Copyright Warning & Restrictions

The copyright law of the United States (Title 17, United States Code) governs the making of photocopies or other reproductions of copyrighted material.

Under certain conditions specified in the law, libraries and archives are authorized to furnish a photocopy or other reproduction. One of these specified conditions is that the photocopy or reproduction is not to be "used for any purpose other than private study, scholarship, or research." If a, user makes a request for, or later uses, a photocopy or reproduction for purposes in excess of "fair use" that user may be liable for copyright infringement,

This institution reserves the right to refuse to accept a copying order if, in its judgment, fulfillment of the order would involve violation of copyright law.

Please Note: The author retains the copyright while the New Jersey Institute of Technology reserves the right to distribute this thesis or dissertation

Printing note: If you do not wish to print this page, then select "Pages from: first page # to: last page #" on the print dialog screen

ABSTRACT

On Adaptive Censored CFAR Detection

by

Loizos Anastasiou Prastitis

In an automatic radar detection system the received signal in every range resolution cell is compared with a threshold to test for the presence of a target. A Neyman-Pearson type test is used which maximizes the probability of detection for a fixed probability of false alarm. For the simple case where the noise is homogeneous a fixed threshold is chosen to achieve the designed constant false alarm rate (CFAR). In the more realistic case the noise background is non-stationary due to clutter and interference. In this situation, the threshold used for testing a particular cell is usually set adaptively using data from nearby resolution cells. A number of such adaptive schemes have been proposed and these are reviewed and the analysis of some of them extended. In this dissertation, new adaptive thresholding techniques for use in nonhomogeneous background environments are proposed and analyzed. It is shown that these new schemes under many conditions perform better than the methods described in the literature in terms of achieving lower probabilities of false alarm and higher probabilities of detection.

First we analyze the greatest-of, GO and smallest-of, SO-CFAR detectors in time diversity transmission. Time diversity transmission is employed to combat deep fades and the loss of the signal. We then present a comparison of the detection performance and the false alarm regulation of the CA,GO and SO-CFAR detectors.

Then we propose and analyze the Automatic Censored Cell Averaging CFAR detector, ACCA-CFAR, which determines whether the test cell is in the clutter or the clear region and selects only those samples that are

identically distributed with the noise in the test cell to form the detection threshold. In the presence of two clutter power transitions in the reference window, the ACCA-CFAR detector is shown to achieve robust false alarm regulation performance while none of the detectors in the literature performs well.

For multiple target situations we propose and analyze the Adaptive Spiky Interference Rejection detector, ASIR-CFAR, which determines and censors the interfering targets by performing cell-by-cell tests, without a priori knowledge about the number of interfering targets. In addition, the results of the Censored Cell Averaging CFAR detector, CCA-CFAR, are extended for multiple pulse transmission and compared with those of the proposed detector.

For multiple target situations in nonhomogeneous clutter the Data Discriminator detector, DD-CFAR, is proposed and analyzed. The DD-CFAR detector performs two passes over the data. In the first pass, the algorithm censors any possible interfering target returns that may be present in the reference cells of the test cell. In the second pass the algorithm determines wheather the test cell is in the clutter or the clear region and selects only those samples that are identically distributed with the noise in the test cell to form the detection threshold. An analysis of the processing time required by the proposed detector is also presented, and compared with the processing time required by other detectors.

Finally we propose and analyze, the Residual Cell Averaging CFAR detector, RCA-CFAR, an adaptive thresholding procedure for Rayleigh envelope distributed signal and noise where noise power residues instead of noise power estimates are processed. The fact that the noise residues become partially correlated to the same degree, if the adjacent samples are

identically distributed, enable us to identify non-homogeneities in the clutter power distribution, by simply observing the consistency in the degree of correlation.

ON ADAPTIVE CENSORED CFAR DETECTION

by

Loizos Anastasiou Prastitis

A Dissertation
Submitted to the Faculty of
New Jersey Institute of Technology
in Partial Fulfillment of the Requirements for the Degree of
Doctor of Philosophy

Department of Electrical and Computer Engineering

January, 1993

APPROVAL PAGE

On Adaptive Censored CFAR Detection

Loizos Anastasiou Prastitis

Dr. Joseph Frank, Thesis Adviser
Associate Professor of Electrical and Computer Engineering, NJIT

Dr. Yun-Qing Shi, Committe Member
Assistant Professor of Electrical and Computer Engineering, NJIT

Dr. Alex M. Haimovich, Committe Member
Associate Professor of Electrical and Computer Engineering, NJIT

Dr. Stelios D. Himonas, Committe Member
Assistant Professor of Electrical Engineering
New York Institute of Technology

Dr. Priyantha L. Perrera, Committe Member
Assistant Professor of Mathematics Department, NJIT

BIOGRAPHICAL SKETCH

Author: Loizos Anastasiou Prastitis

Degree: Doctor of Philosophy in Electrical Engineering

Date: January, 1993

Date of Birth: August 3, 1960

Place of Birth: Famagusta, Cyprus

Undergraduate and Graduate Education:

- Doctor of Philosophy in Electrical Engineering, New Jersey Institute of Technology, Newark, NJ, 1993
- Master of Science in Electrical Engineering, University of Bridgeport, Bridgeport, CT, 1986
- Bachelor of Science in Biomedical Engineering, University of Bridgeport, Bridgeport, CT, 1987
- Bachelor of Science in Electrical Engineering, University of Bridgeport, Bridgeport, CT, 1985

Major: Electrical Engineering

Presentations and Publications:

Prastitis, L.A., J. Frank, and S.D. Himonas. "Optimum Detection of Rayleigh Signals in Nonstationary Noise." *Proceedings of the 1991 IEEE International Phoenix Conference on Computers and Communications*, Phoenix, Arizona, March 1991, pp. 401-407.

Prastitis, L.A., J. Frank, and S.D. Himonas. "On Signal Detection in Partially Correlated Clutter." *Proceedings of the 1991 IEEE Digital Avionics Systems Conference*, Los Angeles, California.

Prastitis, L.A., J. Frank, and S.D. Himonas. "A New Interference Rejection CFAR Processor." *Proceedings of the 1992 Conference on Information Sciences and Systems*, Princeton University, Princeton, New Jersey, pp. 733-738.

Prastitis, L.A., J. Frank, and S.D. Himonas. "Automatic Censored Cell Averaging CFAR Detector in Non-Homogeneous Clutter."

Proceedings of the 1992 International Radar Conference, Brighton, United Kingdom, October 1992, pp.218-221.

This dissertation is dedicated to my Parents

ACKNOWLEDGEMENT

The author would like to express his appreciation to Dr. Joseph Frank for his support, knowledge and insight during my research at N.J.I.T. far in excess of reasonable expectations.

I would also like to express my thankfulness to Dr. Stelios Himonas for contributing his knowledge.

Many thanks are due to the distinguished members of the committee: Dr. Yun-Qing Shi, Dr. Alex Haimovich and Dr. Priyantha L. Perera. Their encouragement and valuable discussions have improved the quality of this dissertation.

The author would also like to thank the valuable members of the Electrical and Computer Engineering department for their help and continuous support.

I also would like to extend a special thanks to my immediate family. Many thanks go to my mother and father and to my wife Athina and all my friends, for their dedication and generous support.

TABLE OF CONTENTS

LIST OF FIGURES

Chapter 1

INTRODUCTION AND OVERVIEW OF PREVIOUS WORK

1.1 Introduction

The received signal in a radar signal processor is always accompanied by noise. The performance of the radar receiver is greatly dependent on the presence of noise, and the receiver is desired to achieve constant false alarm rate, CFAR, and maximum probability of target detection. Thermal noise generated by the radar itself is unavoidable. In addition, returns from other targets referred to as interfering targets, unwanted echoes (clutter) typically from the ground, sea, rain or other participation, chaff and small objects, interfere with the detection of the desired targets. The distinction between clutter and target depends on the purpose of a radar system. For an air surveillance radar, land, rain and weather conditions are clutter sources. For a radar in metereology, weather conditions are regarded as a target, and aircrafts are considered as clutter. Land for instance, is considered the target for a ground mapping radar while weather conditions and aircrafts constitute clutter sources. From experimental data, the clutter backscattering coefficient (effective echoing area) can be modeled by either the Rayleigh, the Log-normal, or the Weibull distribution depending on the type of clutter [1]. If the clutter returns are Rayleigh envelope distributed, and they are identically distributed with the thermal noise, this constitutes the simplest

clutter model. The environment in which the radar operates depends on the above factors that may yield statistically non stationary signals with unknown variance at the receiver input.

In general, the radar system consists of a transmitter and a receiver at the same location with one or two antennas. The transmitted signal is an electromagnetic signal or sometimes an acoustic one [2]. The amplitude of the signal at the receiver input depends on the target radar cross section, RCS, which is a measure of the amount of the electromagnetic energy a radar target intercepts and scatters back towards the receiver. In general, the target RCS fluctuates because targets consists of many scattering elements and returns from each scattering element vary. Target RCS fluctuations are modelled according to the four Swerling target cases [3]. Cases I and II represent targets composed of a large number of independent scatterers none of which dominates, e.g. large aircrafts, rain clutter and terrain clutter. Cases III and IV represent targets that have a single dominant nonfluctuating scatterer together with other smaller independent scatterers, e.g. rockets and missiles. Swerling I and II targets produce signals whose envelopes are Rayleigh distributed, while Swerling cases III and IV targets produce signals whose envelopes are chi-squared distributed. Cases I and III assume slow target RCS fluctuations, and thus signal returns are considered completely correlated pulse-to-pulse but independent scan-to-scan. Cases II and IV assume rapid target RCS fluctuations and therefore signal returns are considered independent pulse-to-pulse. It should be pointed out that for a single pulse transmission per scan, case I is identical to case II, and case III is identical to case IV.

1.2 Radar Signal Detection

The detection of a radar signal embeded in noise can be formulated as a problem in hypothesis testing [4-8]. The null hypothesis, denoted by H_0, is the hypothesis

that the received signal is due to noise only while the alternative hypothesis, denoted by H_1, is the hypothesis that the received signal is due to a target return echo plus noise. The null hypothesis, H_0, should be tested against the alternative hypothesis, H_1 to obtain a decision about the presence or the absence of a target. This test leads to two kinds of error probabilities. The probability of false alarm, P_F, which is to decide H_1 while hypothesis H_0 is true, and the probability of miss which is to decide H_0 while hypothesis H_1 is true. A decision rule that does not require knowledge of a priori signal statistics appropriate for radar signal detection, is designed based on the Neyman-Pearson criterion. The optimum Neyman-Pearson detector, for this case is shown in Figure 1.1, where $r(t)$ denotes the received signal and ω_c the carrier angular frequency. The input signal at the receiver, when a target is present, is an attenueded, randomly phase shifted version of the transmitted pulse embedded in white Gaussian noise [9]. The received signal $r(t)$ is processed by the inphase and quadrature channels as shown in Figure 1.1. For Swerling cases I and II, X and Y are Gaussian random variables with parameter 0 and μ $[N(0,\mu)]$. Under hypothesis H_0 (thermal noise only) $\mu = 2\sigma^2$ and under hypothesis H_1 (signal plus noise) $\mu = 2\sigma^2 + 2a^2$ where $2a^2$ is the signal power. Thus μ is given by

$$\mu = \begin{cases} 2\sigma^2 & \text{for } H_0 \\ 2\sigma^2(1+\frac{a^2}{\sigma^2}) & \text{for } H_1 \end{cases} \tag{1.1}$$

If we define $S = \frac{a^2}{\sigma^2}$, the signal to noise ratio at the receiver input, SNR, μ is given by

$$\mu = \begin{cases} 2\sigma^2 & \text{for } H_0 \\ 2\sigma^2(1+S) & \text{for } H_1 \end{cases} \tag{1.2}$$

As shown in Figure 1.1, the input to the threshold device Q is given by

$$Q = X^2 + Y^2 \tag{1.3}$$

Thus, from the assumed noise model the conditional probability density function, pdf, of Q is given by

$$p_{Q|H_i}(q|H_i) = \begin{cases} \frac{1}{2\sigma^2}e^{-q/\sigma^2} & \text{for} \quad H_0 \\ \frac{1}{\sigma^2(1+S)}e^{-q/\sigma^2(1+S)} & \text{for} \quad H_1 \end{cases} \tag{1.4}$$

The Neyman-Pearson criterion requires that the probability of false alarm, P_F, is less than a desired value, α, and that the probability of target detection should be maximized. This results in the likelihood ratio test, that is,

$$\Lambda(q) = \frac{p_{Q|H_1}(q|H_1)}{p_{Q|H_0}(q|H_0)} \underset{H_0}{\overset{H_1}{\gtrless}} \lambda \tag{1.5}$$

where $\Lambda(q)$ is the likelihood ratio, $p_{Q|H_i}(q|H_i)$ is the conditional probability density function, pdf, of Q when hypothesis H_i, $i = 0, 1$ is true, and λ is the detection threshold which is obtained from the constraint $P_F = \alpha$, that is

$$\int_{\lambda}^{\infty} p_{\Lambda|H_0}(l|H_0)d\lambda = \alpha \tag{1.6}$$

The solution of (1.6) yields a threshold which is a function of the noise variance.

In a real radar environment where the total noise is a nonstationary process whose variance may vary with time, the ideal fixed threshold detector does not achieve any regulation in the probability of false alarm. For a design probability of false alarm, $P_F = 10^{-8}$, a small increase in the noise variance by only 3dB results in an increase of 10^{-4} in the false alarm probability as shown in Figure 1.2.

1.3 The CA-CFAR Detector

As we saw in the previous section, the ideal fixed threshold detector may yield an excessive number of false alarms. This overloads the radar receiver, since in addition to the detection process, other processes are initiated by the radar, such as tracking for example. In order to achieve constant false alarm rate, CFAR, adaptive thresholding procedures are needed. Finn and Johnson in [10], proposed the cell averaging constant false alarm rate, CA-CFAR, detector. The estimate of the noise level in every detection is formed by the nearby noise samples. Then, based on this estimate the detection threshold is set. In other words, the detection threshold is designed

in such a way, to adapt to changes in the environment. The noise observations are obtained by sampling in range and doppler as shown in Figure 1.3. The bandwith of each doppler (bandpass) filter is equal to the bandwith of the transmitted rectangular pulse, B, where $B = 1/\tau$ and τ is the transmitted pulse width. The output of each square-law detector is sampled every τ seconds which corresponds to a range interval of $c\tau/2$. Each sample can be considered as the output of a range-doppler resolution cell with dimensions τ in time and $1/\tau$ in frequency. Therefore we obtain a matrix of range and doppler resolution cells, as shown in Figure 1.4. The CA-CFAR detector is shown in Figure 1.5, where we show the range cells only for a specific doppler frequency. Each resolution cell is tested separetely in order to make a decision. We shall assume that the test cell is the middle one, a customary assumption made in the literature. The cells surrounding the test cell are known as the reference range cells which comprise the reference window. The reference cells to the left of the test cell are referred to as the leading range cells, while the reference cells to the right of the cell under test are referred to as the lagging range cells. We assume that the cell outputs are observations from statistically independent and identically distributed random variables. The conditional probability density function of the output of the jth range cell is given by

$$p_{Q_j}(q_j) = \frac{1}{\mu}\exp(-\frac{q_j}{\mu}) \quad q_j \geq 0 \tag{1.7}$$

for $j = 1, \ldots, N(N = M/2)$. μ denotes the parameter of the distribution from which the observation q_j is generated. It should be pointed out that through out this dissertation, uppercase letters are used to denote random variables, while lower case letters are used to denote the corresponding observations. The value of μ depends on the contents of the jth cell. If the jth cell contains thermal noise only, μ is normalized to unity. If it is immersed in clutter then, $\mu = 1 + C$ where C denotes the average clutter power to thermal noise power at the receiver input. If the jth cell contains a target return then $\mu = 1 + I$, where I denotes the target return average signal power

to thermal noise power ratio at the receiver input. If the jth cell is immersed in the clutter and in addition, contains a target return then $\mu = 1 + C + I$. The cell under test is assumed to be the one in the middle, and is denoted by the subscript 0. The cell under test may contain either noise alone or target plus noise. The conditional probability density function of the output of the test cell is given by

$$p_{Q_0|H_i}(q_0|H_i) = \begin{cases} \frac{1}{2\sigma^2(1+S)} \exp\left(-\frac{q_0}{2\sigma^2(1+S)}\right) & H_1 \\ \frac{1}{2\sigma^2} \exp(-\frac{q_0}{2\sigma^2}) & H_0 \end{cases} \tag{1.8}$$

for Swerling cases I and II, and

$$p_{Q_0|H_i}(q_0|H_i) = \begin{cases} \frac{1}{[2\sigma^2(1+S)]^2}[2\sigma^2 + \frac{S/2}{1+S/2}q_0] \exp[-\frac{q_0}{2\sigma^2(1+S/2)}] & H_1 \\ \frac{1}{2\sigma^2} \exp(-\frac{q_0}{2\sigma^2}) & H_0 \end{cases} \tag{1.9}$$

for Swerling cases III and IV. $2\sigma^2$ is the input noise variance and S is the average received signal to noise ratio, SNR. The received signal $r(t)$ is square law detected and sampled in range by the $N + 1$ range resolution cells as shown in Figure 1.5. We assume that $q_1, \ldots, q_N$ are samples from exponential distribution and that they are independent. The maximum likelihood estimate, $2\hat{\sigma^2}$, of the parameter of the distribution is derived as follows : The likelihood function is

$$\begin{aligned} L[2\sigma^2] &= p(q_1, \ldots, q_N; 2\sigma^2) \\ &= \prod_{j=1}^{N} p(q_j, 2\sigma^2) \\ &= (\frac{1}{2\sigma^2})^n \exp\left[-\frac{1}{2\sigma^2}(\sum_{j=1}^{N} q_j)\right] \end{aligned} \tag{1.10}$$

The derivative of the likelihood function is given by

$$\frac{d[L(2\sigma^2)]}{d2\sigma^2} = -\frac{M}{2\sigma^2} + \frac{1}{(2\sigma^2)^2}\sum_{j=1}^{N} q_j \tag{1.11}$$

Equating the derivative to zero the maximum likelihood estimate of $2\hat{\sigma^2}$ is

$$2\hat{\sigma^2} = \frac{1}{N}\sum_{j=1}^{N} q_j \tag{1.12}$$

Thus, the maximum likelihood estimate of the noise level in the cell under test is equal to the arithmetic mean of the nearby resolution cells. The noise level estimate

is then scaled by a constant T, the threshold multiplier, which is chosen to achieve the desired probability of false alarm α. The output of the cell under test is then compared to the adaptive threshold Tq according to

$$Q_0 \underset{H_0}{\overset{H_1}{\gtrless}} T\,Q \tag{1.13}$$

where Q is the sufficient statistic of noise level in the test cell, $Q = N(2\hat{\sigma^2})$, in order to make a decision about the presence (H_1) or the absence (H_0) of a target in the test cell. The design expression for the probability of detection is

$$\begin{aligned} P_D &= \Pr(Q_0 > TQ|H_1) \\ &= \int_0^\infty dq p_Q(q) \int_{Tq}^\infty p_{Q_0|H_1}(q_0|H_1) dq_0 \end{aligned} \tag{1.14}$$

where $p_Q(q)$ is the pdf of the test statistic Q. Similarly the design expression for the probability of false alarm is

$$\begin{aligned} P_F &= \Pr(Q_0 > TQ|H_0) \\ &= \int_0^\infty dq p_Q(q) \int_{Tq}^\infty p_{Q_0|H_0}(q_0|H_0) dq_0 \end{aligned} \tag{1.15}$$

The probability density function, pdf, of Q is $p_Q(q) = G(N,1)$, where $G(N,1)$ is the Gamma distribution with parameter N and 1. Thus,

$$p_Q(q) = \frac{1}{\Gamma(N)} q^{N-1} \exp(-q) \tag{1.16}$$

Assuming that the primary target in the test cell is fluctuating according to Swerling II model, substituting equations (1.8) and (1.16) into equation (1.14) the probability of detection is

$$P_D = \left[1 + \frac{T}{1+S}\right]^{-N} \tag{1.17}$$

Setting $S = 0$, in equation (1.17), the design expression for the probability of false alarm is

$$P_F = (1+T)^{-N} \tag{1.18}$$

The scaling constant T is then computed from equation (1.18) thus,

$$T = (P_{FA})^{-\frac{1}{N}} - 1 \tag{1.19}$$

It is clear from equations (1.17) and (1.18), that both the probability of detection and the probability of false alarm are independent of the noise parameter μ. As the number of reference range cells becomes large ($N \rightarrow \infty$), the probability of detection approaches

$$\begin{aligned} P_D &= \lim_{N\rightarrow\infty}(1 + \frac{T}{1+S})^{-N} \\ &= \exp(-\frac{T}{1+S}) \end{aligned} \tag{1.20}$$

and the probability of false alarm approaches

$$\begin{aligned} P_F &= \lim_{N\rightarrow\infty}(1 + T)^{-N} \\ &= \exp(-T) \end{aligned} \tag{1.21}$$

Equations (1.20) and (1.21) are the expressions which describe the performance of the ideal (fixed threshold) detector. Thus, for homogeneous clutter background environment, the CA-CFAR detector is the optimum detector in the sense that its probability of detection approaches that of the ideal fixed threshold detector, as the number of reference noise samples becomes very large.

The CA-CFAR detector achieves the design probability of false alarm and a high detection probability in a homogeneous background environment, that is, when the received noise samples are identically distributed and statistically independent, as we saw earlier. In a real environment however the noise samples may not be homogeneous. We will study the detection performance as well as the false alarm regulation properties of the CA-CFAR detector and all other detectors considered in this dissertation, based on the following four models of background environment.

Model A: Clutter power transitions

This model is defined to describe the situation in which there is a single transition in the clutter power distribution as shown in Figures 1.6 and 1.7. In practice, the clutter power transition may represent the boundary of a precipitation area. In Figure 1.6 the cell under test is in the clutter, while in Figure 1.7 the test cell is in the clear. A cell is said to be in the clear if it contains only thermal noise. As mentioned earlier, the test cell is assumed to be in the middle of the reference window. Assuming that m is the number of range cells immersed in clutter, then the test cell is in the clutter, if and only if $m > N/2$, where N is the even total number of reference range cells. If $m < N/2$, the test cell is in the clear.

Model B: Two clutter power transitions

This model is defined to describe the situation in which there are two clutter power transitions in the clutter power distribution, as shown in Figures 1.8 and 1.9. If m_1 and m_2 represent the location of the clutter power transitions in the leading and lagging reference window respectively, and the range cells between m_1 and m_2 are immersed in clutter, the test cell is said to be in the clutter if $m_1 < N/2 < m_2$ as shown in Figure 1.8. On the other hand if m_1 and $N - m_2$ range cells are immersed in clutter, the test cell is said to be in the clear if $m_1 < N/2 < m_2$ as shown in Figure 1.9.

Model C: Spikes in individual cells.

This model is defined to describe the situation where the clutter background environment is composed of homogeneous white Gaussian noise plus interfering targets. The targets appear as spikes in the individual range cells as shown in Figure 1.10. These targets may fall in either the leading or the lagging reference range cells or in both the leading and lagging range cells.

Model D: Clutter and Spikes in reference window

This model describes the most general case in which not only there is a transition

in the clutter power distribution, but also interfering target returns. Typical cases of this model are presented in Figure 1.11.

1.4 Threshold Exceedance Probability

In this section we derive an expression for the threshold exceedance probability. This expression will be used in the next section and through out this dissertation to derive expressions for the false alarm and the detection probabilities of the detectors that are considered. The threshold exceedance probability, $Pr(E_i)$, is defined to be

$$Pr(E_i) = Pr(Q_0 > TQ|H_i), \quad i = 0, 1 \tag{1.22}$$

where Q is the sufficient statistic of the noise level in the cell under test whose probability density function, pdf, is denoted by $p_Q(q)$, and Q_0 is the random variable denoting the output of the test cell. The threshold exceedance probability is equal to P_F for $i = 0$, while for $i = 1$, it is equal to the probability of detection P_D. Defining a new random variable R according to

$$R = Q_0 - TQ \tag{1.23}$$

the threshold exceedance probability of equation (1.22) can be written as

$$Pr(E_i) = Pr(R > 0|H_i), \quad i = 0, 1 \tag{1.24}$$

Let the conditional pdf of R given hypothesis H_i, $i = 0, 1$, be $p_{R|H_i}(r|H_i)$. Therefore, the threshold exceedance probability is given by

$$Pr(E_i) = \int_0^\infty p_{R|H_i}(r|H_i)dr, \quad i = 0, 1 \tag{1.25}$$

The moment generating function, mgf, of R under hypothesis H_i is defined to be

$$\begin{aligned} \Phi_{R|H_i}(\omega) &= E[\exp(-\omega R)|H_i] \\ &= \int_\infty^\infty p_{R|H_i}(r|H_i)\exp(-\omega r)dr, \end{aligned} \tag{1.26}$$

where $E[\cdot]$ denotes the expectation operator. Inverting the integral of equation (1.26), we may express the conditional pdf of R in terms of its mgf as,

$$p_{R|H_i}(r|H_i) = \frac{1}{2\pi i}\int_c \Phi_{R|H_i}(\omega)\exp(\omega R)d\omega \quad i = 0, 1 \tag{1.27}$$

The contour of integration c consists of a vertical path in the complex ω-plane crossing the negative real axis at $\omega = c_1$. It is closed in an infinite semicircle in the left half ω-plane. c_1 is chosen so that the contour c encloses all the poles of $\Phi_{R|H_i}(\omega)$ that lie in the left half ω-plane. Substituting equation (1.27) into (1.25) and performing the integration with respect to r, the threshold exceedance probability is obtained to be

$$Pr(E_i) = -\frac{1}{2\pi i}\int_c \omega^{-1}\Phi_{R|H_i}(\omega)d\omega \tag{1.28}$$

1.5 The CA-CFAR Detector in Nonhomogeneous Background Environment

In this section we derive expressions for the probability of detection and the probability of false alarm for the CA-CFAR detector in the presence of a clutter power transition in the reference window of the cell under test. Also the case of the presence of interfering targets is studied.

The detection performance as well as the false alarm regulation properties of the CA-CFAR detector may be seriously degraded for the four models described in section 1.3. If the test cell is in the clear region but a group of reference cells are immersed in the clutter (Figures 1.7 and 1.9), a *masking effect* results. That is, the threshold is raised unnecessarily and therefore the probability of detection (along with the false alarm probability) is lowered significantly, even though there may be a high SNR in the cell of interest. On the other hand, if the test cell is in the clutter but a group of reference cells are in the clear (Figures 1.6 and 1.8), the probability of false alarm increases intolerably. When interfering targets lie in the reference cells of the

target under consideration (Figure 1.10), denoted hereafter as the primary target, the threshold is raised and detection of the primary target is seriously degraded. This is known as the *capture effect*. Assuming that m samples in the reference window are in the clear and the remaining $N-m$ samples including the test cell are in the clutter, Q is given by

$$Q = \sum_{j=1}^{m} q_j + \sum_{j=m+1}^{N} q_j \tag{1.29}$$

where

$$p_{Q_j}(q_j) = \begin{cases} \exp(-q_j) & j = 1,\ldots,m \\ \frac{1}{1+C}\exp(-\frac{q_j}{1+C}) & j = m+1,\ldots,N \end{cases} \tag{1.30}$$

and C denotes the clutter to thermal noise power ratio at the receiver input. The expression for the probability of detection is defined to be

$$\begin{aligned} P_D &= \Pr(Q_0 > TQ|H_1) \\ &= -\frac{1}{2\pi i}\int_c \omega^{-1}\Phi_{R|H_1}(\omega)d\omega \end{aligned} \tag{1.31}$$

where $\Phi_{R|H_1}(\omega)$ is the moment generating function, mgf, of $R = Q_0 - TQ$ and is given by

$$\Phi_{R|H_1}(\omega) = \frac{(1+C+S)^{-1}(1-\omega T)^{-m}}{(\omega + \frac{1}{(1+C+S))}(1-\omega T(1+C))^{N-m}} \tag{1.32}$$

Substituting equation (1.32) into (1.31) the probability of detection is obtained to be

$$P_D = (1+C)^{m-N}\left[\frac{1}{1+C} + \frac{T}{(1+C+S)}\right]^{m-N}\left[1 + \frac{T}{1+C+S}\right]^{-m} \tag{1.33}$$

In equation (1.31), the contour of integration c is crossing the real ω-axis at $\omega = c_1$ and is closed in an infinite semicircle in the left half ω-plane. c_1 is selected so that c encloses all poles of $\Phi_{R|H_1}(\omega)$ that lie in the open left half ω-plane. Setting $S = 0$ in equation (1.33) the probability of false alarm is

$$P_F = (1+T)^{N-m}\left[1 + \frac{T}{1+C}\right]^{-m} \tag{1.34}$$

In the case where the test cell is in the clear and m reference samples are in the clutter, Q is given in expression (1.29) where

$$p_{Q_j}(q_j) = \begin{cases} \exp(-q_j) & j = m+1,\ldots,N \\ \frac{1}{1+C}\exp(-\frac{q_j}{1+C}) & j = 1,\ldots,m \end{cases} \tag{1.35}$$

Following the same procedure as before the probability of detection is derived to be

$$P_D = (1+C)^{-m}(1/(1+C)+T/(1+S))^{-m}(1+T/(1+S))^{m-N} \tag{1.36}$$

Setting $S = 0$ in the above equation, the probability of false alarm is given by

$$P_F = (1+(1+C)T)^{-m}(1+T)^{m-N} \tag{1.37}$$

Similarly, when m interfering targets appear in the reference window with Q given in equation (1.29) the probability of detection is

$$P_D = \left[1+(1+I)\frac{T}{(1+S)}\right]^{-m}\left[1+\frac{T}{(1+S)}\right]^{m-N} \tag{1.38}$$

where I is the interference to noise ratio. In Figure 1.12 we study the false alarm regulation performance of the CA-CFAR detector when a clutter power transition is present in the leading reference window and the test cell is in the clear. We assume $N = 16$ and a design probability of false alarm, $\alpha = 10^{-4}$. Clearly, the CA-CFAR detector does not achieve the design probability of false alarm due to the fact that the noise level estimate in the test cell is underestimated and a masking effect results. In Figure 1.13 we show the probability of detection of the CA-CFAR when one and two interfering targets are present in the reference window. We assume a window of $N = 16$ and a design probability of false alarm of $\alpha = 10^{-4}$. In the presence of one interfering target, the probability of detection degrades as compared to the homogeneous environment as shown in Figure 1.13, due to the capture effect. The degradation is even more acute in the presence of two interfering targets.

1.6 CFAR Detectors

To alleviate the problems mentioned above, different techniques have been proposed in the literature [11-30]. The problem of the increase of the false alarm probability due to the presence of a step discontinuity in the distributed clutter, has been treated

by Hansen and Sawyers [11,12]. They proposed the greatest-of-selection logic in cell averaging constant false alarm rate detector, GO-CFAR, to control the increase in the false alarm probability. A detailed analysis of the false alarm regulation capabilities of the GO-CFAR detector has been performed by Moore and Lawrence [13]. In [14], Weiss has shown that if one or more interfering targets are present, the GO-CFAR detector performance is very poor. He suggested the use of the smallest-of-selection logic in cell averaging constant false alarm rate detector, SO-CFAR. The SO-CFAR detector was first proposed by Trunk [15] in order to improve the resolution of closely spaced targets. In order to improve the probability of detection of the CA-CFAR, the GO-CFAR and SO-CFAR detectors, Barkat and Varshney [16] and Barkat [17] proposed the use of multiple estimators to obtain the detection threshold. For multiple target situations, when an a priori estimate about the level of interference can be obtained from the radar's tracking system, it is possible to lower the adaptive threshold, thereby minimizing the capture effect which deteriorates the performance of the CA-CFAR detector. Mc-Lane in [18], proposed a modified CA-CFAR detector which employs threshold compensation based on that a priori information about the location of the targets. An extension of this procedure to the GO-CFAR and the SO-CFAR detectors was performed by Al-Hussainni and Imbrahim [19]. Furthermore, Barkat and Varshney [20] proposed the weighted cell-averaging CFAR, WCA-CFAR, detector by assigning optimum weights to the sums of the leading and lagging range cells such that CFAR is achieved while the probability of detection is maximized. Barboy [21] proposed an interative censoring scheme to detect a number of targets which may be present in the reference window.

Recently, a new class of order statistics-based thresholding techniques have appeared in the literature [22-27]. Rohling [22] introduced an order statistic based estimation technique to achieve CFAR for nonhomogeneous environments. He proposed the order-statistic CFAR, OS-CFAR, detector which chooses one ordered sam-

ple to represent the noise level estimate in the cell under test. Elias-Fuste et al. [23] proposed two new OS-CFAR detectors that require only half the processing time of the OS-CFAR detection [22]. One is the ordered statistic greatest of OSGO-CFAR, while the other is an ordered statistic smallest of the OSSO-CFAR detector. Rickard and Dillard [24], proposed the censored Mean Level Detector, CMLD, in which the largest samples are censored and the noise level estimate is obtained from the remaining noise samples. For a fixed number of interfering Swerling targets II, Ritcey [25] studied the performance of the CMLD. Al-Hussainni [26] extended this procedure to the greatest-of-detector. Gandhi and Kassam [27], proposed a generalization of the OS-CFAR detector and the CMLD, known as the trimmed mean, TM-CFAR, detector. The TM-CFAR detector implements trimmed averaging after ordering the samples in the reference window. In the order-statistic detectors, mentioned above the censoring points are preset. This implies that these detectors achieve robust performance given some a priori knowledge about the background environment. In general however, such a priori information may not be available, and these detectors they may suffer similar masking and capture effects as well as increase in the false alarm probability, like the CA-CFAR detector. To alleviate these problems in the above mentioned fixed censoring schemes, adaptive censoring procedures have been proposed in the literature [28-30]. In [28], the generalized censored mean level detector, GCMLD, was proposed. The GCMLD employs a signal processing algorithm which adaptively selects the censoring point by performing cell-by-cell tests. The GCMLD is robust when the reference window contains interfering targets in homogeneous noise. In [29], the generalized two level, GTL-CMLD was proposed. The GTL-CMLD achieves robust performance in the presence of both interfering targets and clutter power transitions. In [30] the adaptive censored greatest-of, ACGO-CFAR detector has been proposed. In this scheme, two tentative estimates of the noise level in the test cell are obtained by independantly processing the outputs of the leading

and lagging reference range cells. The final estimate of the noise level is set to be the maximum of the two tentative estimates which are obtained by introducing a cell-by-cell criterion for accepting or rejecting reference samples.

1.7 Dissertation Organization

In this dissertation, robust detection techniques for CFAR processing in non-homogeneous environments are considered. First, in chapter II we study the GO and SO-CFAR detectors for single pulse transmission. Due to the fact that in many practical situations time diversity transmission is employed in order to combat deep fades and loss of signal, the results of the SO and GO-CFAR detectors are extended for multiple pulse transmission. In chapter III, we propose a CFAR detection algorithm, the Automatic Censored Cell Averaging CFAR detector, ACCA-CFAR, which determines whether the test cell is in the clutter or the clear region and selects only those samples which are identically distributed with the noise in the test cell to form the detection threshold. We show that the required processing time for a decision to be reached is less than that of the order-based statistics processor, the ACGO-CFAR detector. When two clutter power transitions are present, the false alarm regulation properties of the proposed detector are shown to be more robust as compared to those of the GO and ACGO-CFAR detectors. In chapter IV we propose the Adaptive Spiky Interference Rejection, ASIR-CFAR, detector which determines and censores the interfering targets by performing cell-by-cell tests. The detection performance of the ASIR-CFAR detector is compared to those of the GCMLD and CCA-CFAR detectors in multiple target situations. It is shown that when the probability of false alarm becomes stricter and the reference window becomes smaller the detection performance of the proposed detector is better as compared to those of the GCMLD snd the CCA-CFAR detectors. Also we study the effect of the probability of false censoring on the design probability of false alarm for both the GCMLD and the ASIR-CFAR detectors. In addition, we

show that the required processing time of the proposed detector is less than that of the GCMLD detector. The results of CCA-CFAR detector are also extended for time diversity transmission. In chapter V we propose and analyze the Data Discriminator, DD-CFAR processor in the presence of both interfering targets and clutter power transitions in the reference window of the primary target. The DD-CFAR processor performs two passes over the data. In the first pass, the algorithm censors any possible interfering target returns that may be present in the reference cells of the test cell. In the second pass the algorithm determines whether the test cell is in the clutter or the clear region and selects only those samples that are identically distributed with the noise in the test cell. The false alarm regulation and detection performance of the DD-CFAR detector are compared to those of the ACGO, TM, GO and SO-CFAR detectors. Finally in chapter VI, we propose an adaptive thresholding procedure for Rayleigh envelope distributed signals and noise, where noise power residues instead of noise power estimates are processed. We show that it is the optimum constant false alarm rate, CFAR, detector when the noise samples are statistically independent and identically distributed in the sense that its detection performance approaches that of the ideal (fixed threshold detector) as the number of noise samples becomes large. However, an attractive feature of the proposed detector is that the noise residues become partially correlated to the same degree, if the adjacent samples are identically distributed, and this enables us to identify non-homogeneities in the clutter power distribution which may be censored, by simply observing the consistency of the degree of correlation between adjacently received samples.

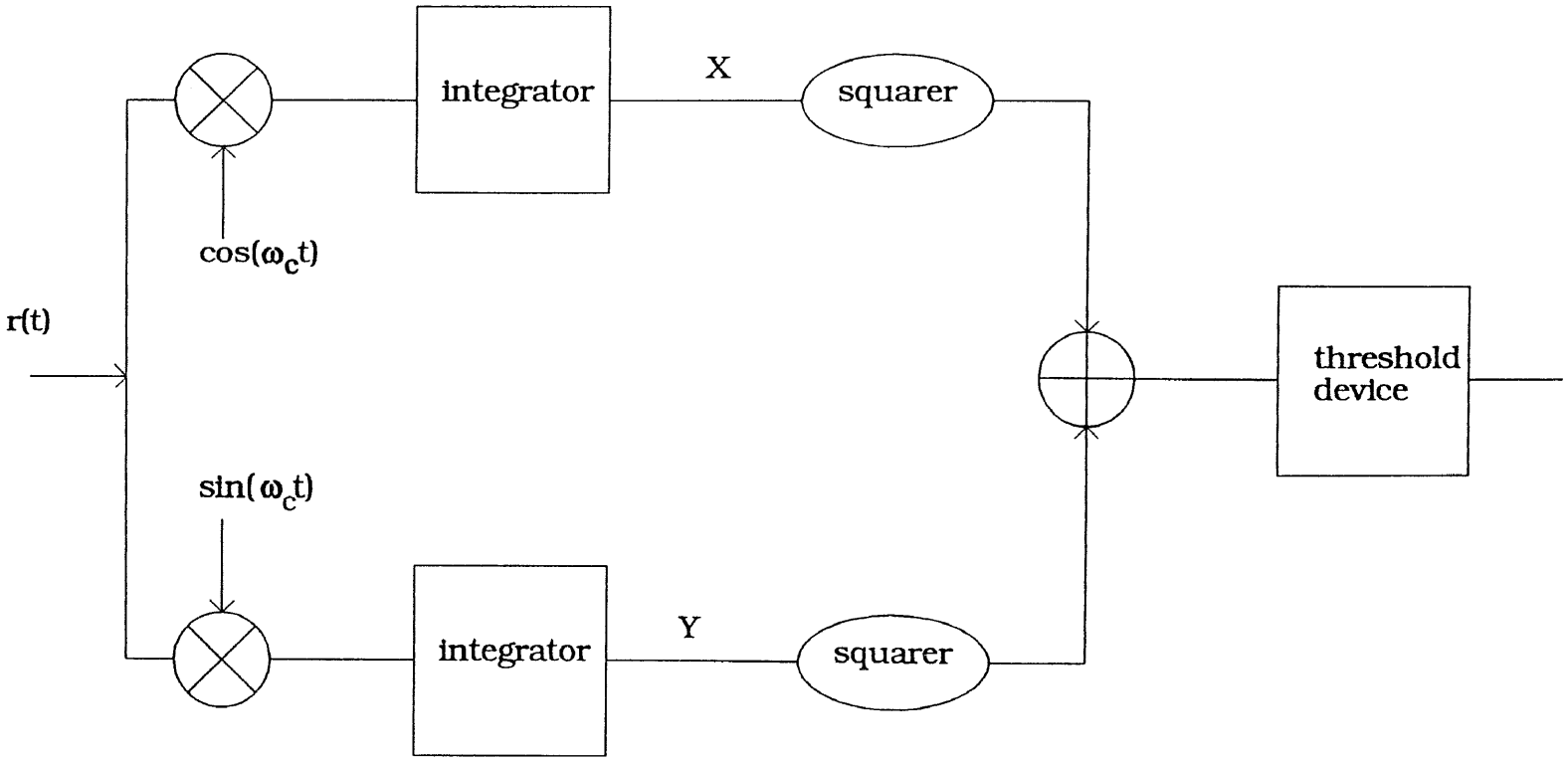

Figure 1.1 Optimum receiver, squarer realization

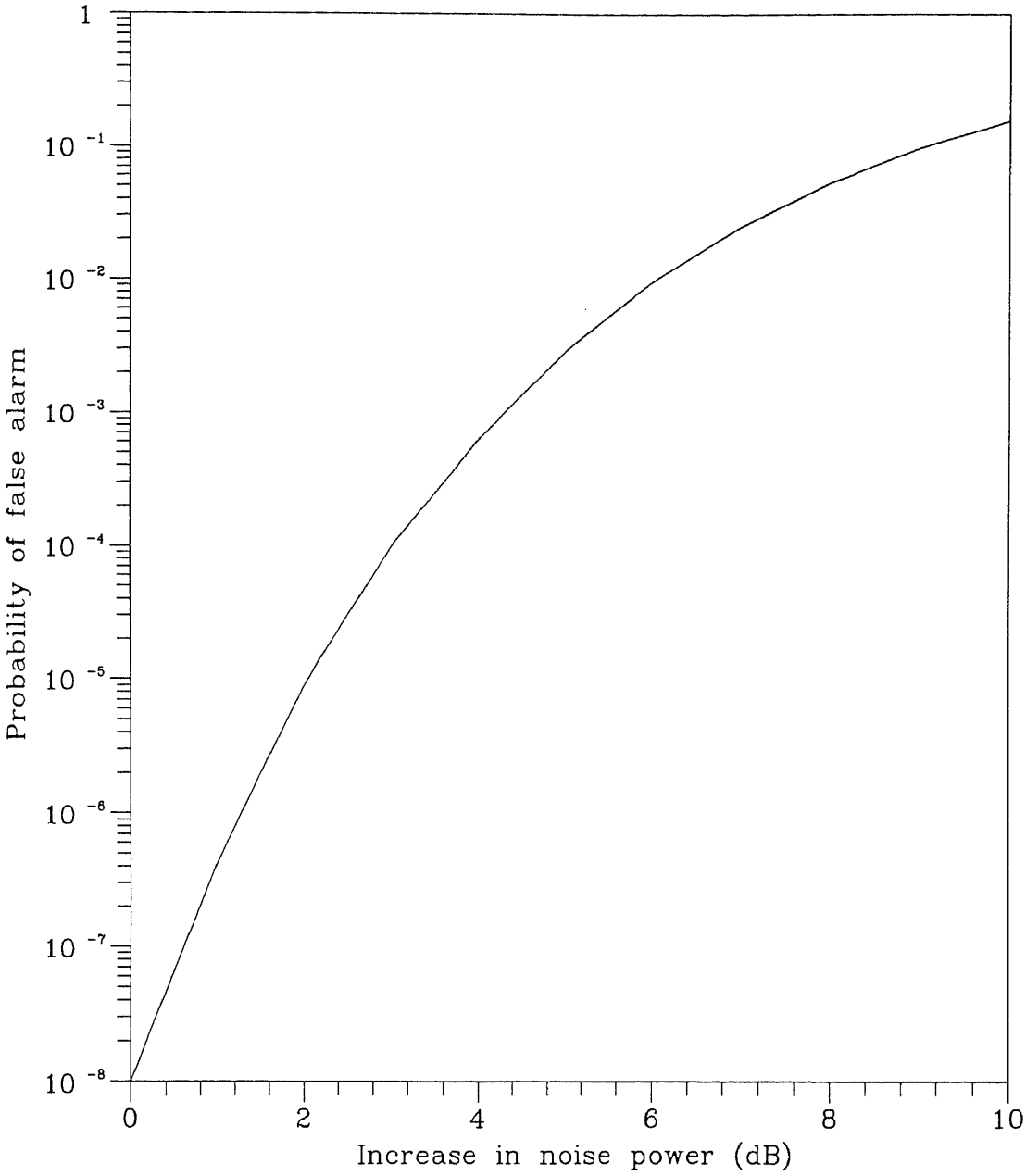

Figure 1.2 The effect of increased noise on the probability of false alarm of a fixed threshold detector.

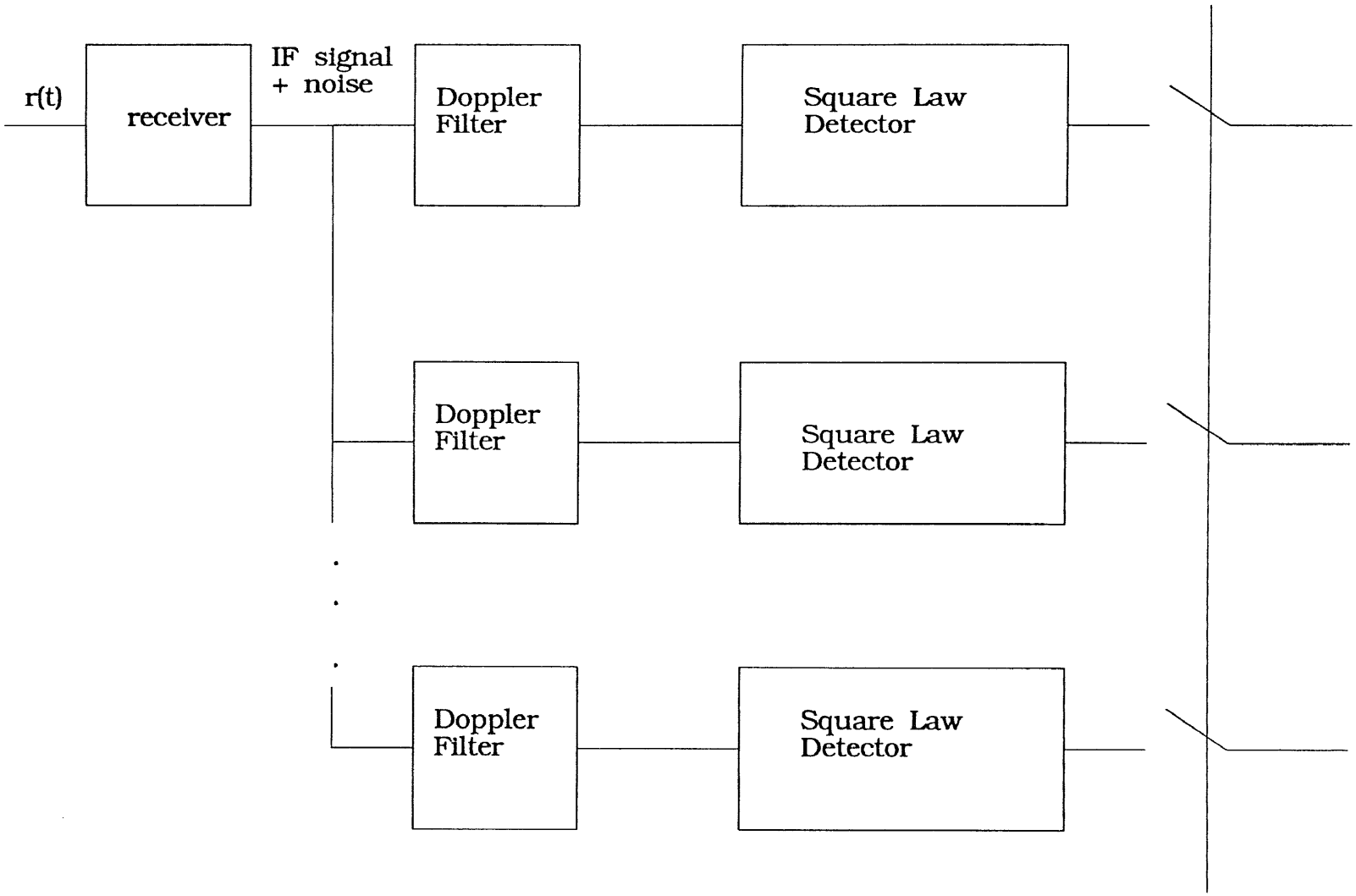

Figure 1.3 Range and doppler sampling process.

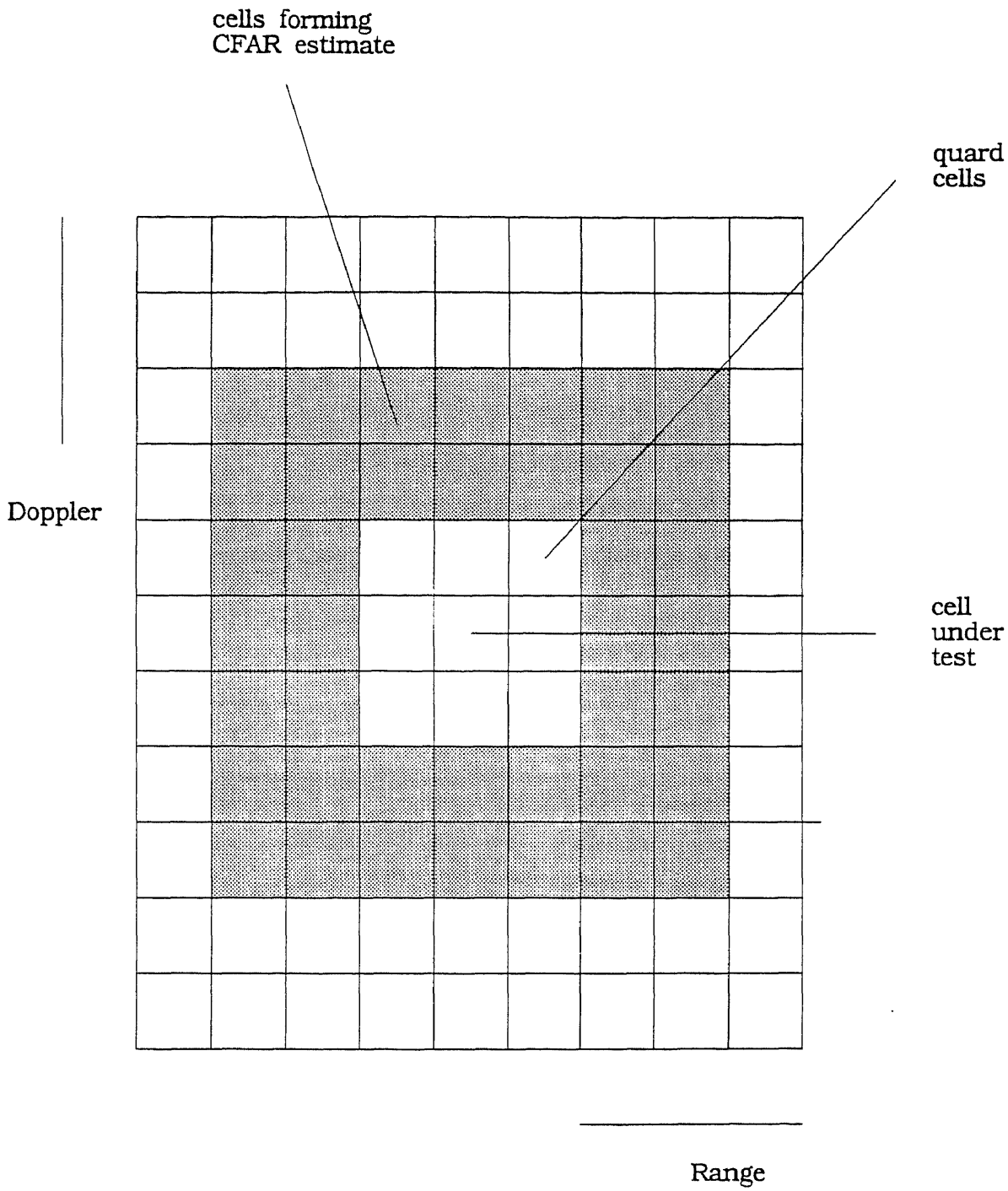

Figure 1.4 Matrix of range and doppler cells.

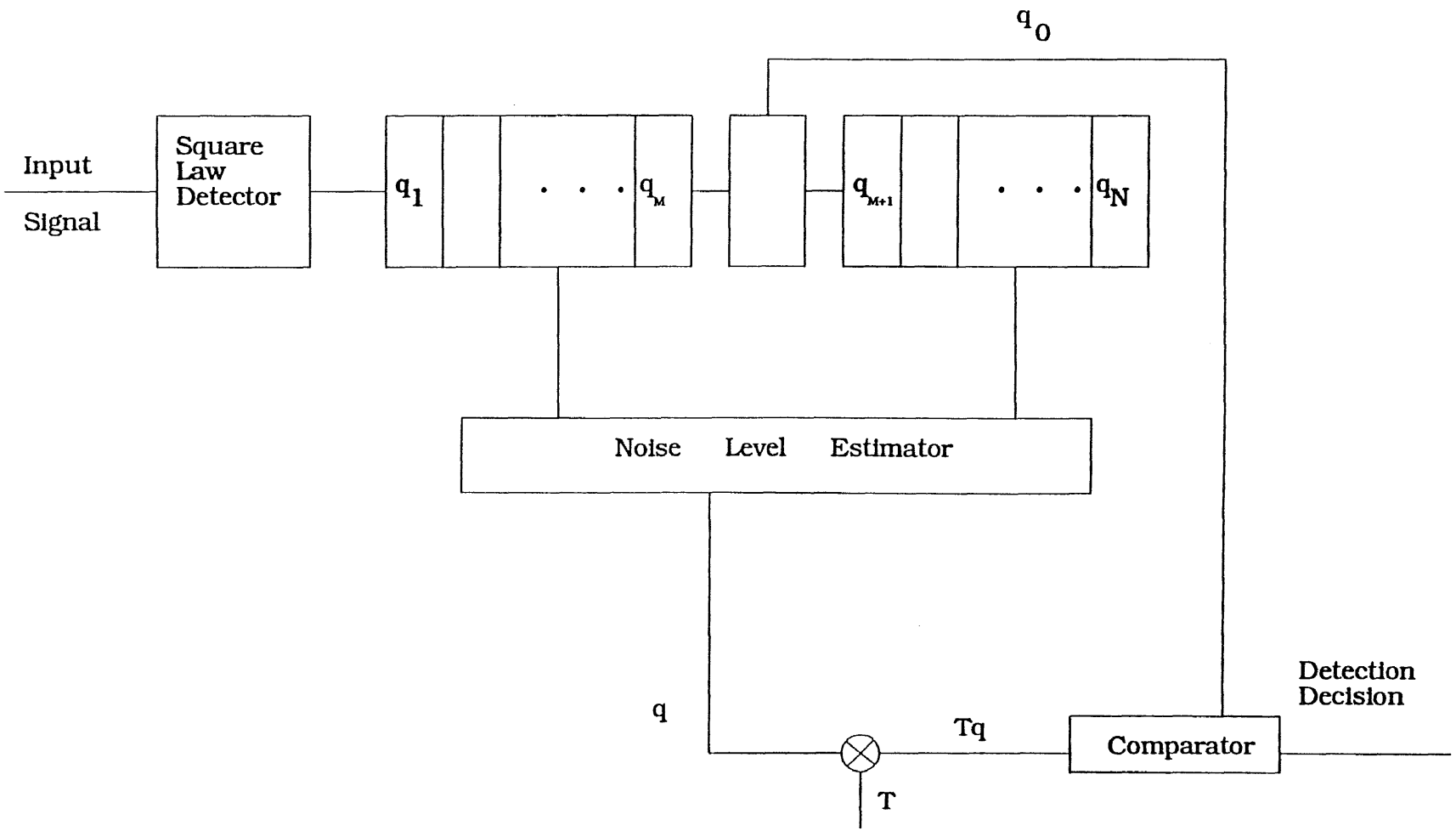

Figure 1.5 Cell Averaging CFAR Detector

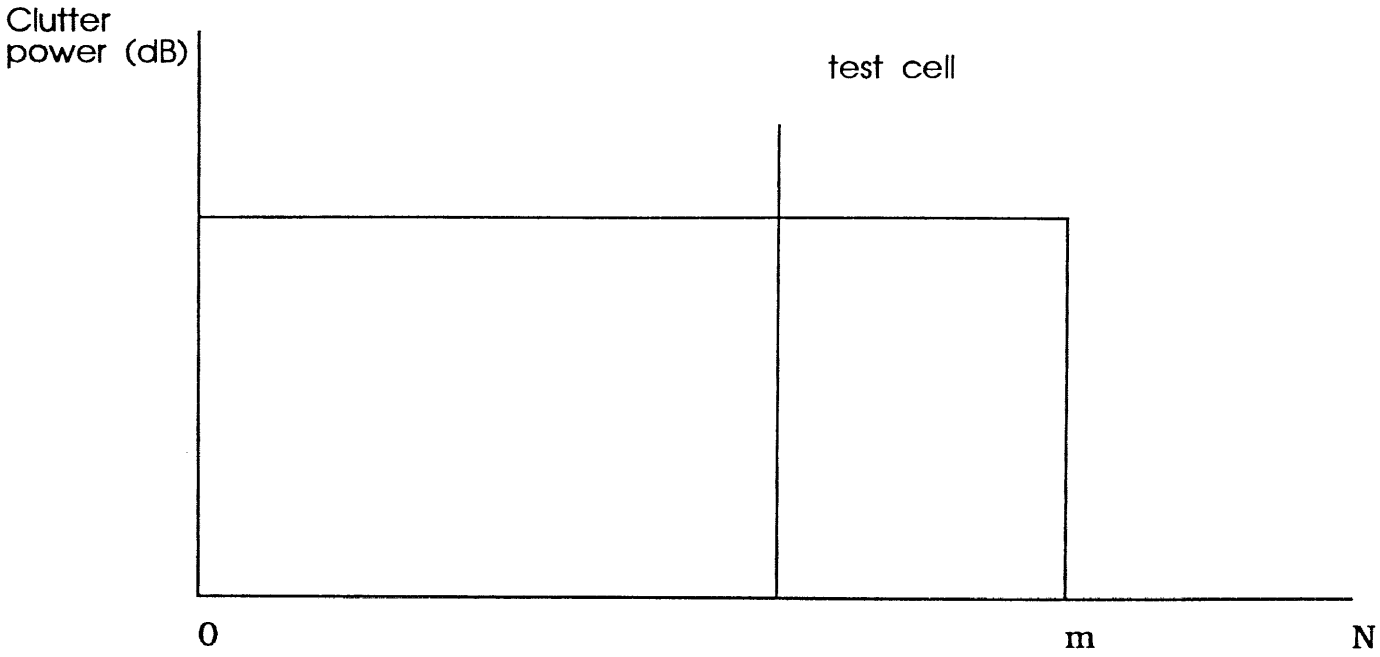

Figure 1.6 Model of a clutter power transition when the test cell and m reference samples are in the clear.

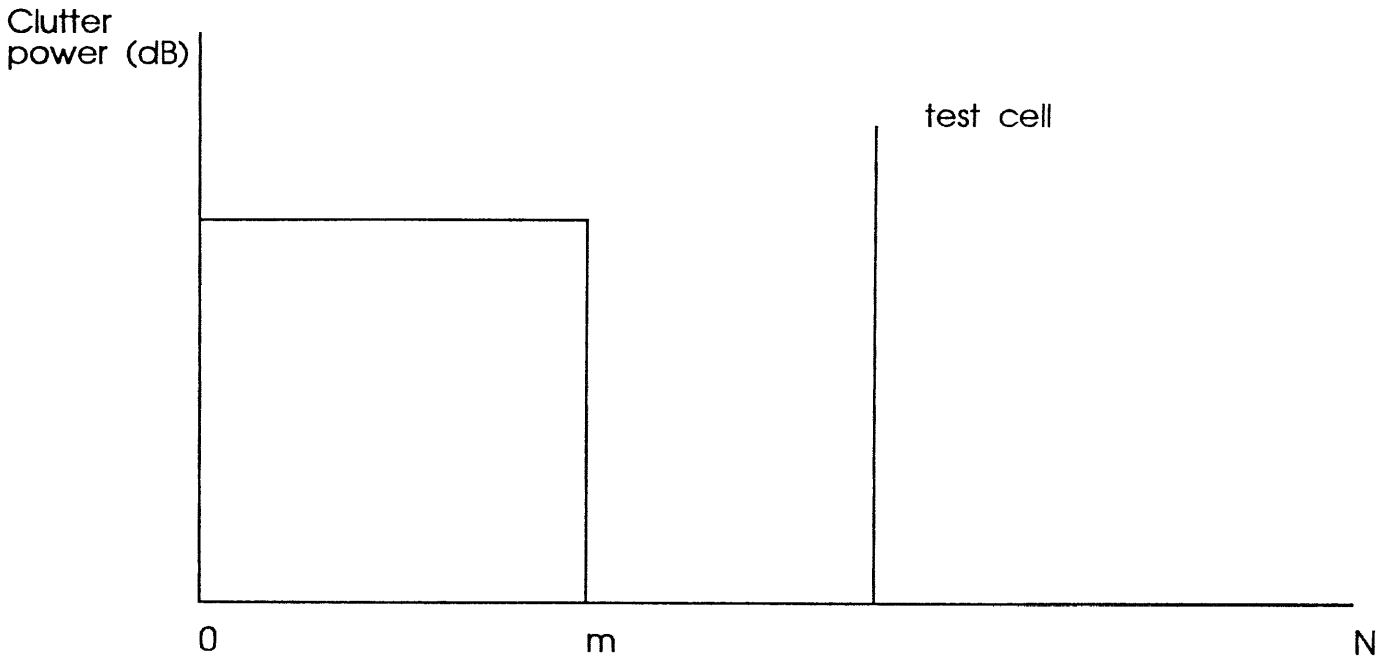

Figure 1.7 Model of a clutter power transition when the test cell is in the clear and m reference cells are in the clutter.

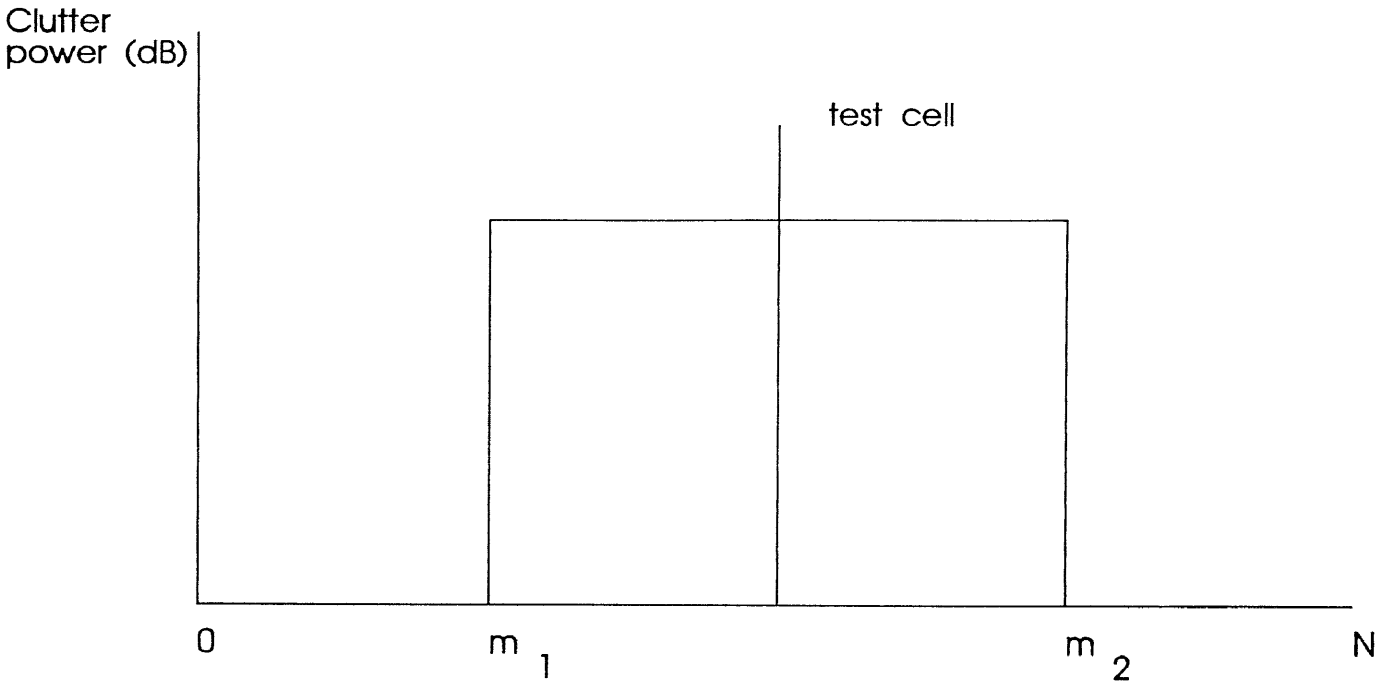

Figure 1.8 Model of two clutter power transitions present, one in the leading and the other in the lagging reference window. Test cell is in the clutter.

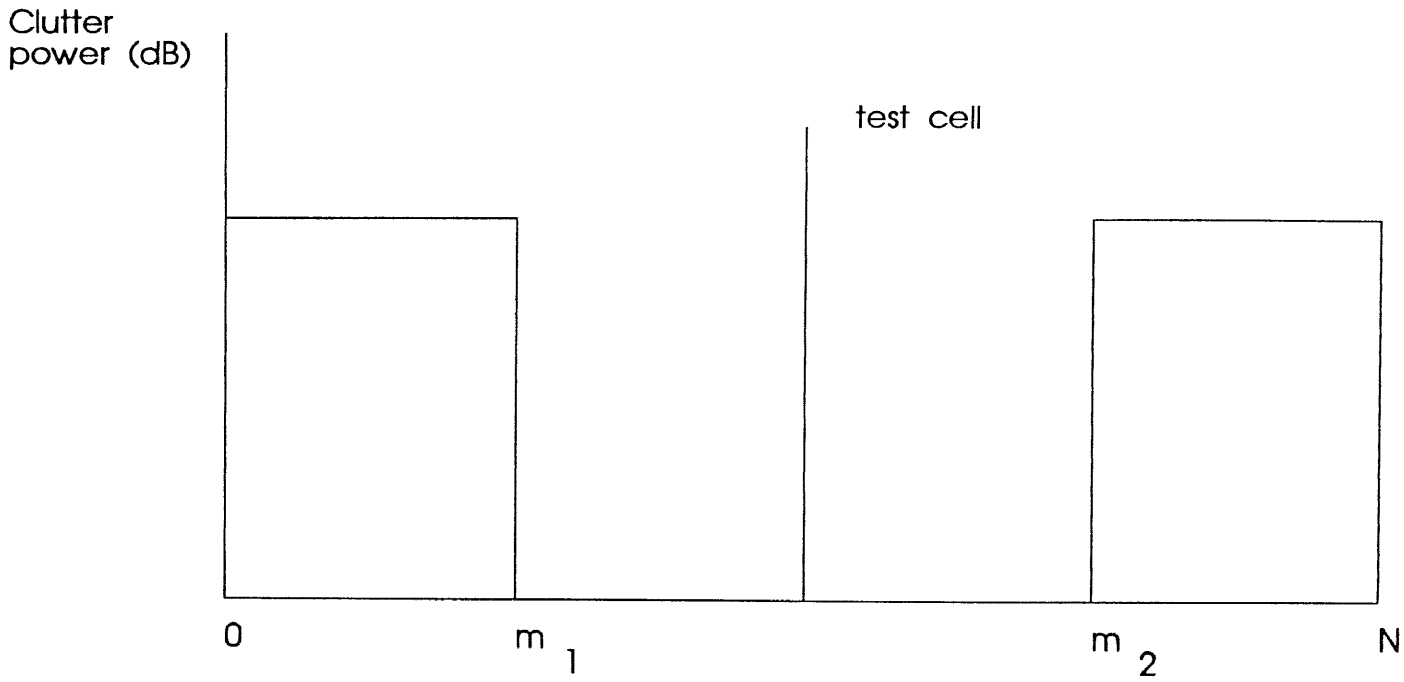

Figure 1.9 Model of two clutter power transitions present. The test cell is in the clear and some of the reference cells are in the clutter.

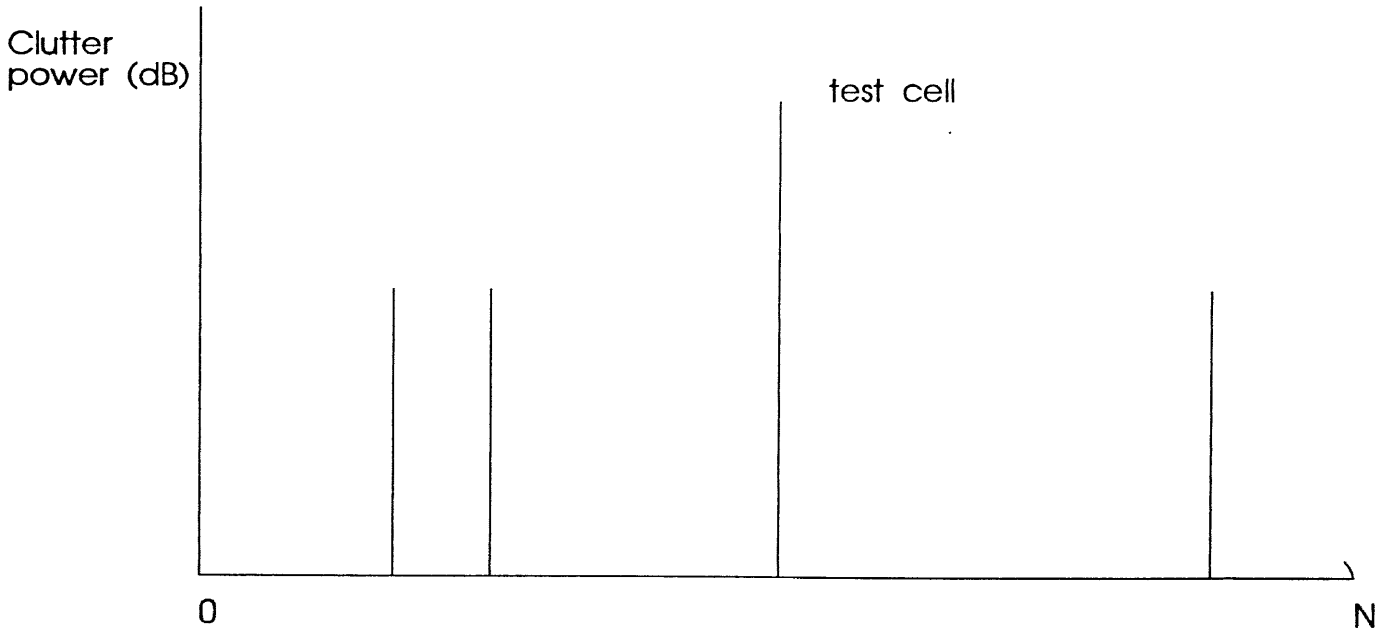

Figure 1.10 Sample model of homogeneous background environment with a number of spikes present in the reference window.

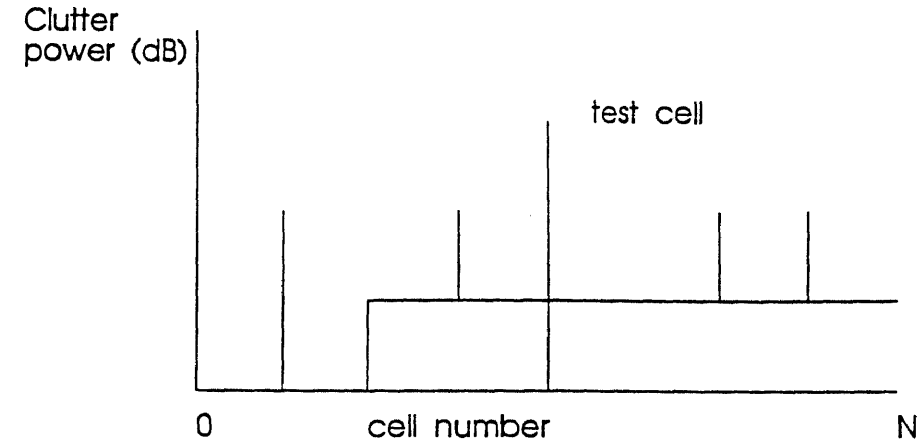

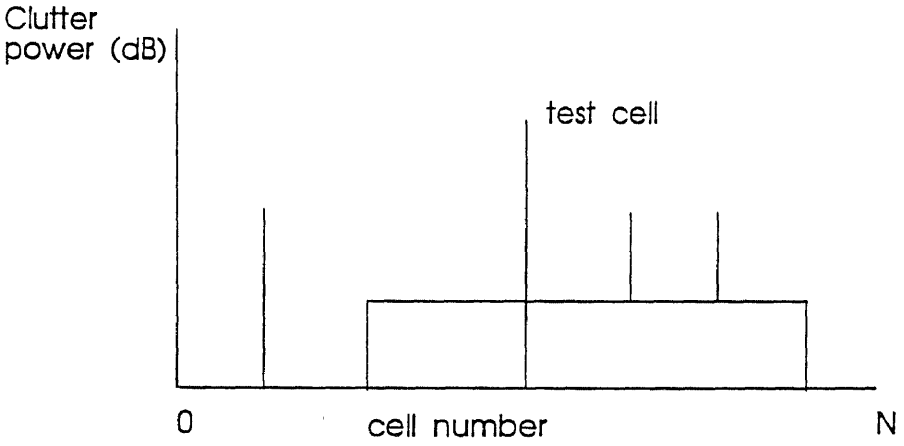

Figure 1.11 Sample clutter power distributions when one and two transitions are present and spikes appear in the reference window.

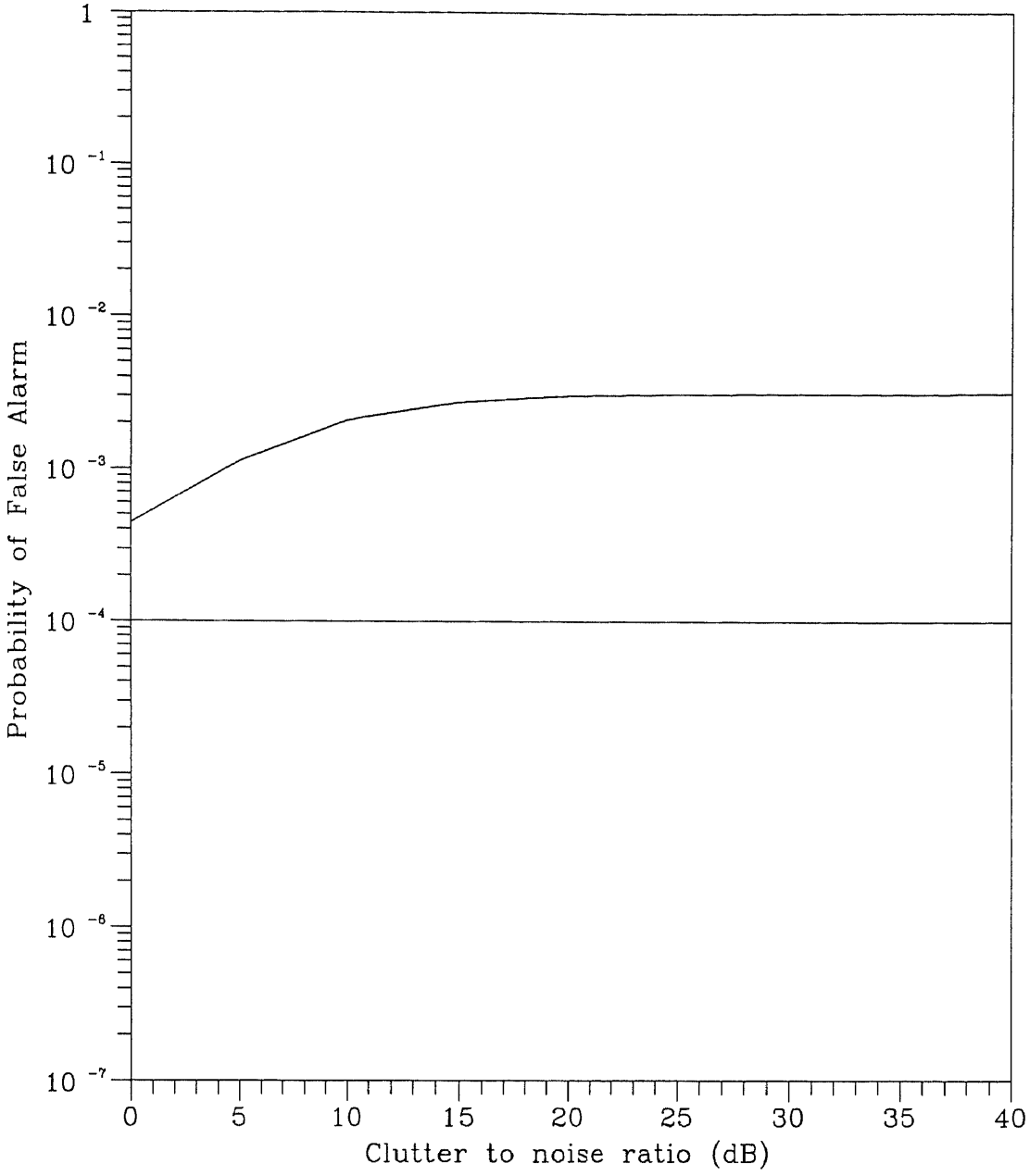

Figure 1.12. Probability of false alarm of the CA-CFAR in the presence of a clutter power transition.
N=16, $\alpha=10^{-4}$.

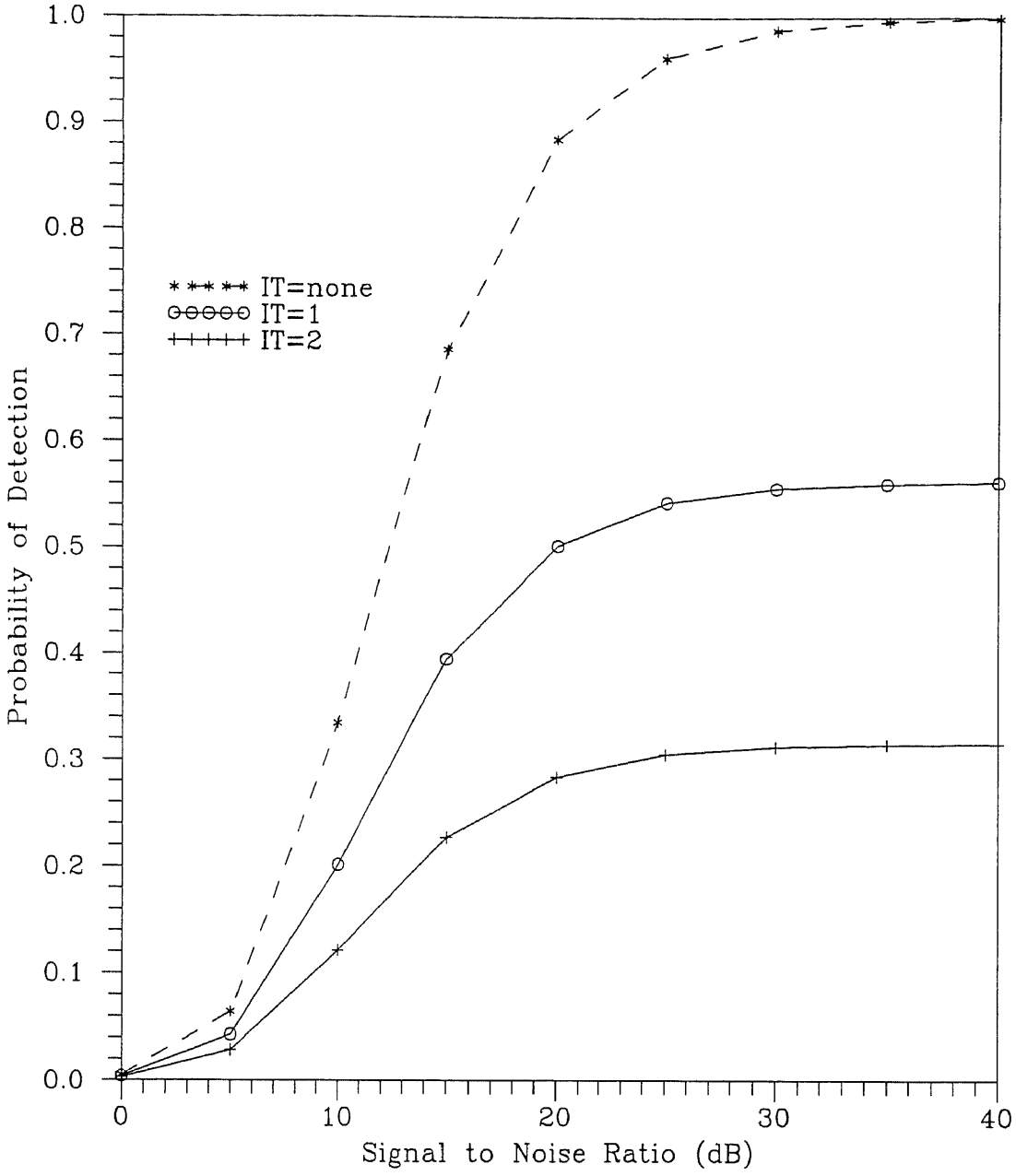

Figure 1.13. Probability of detection of the CA-CFAR detector in the presence of interfering targets. N=16, $\alpha=10^{-4}$.

Chapter 2

THE GO AND SO-CFAR DETECTORS IN TIME DIVERSITY COMBINING

2.1 Introduction

As we saw in the previous chapter, the presence of discontinuities in the background environment, such as that produced at chaff or clutter edges, of the conventional cell averaging, CA-CFAR detector, may cause the probability of false alarm to increase intolerably when the cell under test is immersed in clutter. On the other hand when the test cell is in the clear and a group of reference cells are in the clutter, a masking effect results. Thus, depending on the location of the clutter edge we want to choose the group of samples that are identically distributed with the noise in the test cell to form the estimate of the noise level in the cell under test. If the test cell is in the clutter and a clutter power transition is present in the reference window, the maximum of the sums of the outputs of the leading and lagging range cells is chosen to represent the estimate of the noise level in the test cell. This yields the greatest-of-selection logic in cell averaging CFAR detector which is referred to as the GO-CFAR detector. In the case where the test cell is in the clear the minimum of the sums of the outputs of the leading and lagging range cells is chosen. This yields the smallest-of-selection logic in cell averaging CFAR detector which is referred to as SO-CFAR detector. Also, the presence of interfering target returns in the reference window of the primary target,

causes degradation of the probability of detection. Thus, assuming that a number of interfering targets are present either in the leading or lagging range cells, the noise level estimate in the cell under test is chosen to be the minimum of the sums of the outputs of the leading and lagging range cells (smallest-of-selection).

In communication systems, some parameters of the received signal such as the amplitude or phase may flactuate with time and this phenomenon is referred to as fading [6]. Similarly, in radar the received signal might fade due to target fluctuations, so time diversity transmission, in which multiple pulses are transmitted, is employed. In this chapter, not only we analyze the GO and SO-CFAR detectors for single pulse transmission but in addition, we extend the analysis of [11,12,14] for a more realistic approach where multiple pulses are transmitted.

In section 2.2, the GO and SO-CFAR detectors are described and analyzed for single pulse transmission. In section 2.3 the analysis for the GO and SO-CFAR detectors is extended for multiple pulse transmission. In section 2.4 we show the simulation results in comparing the three detectors (CA,GO,SO-CFAR) for different background environments. In section 2.5 we present a summary along with our conclusions.

2.2 The GO and SO-CFAR Detectors for a Single Pulse Transmission System

In this section, we study the performance of the GO and SO-CFAR detectors when one pulse per antenna scan is transmitted. As shown in Figure 2.1, the input to the selection logic is the sum of the outputs of the leading window, U and the sum of the outputs of the lagging window V. The output of the selection logic depends on the particular CFAR processor. To control the increase of the probability of false alarm due to the presence of a clutter power transition in either the leading or the lagging reference window, while the test cell is in the clutter, the GO-CFAR detector was proposed in [11,12]. In the GO-CFAR detector the estimate of the noise level in the

cell under test is set to be the maximum of the sums of the output of the leading and lagging range cells.

Thus, in the case of the GO-CFAR detector, the output of the selection logic is the maximum of U and V, and

$$Q = \max(U, V) \tag{2.1}$$

where

$$U = \sum_{j=1}^{M} q_j \tag{2.2}$$

and

$$V = \sum_{j=M+1}^{N} q_j \tag{2.3}$$

The random variables U and V are governed by the Gamma distribution with parameters M and 1, $G(M,1)$, where $G(M,1)$ is the pdf of a Gamma distribution with parameter M and 1. Thus,

$$p_U(q) = p_V(q) = \frac{1}{\Gamma(M)} q^{M-1} \exp^{-q}, \qquad q \geq 0 \tag{2.4}$$

The cumulative distribution function, (cdf), of U and V is therefore given by

$$P_U(q) = P_V(q) = \int_0^q \frac{1}{\Gamma(M)} q^{M-1} \exp(-q) dq \tag{2.5}$$

Also, the cumulative distribution function, cdf, of Q which is given in equation (2.1) is, [31]

$$P_Q(q) = P_U(q) P_V(q) \tag{2.6}$$

The probability density function, pdf, of Q is equal to the derivative of the cdf of Q, that is,

$$\begin{aligned} p_Q(q) &= \frac{d}{dq} P_Q(q) = 2 p_U(q) P_U(q) \\ &= 2 \frac{1}{\Gamma(M)} q^{M-1} \exp(-q) \int_0^q \frac{q^{M-1}}{\Gamma(M)} \exp(-q) dq \end{aligned} \tag{2.7}$$

The integral in the above expression is the incomplete Gamma function which can be expressed as finite series expansion

$$\gamma(M,q) = \Gamma(M)\left[1 - \exp(-q)\sum_{k=0}^{M-1}\frac{q^k}{k!}\right] \tag{2.8}$$

Substituting equation (2.8) into equation (2.7), the pdf of the test statistic Q is obtained to be

$$p_Q(q) = \frac{2q^{M-1}\exp(-q)}{\Gamma(M)}\left[1 - \exp(-q)\sum_{k=0}^{\frac{N}{2}-1}\frac{q^k}{k!}\right] \tag{2.9}$$

The expresssion for the probability of detection of the GO-CFAR detector is obtained by substituting equation (2.9) into equation (1.14), that is,

$$P_D = 2\left(1+\frac{T_{GO}}{1+S}\right)^{-M} - 2\sum_{k=0}^{M-1}\binom{M+k-1}{k}\left(2+\frac{T_{GO}}{1+S}\right)^{-(M+k)} \tag{2.10}$$

For $S = 0$ the above expression yields the design probability of false alarm, P_F

$$P_F = 2(1+T_{GO})^{-M} - 2\sum_{k=0}^{M-1}\binom{M+k-1}{k}(2+T_{GO})^{-(M+k)} \tag{2.11}$$

Equation (2.11) is the design expression for the probability of false alarm and is used to calculate the scaling constant T_{GO}, by solving $P_F = \alpha$.

The GO-CFAR detector performs well when a clutter power transition is present in either the leading or the lagging reference window while the test cell is in the clutter. However, in the presence of interfering targets or when a clutter power transition is present while the test cell is in the clear, the detection performance of the GO-CFAR detector degrades significantly. To alleviate this problem the smallest-of-selection logic, SO-CFAR was proposed in [14]. In the SO-CFAR detector the estimate of the noise level in the cell under test is set to be the minimum of the sum of the outputs of the leading and lagging range cells. Thus, in the case of the SO-CFAR detector the test statistic, Q, is given by

$$Q = \min(U, V) \tag{2.12}$$

where U and V are given in equations (2.2) and (2.3) respectively. Thus, the pdf of the test statistic Q [31] is given by

$$\begin{aligned} p_Q(q) &= p_U(q)[1 - P_V(q)] + p_V(q)[1 - P_U(q)] \\ &= p_U(q) + p_V(q) - [p_U(q)P_V(q) + p_V(q)P_U(q)] \\ &= p_U(q) + p_V(q) - p_Q^{GO}(q) \end{aligned} \tag{2.13}$$

Substituting the expression given in equation (2.4) into equation (2.13), where $p_Q^{GO}(q)$ is the pdf of the test statistic for the GO-CFAR detector and is given in equation (2.9), the pdf of the test statistic for the SO-CFAR detector is obtained to be

$$p_Q(q) = \frac{2q^{M-1}\exp(-2q)}{\Gamma(M)} \sum_{k=0}^{M-1} \frac{q^k}{k!} \tag{2.14}$$

Substituting the above expression into equation (1.14) the probability of detection of the SO-CFAR detector is given by

$$P_D = 2\left(2 + \frac{T_{SO}}{1+S}\right)^{-M} \sum_{k=0}^{M-1} \binom{M+k-1}{k} \left(2 + \frac{T_{SO}}{1+S}\right)^{-k} \tag{2.15}$$

Setting $S = 0$ in equation (2.15) we obtain that the design expression for the probability of false alarm, P_F, for the SO-CFAR detector is,

$$P_F = 2(2 + T_{SO})^{-M} \sum_{k=0}^{M-1} \binom{M+k-1}{k} (2 + T_{SO})^{-k} \tag{2.16}$$

As in the case of the the GO-CFAR detector, equation (2.16) is used to calculate the scaling constant T_{SO}, so that $P_F = \alpha$. The scaling constants for the SO and GO-CFAR detectors are shown in appendix A for different sizes of reference window ($N = 16, 24, 32$) and three design values of probability of false alarm ($10^{-4}, 10^{-6}, 10^{-8}$). Next, we consider the CA,GO and SO-CFAR in a time diversity system.

2.3 The GO and SO-CFAR Detectors in Time Diversity Transmission

Assuming that L pulses are processed, the received signal $r(t)$ is square law detected and sampled in range by the $N+1$ resolution cells resulting in a matrix of $L \times (N+1)$

observations that are denoted by q_{ij}, $i = 1,\ldots,L$ and $j = 1,2,\ldots,N$ as shown in Figure 2.2 Notice that we use j to index the cell number, whereas, i denotes the observations corresponding to the ith pulse from the jth cell. As before, the $q_{ij}, i = 1,\ldots,L$ and $j = 0,\ldots,N(M = N/2)$ are exponentially distributed random variables. In this case, we do not process a single observation, that is, we first form the sum of the L observations from each range cell,

$$q_j = \sum_{i=1}^{L} q_{ij} \quad j = 0,\ldots,N \tag{2.17}$$

q_j given in equation (2.17) are then processed as before by various detectors. The difference is that in carrying out the analysis, the composite data are not observations from exponentially distributed random variables, but they may viewed as observations from chi-squared random variables with $2L$ degrees of freedom [32], since each composite observation is the sum of L exponentially distributed observations. Similarly, the test sample q_0 is the sum of the L exponential observations from the test cell, i.e.

$$q_0 = \sum_{i=1}^{L} q_{i0} \tag{2.18}$$

The conditional pdf of the test statistic Q_0 is now given by

$$p_{Q_0}(q_0) = \begin{cases} \frac{q_0^{L-1}}{\Gamma(L)} \exp(-q_0) & H_0 \\ \frac{q_0^{L-1} \exp[-q_0/(1+S)]}{\Gamma(L)(1+S)^L} & H_1 \end{cases} \tag{2.19}$$

The pdf of the noise level estimate of Q depends on the particular detector.

In the case of the cell averaging CFAR detector, CA-CFAR, Q is the sum of all composite reference observations $Q_1,\ldots,Q_N$. If $Q_j, j = 1,\ldots,N$ are identically distributed with the noise in the test cell, their probability density function, pdf, is given by

$$p_{Q_j}(q_j) = \frac{q_j^{L-1}}{\Gamma(L)} \exp(-q_j) \tag{2.20}$$

Therefore, the pdf of Q is given by

$$p_Q(q) = \frac{q^{NL-1}}{\Gamma(NL)} \exp(-q) \tag{2.21}$$

The expression for the probability of detection is

$$P_D = \int_0^\infty dq p_Q(q) \int_{T_q}^\infty p_{Q_0|H_1}(q_0|H_1) dq_0 \tag{2.22}$$

Substituting equation (2.21) into (2.22) we have

$$P_D = \sum_{r=0}^{L-1} \frac{T^{L-1-r}(L-1-r)!^{-1}}{(NL-1)!(1+S)^{L-r-1}} \int_0^\infty q^{NL+L-2-r} \exp[-q(1+\frac{T}{1+S})] dq \tag{2.23}$$

Performing the above integration the probability of detection is obtained to be

$$P_D = \sum_{r=0}^{L-1} \begin{pmatrix} NL+L-2-r \\ L-1-r \end{pmatrix} \frac{T^{L-1-r}}{(1+S)^{L-r-1}} (1+\frac{T}{1+S})^{-(NL+L-1-r)} \tag{2.24}$$

Setting $S = 0$ in equation (2.24) the probability of false alarm for the CA-CFAR detector is

$$P_F = \sum_{r=0}^{L-1} \begin{pmatrix} NL+L-2-r \\ L-1-r \end{pmatrix} T^{L-1-r}(1+T)^{-(NL+L-1-r)} \tag{2.25}$$

Considering now the GO-CFAR detector, the estimate of the noise level in the cell under test is given by equation (2.1) where U and V are the sum of the composite observations of the leading and lagging range cells respectively, that is,

$$U = \sum_{j=1}^{M} q_j \tag{2.26}$$

and

$$V = \sum_{j=M+1}^{N} q_j \tag{2.27}$$

Thus,

$$q = \max \left\{ \left(\sum_{j=1}^{M} q_j \right), \left(\sum_{j=M+1}^{N} q_j \right) \right\} \tag{2.28}$$

In the case of the SO-CFAR detector, the estimate of the noise level in the cell under test is given by equation (2.12). Thus, for the SO-CFAR detector

$$q = \min \left\{ \left(\sum_{j=1}^{M} q_j \right), \left(\sum_{j=M+1}^{N} q_j \right) \right\} \tag{2.29}$$

Substituting equation (2.19) into equation (2.22), yields

$$P_D = \int_0^\infty p_Q(q) \sum_{k=0}^{L-1} \frac{\exp(-\frac{T_{GO}}{1+S}q)(\frac{T_{GO}}{1+S}q)^{L-1-k}}{(L-1-k)!(1+S)^L} dq \tag{2.30}$$

The pdf of the test statistic given in (2.28) for the GO-CFAR detector is derived to be

$$p_Q(q) = \frac{2q^{ML-1}\exp(-q)}{\Gamma(ML)} - \frac{2}{\Gamma(ML)}\sum_{k=0}^{ML-1}\frac{\exp(-2q)q^{ML-1+k}}{k!} \tag{2.31}$$

Substituting (2.31) into (2.30), the expression for the probability of detection for the GO-CFAR detector is

$$\begin{aligned} P_D^{GO} &= \sum_{k=0}^{L-1}\frac{2\frac{T_{GO}}{1+s}^{L-1-k}}{(L-1-k)!\Gamma(ML)}\int_0^\infty q^{ML+L-k-2}\exp(-(1+\frac{T_{GO}}{1+s})q)dq \\ &\quad - \frac{2}{\Gamma(ML)}\frac{\frac{T_{GO}}{1+S}^{L-r-1}}{k!(L-1-r)!}\sum_{k=0}^{ML-1}\sum_{r=0}^{L-1}\int_0^\infty q^{ML+L+k-2-r}\exp(-(2+\frac{T_{GO}}{1+S})q)dq \end{aligned} \tag{2.32}$$

which yields

$$\begin{aligned} P_D^{GO} &= 2\sum_{k=0}^{L-1}\binom{ML+L-k-2}{ML-1}\cdot\frac{\frac{T_{GO}}{1+S}^{L-1-k}}{(1+\frac{T_{GO}}{1+S})^{ML+L-k-1}} \\ &\quad -2\sum_{k=0}^{ML-1}\sum_{r=0}^{L-1}\frac{(ML+k+L-2-r)!}{(ML-1)!k!(L-1-r)!}\frac{\frac{T_{GO}}{1+S}^{L-1-r}}{(2+\frac{T_{GO}}{1+S})^{ML+k+L-1-r}} \end{aligned} \tag{2.33}$$

For $S = 0$, the above expression yields the design expression for the probability of false alarm, P_F, for multiple pulse transmission for the GO-CFAR detector, that is,

$$\begin{aligned} P_F^{GO} &= 2\sum_{k=0}^{L-1}\binom{ML+L-k-2}{ML-1}\cdot\frac{T_{GO}^{L-1-k}}{(1+T_{GO})^{ML+L-k-1}} \\ &\quad -2\sum_{k=0}^{ML-1}\sum_{r=0}^{L-1}\frac{(ML+k+L-2-r)!}{(ML-1)!k!(L-1-r)!}\frac{T_{GO}^{L-1-r}}{(2+T_{GO})^{ML+k+L-1-r}} \end{aligned} \tag{2.34}$$

Equation (2.34) is used to compute the threshold multipliers T_{GO}, by solving $P_F = \alpha$.

Using equation (2.13), the pdf of the test statistic given in (2.29) for the SO-CFAR detector is derived to be

$$p_Q(q) = \frac{2}{\Gamma(ML)}\sum_{k=0}^{ML-1}\frac{\exp(-2q)q^{ML-1+k}}{k!} \tag{2.35}$$

Substituting equation (2.35) into equation (2.30) the design expression for the probability of detection for the SO-CFAR is obtained to be

$$P_D^{SO} = \sum_{k=0}^{L-1}\frac{2(\frac{T_{SO}}{1+S})^{L-1-k}(L+ML-2-k)!}{(L-1-k)!\Gamma(ML)(1+\frac{T_{SO}}{1+S})^{ML+L-k-1}} \tag{2.36}$$

$$-2\sum_{k=0}^{L-1}\begin{pmatrix} ML+L-k-2 \\ ML-1 \end{pmatrix}\cdot\frac{\frac{T_{SO}}{1+S}^{L-1-k}}{(1+\frac{T_{SO}}{1+S})^{ML+L-k-1}}$$
$$+2\sum_{k=0}^{ML-1}\sum_{r=0}^{L-1}\frac{(ML+k+L-2-r)!}{(ML-1)!k!(L-1-r)!}\frac{\frac{T_{SO}}{1+S}^{L-1-r}}{(2+\frac{T_{SO}}{1+S})^{ML+k+L-1-r}} \quad (2.37)$$

As in the case of the GO-CFAR letting $S = 0$, the above expression gives the design probability of false alarm for the SO-CFAR detector that is,

$$P_F^{SO} = \sum_{k=0}^{L-1}\frac{2(T_{SO})^{L-1-k}(L+ML-2-k)!}{(L-1-k)!\Gamma(ML)(1+T_{SO})^{ML+L-k-1}} \quad (2.38)$$
$$-2\sum_{k=0}^{L-1}\begin{pmatrix} ML+L-k-2 \\ ML-1 \end{pmatrix}\cdot\frac{T_SO^{L-1-k}}{(1+T_{SO})^{ML+L-k-1}}$$
$$+2\sum_{k=0}^{ML-1}\sum_{r=0}^{L-1}\frac{(ML+k+L-2-r)!}{(ML-1)!k!(L-1-r)!}\frac{T_{SO}^{L-1-r}}{(2+T_{SO})^{ML+k+L-1-r}} \quad (2.39)$$

The threshold multiplier T_{SO} for the SO-CFAR is computed from the above expression by solving $P_F = \alpha$. The scaling constants for $L = 4$, are also shown in appendix A.

2.4 Results

In this section we evaluate and compare the false alarm and detection performance of the CA, SO and GO-CFAR detectors for different background environments. In Figures 2.3 and 2.4 we study the detection performance of the CA, GO and SO-CFAR detectors in homogeneous background environment. We assume a reference window of $N = 16$ and design probability of false alarm, $\alpha = 10^{-4}$. In Figure 2.3, where single pulse transmission ($L = 1$) is assumed the detection performance of all three detectors is approximately the same. The additional detectability loss introduced by the GO-CFAR detector is very small and falls in the range of 0.1 to 0.3dB as shown in Figure 2.3. In the case of the SO-CFAR detector the additional detectability loss is shown to be approximately 1dB. In Figure 2.4, where multiple transmission is employed ($L = 4$), the detection performance of all three detectors is also shown to be approximately the same. However, the detection performance as compared to the case

with $L = 1$ (Figure 2.3) is significantly improved due to the enhanced performance offered by the time diversity transmission. For signal to noise ratio 15dB and above the probability of detection for all three detectors is equal to one. In Figures 2.5 and 2.6 the detection performance of the CA,GO and SO-CFAR detectors in the presence of one and two interfering targets is studied. We assume $N = 16$ and a design probability of false alarm $\alpha = 10^{-4}$. In Figure 2.5, the SO-CFAR detector is shown to be superior to both the CA and GO-CFAR detectors for $L = 1, 4$. Both the CA and GO-CFAR detectors suffer from the capture effect since the interfering target in the reference window of the primary target raises the adaptive threshold. In Figure 2.6 where two interfering targets are present, one in the leading and the other in the lagging reference window the detection performance of all three detectors is seriously degraded due to the capture effect. The SO-CFAR detector also suffers from the capture effect in this case since both the leading and lagging reference window contain interfering targets. Note that in both Figures 2.5 and 2.6 when $L = 4$ the detection performance improves due to the diversity transmission.

In Figures 2.7 and 2.8 we study the false alarm regulation of the CA, SO and GO-CFAR detectors ($L = 1, 4$) in the presence of a clutter power discontinuity ($C = 30$dB) in the reference window. We assume that the test cell is immersed in clutter and that $N = 16$. In both Figures when the number of cells immersed in clutter is sixteen i.e. homogeneous environment, all detectors achieve the design probability of false alarm $\alpha = 10^{-4}$. However, when the clutter edge is in the test cell the false alarm probability of the SO-CFAR detector approaches unity and that of the CA and GO-CFAR detectors is approximately one and two orders of magnitude higher than the desired value ($\alpha = 10^{-4}$). The false alarm regulation of the GO-CFAR detector is shown to be superior to that of both the CA and SO-CFAR detectors.

2.5 Summary and Conclusions

In this chapter, we described and analyzed the CA,GO and SO-CFAR detectors for single pulse transmission. Then we have extended the analysis of the GO and SO-CFAR detectors in [11,12,14] for time diversity transmission. In the presence of a clutter power transition in the leading or the lagging reference window we showed that the GO-CFAR detector performs better than the CA-CFAR detector. The SO-CFAR detector was shown to be robust in the presence of interfering targets in either the leading or lagging reference window of the cell under test. Finnally, we compared the SO and the GO-CFAR detectors when time diversity transmission is employed. The detection probability of both detectors was significantly improved due to the enhanced performance offered by the time diversity transmission.

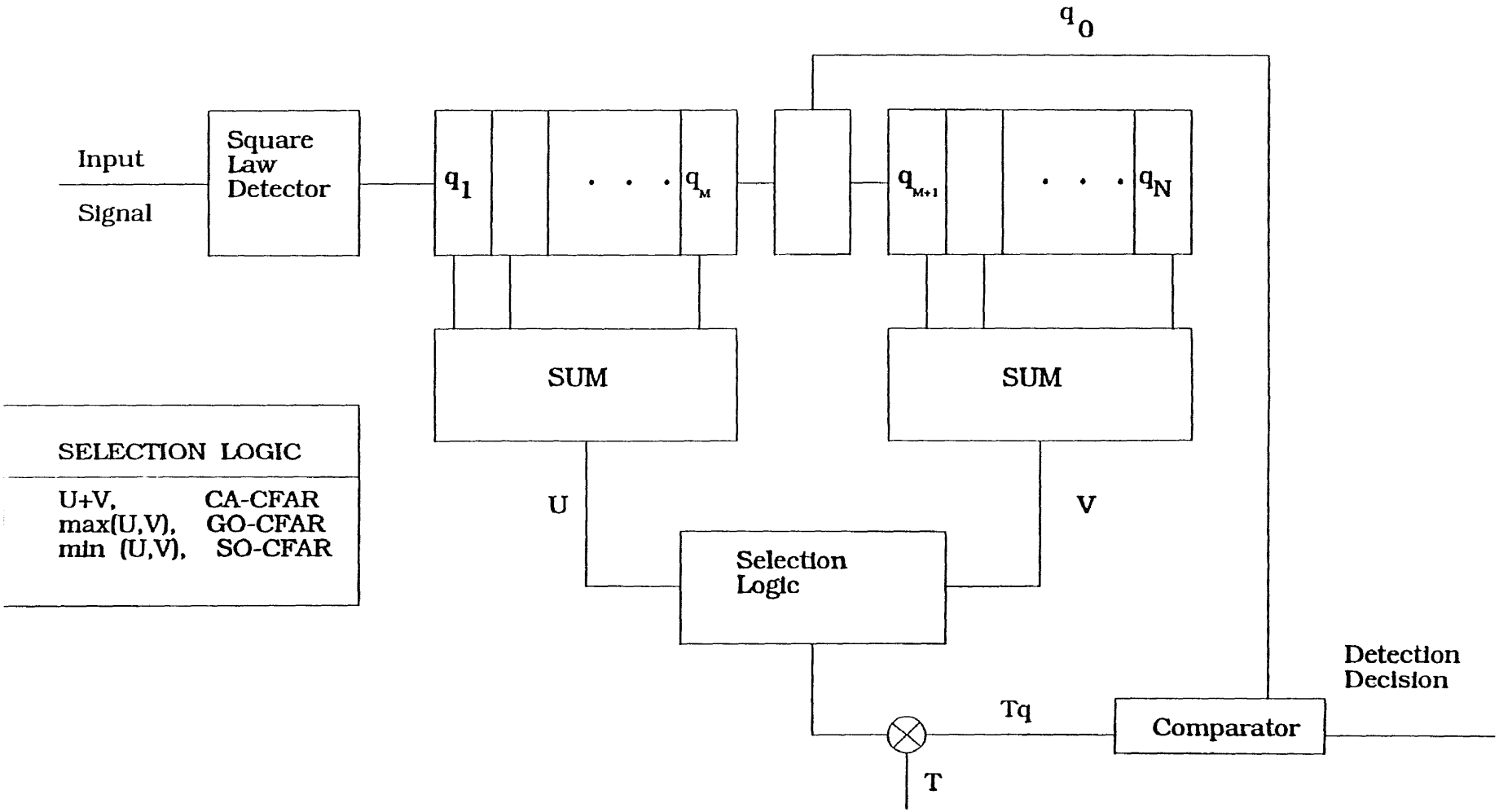

Figure 2.1 CFAR Detector

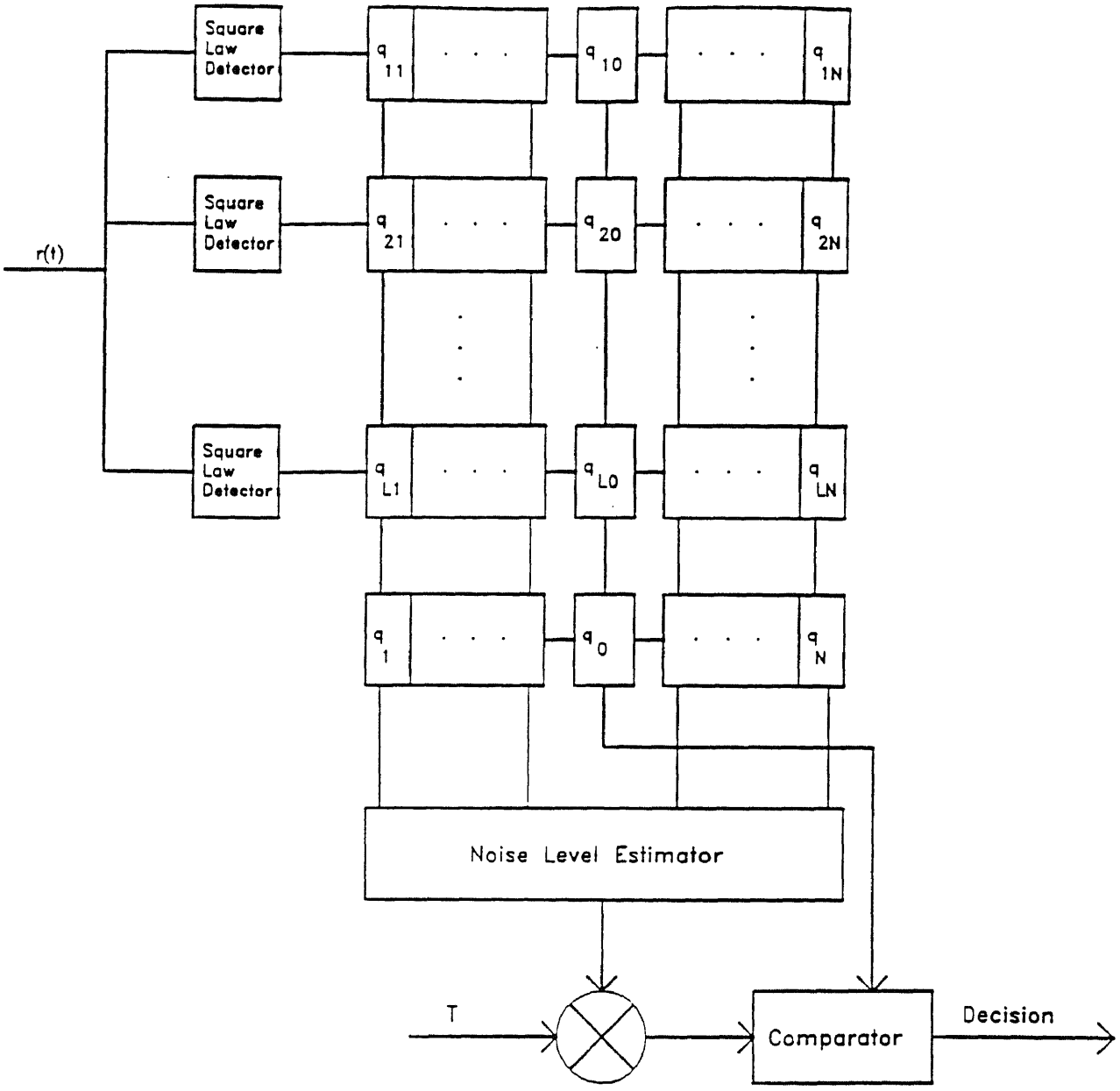

Figure 2.2 CFAR Detector.

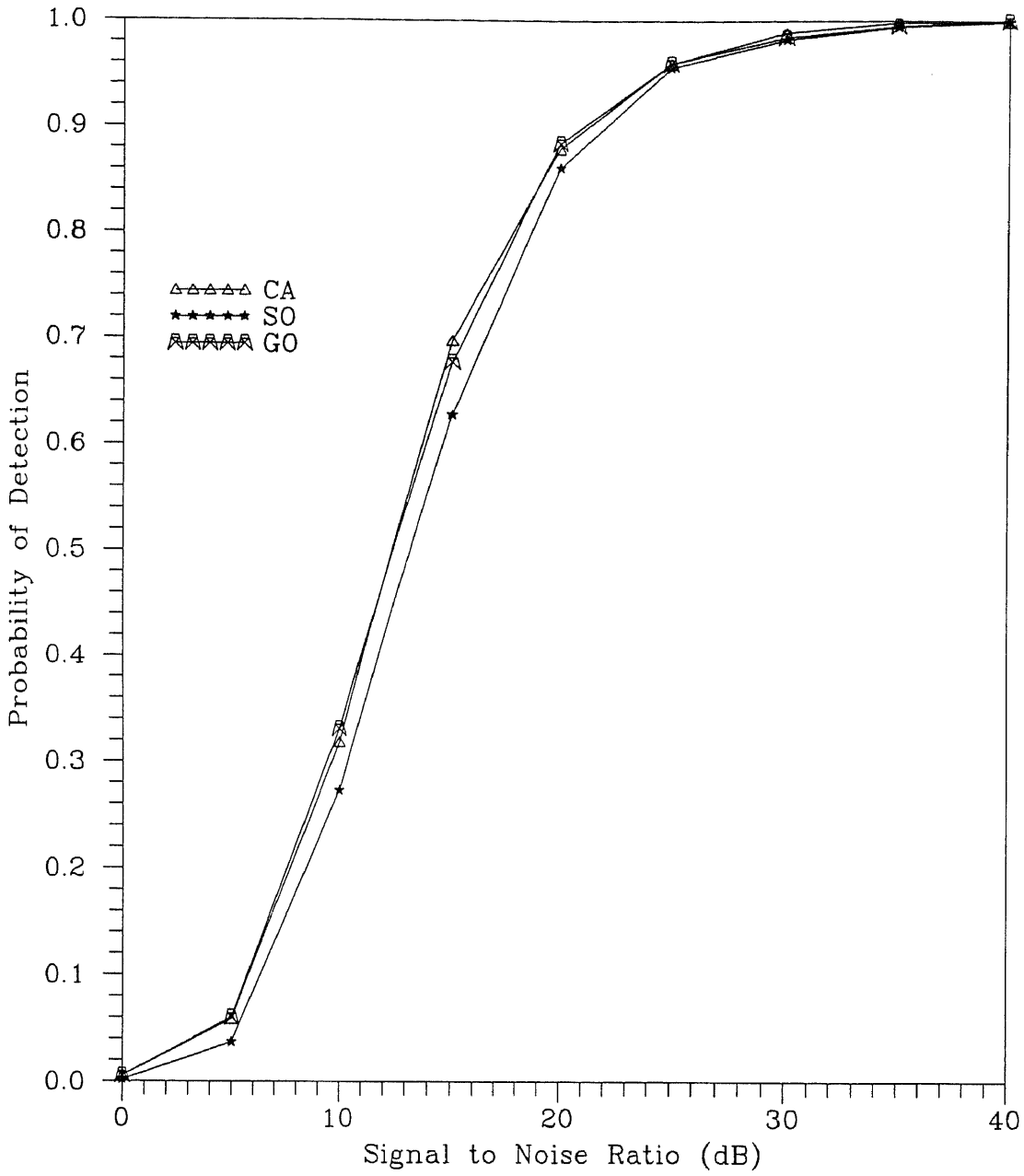

Figure 2.3. Probability of detection CA,GO,SO−CFAR detectors in homogeneous background environment. N=16, L=1, $\alpha=10^{-4}$.

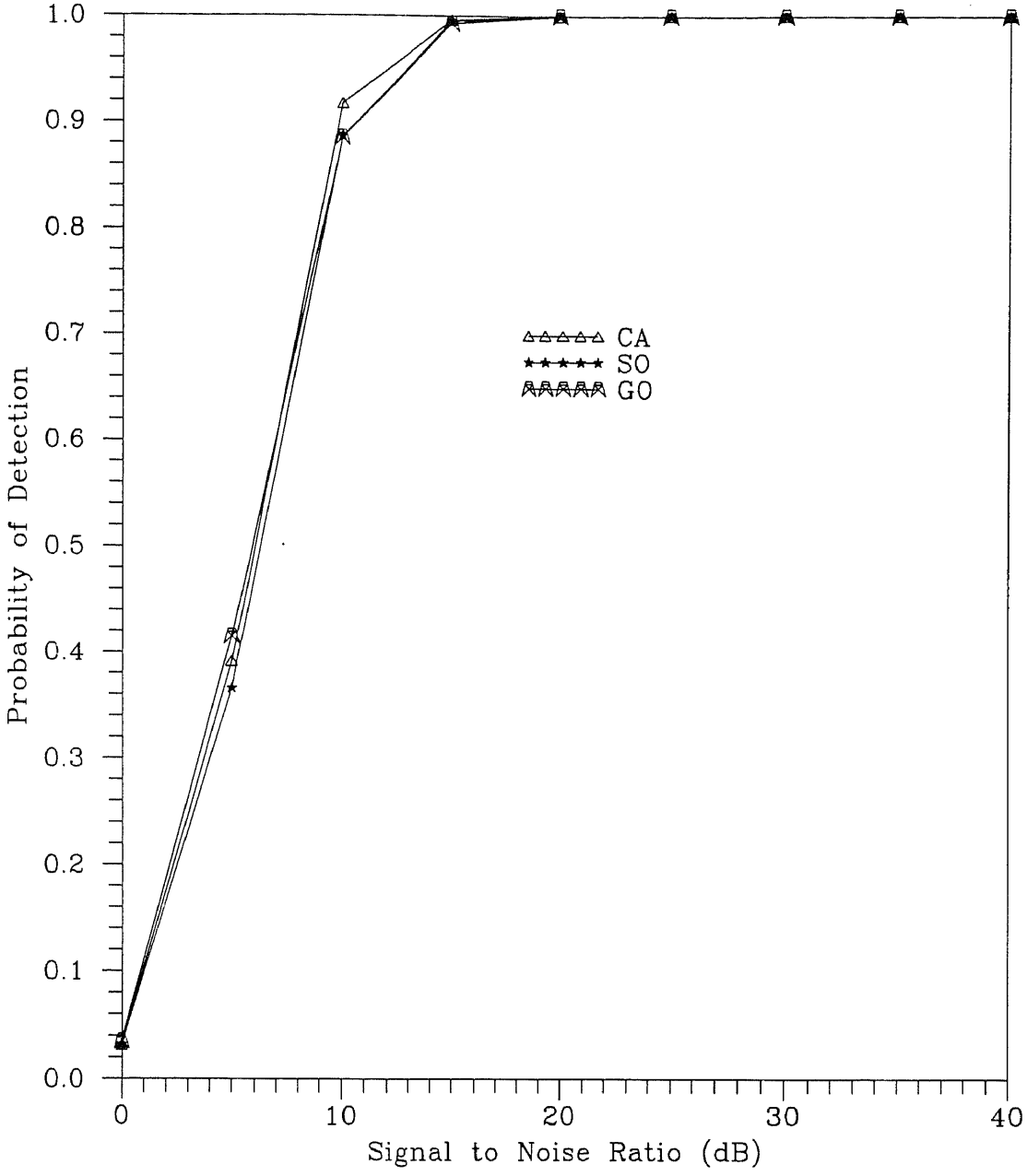

Figure 2.4. Probability of detection CA,GO,SO-CFAR detectors in homogeneous background environment. N=16, L=4, $\alpha=10^{-4}$.

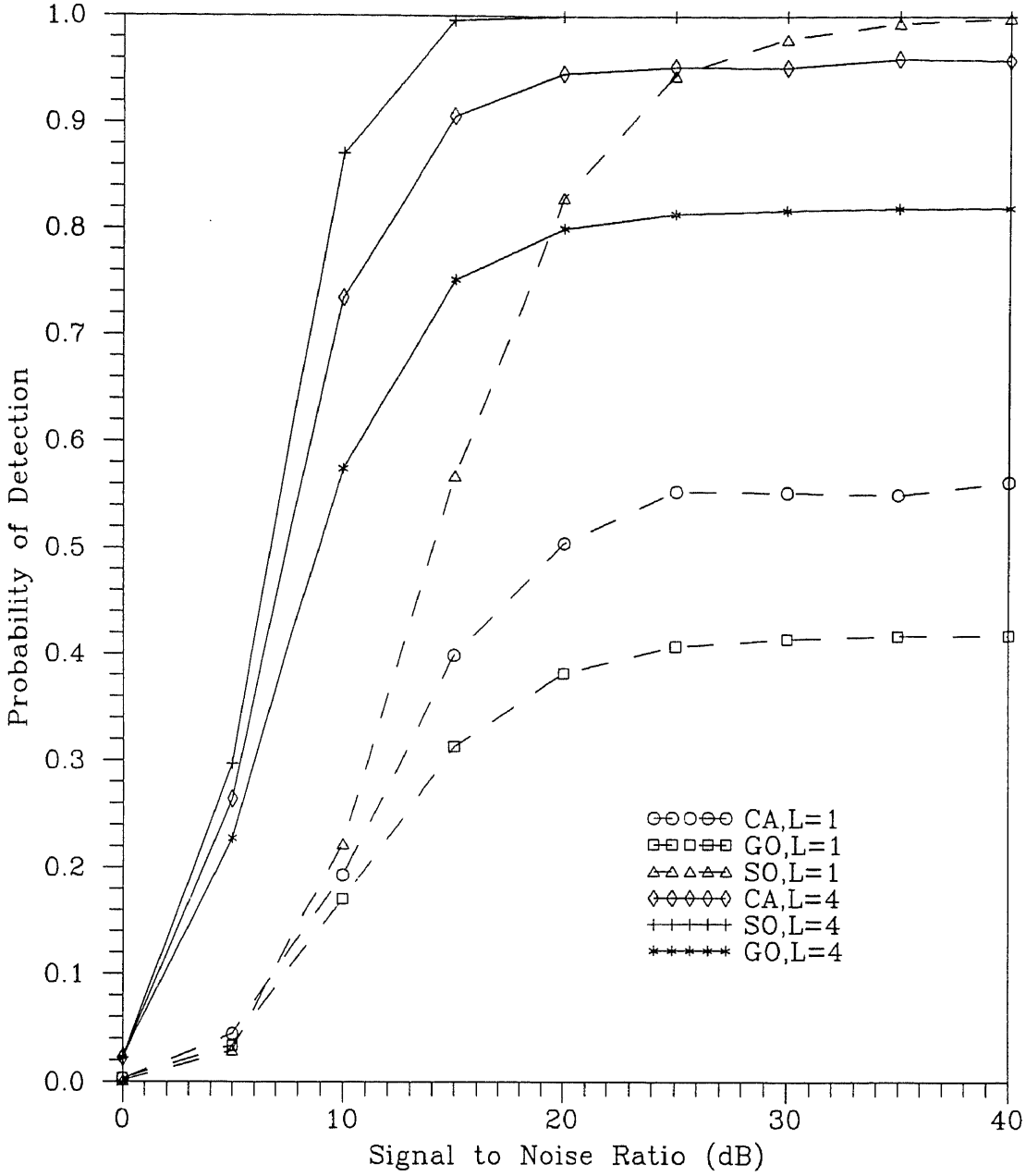

Figure 2.5. Probability of detection CA,GO and SO-CFAR detectors in the presence of one interfering target. N=16, $\alpha=10^{-4}$.

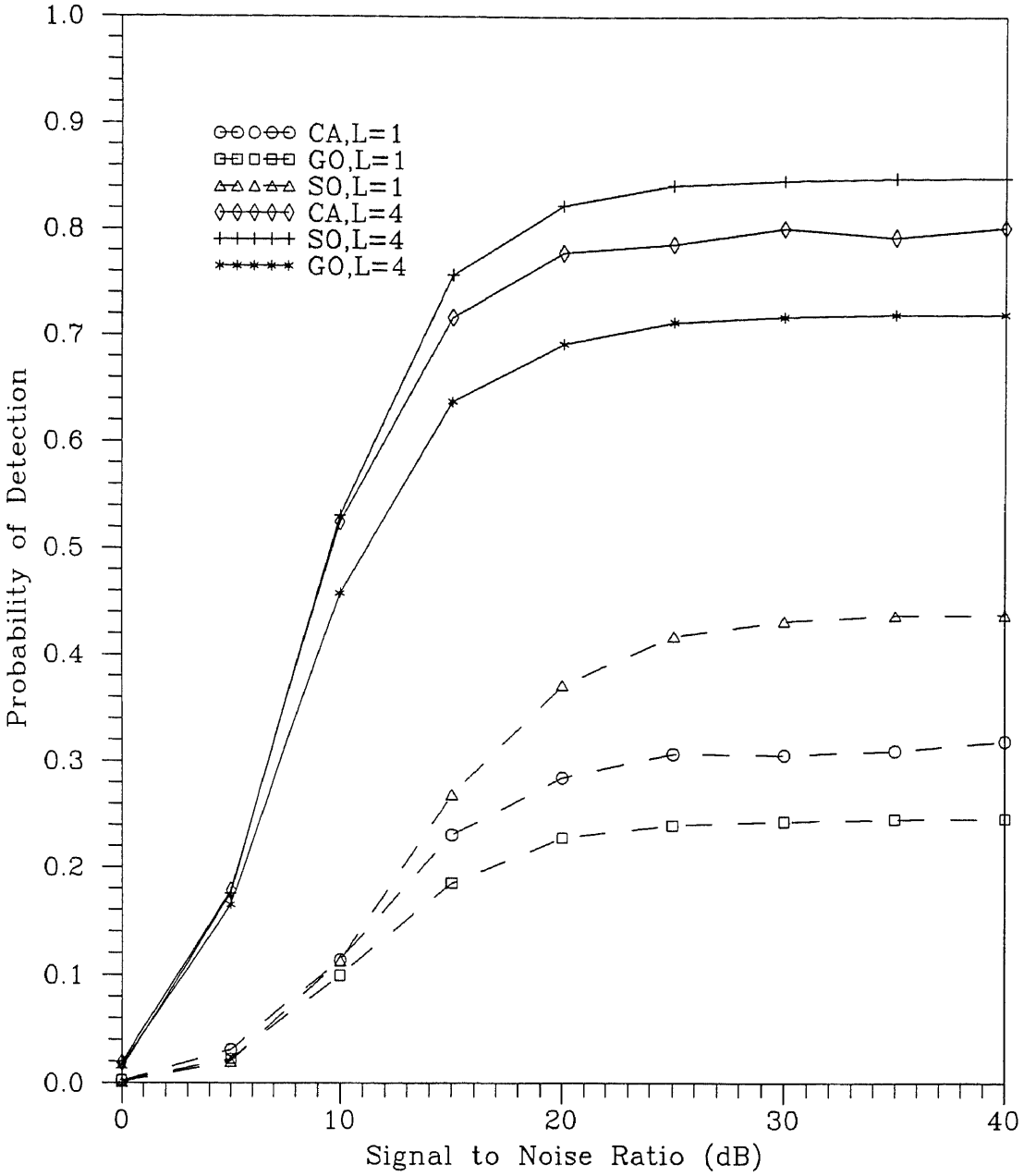

Figure 2.6. Probability of detection CA,GO and SO-CFAR detectors in the presence of two interfering targets one in the leading and the other in the lagging reference window. N=16, $\alpha=10^{-4}$.

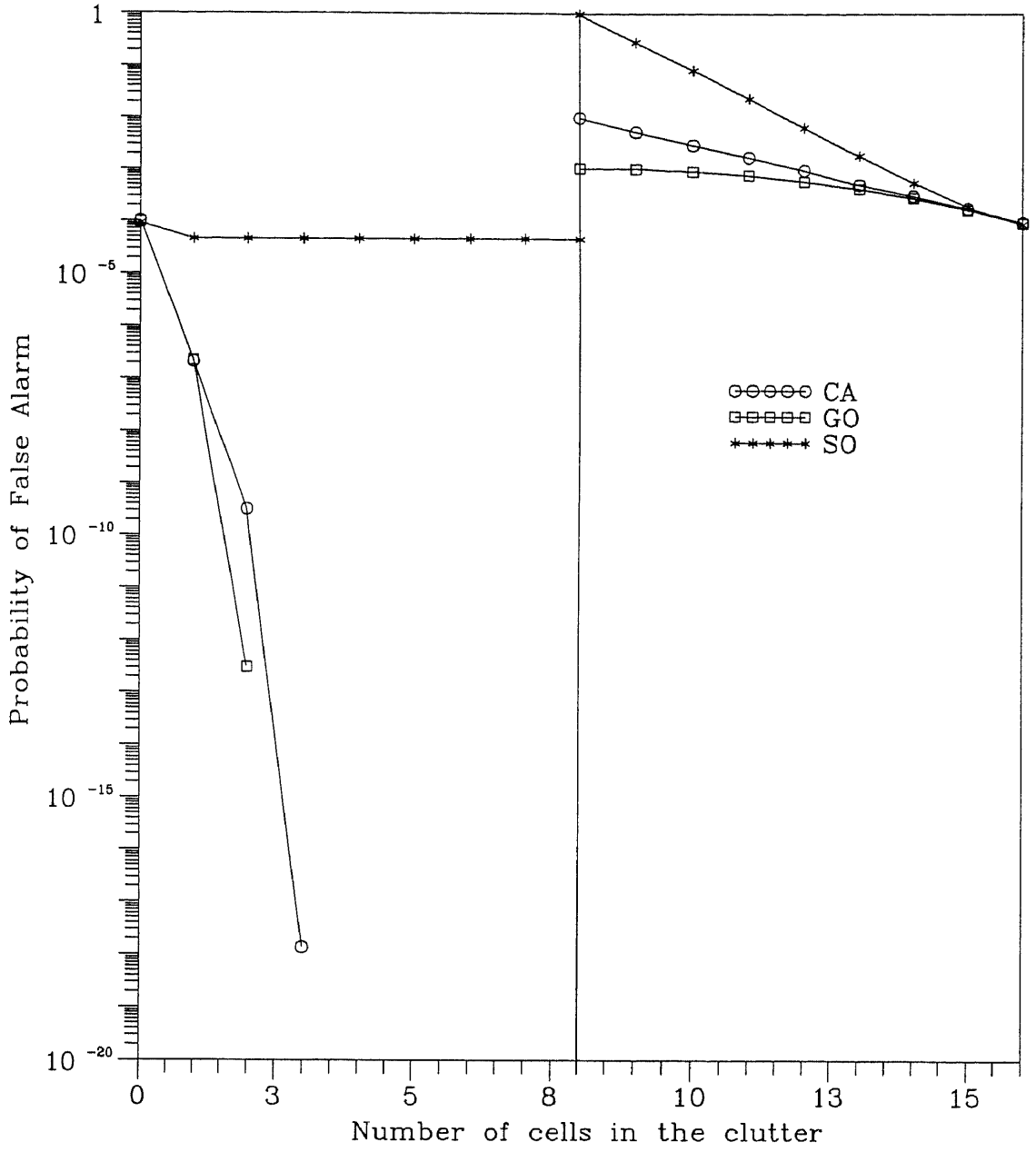

Figure 2.7. Probability of false alarm of the GO,SO and the CA-CFAR detectors in the presence of a clutter power transition.

N=16, C=30dB, L=1, $\alpha=10^{-4}$.

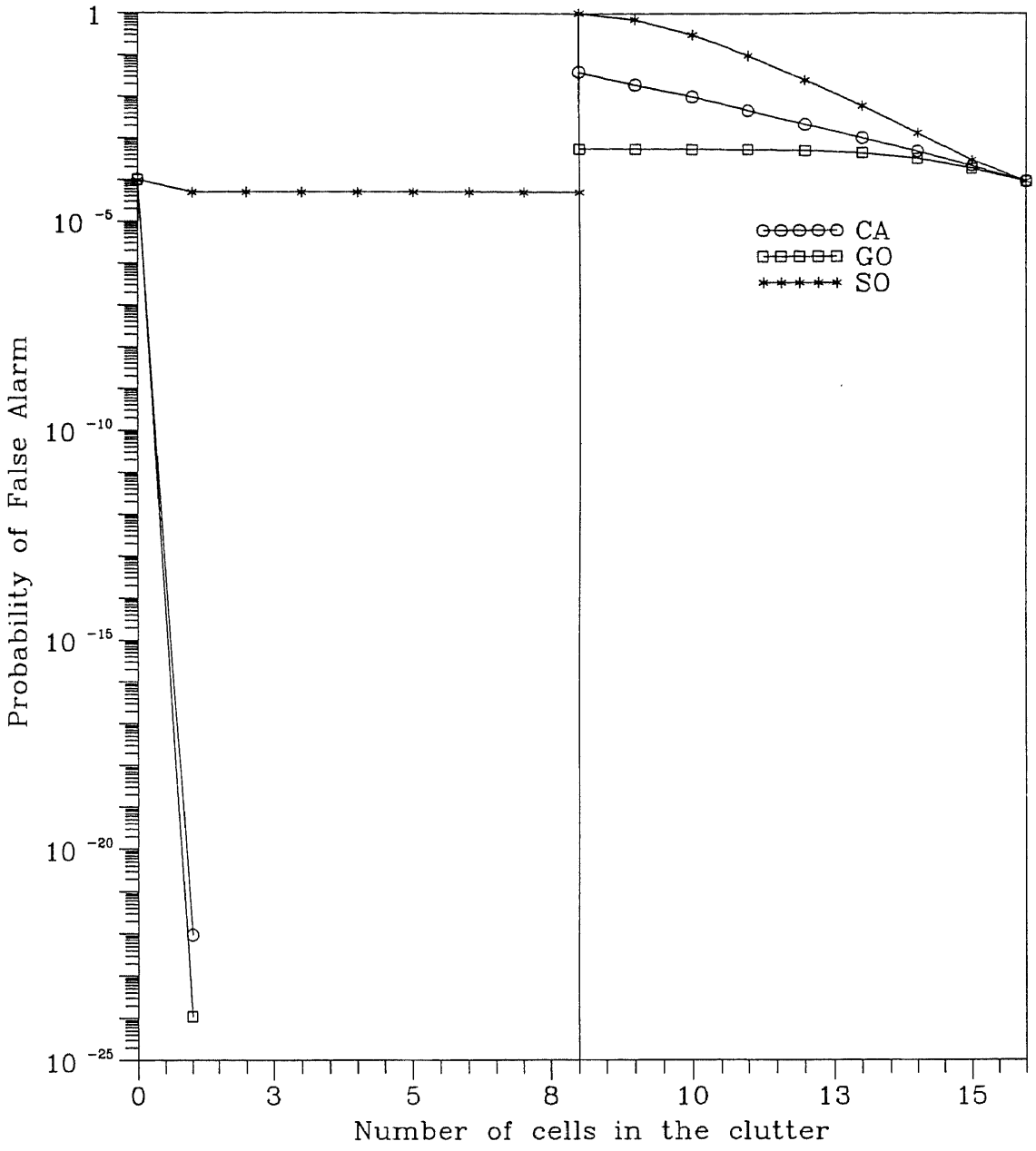

Figure 2.8. Probability of false alarm of the GO,SO and the CA-CFAR detectors in the presence of a clutter power transition.
N=16, C=30dB, L=4, $\alpha=10^{-4}$.

Chapter 3

AN AUTOMATIC CENSORED CELL AVERAGING CFAR DETECTOR IN NONHOMOGENEOUS CLUTTER

3.1 Introduction

When the clutter background environment is not homogeneous, as we saw earlier, the performance of the CA-CFAR detector is seriously degraded. If the test cell is in the clear but some of the reference cells lie in the clutter, the threshold is raised unnecessarily and therefore the probability of detection is degraded. On the other hand, if the test cell is in the clutter but a group of reference cells is in the clear, the CA-CFAR detector underestimates the noise level in the test cell thus yielding an excessive number of false alarms. In order to alleviate the above problems, different techniques have been proposed in the literature. The GO-CFAR detector, that selects the maximum of the outputs of the leading and lagging reference window was studied in the previous chapter. It was shown that the additional detectability loss due to the greatest-of selection logic was in the range of 0.1 to 0.3dB. However, in the case where the test cell is in the clear and some of the reference cells are immersed in clutter, its detection performance is seriously degraded.

In order to alleviate the above problems, a number of order statistics-based thresholding techniques have been proposed in the literature [22-30]. In the order statistics-based processors, the reference samples are first ordered in ascending order and then depending on the particular processor a censoring procedure is applied to identify the reference samples that are not identically distributed with the noise in the test cell. In [22-27] the censoring point(s) is(are) preset. This implies that a priori knowledge about the background environment is needed for these detectors to perform well. In [28-30] a signal processing algorithm which adaptively selects the censoring points by performing cell-by-cell tests is used.

In this chapter, we propose an adaptive censoring algorithm which like the detectors in [27,30] performs cell-by-cell tests to censor the unwanted samples, but does not rank order the reference observations. In addition, the proposed detector which is referred to as the automatic cenored cell averaging (ACCA) CFAR detector is designed to be robust when more than one clutter power transition occurs in the reference window, while the processors in [27,30] make no such provision.

In section 3.2, we briefly describe the ACGO-CFAR detector. In section 3.3, we present a description of the ACCA-CFAR detector. The mathematical analysis to derive the design equations used to implement the proposed detector is presented in section 3.4. In section 3.5 we study the computational complexity of the ACCA and ACGO-CFAR detectors in terms of processing time requirements. In section 3.6, the detection performance and the false alarm regulation of the ACCA-CFAR detector are evaluated by means of computer simulations. Its performance is compared with the performances of the GO-CFAR and ACGO-CFAR detectors for homogeneous and non-homogeneous background environment. Our conclusions are briefly stated in section 3.7.

3.2 The ACGO-CFAR Detector

The order statistics-based thresholding techniques in [22,24,25,27], require some a priori knowledge about the background environment in order to censor the unwanted samples, since the censoring points are preset. In [30], the Adaptive Censored Greatest-of CFAR detector, which adaptively selects the censoring points was proposed for various non-homogeneous background environments. In the ACGO-CFAR detector, the censoring algorithm is applied independently and in parallel to both the outputs of the leading range cells $q_j, j = 1, \ldots, M(M = N/2)$ and the outputs of the lagging range cells q_j, $j = M + 1, \ldots, N$. The outputs of the leading and the lagging cells are rank ordered independently of each other to yield the ordered sequences

$$q_{(1)} \leq q_{(2)} \leq, \ldots, q_{(M)} \tag{3.1}$$

and

$$q_{(M+1)} \leq q_{(M+2)} \leq, \ldots, q_{(N)} \tag{3.2}$$

respectively. The censoring algorithm then, compares the ordered sample $q_{(k+1)}$ to the threshold $T_k S_k$ at the kth step. A decision is obtained according to

$$q_{(k+1)} \underset{H_0}{\overset{H_1}{\gtrless}} T_k \, S_k \tag{3.3}$$

where T_k is the kth scaling constant which is selected so that the desired probability of false censoring, P_{FC}, is achieved. In equation (3.3), S_k denotes the sum of the lower k ordered samples, that is,

$$S_k = \sum_{j=1}^{k} q_{(j)} \tag{3.4}$$

The censoring procedure stops if a particular test hypothesis H_1 is decided to be true or when all samples in the group of cells under consideration are tested. The estimate q of the noise level in the test cell is set to be the maximum of u and v, that is,

$$q = \max(u, v) \tag{3.5}$$

where

$$u = \frac{1}{m_1} \sum_{j=1}^{m_1} q_{(j)} \tag{3.6}$$

and

$$v = \frac{1}{m_2} \sum_{j=1}^{m_2} q_{(N/2+j)} \tag{3.7}$$

m_1 and m_2 are the samples in the leading and lagging reference window respectively, that survive the censoring procedure. The probability of false censoring, P_{FC}, the ordered samples $q_{(k+1)}, \ldots, M$ at the kth step of the censoring procedure is the probability that hypothesis H_1 is decided to be true while hypothesis H_0 is actually true. The probability of false alarm, P_{FC}, is derived to be [30]

$$P_{FC} = \binom{M}{k} \frac{1}{[1 + T_k(M-k)]^k} \tag{3.8}$$

The probability of false alarm, P_F, is equal to the probability that the output of the cell under test, Q_0 is greater than the detection threshold, Tq, under hypothesis H_0, that is,

$$P_F = \Pr(Q_0 > TQ | H_0) \tag{3.9}$$

where Q denotes the estimator of the noise level in the test cell given in equation (3.5). The design equation for the probability of false alarm, P_F, is derived to be [30]

$$\begin{aligned} P_F \;=\; & \left(1 + \frac{T}{m_1}\right)^{-m_1} + \left(1 + \frac{T}{m_2}\right)^{-m_2} \\ & - {m_1}^{m_1} \sum_{k=0}^{m_2-1} \binom{m_1 + k - 1}{k} {m_2}^k (T + m_1 + m_2)^{-(m_1+k)} \\ & - {m_2}^{m_2} \sum_{k=0}^{m_1-1} \binom{m_2 + k - 1}{k} {m_1}^k (T + m_1 + m_2)^{-(m_2+k)} \end{aligned} \tag{3.10}$$

The scaling constant T, is computed by solving the equation $P_F = \alpha$. In Figure 3.1, we study the censoring capabilities of the ACGO-CFAR detector where out of $M = 8$ statistically independent random variables, m were generated with mean $\mu = 1$ and the remaining $r = M - m$ with mean $\mu = 1 + I$; I denotes the interference to noise ratio. The censoring is more robust as the interference becomes stronger. Also, as

the number of samples containing interference increases the probability of censoring these samples for a given I decreases.

3.3 The ACCA-CFAR Detector

In this section, we present the algorithm, that the ACCA-CFAR detector uses to censor the unwanted samples in the reference cells, that may/or not contain an extended clutter edge and obtain an estimate of the noise level in the cell under test. A censoring procedure is implemented to make an assessment of the background environment. The censoring procedure begins by first initializing two parameters, $k_1 = 0$ and $k_2 = N$. q_1 is then compared with a scaled version of q_2, $T_c q_2$, where T_c is the scaling constant which is selected to satisfy the design probability of false censoring, P_{FC}. If $q_1 > T_c q_2$ then the mean of $Q_1(\overline{Q_1})$ is decided to be greater than the mean of $Q_2(\overline{Q_2})$(where we use uppercase letters to denote random variables and lowercase letters to denote there corresponding observations). Thus, a high to low clutter power transition is assumed to occur in cell 1 (hypothesis H_{10}) and k_1 is updated to 1. In this event, the algorithm continues with the next step in which the samples q_2 and q_3 are considered. On the other hand, if $q_1 < T_c q_2$ two possible cases arise. Either q_1 and q_2 are identically distributed (hypothesis H_{00}) or a low to high clutter power transition occurs (hypothesis H_{01}). In order to determine which one of H_{00} or H_{01} is true, we then compare q_2 with $T_c q_1$. If $q_2 > T_c q_1$ hypothesis H_{01} is decided to be true and $k_1 = 1$. If $q_2 < T_c q_1$ hypothesis H_{00} is decided to be true and k_1 remains unchanged, i.e., $k_1 = 0$. The algorithm continues in the same manner until all the samples from the leading cells are tested. The value of k_1 is updated every time H_{10} or H_{01} is true. Observe that up to this point the maximum possible value of k_1 is $M - 1$. Then, the last sample from the leading cells, q_M, is compared with a scaled version of the first sample from the lagging cells, $T_c q_{M+1}$. If $q_M > T_c q_{M+1}$ we decide that $\overline{Q_M} > \overline{Q_{M+1}}$, i.e., hypothesis H_{10} is true. Since the test cell is located between

the cells indexed by M and $M+1$, the clutter power transition may occur in either the Mth cell or the test cell. It should be pointed out that in this test , it is not possible to determine the exact location of the clutter edge as the test cell is not considered by the censoring algorithm. In order to avoid an excessive number of false alarms in the event that the transition occurs in the test cell, we assume that the noise in the test cell is identically distributed with Q_M and the second parameter k_2 is set equal to M. At this point the algorithm stops and the estimate noise in the test cell is obtained by combining $q_{K_1+1}, \ldots, q_{K_2}$ which have been determined to be identically distributeed with the noise in the test cell. On the other hand, if $q_M < T_c q_{M+1}$ either H_{00} or H_{01} might be true. As before, we compare q_{M+1} with $T_c q_M$. If $q_{M+1} > T_c q_M$ hypothesis H_{01} is decided to be true. Again the clutter power transition may occur in either the test cell or the $(M+1)$th reference cell. As in the previous case, we decide that the edge is located in the test cell and therefore $k_1 = M$, while k_2 remains unchanged, that is, all the leading samples are censored. If $q_{M+1} < T_c q_M$ hypothesis H_{00} is decided to be true and both k_1 and k_2 hold on to these previous values. The algorithm continues in the same manner until a clutter power transition is detected. When a clutter power transition is detected, the value of k_2 is updaded accordingly while the value of k_1 does not change when the lagging samples are being tested. If no transition is detected $k_2 = N$. Observe that when a transition is detected in the lagging cells, the algorithm stops without testing the remaining of the lagging cells. This is due to the fact that after the transition, it is not possible to determine whether any of the remaining cells are identically distributed with the noise in the test cell or not. After the censoring procedure finishes, the noise level estimate, q, is set to be

$$q = \sum_{i=k_1+1}^{k_2} q_i \tag{3.11}$$

The output of the test cell is then compared to the adaptive threshold $T(J)q$, that is,

$$q_0 \underset{H_0}{\overset{H_1}{\gtrless}} T(J)q \tag{3.12}$$

in order to determine the presence (H_1) or absence (H_0) of a target in the test cell. The scaling constant $T(J)$ is chosen so that the design false alarm probability, α, is satisfied. The variable $J = k_2 - k_1$ is the number of samples that are included in the threshold estimation process.

In Figure 3.2, we study the censoring capabilities of the proposed censoring algorithm where out of $N = 16$ ststistically independent random variables 4 were generated with parameter $\mu = 0$ and the remaining 12 with parameter $\mu = C$. The simulation was conducted for $L = 1$ and 4 and $\beta = 6 \times 10^{-3}$, 4×10^{-3}, 10^{-3} and 10^{-4}. As expected, the probability of detecting the clutter power transition increases as C increases. The unwanted samples are censored more efficiently (i) as β increases because the adaptive threshold in each step of the censoring process decreases, and (ii) as L increases due to the enhanced performance offered by the diversity in the system configuration. For example when the clutter to noise ratio is 30dB and $L = 1$, the probability of edge detection increases from approximately 0.5 to 0.9, when β increases from 10^{-3} to 6×10^{-3}. On the other hand if L is changed to $L = 4$ for the same clutter to noise ratio, the probability of edge detection approaches unity.

3.4 Analysis of the ACCA-CFAR Detector

The probability of false censoring, P_{FC}, is defined as the probability to falsely decide the presence of a step discontinuity in the reference window when in fact no discontinuity is present. P_{FC}, can be written as a contour integral of the moment generating function, mgf, of the equivalent statistic $R_j = Q_j - T_c Q_{j-1}$ where q_j and q_{j-1} are the observations from the jth and $(j-1)$th reference cells respectively. The

scaling constant T_c is selected so that the desired probability of false censoring, β, is achieved. Thus,

$$\begin{aligned} P_{FC} &= \Pr(R_j > 0 | H_{00}) \\ &= -\frac{1}{2\pi i}\int_c \omega^{-1}\Phi_{R_j|H_{00}}(\omega)d\omega \end{aligned} \tag{3.13}$$

where the mgf of the equivalent statistic R_j is given by

$$\begin{aligned} \Phi_{R_j|H_{00}} &= E\left[\exp(-\omega(\sum_{i=1}^{L} q_{ij} - T_c\sum_{i=1}^{L} q_{i(j-1)}))\right] \\ &= \int_0^\infty \cdots \int_0^\infty \exp\left(-\sum_{i=1}^{L} q_{ij}\right)\exp\left(-\omega\sum_{i=1}^{L} q_{ij}\right) dq_{ij}\ldots dq_{Lj} \\ &\quad \cdot \int_0^\infty \cdots \int_0^\infty \exp\left(-\sum_{i=1}^{L} q_{i,j-1}\right)\exp\left(T_c\omega\sum_{i=1}^{L} q_{i,j-1}\right) dq_{i,j-1}\ldots dq_{L,j-1} \\ &= \left[\left(\frac{1}{1+\omega}\right)\left(\frac{1}{1-T_c\omega}\right)\right]^L \end{aligned} \tag{3.14}$$

In equation (3.13), the contour of integration c is crossing the real ω-axis at $\omega = c_1$ and is closed in an infinite semicircle in the left half ω-plane. c_1 is selected so that c encloses all the poles of $\Phi_{R_j|H_{00}}(\omega)$ that lie in the open left half ω-plane. Substituting equation (3.14) into equation (3.13), the residue at $\omega = -1$ is

$$\begin{aligned} \mathrm{Res}_{\omega\to -1} &= \frac{1}{(L-1)!}\lim_{\omega\to -1}\frac{d^{L-1}}{d\omega^{L-1}}\left\{\frac{1}{\omega(1-T_c\omega)^L}\right\} \\ &= \frac{1}{(L-1)!}\lim_{\omega\to -1}\sum_{k=0}^{L-1}\binom{L-1}{k}\frac{d^k(1-T_c\omega)^{-L}}{d\omega^k}\frac{d^{L-1-k}(\omega^{-1})}{d\omega^{L-1-k}} \end{aligned} \tag{3.15}$$

and by using

$$\begin{aligned} \frac{d^n[uv]}{dx^n} &= \binom{n}{0}v\frac{d^n u}{dx^n} + \binom{n}{1}\frac{dv}{dx}\frac{d^{n-1}u}{dx^{n-1}} + \binom{n}{2}\frac{d^2v}{dx^2}\frac{d^{n-2}u}{dx^{n-2}} + \\ &\quad \ldots + \binom{n}{k}\frac{d^K u}{dx^k}\frac{d^{n-k}u}{dx^{n-k}} + \ldots \binom{n}{n}u\frac{d^n u}{dx^n} \end{aligned} \tag{3.16}$$

the probability of false censoring is derived to be

$$P_{FC} = \sum_{k=0}^{L-1}\binom{L+k-1}{k}\frac{T_c^k}{(1+T_c)^{L+k}} \tag{3.17}$$

The scaling constant T_c is computed from equation (3.17) by solving $P_{FC} = \beta$

The probability of false alarm, P_F, is equal to the probability that the output of the cell under test, q_0, exceeds the detection threshold, $T(J)q$, under hypothesis H_0. That is, from the test of expression (3.12), the probability of false alarm is given by

$$P_F = \Pr(Q_0 > T(J)Q|H_0) \tag{3.18}$$

where Q denotes the estimator of the noise level in the test cell which is given by equation (3.11). Following the same procedure as in the derivation of the expression for the probability of false ecensoring, the probability of false alarm, P_F, is the contour integral

$$P_F = -\frac{1}{2\pi i}\int_c \omega^{-1}\Phi_{R|H_0}(\omega)d\omega \tag{3.19}$$

where the equivalent statistic R is given by

$$R = Q_0 - T(J)Q \tag{3.20}$$

The contour of integration is the same as that of equation (3.13) except c_1 is selected so that all the poles of $\Phi_{R|H_0}(\omega)$ that lie in the open left half ω-plane are enclosed. The moment generating function, mgf, of R under H_0 is given by

$$\begin{aligned}
\Phi_{R|H_0}(\omega) &= E[\exp(-\omega(\sum_{i=1}^{L} q_{i0} - T\sum_{j=1}^{J}\sum_{i=1}^{L} q_{ij}))] \\
&= \int_0^\infty \cdots \int_0^\infty \exp\left(-\omega\sum_{i=1}^{L} q_{i0}\right)\exp\left(-\sum_{i=1}^{L} q_{i0}\right) dq_{i0}\ldots dq_{L0} \\
&\quad \cdot \int_0^\infty \cdots \int_0^\infty \exp\left(\omega T\sum_{j=1}^{J}\sum_{i=1}^{L} q_{ij}\right)\exp\left(-\sum_{j=1}^{J}\sum_{i=1}^{L} q_{ij}\right) dq_{ij}\ldots dq_{Lj} \\
&= (1+\omega)^{-L}(1-T\omega)^{-JL}
\end{aligned} \tag{3.21}$$

Substitution of equation (3.21) into (3.19) and with the residue at $\omega = -1$ given by

$$\begin{aligned}
\mathrm{Res}_{\omega\to -1} &= \frac{1}{(L-1)!}\lim_{\omega\to -1}\frac{d^{L-1}}{d\omega^{L-1}}\left\{\frac{\omega^{-1}}{\omega(1-T\omega)^{JL}}\right\} \\
&= \frac{1}{(L-1)!}\lim_{\omega\to -1}\sum_{k=0}^{L-1}\binom{L-1}{k}(-1)^{L-1-k}\omega^{-(L-k)}
\end{aligned}$$

$$\cdot\frac{(JL+k-1)!}{(JL-1)!}\frac{T^k}{(1-T\omega)^{JL+k}} \tag{3.22}$$

the probability of false alarm, P_F, is derived to be

$$P_F = \sum_{k=0}^{L-1}\left(\begin{array}{c} JL+k-1 \\ k \end{array}\right) T(J)^k(1+T(J))^{-(JL+k)} \tag{3.23}$$

Equation (3.23) is used to calculate the threshold multipliers $T(J), J = 1,\ldots,N$, so that $P_F = \alpha$. Observe that equation (3.23) is the expression for the probability of false alarm under the assumption that the censoring procedure correctly identifies the J reference samples that are identically distributed with the noise in the cell under test. In general however, some samples that are identically distributed with the noise in the cell under test may be censored or some samples that are not identically distributed with the noise in the test cell may be included in the threshold estimation process. The exact expression of the probability of false alarm is given by

$$P_F = \sum_{k_1=1}^{M}\sum_{k_2=M+1}^{N} P_F(M-k_1,k_2)Pr(M-k_1,k_2) \tag{3.24}$$

where $P_F(M-k_1,k_2)$ denotes the conditional probability of false alarm given that $M-k_1$ samples from the leading and $k_2-(M+1)$ samples from the lagging cells are included in the threshold estimation process, and $Pr(M-k_1,k_2)$ is the joint probability mass function of $M-k_1$ and k_2. The joint probability mass function can be written as

$$Pr(M-k_1,k_2) = Pr(M-k_1)Pr(k_2) \tag{3.25}$$

since the random variables of the leading reference window are independent of those of the lagging reference window. Assuming that the censoring procedure identifies correctly all the samples that identically distributed with the cell under test, i.e. $\Pr(M-k_1)$ =$\Pr(k_2)$ = 1, equation (3.24) reduces to equation (3.23). The use of expression (3.23) to calculate the parameter T(J), is justified under the assumption made in designing a CFAR processor, that is, CFAR processors assume that the reference noise observations are representative of the noise in the test cell. [27,29,30]

In Figures 3.3 and 3.4 we present the probability of false alarm versus the probability of false censoring for $L = 1, 4$ and $\alpha = 10^{-4}$ for the ACCA-CFAR detector. We observe that when $L = 1$ and the desired P_{FC} is less than 6×10^{-3} the probability of false alarm that is achieved by the ACCA-CFAR detector is equal to the design value. On the other hand, when the desired probability of false censoring is greater than 6×10^{-3} the probability of false alarm increases above the design value. Thus, to avoid overcensoring which causes underestimation of the noise level in the test cell, when $L = 1$ and $\alpha = 10^{-4}$ we choose the desired value of P_{FC} to be 6×10^{-3}. It should be pointed out that the maximum value of P_{FC} with which α is achieved is chosen to avoid reducing the censoring cababilities of the proposed algorithm, since it will discourage censoring possible clutter edge(s). Similarly, when $L = 4$ and $\alpha = 10^{-4}$ we choose the desired value of P_{FC} to be 4×10^{-3}.

3.5 Time processing requirements

An attractive feature of the proposed detector as compared with order statistics-based processors is the reduced amount of processing time required to implement the censoring procedure which makes an assessment of the background environment and then makes a decision about the presence or absence of a target in the cell under test. In Figure 3.5, we compare the processing times of the detectors for $L = 1$. We have assumed that in the order statistic processor (ACGO-CFAR) the heap sorting algorithm which is the fastest sorting routine [33] is used to rank order the data. When the heap sort is used, $N \log_2 N$ comparisons are required to sort the data. We have also assumed that a single DSP processor [34,35], employing special floating point hardware so that multiplications and additions take the same amount of time to be executed, is used. The maximum required number of machine cycles for the three detectors are derived to be

$$\tau_{ACGO} = 2N log_2 \frac{N}{2} + 4N + 1 \tag{3.26}$$

$$\tau_{ACCA} = 7N - 4 \tag{3.27}$$

We observe that when

$$N \geq 2^{4.5} \tag{3.28}$$

the execution time of the ACCA-CFAR detector is smaller than the execution time of the ACGO-CFAR detector.

3.6 Results

The false alarm regulation and detection performance of the ACCA-CFAR detector have been evaluated by means of computer simulations. The results are compared with those of the GO and ACGO-CFAR detectors. The ACGO and GO-CFAR detectors are analyzed in detail in [30] and [11,12] respectively. In the case of multiple pulses ($L = 4$), the ACCA detector is compared only with the GO-CFAR detector. The ACGO-CFAR detector is not shown because the order statistics analysis required to compute the threshold multiplier is extremely cumbersome. The GO-CFAR detector sums independently the outputs of the leading and the lagging range cells and selects the maximum of the two to be the estimate of the noise in the test cell. The ACGO-CFAR detector obtaines two tentative estimates of the noise level in the test cell by independently processing the outputs of the leading and lagging range cells. The final estimate of the noise level in the cell under test is set to be the maximum of the two tentative estimates.

Unwanted samples in the reference window may be continously distributed in the form of a clutter as shown in Figure 3.6. In Figures 3.6a,3.6b,3.6c the reference window is shown with the test cell immersed in the clutter and some of the reference noise samples in the clear, where in Figure 3.6d the test cell is in the clear and some of the reference samples are in the clutter. The false alarm regulation performance of the ACCA-CFAR detector is compared with those of the GO and ACGO-CFAR detectors

based on the different environments shown in Figure 3.6. As mentioned earlier, when the test cell is in the clutter, and some of the reference cells are in the clear, (as shown Figures 3.6a,3.6b,3.6c) the conventional CA-CFAR detector underestimates the noise in the test cell, yielding an excessive probability of false alarm. On the other hand when the test cell is in the clear and a group of reference cells is in the clutter, (Figure 3.6d) a masking effect results. That is, the threshold is raised unnecesarily resulting in poor detection performance. In Figures 3.7 and 3.8 the false alarm regulation properties of the ACCA-CFAR detector are shown for various values of the background noise level. The results show the CFAR properties of the ACCA-CFAR detector for $N = 16$ reference noise samples and for single ($L = 1$) and multiple pulse ($L = 4$) transmission. Three desired probabilities of false alarm are considered $(10^{-2}, 10^{-3}, 10^{-4})$ and the probability of false censoring is assumed to be 6×10^{-3} in Figure 3.7 and 4×10^{-3} in Figure 3.8. In both cases where $L = 1$ and $L = 4$ the false alarm probability of the proposed detector is shown to be robust for all the three values of desired probability of false alarm considered.

In Figures 3.9 and 3.10, the probability of false alarm of the ACCA, GO and ACGO-CFAR detectors is shown, when the test cell and r reference cells are in the clutter. In both Figures all the detectors achieve the desired probability of false alarm when the number of reference cells is 16, i.e. homogeneous case. As the clutter power transition increases, the false alarm regulation of the ACCA-CFAR detector is superior as compared with the case of the GO and ACGO-CFAR detectors. Although the probability of detecting the clutter edge when $C = 15$dB is greater than the probability of detecting the clutter edge when $C = 5$dB, the probability of false alarm in the latter case is lower. This is due to the fact that the censoring procedure sometimes may miss the clutter edge in the leading window, since the clutter power transition is low and as a result the cells that are immersed in clutter will raise the threshold, thus, the probability of false alarm is lowered. In the case of the ACGO-

CFAR detector, the probability of false alarm increases as the clutter to noise ratio increase as shown in Figure 3.9. When $L = 4$ and the clutter power transition is high (30dB) as shown in Figure 3.10, the performance of the ACCA-CFAR detector is superior to that of the GO-CFAR detector, even in the case where the clutter edge is next or in the test cell. This is due to the fact that as we saw in Figure 3.2, the unwanted samples are censored more effectively as L increases due to the improvement in the probability of edge detection provided by the diversity in the system configuration.

In Figures 3.11 and 3.12, we present the probability of false alarm that is achieved by the ACCA, GO and ACGO-CFAR detectors when a group of reference cells surrounding the test cell are immersed in the clutter, that is, two clutter edges are present, one in the leading and one in the lagging reference window. The ACGO-CFAR detector is shown only in Figure 3.11 for $L = 1$. We observe that the false alarm control properties of the ACCA-CFAR detector are more robust than those of the GO-CFAR detector, especially when the clutter to thermal noise ratio, CNR is high. This is due to the fact that the censoring procedure of the ACCA-CFAR detector is more effective as the clutter to noise ratio increases. Also the GO-CFAR detector that selects the maximum of the individual sums of the leading and the lagging range cells, underestimates the noise level in the test cell, since some of the range cells that are in the clear will be included in the threshold estimation, thus lowering the adaptive threshold. In this environment, the false alarm regulation properties of the ACGO-CFAR detector are poor. This is due to the fact that in the application of the censoring procedure, all the cells in both the leading and lagging windows that are in the clutter are censored. Consequently, the total noise in the test cell is severely underestimated and the clutter in the test cell appears as a target return causing the probability of alarm to approach unity as C increases. In all the cases where $L = 4$, and as the clutter transition becomes higher the false alarm regulation

of the ACCA-CFAR detector is superior compared to that of the GO-CFAR detector. In both Figures when two clutter power transitions are present the robust performance of the proposed detector as compared to the GO and ACGO-CFAR detectors is demonstrated.

In Figures 3.13 and 3.14, the false alarm regulation probability of the GO, ACGO and ACCA-CFAR detectors is examined, in the case where the leading window is in the clear and the clutter edge is at the test cell and extended gradually as k increases through out the lagging window. When $L = 1$ the performance of both the ACCA and GO CFAR detectors are more robust as compared to that of the ACGO-CFAR detector since the ACGO-CFAR detector for high clutter to noise ratio censors all the cells immersed in clutter in the lagging window, and since the test cell is in the clutter the noise in the cell under test is severely underestimated. As the number of reference cells immersed in clutter in the lagging window increases, the GO-CFAR detector which chooses the maximum sum of the outputs of the leading and lagging window is superior, since this constitutes the best environment for the GO-CFAR detector. When $L = 4$ and the clutter power transition is high, the false alarm regulation of the ACCA-CFAR detector is more robust than that of the GO-CFAR detector. Also in the case where some of the reference cells in the lagging window are in the clear the false alarm regulation of the GO-CFAR is worst than that of the proposed detector. On the other hand as the number of reference noise samples that are in the clutter increases, the false alarm properties of the GO-CFAR detector are superior since this constitutes the best environment for the GO-CFAR detector.

In 3.15 and 3.16, two clutter power transitions are present, one in the leading and one in the lagging reference window. The false alarm regulation achieved by the GO-CFAR detector is inferior in all cases since the maximum of the sums of the leading and lagging reference window will be chosen, and consequently some of the reference samples that are in the clear will be included in the threshold estimation.

In Figure 3.16 where $L = 4$, the false alarm regulation of the ACCA-CFAR detector is superior, as compared with the probability of false alarm of the GO-CFAR detector, demonstrating the robustness of the ACCA-CFAR detector in such acute environments where two clutter power transitions are present.

In Figures 3.17 and 3.18, we show the false alarm regulation of the ACCA and ACGO-CFAR detectors, in the case where a group of reference cells are immersed in the clutter and the test cell is in the clear. The false alarm regulation properties of the GO-CFAR detector are not shown, since the test cell is in the clear and a group of reference cells is in the clutter. Thus, the GO-CFAR detector raises the threshold unnecessarily, and the probability of detection along with the false alarm probability are lowered significantly. In the case of the ACCA-CFAR detector, the probability of false alarm is lower when $C = 5, 15$dB as shown in Figure 3.17. This is due to the fact that the censoring procedure of the ACCA-CFAR detector may sometimes miss the clutter edge when the clutter to noise ratio is low (Figure 3.2) and consequently the adaptive threshold is raised, yielding in low probability of false alarm. However, in Figure 3.18 where $L = 4$, the ACCA-CFAR detector achieves the design probability of false alarm since the clutter edge in the lagging window is detected more effectively due to the diversity transmission. The probability of censoring the clutter edge when $C = 15$ and 30dB is greater than the probability of censoring the clutter edge when $C = 5$dB, thus in the latter case, some of the reference samples immersed in clutter are included in the threshold estimation. This causes the threshold to be raised unneccesarily yielding in lower probability of false alarm.

In Figures 3.19 and 3.21 we show the detection performance of the ACCA-CFAR detector. In Figure 3.19, we show the probability of detection of the ACCA,GO,CA, Ideal and ACGO-CFAR detectors in homogeneous background environment. The probability of detection in all cases is shown to be almost identical with the ideal detector to be superior as expected. In Figure 3.20, we show the probability of

detection of the ACGO, GO and ACCA-CFAR detectors, when the test cell and a group of reference cells are in the clutter. The detection performance of all three detectors is shown to be approximately the same. In Figure 3.21, the probability of detection of the ACCA and ACGO-CFAR detectors is studied in the case where a number of reference cells in the lagging window is immersed in the clutter and the test cell is in the clear. In both cases where $C = 10$dB and $C = 20$dB the detection performance of the ACCA-CFAR detector is better than that of the ACGO. This is due to the fact that in the ACGO detector, as the number of cells that contain interference increases, the censoring capabilities of the ACGO-CFAR detector are degraded as shown in Figure 3.1. In the above environment the samples containing interference are not effectively censored since in the lagging reference window, out of eight range cells, five are immersed in the clutter. It should be pointed out however, that as the number of samples containing interference becomes smaller, the ACGO-CFAR detection performance will improve significantly.

3.7 Summary and Conclusions

In this chapter, we have considered the problem of CFAR detection in nonhomogeneous background environments. We have proposed the ACCA CFAR detector, which determines whether the test cell is in the clutter or the clear region and selects only those samples which are identically distributed with the noise in the test cell to form the detection threshold. The ACCA-CFAR detector does not require rank ordering of the received data, thus, reducing the processing time considerably. The processing time required for the ACCA-CFAR detector was shown to be less than the time required by the ACGO-CFAR detector as the number of reference noise samples increases. In addition, when two clutter power transitions are present (leading and lagging window) the false alarm regulation properties of the ACCA-CFAR detector are superior, as compared to those of the GO and ACGO-CFAR detectors.

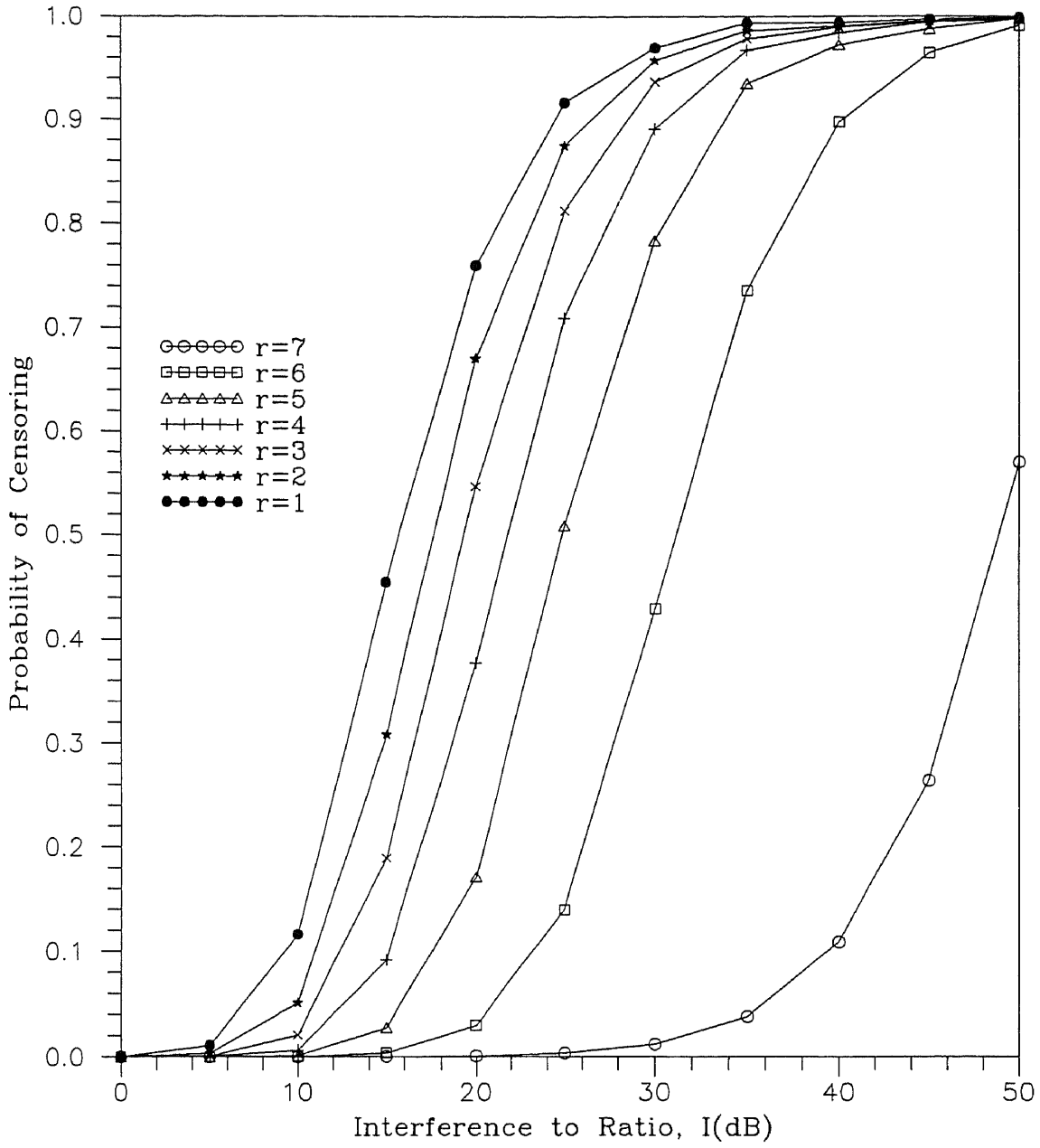

Figure 3.1. Probability of censoring all the r samples that actually contain interference in the ACGO-CFAR detector. M=8, $\alpha=10^{-4}$.

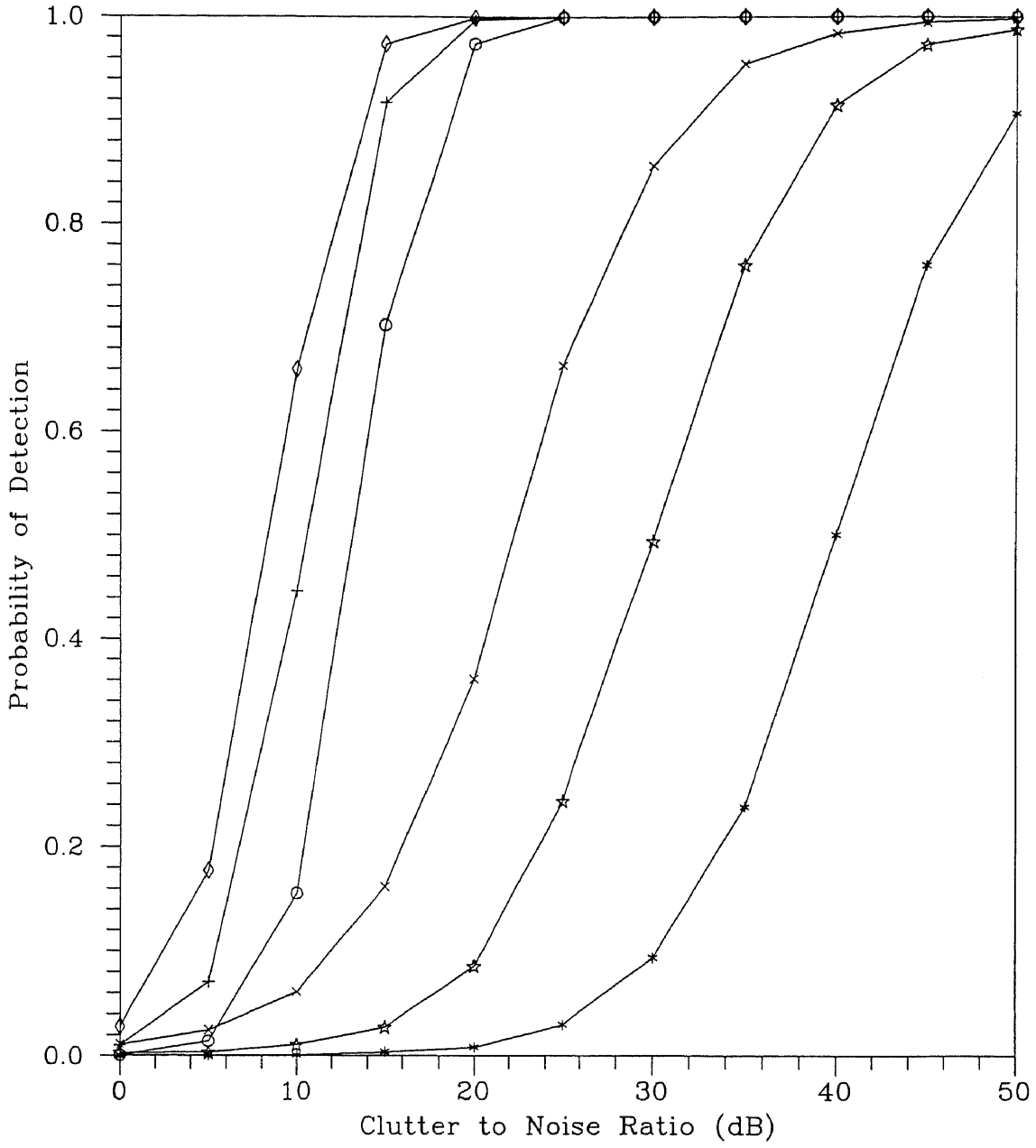

Figure 3.2. Probability of edge detection versus clutter to noise ratio (CNR) of the ACCA–CFAR detector.
N=16, $\alpha=10^{-4}$, Transition at cell 4.

×××××× L=1, $\beta=6\times10^{-3}$
☆☆☆☆☆☆ L=1, $\beta=10^{-3}$
****** L=1, $\beta=10^{-4}$
◊◊◊◊◊ L=4, $\beta=4\times10^{-3}$
++++++ L=4, $\beta=10^{-3}$
○○○○○ L=4, $\beta=10^{-4}$

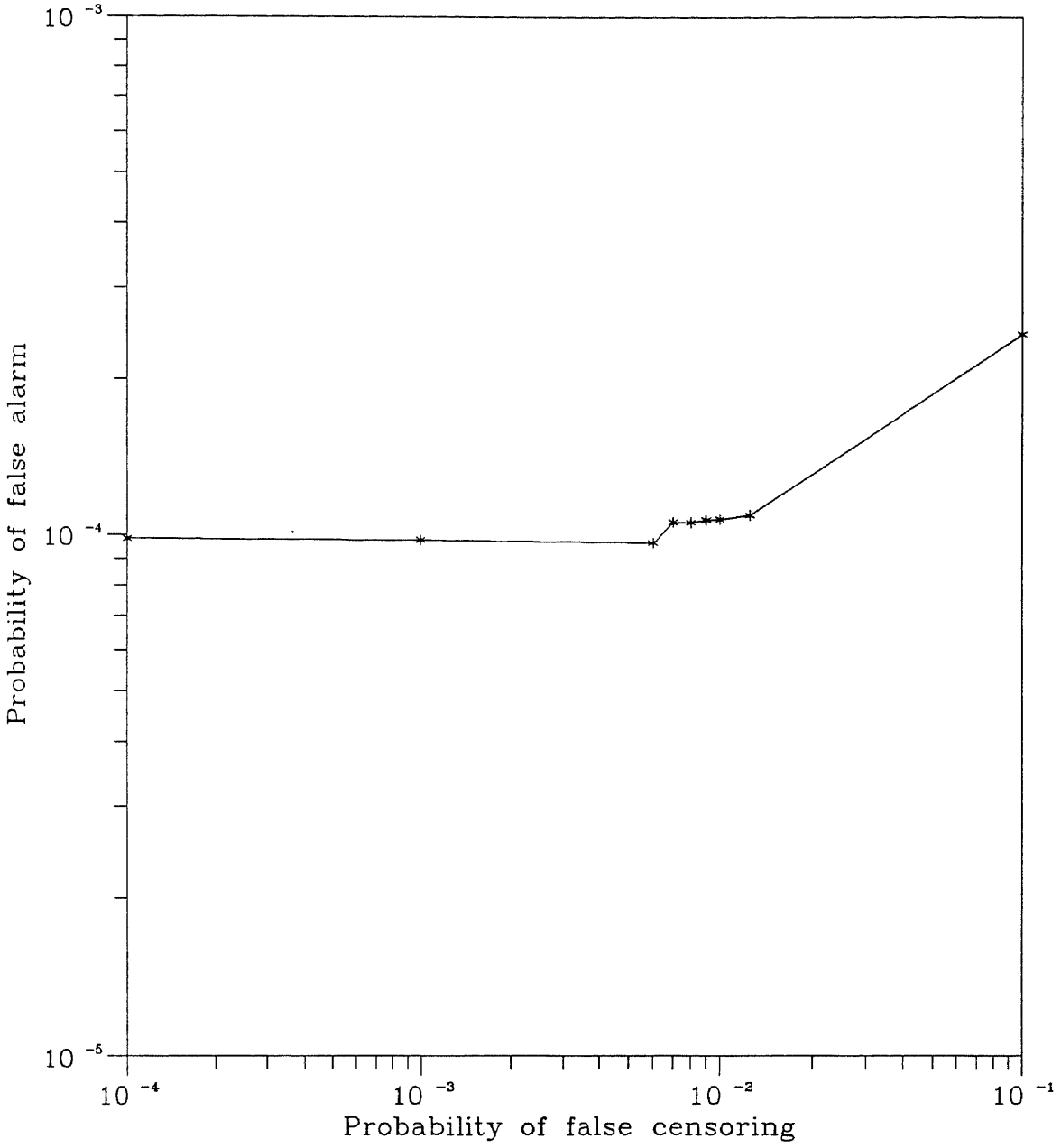

Figure 3.3. Probability of false alarm versus probability of false censoring of the ACCA–CFAR detector.
N=16, L=1, $\alpha=10^{-4}$

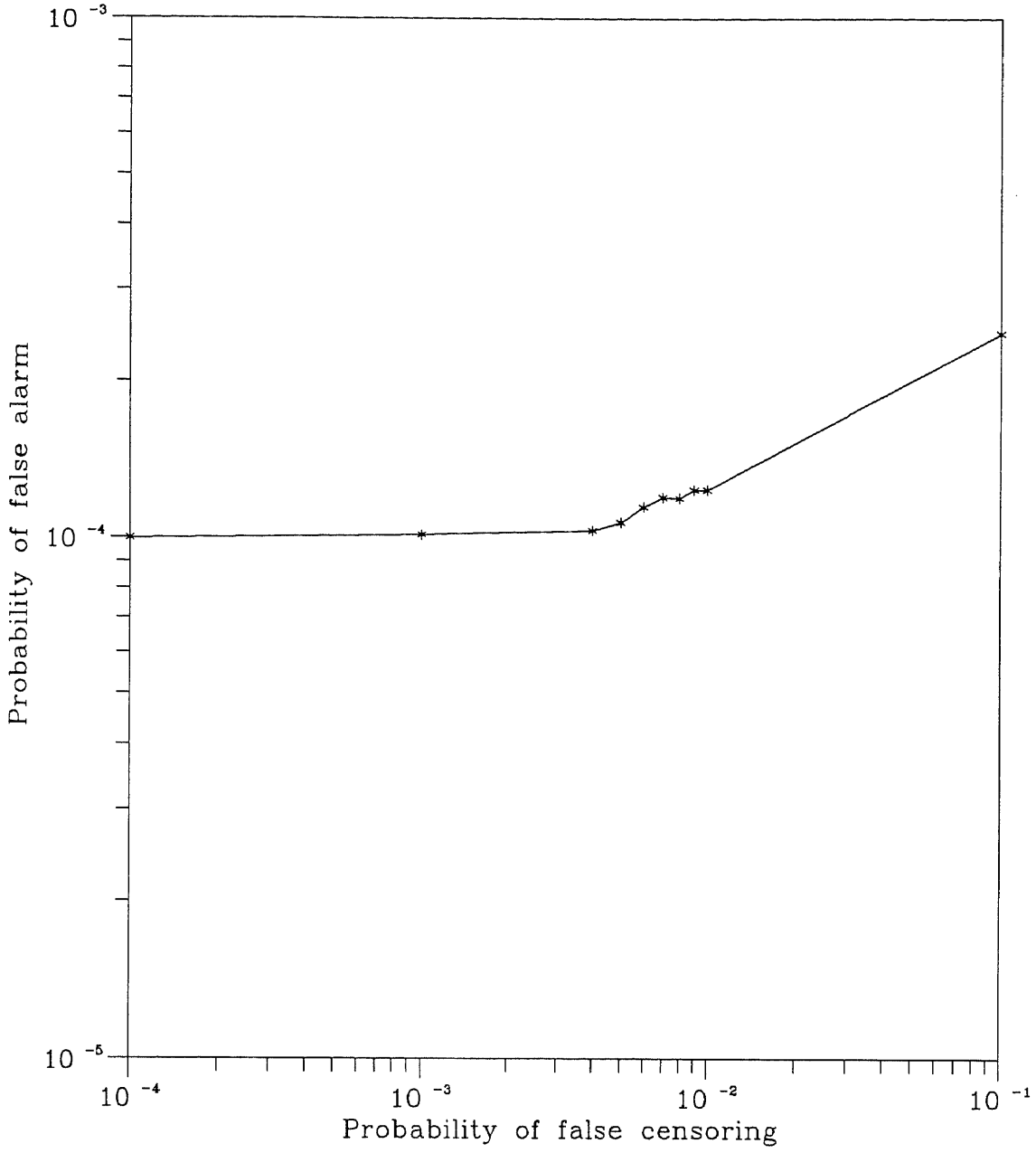

Figure 3.4. Probability of false alarm versus probability of false censoring of the ACCA-CFAR detector.
N=16, L=4, $\alpha=10^{-4}$

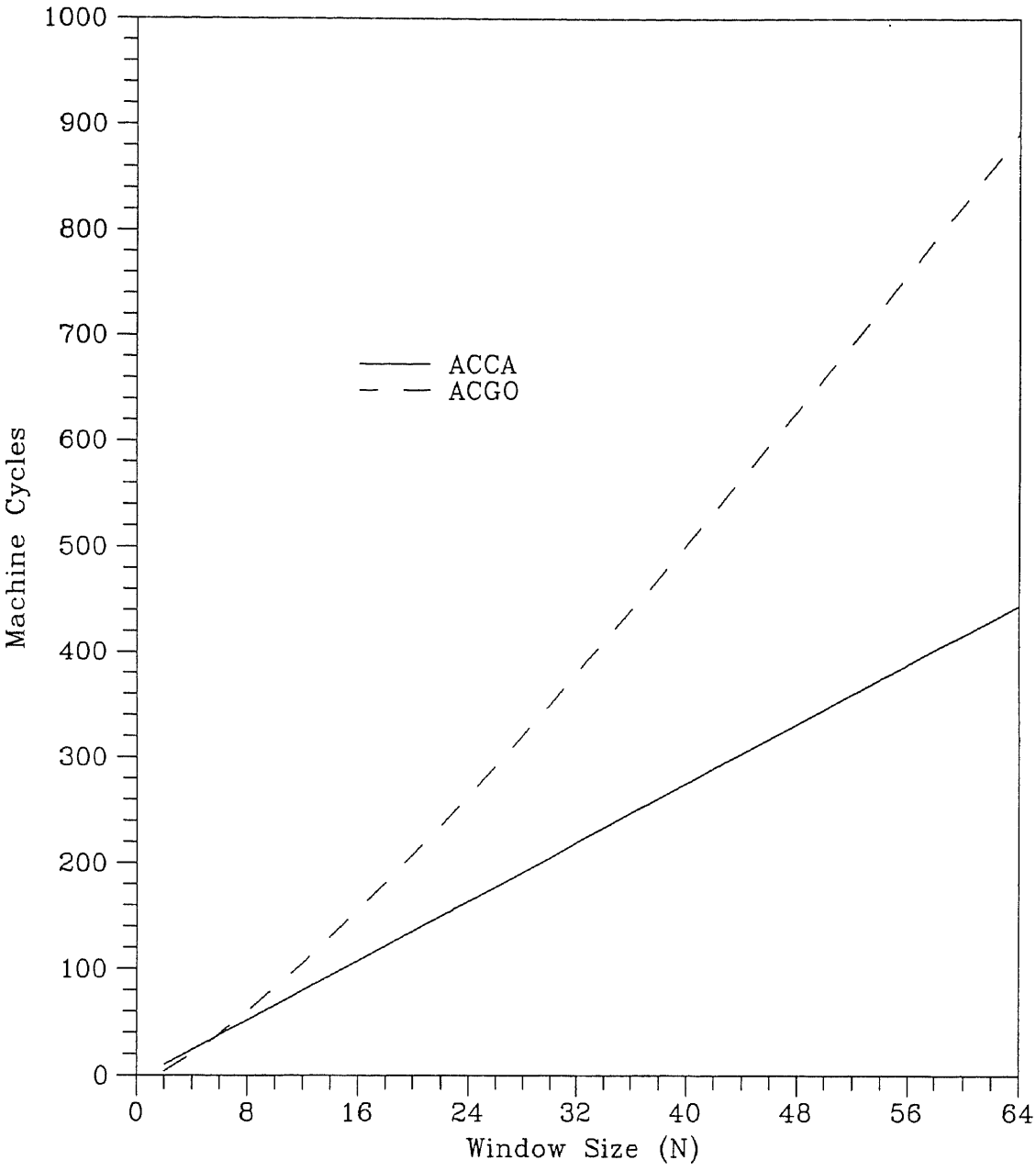

Figure 3.5. Total execution time in machine cycles versus the window size.

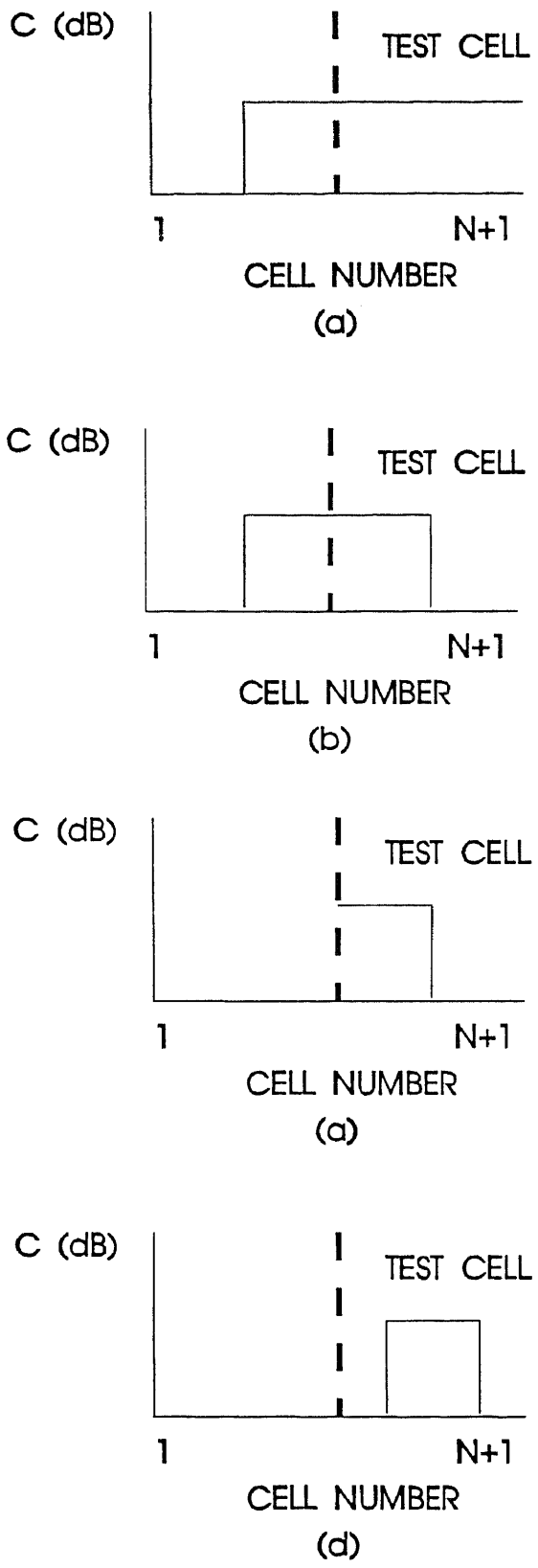

Figure 3.6 Clutter Environments

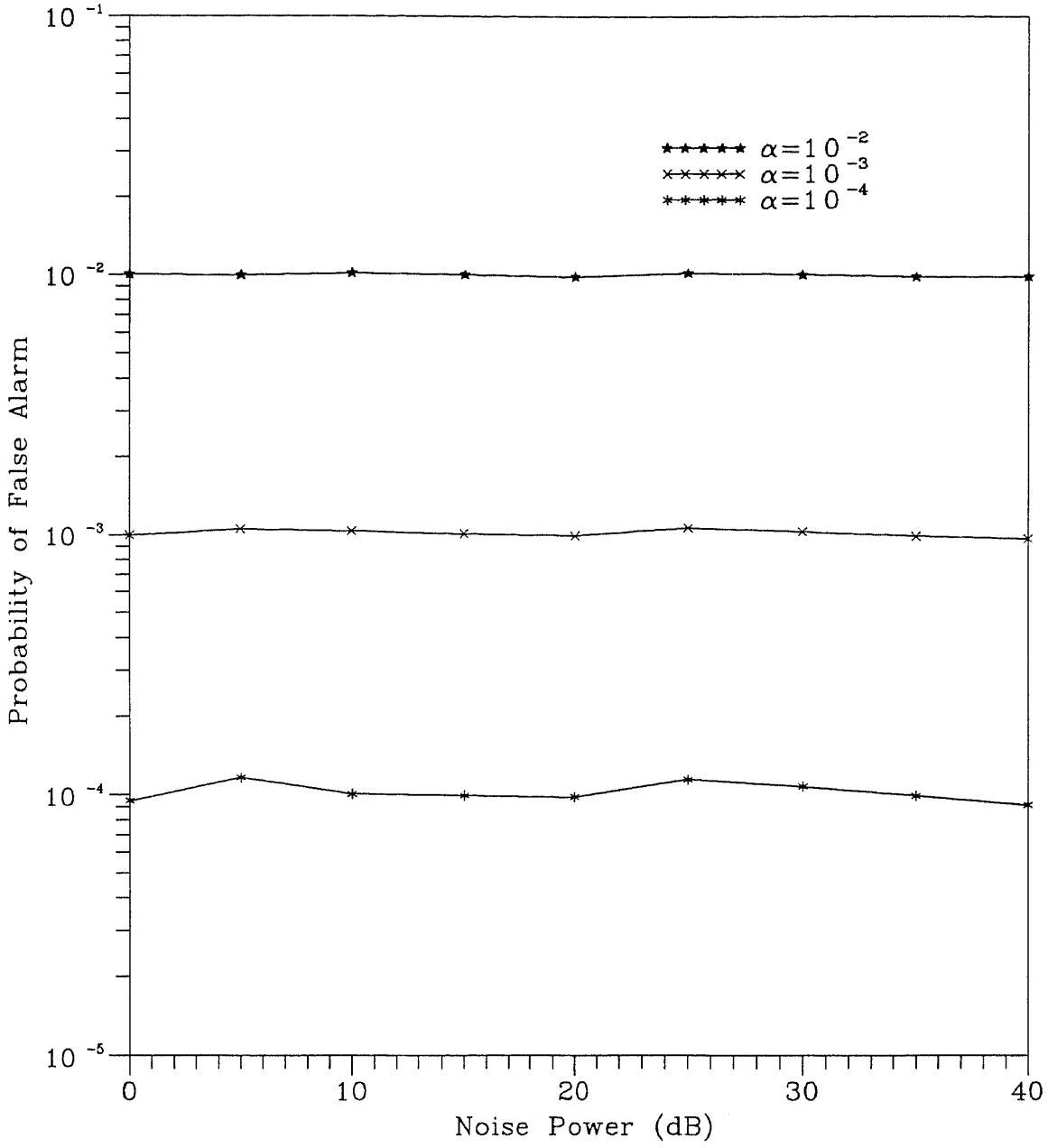

Figure 3.7. Probability of false alarm versus noise power (dB). N=16, L=1, $\beta=6\times10^{-4}$

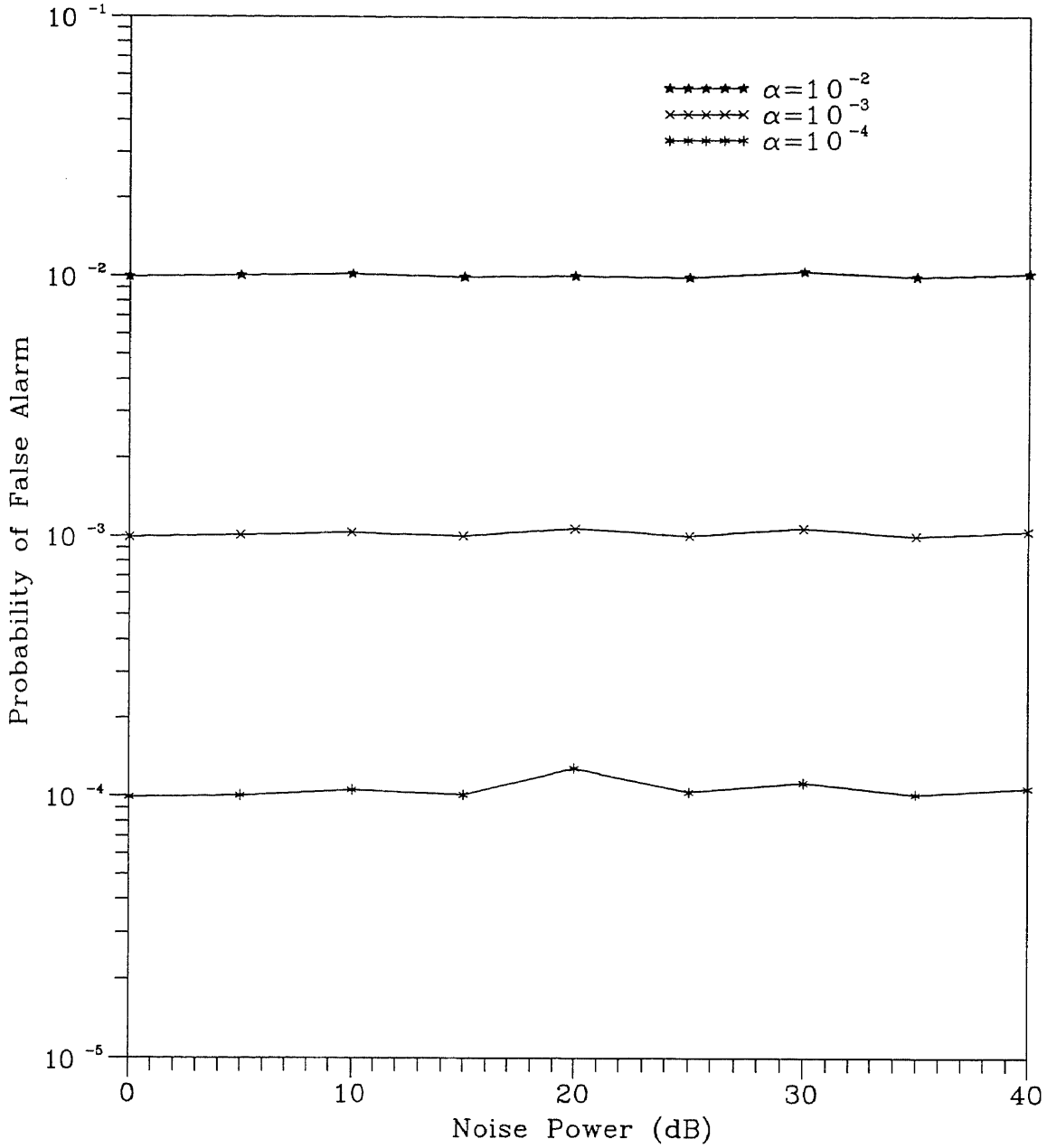

Figure 3.8. Probability of false alarm versus noise power.(dB) N=16, L=4, $\beta=4\times10^{-4}$

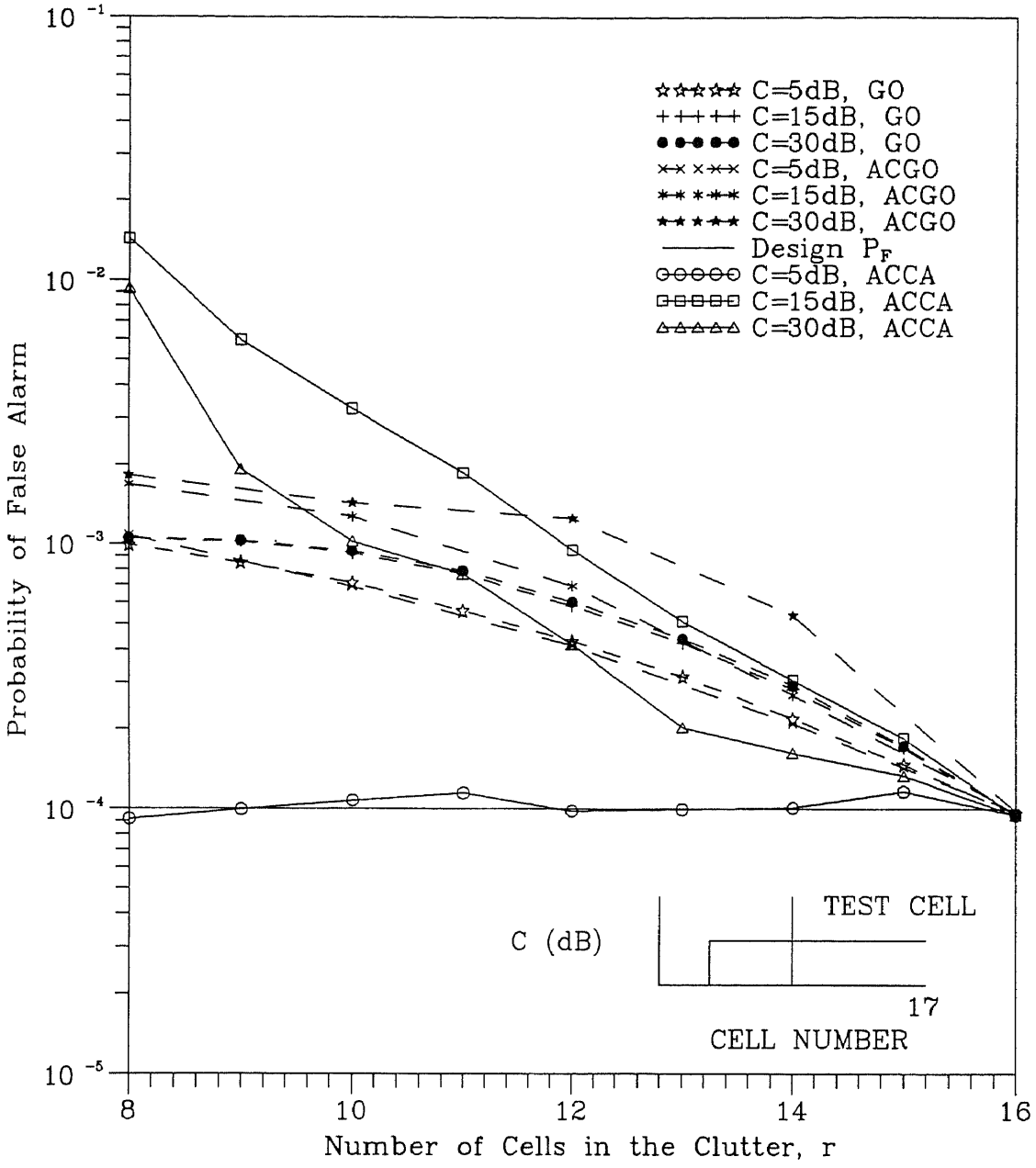

Figure 3.9. Probability of false alarm of the ACCA,GO and the ACGO-CFAR detectors when test cell and r reference cells are in the clutter, and m reference cells are in the clear.
N=16, L=1, $\alpha=10^{-4}$, $\beta=6\times10^{-3}$

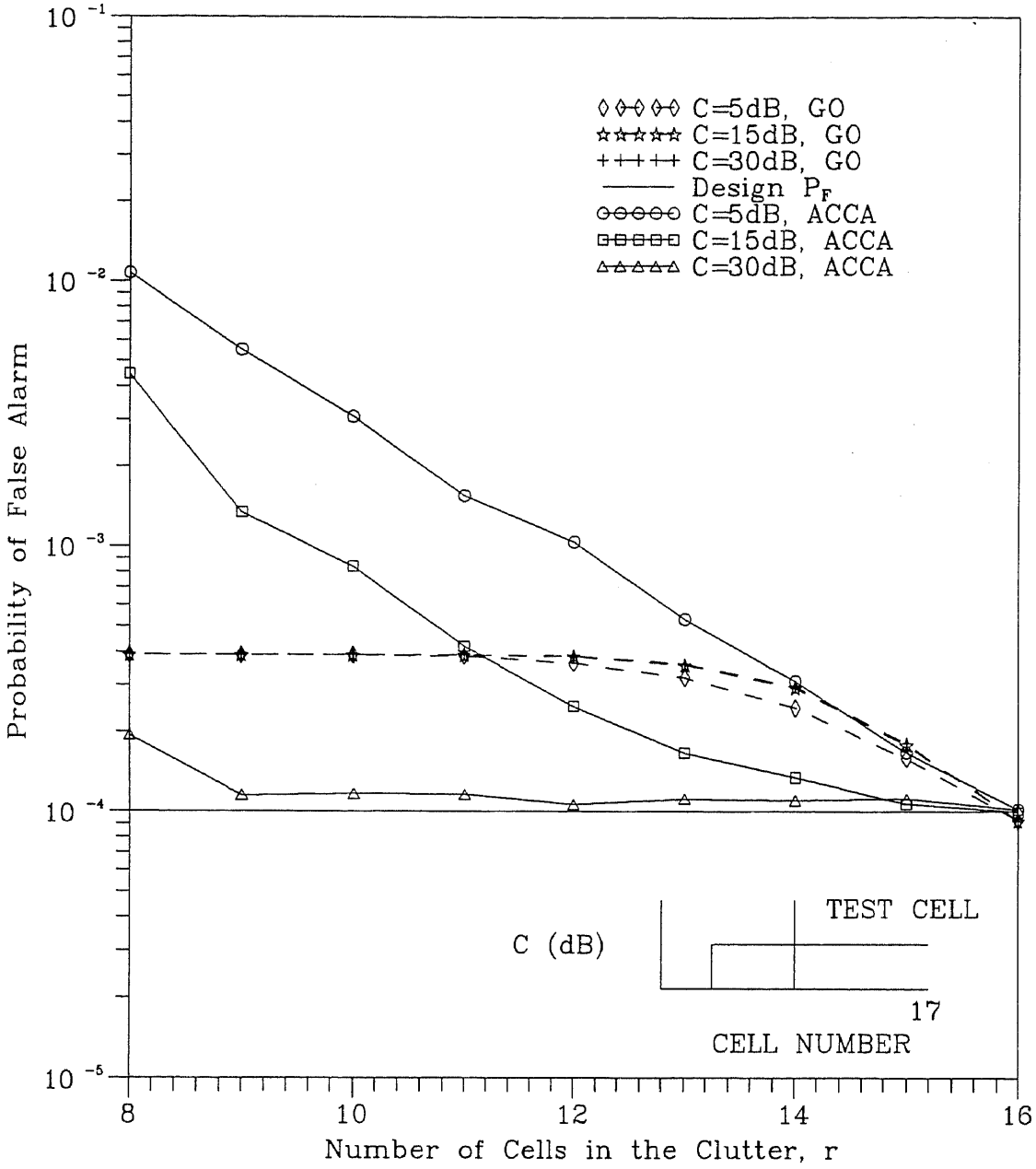

Figure 3.10. Probability of false alarm of the ACCA and the GO-CFAR detectors when test cell and r reference cells are in the clutter, and m reference cells are in the clear.
N=16, L=4, $\alpha=10^{-4}$, $\beta=4\times10^{-3}$

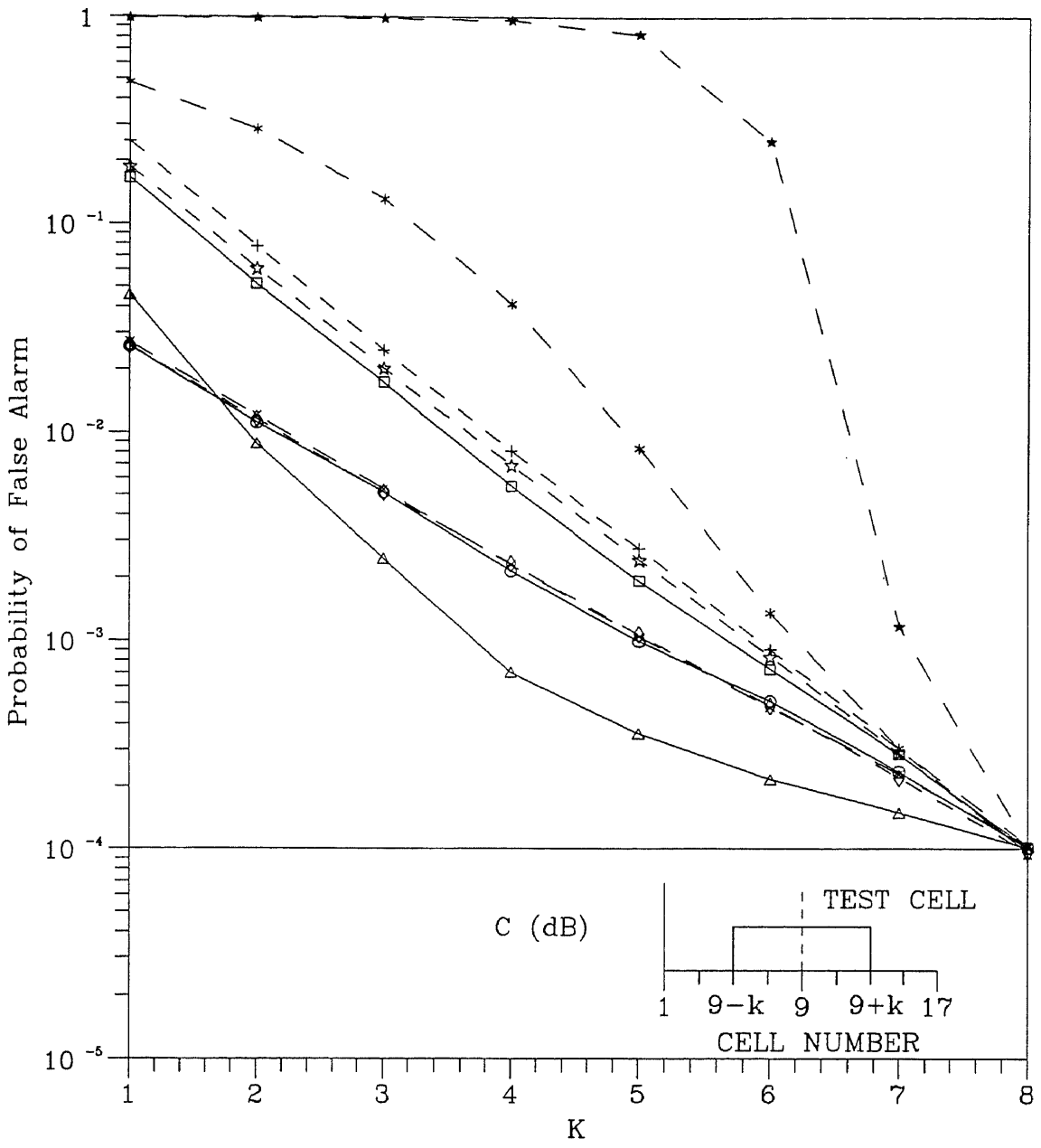

Figure 3.11. Probability of false alarm of the ACCA,GO and the ACGO-CFAR detectors when test cell and r reference cells are in the clutter, and m reference cells are in the clear.
N=16, L=1, $\alpha=10^{-4}$, $\beta=6\times10^{-3}$

C=5dB, ACCA
C=15dB, ACCA
C=30dB, ACCA
C=5dB, GO
C=15dB, GO
C=30dB, GO
C=5dB, ACGO
C=15dB, ACGO
C=30dB, ACGO
Design P_F

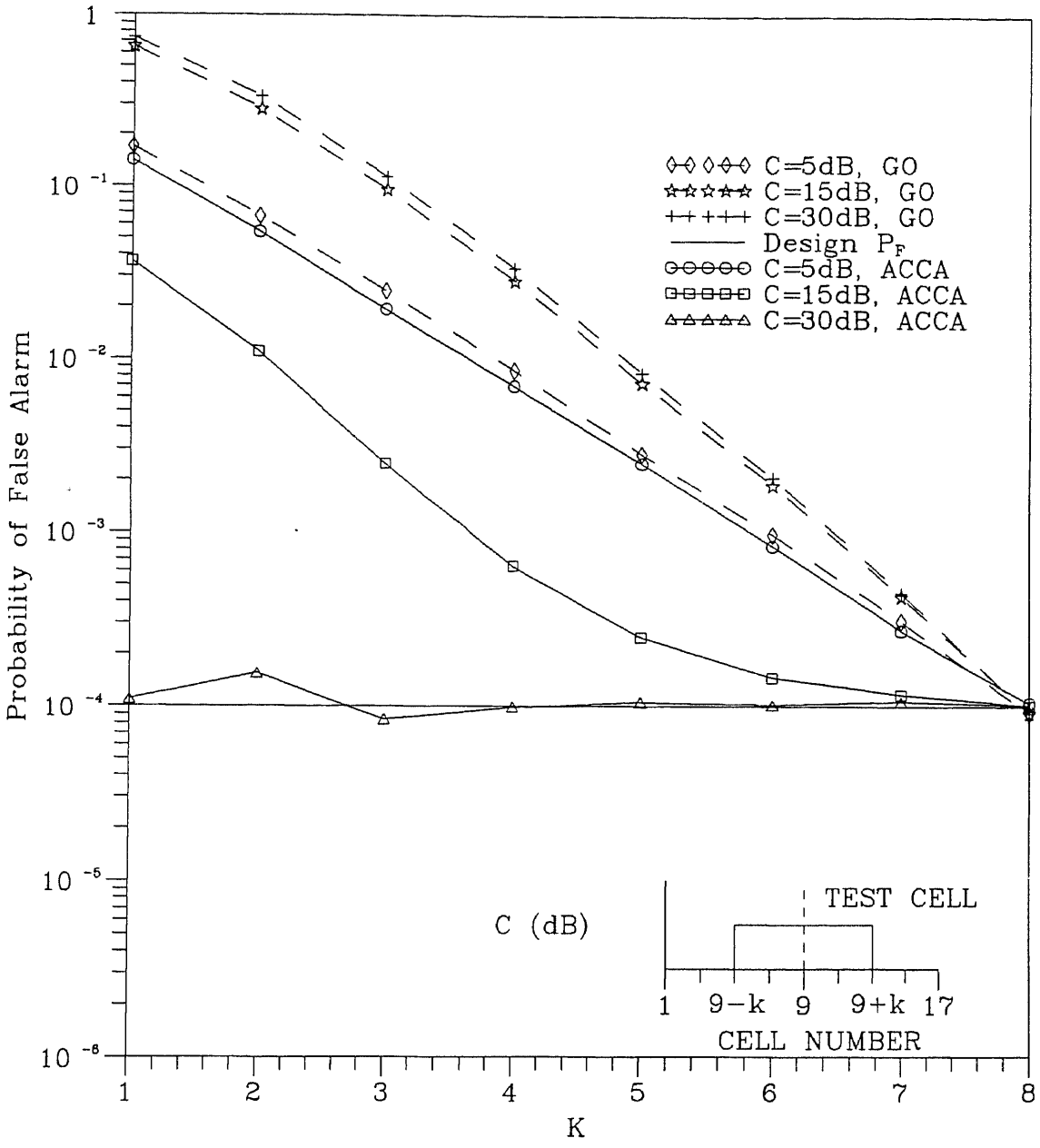

Figure 3.12. Probability of false alarm of the ACCA and the GO-CFAR detectors when test cell and r reference cells are in the clutter, and m reference cells are in the clear.
N=16, L=4, $\alpha=10^{-4}$, $\beta=4\times10^{-3}$

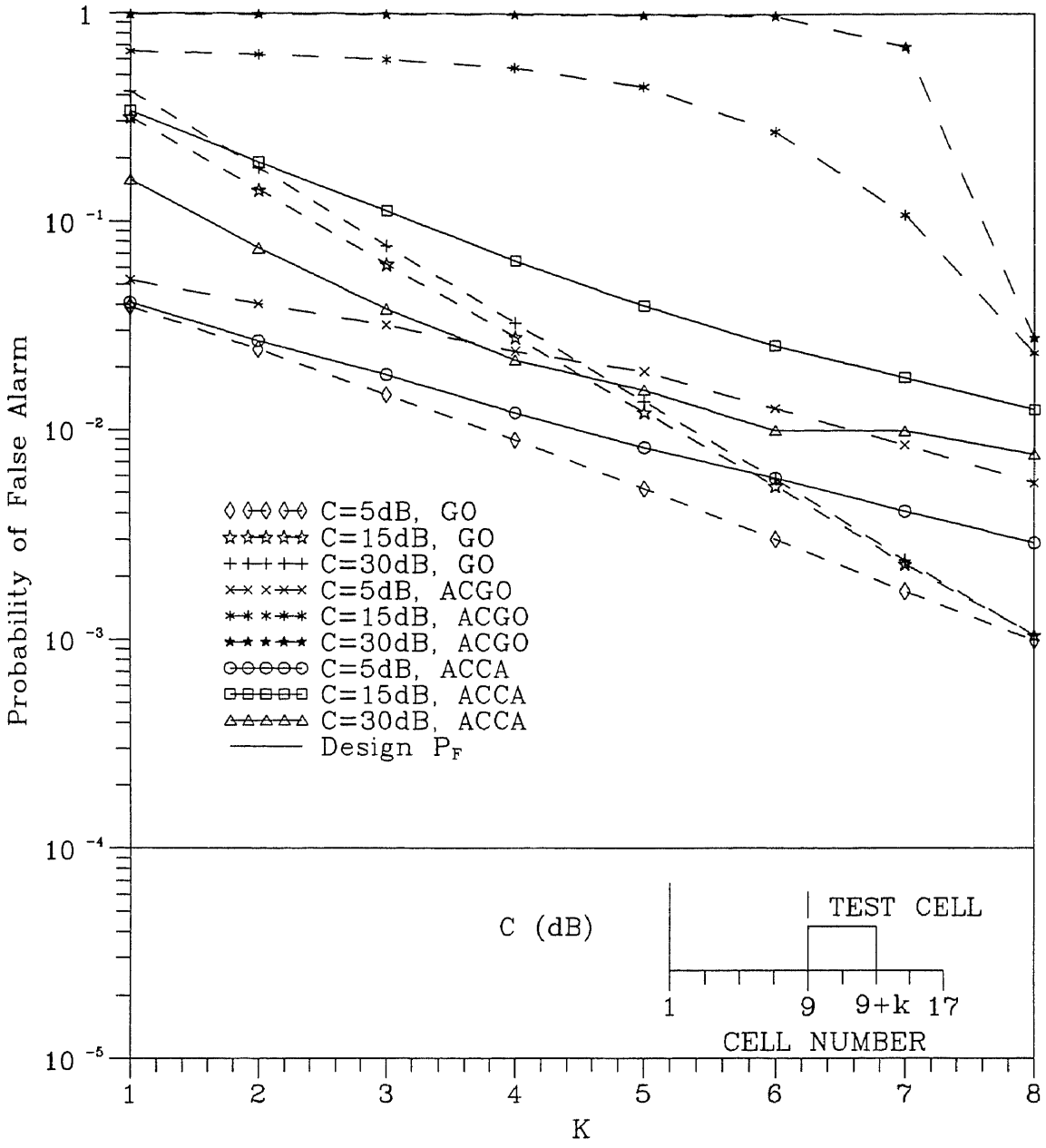

Figure 3.13. Probability of false alarm of the ACCA,GO and the ACGO-CFAR detectors when test cell and r reference cells are in the clutter, and m reference cells are in the clear.
N=16, L=1, $\alpha=10^{-4}$, $\beta=6\times10^{-3}$

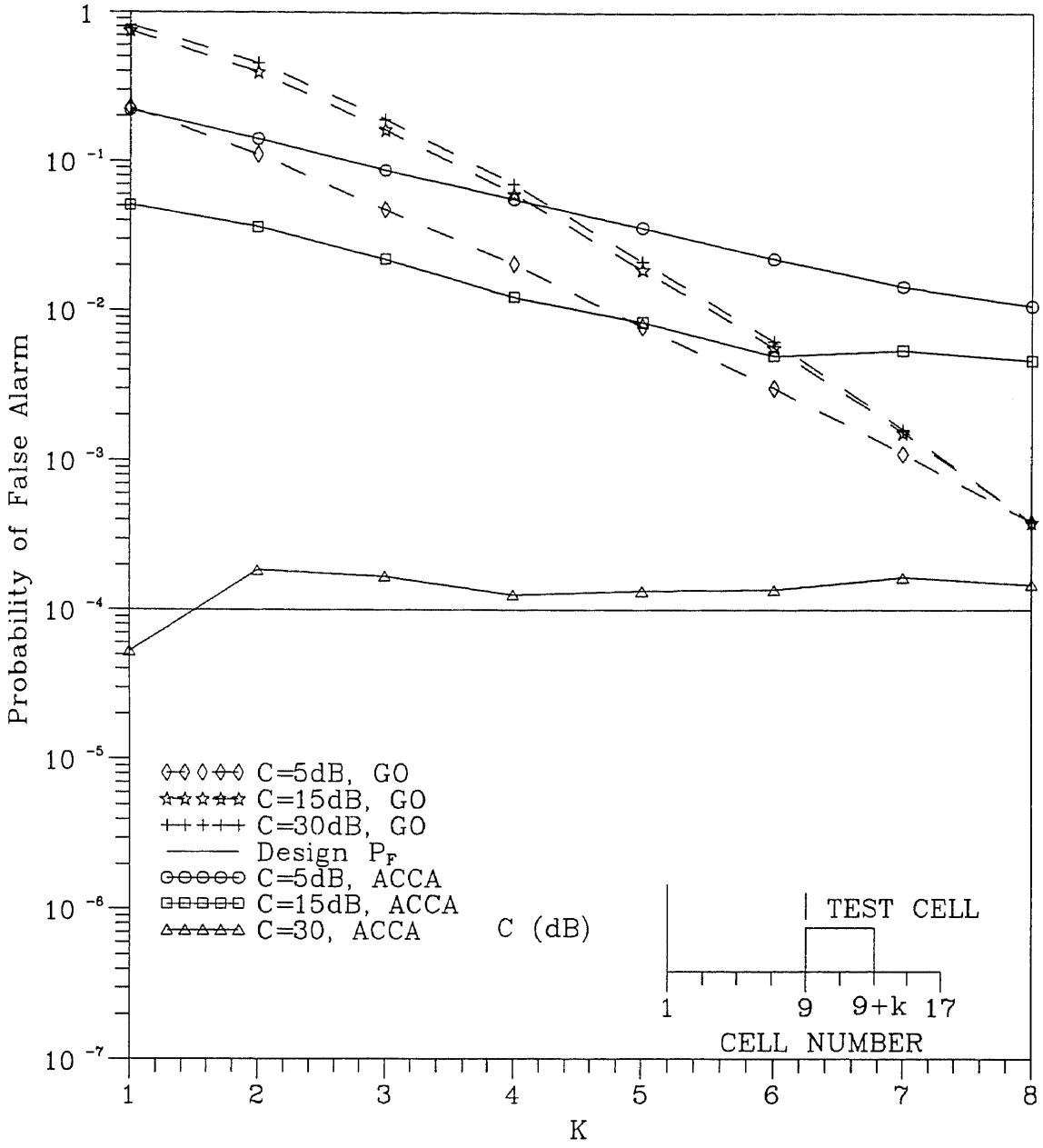

Figure 3.14. Probability of false alarm of the ACCA and the GO–CFAR detectors when test cell and r reference cells are in the clutter, and m reference cells are in the clear. N=16, L=4, $\alpha=10^{-4}$, $\beta=4\times10^{-3}$

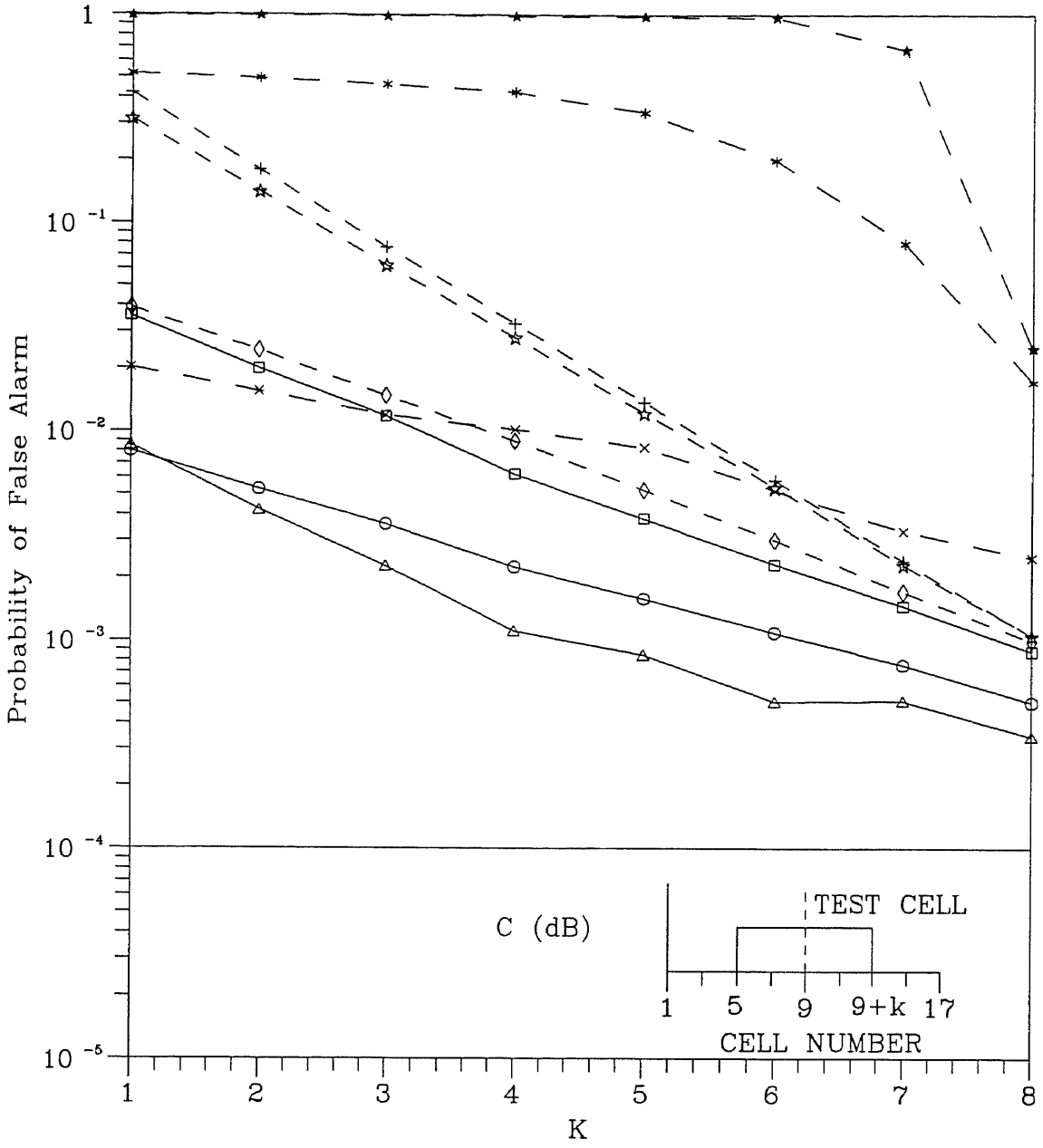

Figure 3.15. Probability of false alarm of the ACCA,GO and the ACGO-CFAR detectors when test cell and r reference cells are in the clutter, and m reference cells are in the clear.
N=16, L=1, $\alpha=10^{-4}$, $\beta=6\times10^{-3}$

◇◇◇◇◇ C=5dB, GO
☆☆☆☆☆ C=15dB, GO
+++++ C=30dB, GO
×××××× C=5dB, AGO
✳✳✳✳✳ C=15dB, AGO
★★★★★ C=30dB, AGO
○○○○○ C=5dB, ACCA
□□□□□ C=15dB, ACCA
△△△△△ C=30dB, ACCA
——— Design P_F

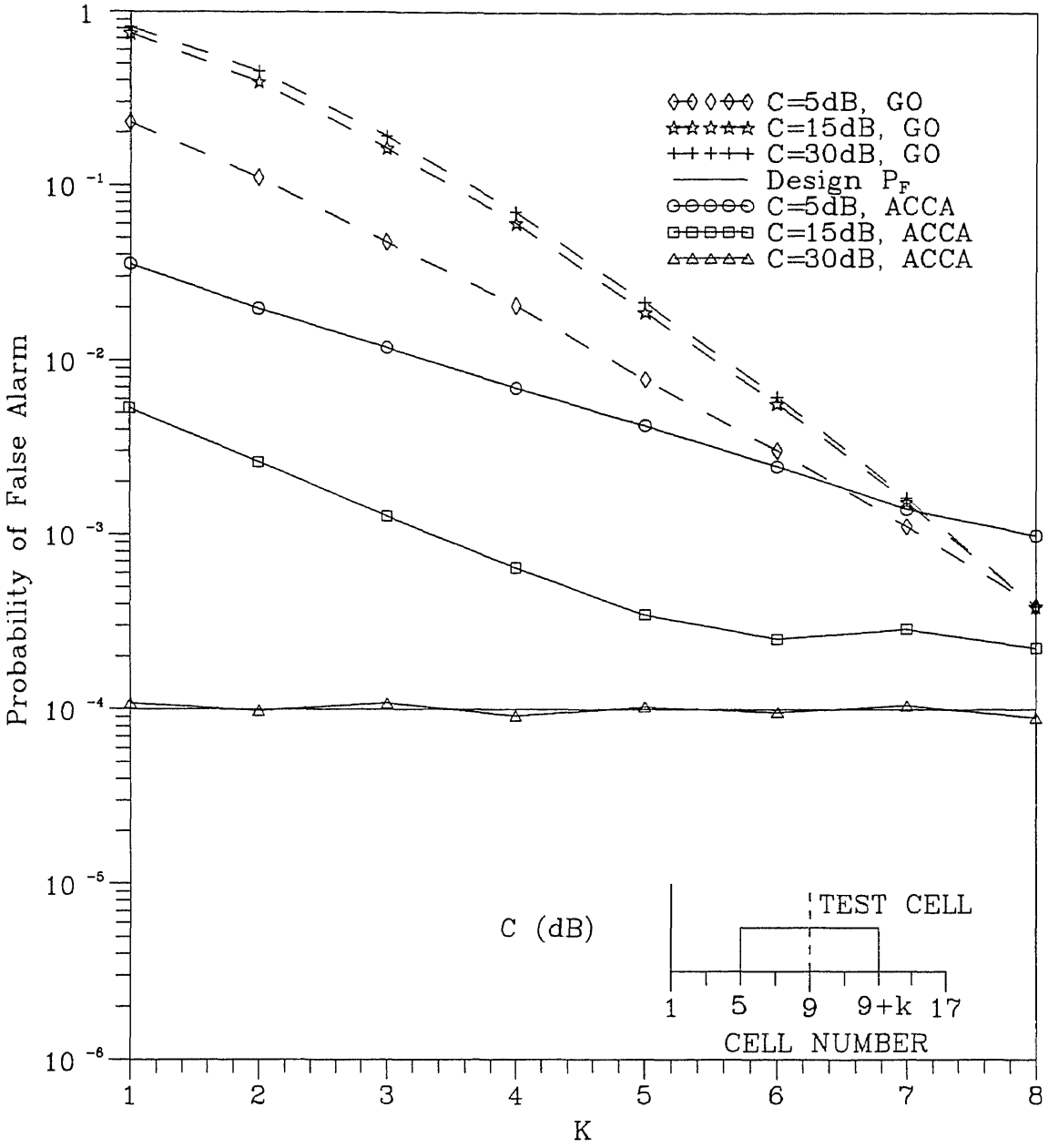

Figure 3.16. Probability of false alarm of the ACCA and the GO-CFAR detectors when test cell and r reference cells are in the clutter, and m reference cells are in the clear. N=16, L=4, $\alpha=10^{-4}$, $\beta=4\times10^{-3}$

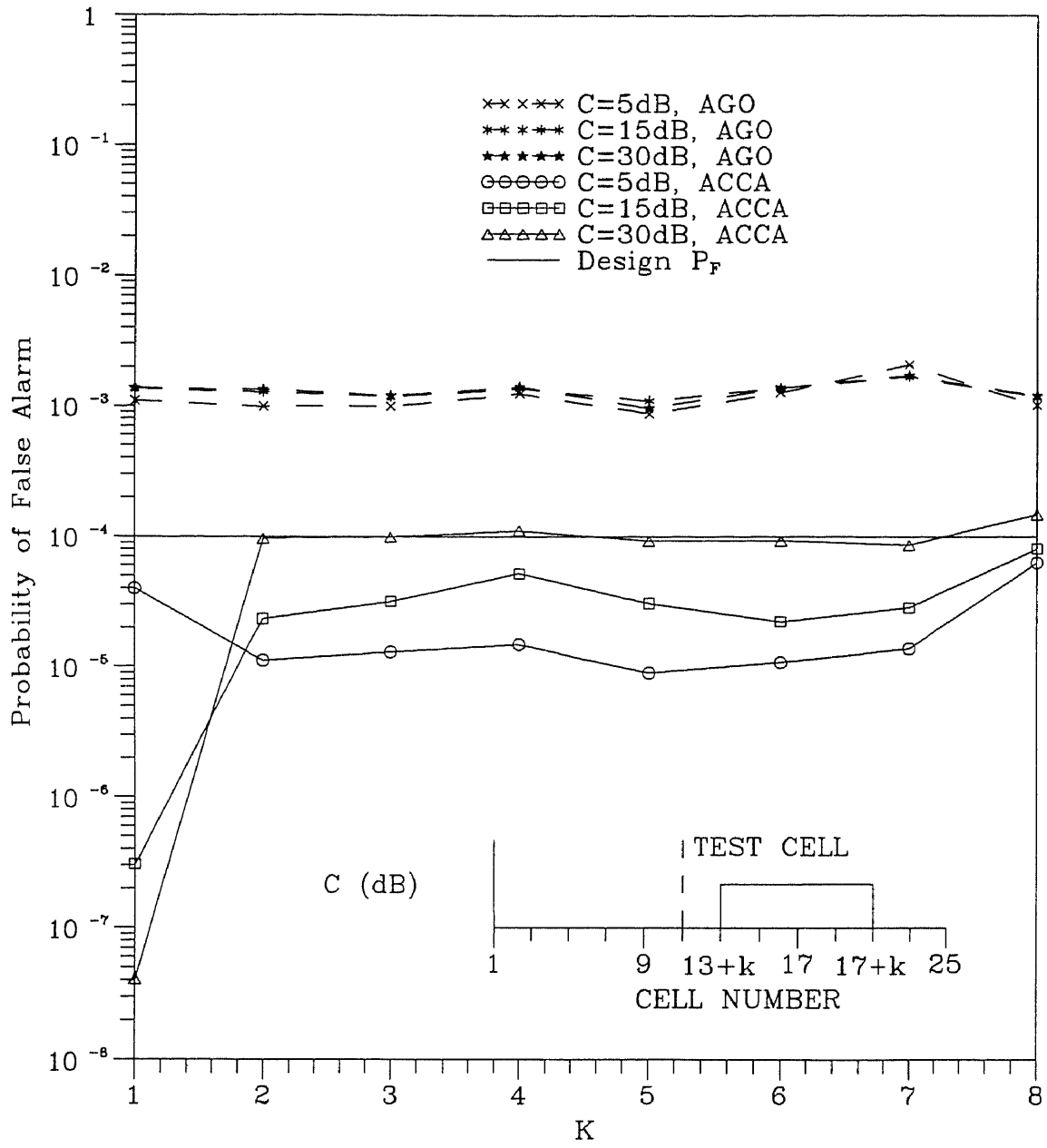

Figure 3.17. Probability of false alarm of the ACCA and the ACGO-CFAR detectors when test cell and m reference cells are in the clear, and r reference cells are in the clutter.
N=24, L=1, $\alpha=10^{-4}$, $\beta=6\times10^{-3}$

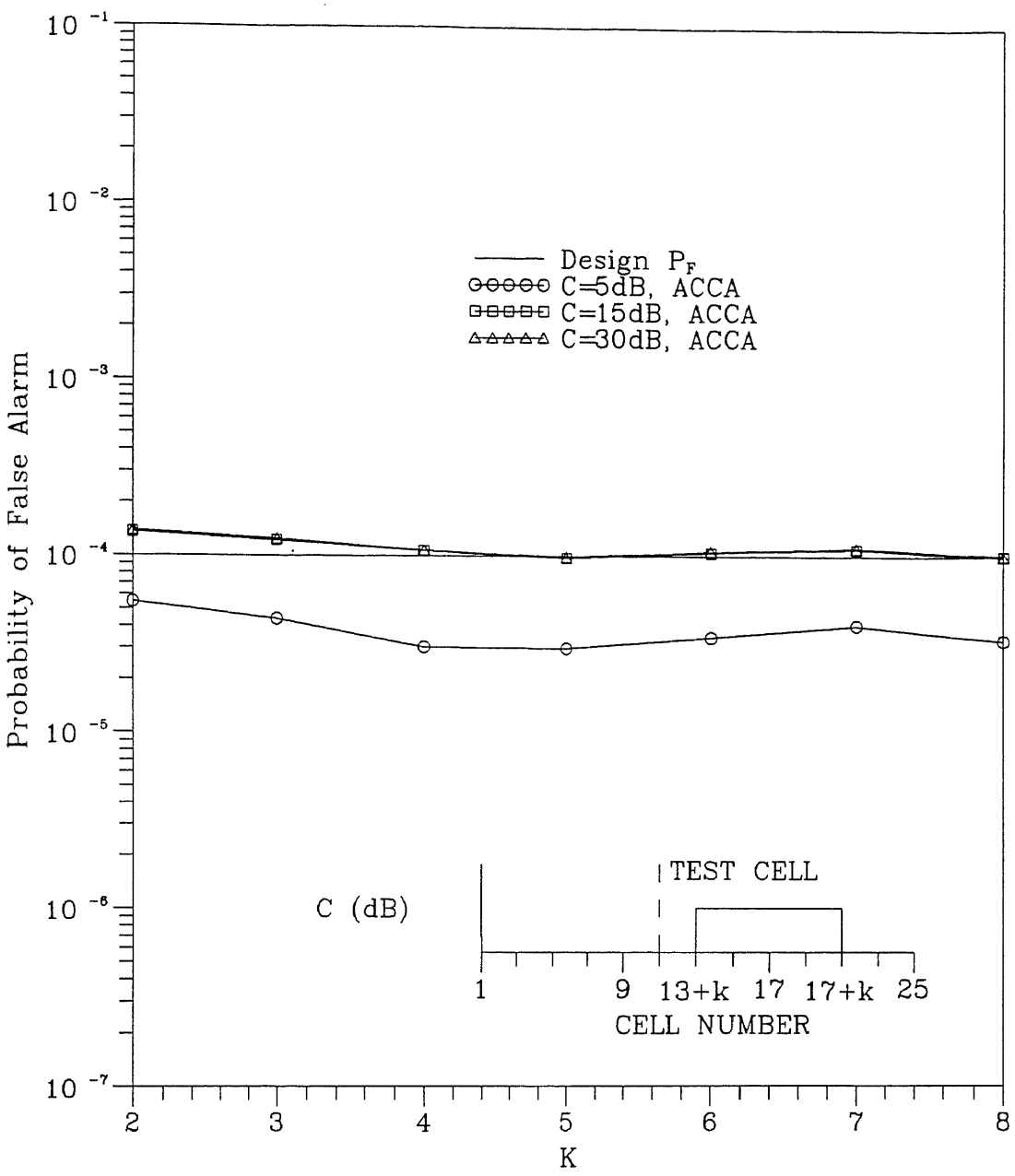

Figure 3.18. Probability of false alarm of the ACCA detector when test cell and m reference cells are in the clear, and r reference cells are in the clutter.
N=24, L=4, $\alpha=10^{-4}$, $\beta=4\times10^{-3}$

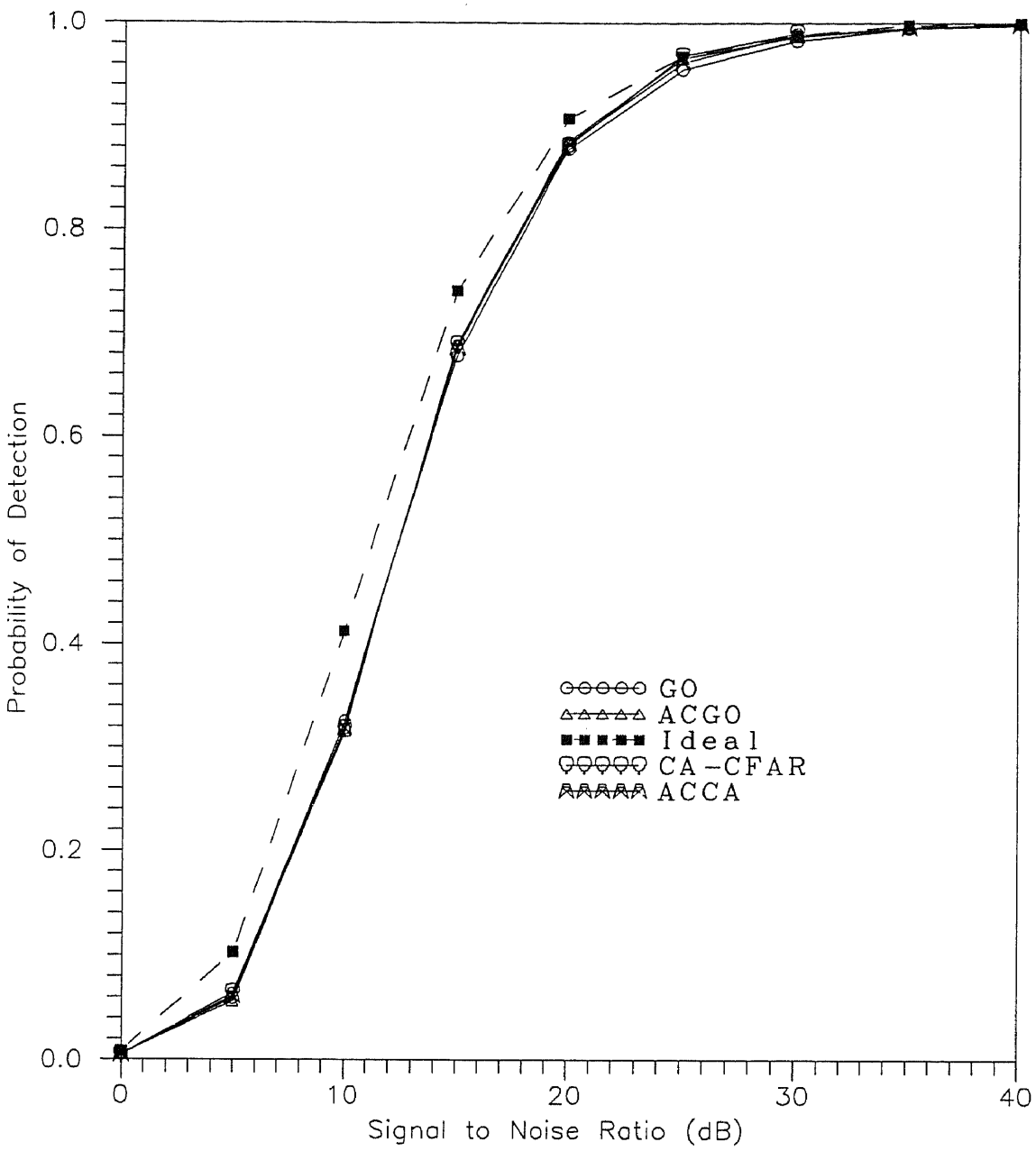

Figure 3.19. Probability of detection of the ACCA,GO,CA Ideal and the ACGO-CFAR detectors in homogeneous background environment.
N=16, L=1, $\alpha=10^{-4}$, $\beta=6\times10^{-3}$.

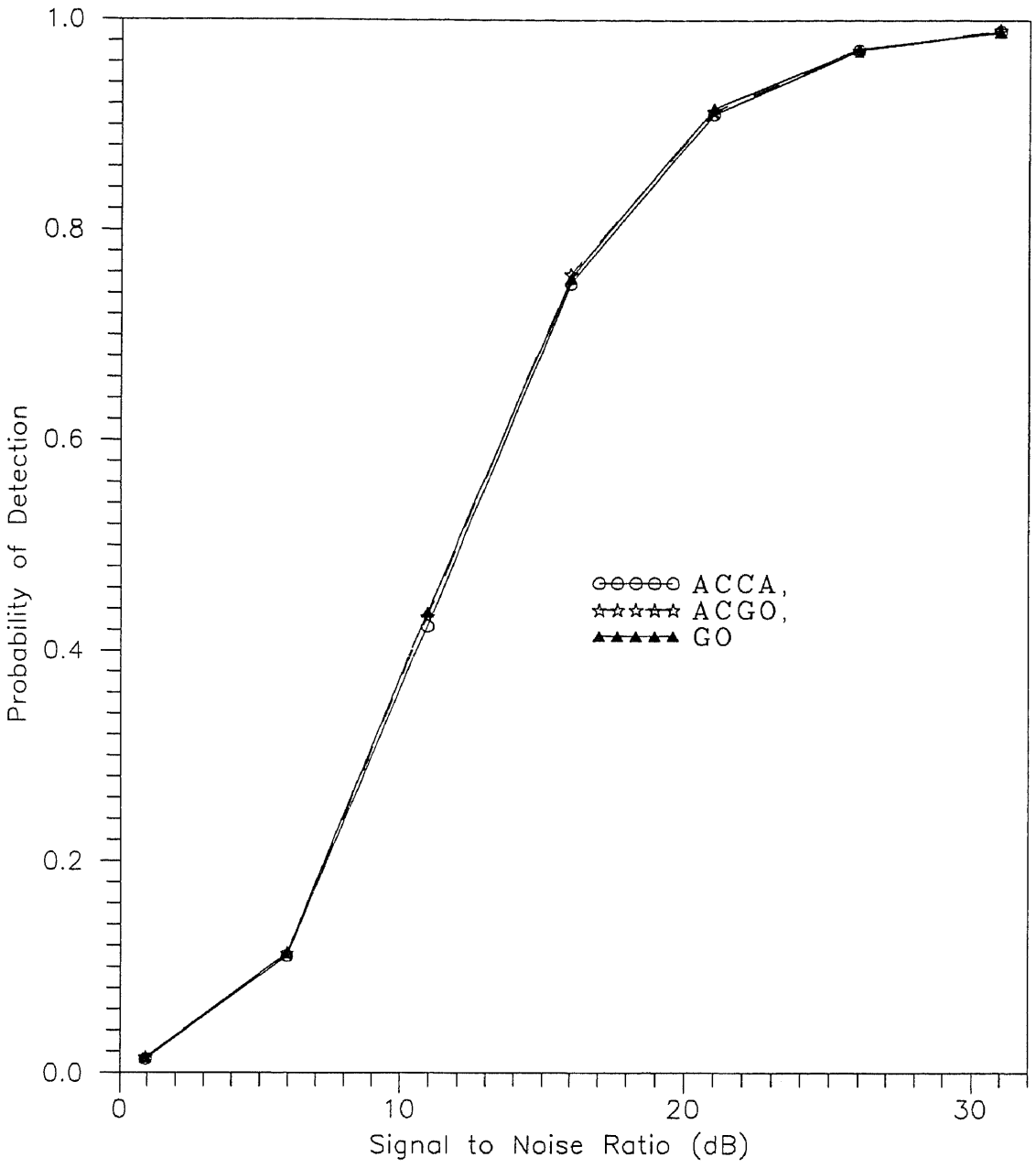

Figure 3.20. Probability of detection of the ACCA,GO and the ACGO–CFAR detectors when test cell and r reference cells are in the clutter, and m reference cells are in the clear. N=16, C=20dB, L=1, $\alpha=10^{-4}$, $\beta=6\times10^{-3}$.

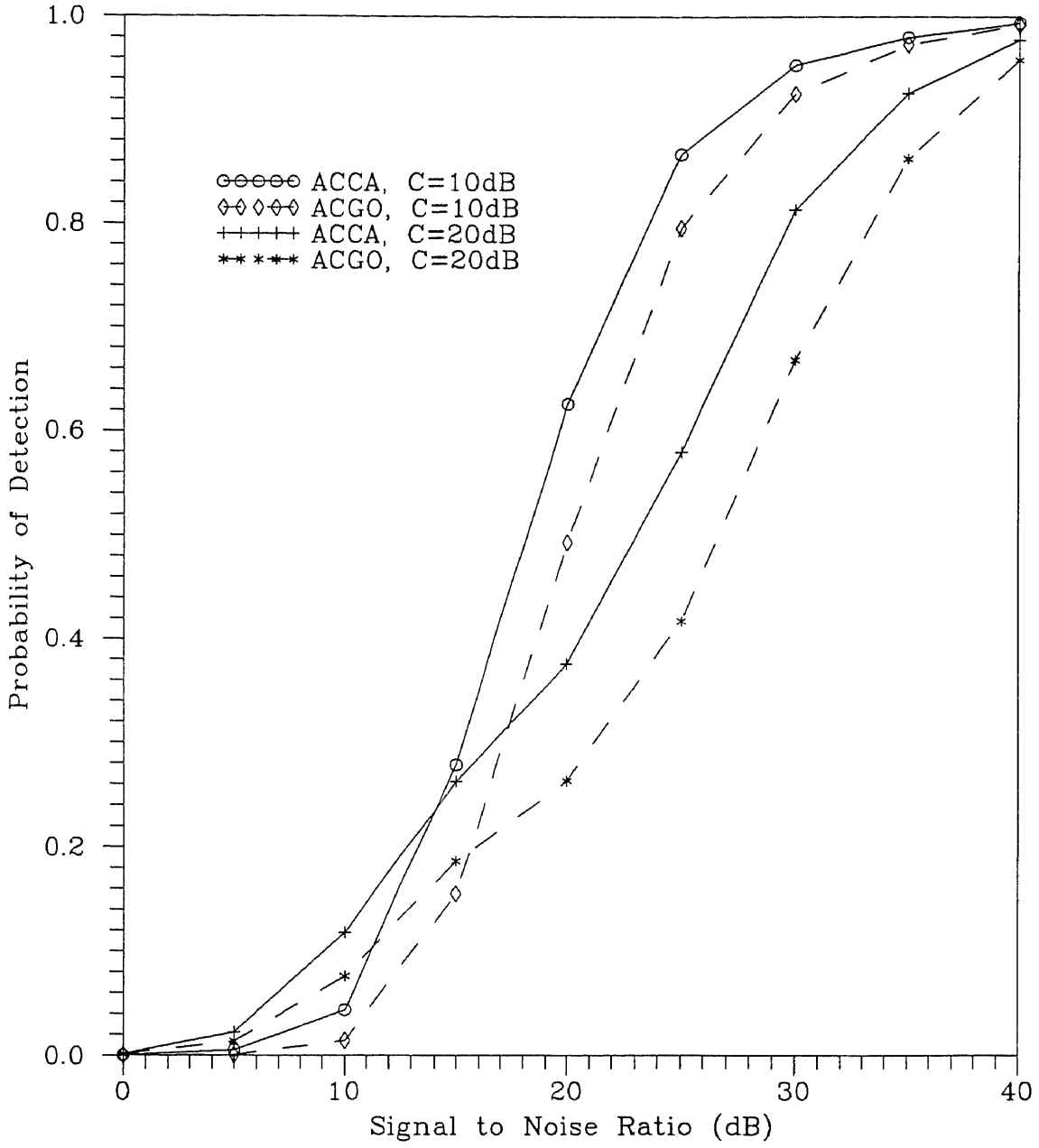

Figure 3.21. Probability of detection of the ACCA and the ACGO-CFAR detectors when test cell and m reference cells are in the clear.
N=16, L=1, $\alpha=10^{-4}$, $\beta=6\times10^{-3}$

Chapter 4

AN ADAPTIVE SPIKY INTERFERENCE REJECTION CFAR DETECTOR

4.1 Introduction

The presence of interfering targets in the reference window of the conventional CA-CFAR detector, causes the adaptive threshold to be raised unnecessarily, and consequently the probability of detection degrades dramatically especially when the number of interfering targets increases. To overcome this problem the SO-CFAR detector was proposed in [14]. However, in the event that interfering targets appear in both the leading and lagging reference window, the SO-CFAR detector also suffers from the capture effect as we saw in chapter 2. In order to alleviate this problem, a number of detection algorithms whose objective is to censor the unwanted spikes, have been proposed in the literature [22-27]. These detection algotithms, first rank order the received observations and use a linear combination of the ordered samples to estimate the detection threshold. The weights of the higher order samples are set equal to zero so that the largest returns which are likely to correspond to interference are not included in the threshold estimation process. The major drawback of these algorithms is that the censoring point is preset. In the event that the number of the samples that are censored is greater than the actual number of interfering targets in the reference window, some of the largest noise samples are censored as well. Therefore, the noise

level in the test cell is underestimated causing an excessive number of false alarms. On the other hand, these detectors suffer from the capture effect if the number of samples that are censored is smaller than the actual number of interfering targets in the reference window. These detectors perform well only when the number of samples that are censored is equal to the number of interfering targets. Thus, a priori information about the number of interfering targets is required for these detectors to perform well. In general, such a priori information is not available. To overcome this problem adaptive censoring algorithms are needed [21,28]. Barboy et al. [21] proposed the censored cell avaraging CCA-CFAR detector where several passes over the data may be required to detect a number of targets that may be present in the window of interest. In [28], the generalized censored mean level detector (GCMLD) has been proposed. The GCMLD employes a signal processing algorithm which adaptively selects the censoring point by performing cell-by-cell tests.

In this chapter, we propose and analyze the Adaptive Spiky Interference Rejection ASIR-CFAR detector which determines and censors the samples that correspond to interfering targets by performing cell-by-cell tests. The remaining samples are combined to form the detection threshold. The ASIR-CFAR detector, like the CCA and GCMLD detectors, does not require a priori knowledge of the interfering environment to perform well. The detection probability of the ASIR, GCMLD and CCA-CFAR detectors in multiple target situations are evaluated and compared. In the case of multiple pulses (L=4), the ASIR-CFAR detector is compared only with the CCA-CFAR detector. The GCMLD detector is not shown because the order statistic analysis required to compute the threshold multipliers is extremely cumbersome. Also, we study the false alarm regulation of the GCMLD and the ASIR-CFAR detectors, for different values of probability of false censoring. A comparison of the ASIR-CFAR detector with that of the GCMLD detector in terms of the required processing time for their implementation is also examined.

In addition, the analysis of the CCA-CFAR detector is extended for for time diversity systems. In real radar systems, time diversity transmission is often used to circumvent the high probability of a deep fade on a single pulse transmission which may result in loss of the signal [36].

In section 4.2, the CCA-CFAR detector is analyzed and we present the mathematical analysis to derive the design equations used for the CCA-CFAR detector in time diversity transmission. In section 4.3 we briefly describe the GCMLD detector. In section 4.4, we present a description of the ASIR-CFAR detector, and we study the effect of the false censoring probability on the design probability of false alarm for both the proposed detector and that of the GCMLD. In section 4.5 the mathematical analysis to derive the design equations used to implement the proposed detector. In section 4.6, the detector performance of the ASIR-CFAR detector is evaluated by means of computer simulations. Its performance is compared with the performance of the CCA-CFAR and GCMLD detector for homogeneous and non-homogeneous background environments. Our conclusions are briefly stated in section 4.7.

4.2 Analysis of the CCA-CFAR Detector

In the CCA-CFAR detector, the procedure for detecting the targets that may lie in the window of interest is as follows [21]:

(i) The sum, s_{N_0}, of the outputs of all the cells (including the one in the middle of the window) is formed,

$$s_{N_0} = \sum_{j=0}^{N} q_j \tag{4.1}$$

where $N_0 = N + 1$. Then, the output of each cell in the entire window is compared to the threshold

$$b_1 = a_0 s_{N_0} \tag{4.2}$$

The samples which exceed this threshold are declared to correspond to target returns. These samples are discarded and the remaining ones which are reindexed are summed to form

$$s_{N_1} = \sum_{j=0}^{N_1-1} q_j \qquad N_1 = N_0 - j_1, \tag{4.3}$$

where j_1 is the number of samples censored in the first step. Notice that the remaining samples have been reindexed.

(ii) The outputs of these remaining cells are compared with a new threshold

$$b_2 = a_1 s_{N_1} \tag{4.4}$$

As in the first step, the j_2 observations that exceed the threshold are decided to correspond to target returns and are not included in the threshold of the third step which is

$$s_{N_2} = \sum_{j=0}^{N_2-1} q_j \qquad N_2 = N_0 - j_1 - j_2 \tag{4.5}$$

The procedure continues in the same manner until no samples exceed the threshold. At the first iteration step the probability of false alarm in any one of the $N+1$ range cells in the window of interest, say the one in the middle, is given by

$$P_F = \Pr(Q_0 > a_0 S_{N_0} | H_0) \tag{4.6}$$

The probability of false alarm can be written as the contour integral

$$P_F = -\frac{1}{2\pi i} \int_C \omega^{-1} \Phi_{R|H_0}(\omega) d\omega \tag{4.7}$$

where the equivalent statistic R is given by

$$R = Q_0 - a_0 S_{N_0} \tag{4.8}$$

In equation (4.7), the contour of integration c is crossing the real ω-axis at $\omega = c_1$ and is closed in an infinite semicircle in the left half ω-plane. C_1 is selected so that

c encloses all the poles of $\Phi_{R|H_0}(\omega)$ that lie in the open half ω-plane. The moment generating function, mgf, of the equivalent statistic R under H_0 is given by

$$\begin{aligned}\Phi_{R|H_0}(\omega) &= E\left[\exp(-\omega\sum_{i=1}^{L} q_{i0}\right] E\left[\exp(\frac{\omega a_0}{1-a_0})\sum_{i=1}^{L}\sum_{j=1,j\neq 0}^{N_0-1} q_{ij}\right] \\ &= (1+\omega)^{-L}(1-\frac{a_0\omega}{1-a_0})^{-L(N_0-1)} \end{aligned} \tag{4.9}$$

Substituting equation (4.9) into (4.7) and with the residue at $\omega = -1$ given by

$$\text{Res}_{\omega\to -1} = \frac{1}{(L-1)!}\lim_{\omega\to -1}\frac{d^{L-1}}{d\omega^{L-1}}\left[\omega^{-1}(1-\frac{\omega a_0}{1-a_0}^{-L(N_0-1)}\right] \tag{4.10}$$

the probability of false alarm is derived to be

$$P_F = \sum_{k=0}^{L-1}\left(\begin{array}{c} L(N_0-1)+k-1 \\ k \end{array}\right)\frac{(\frac{a_0}{1-a_0})^k}{(1+\frac{a_0}{1-a_0})^{L(N_0-1)+k}} \tag{4.11}$$

If we let $L = 1$(single pulse transmission) in equation (4.11) then,

$$P_F = (1-a_0)^{N_0-1} \tag{4.12}$$

The threshold multiplier for the first iteration a_0 is computed by solving $P_F = \alpha$. In [21], the exact threshold multipliers for the subsequent iterations have not been computed because the analysis is too cumbersome. Instead they are computed from

$$(1-a_{j-1})^{N_j-1} = \alpha \tag{4.13}$$

which is similar to (4.12). Following the same approach, the threshold multipliers in time diversity transmission are computed from

$$P_F = \sum_{k=0}^{L-1}\left(\begin{array}{c} L(N_j-1)+k-1 \\ k \end{array}\right)\frac{(\frac{a_0}{1-a_0})^k}{(1+\frac{a_0}{1-a_0})^{L(N_j-1)+k}} \tag{4.14}$$

which is similar to (4.11). Next we give a brief description of the GCMLD detector along with the design equations.

4.3 The GCMLD Detector

The Generalized Censored Mean Level Detector, GCMLD, which does not require any prior knowledge about the number of interfering targets and achieves robust CFAR performance was proposed in [28]. The number of interfering targets is determined by a censoring procedure which is applied to both the leading and the lagging range cells independantly.

The outputs of the range cells are ranked in ascending order according to their magnitude to yield the $N(M = N/2)$ ordered samples

$$q_{(1)} \leq q_{(2)} \leq \cdots q_{(M)} \tag{4.15}$$

Let the lowest ordered sample, $q_{(1)}$, represent the estimate of the background noise level. $q_{(2)}$ is then compared to the threshold $T_1 q_{(1)}$, where T_1 is a scaling constant chosen to achieve a desired probability of false censoring, P_{FC}, the rank-ordered samples $q_{(j)}, j = 2, \ldots, M$. If $q_{(2)}$ is greater than $T_1 q_{(1)}$, it is decided that the samples corresponding to $q_{(j)}, j = 2, \ldots, M$ are returns from interfering targets and therefore will be censored. If $q_{(2)}$ is less than $T_1 q_{(1)}$, then $q_{(2)}$ it is decided to correspond to a noise sample without interference. In this case, the sum of the lower two ordered samples $S_2 = q_{(1)} + q_{(2)}$ is formed. $q_{(3)}$ is the compared to a new adaptive threshold $T_2 S_2$. If $q_{(3)}$ exceeds $T_2 S_2$, it is declared to correspond to an interfering target return and it is censored together with the samples that are greater than $q_{(3)}$. Otherwise, $q_{(3)}$ is declared to be a noise sample without interference. In general, at the kth step, $q_{(k+1)}$ is compared to $T_k S_k$, and a decision is made according to

$$q_{k+1} \underset{H_0}{\overset{H_1}{\gtrless}} T_k \, S_k \tag{4.16}$$

where T_k is the kth scaling constant, and S_k is the sum of the lower k ordered samples. Using the expression in (4.16), the probability of false censoring, P_{FC}, is given by [28]

$$P_{FC} = \frac{(M - k + 1)}{(1 + T_{M-k})^{M-k}} \tag{4.17}$$

Assuming that m_1 samples are censored from the leading cells and m_2 samples are censored from the lagging cells, then the remaining samples in the leading and the lagging window are combined to form an estimate, q, of the noise level in the cell under test. q is then scaled by the constant T to achieve the desired probability of false alarm, P_F, which is given by [28]

$$P_F = \frac{1}{(1+T)^{N-m}} \tag{4.18}$$

4.4 The ASIR-CFAR Detector

In this section, the ASIR-CFAR detector is described and analyzed. Without loss of generality, we assume that no two adjacent range cells may contain spiky interference for this situation may be viewed as the case of a group of cells in the clutter, which was the topic of chapter 3. The censoring procedure starts by comparing q_1 with a scaled version of q_2, $T_i q_2$. The scaling constant T_i is selected to satisfy the desired probability of false censoring γ. The desired choice of γ is presented later in the paper. If $q_1 > T_i q_2$, it is declared to correspond to an interfering target return. Consequently, q_1 is censored. If $q_1 < T_i q_2$, one or two possible hypotheses might be true; either q_1 and q_2 are both noise only samples or q_2 is an interfering target return. The second step of the censoring procedure depends on the outcome of the first one. If q_1 has been declared to be an interfering target return, the censoring algorithm proceeds by testing q_3 since q_2 must be a noise only sample as no two adjacent range cells contain interfering targets. On the other hand, if the outcome of the first step is $q_1 < T_i q_2$, we proceed by testing q_2.

• In the former case, q_3 is compared to both $T_i q_2$ and $T_i q_4$. If $q_3 > T_i q_2$ and $q_3 > T_i q_4$, q_3 is decided to correspond to an interfering target return and is therefore censored. In a similar manner as bofore the algorithm proceeds by testing q_5. If these two conditions are not satisfied, q_3 is decided to be a noise sample and q_4 is then tested.

• In the latter case, q_2 is compared to both $T_i q_1$ and $T_i q_3$. If $q_2 > T_i q_1$ and $q_3 > T_i q_3$, q_2 is censored as it is declared to correspond to an interfering target return and the algorithm proceeds by testing q_4, otherwise, q_4 is tested in the next step.

In general, q_j is compared to $T_i q_{j-1}$ and $T_i q_{j+1}$. If $q_j > T_i q_{j-1}$ and $q_j > T_i q_{j+1}, q_j$ is censored and the algorithm proceeds by testing q_{j+2}. Otherwise, q_j is not censored and q_{j+1} is tested in the next step. The procedure continues in the same manner until a decision about q_{N-1} is made. If q_{N-1} is decided to be an interfering target return, the algorithm stops since its adjacent observation q_N cannot correspond to an interfering target return. If q_{N-1} has not been censored, a decision about q_N is made by comparing it with $T_i q_{N-1}$. If $q_N > T_i q_{N-1}$, q_N is censored. Otherwise q_N is included in the threshold estimation process. After the censoring procedure finishes, the noise level estimate, q, is defined to be the sum of the uncensored samples. The output of the test cell is then compared to the adaptive threshold $T(J)q$, that is,

$$q_0 \underset{H_0}{\overset{H_1}{\gtrless}} T(J)\, q \tag{4.19}$$

in order to determine the presence (H_1) or absence (H_0) of a target in the test cell. The scaling constant $T(J)$ is chosen so that the design false alarm probability, P_F, is satisfied. Assuming m samples are censored by the censoring procedure, then the veriable J ($J = N - m$), is the number of samples that survive the censoring process. In Figures 4.1 and 4.2 we plot the probability of false alarm versus the probability of false censoring for $L = 1, 4$ and $\alpha = 10^{-4}$ and 10^{-6}, for the GCMLD and the ASIR-CFAR detectors. Note that by setting the design value of $P_{FC} = \gamma$, we desire to falsely declare a noise sample as a sample of a return echo from an interfering target with probability γ, while by setting the value of $P_F = \alpha$ means that we desire to falsely declare a noise sample in the test cell as a target return with probability α. If $\gamma > \alpha$ overcensoring is encouraged which cause the actual probability of false alarm to increase. If $\gamma < \alpha$ censoring is discouraged and the interfering targets are

censored with lower probability causing impaired target detectability. We observe that when $\alpha = 10^{-4}$ and the desired P_{FC} is less than 2×10^{-3} the probability of false alarm that is achieved by th ASIR-CFAR detector is equal to the design value. On the other hand, when the desired P_{FC} is greater than 2×10^{-3} the probability of false alarm increases above the design value. This is due to the fact that when P_{FC} is large overcensoring is encouraged. Therefore, the probability of censoring some of the largest noise samples, which causes underestimation of the noise level in the test cell, is high. Thus, when $\alpha = 10^{-4}$ we choose the desired value of P_{FC} to be 2×10^{-3}. Observe that the maximum value of P_{FC} with which α is achieved is selected because any P_{FC} smaller than that will discourage censoring of possible interfering targets thereby reducing the censoring capabilities of the proposed algorithm. Similarly, when $\alpha = 10^{-6}$ the optimum choice of P_{FC} is 10^{-3}. Similarly for the case of multiple pulse ($L = 4$) when $\alpha = 10^{-4}$ or 10^{-6} the optimum choice of P_{FC} is 3×10^{-3} and 2×10^{-3} respectively. In Figure 4.2, we show the probability of false alarm versus the probability of false censoring for $N = 16$ and 32 and $\alpha = 10^{-4}$ and 10^{-6}, for the GCMLD detector. In [28] where the GCMLD was proposed and analyzed no study was presented on the effect of the probability of false censoring on the probability of false alarm. So in the case of the GCMLD we also study the effect of the probability of false censoring on the probability of false alarm and we choose the optimum value for the probability of false censoring. The probability of false censoring was chosen to be the same as the probability of false alarm. We observe that when $\alpha = 10^{-4}$ and the desired probability of false censoring is less than 10^{-4} the probability of false alarm achieved by the GCMLD detector is equal to the design value for both $N = 16$ and 32. On the other hand when the desired probability of false censoring is greater than 10^{-4} the probability of false alarm increases above the desired value for both $N = 16$ and 32. Similarly, when $\alpha = 10^{-6}$ the optimum choice for the probability of false censoring is 10^{-6}. Thus, in the case of the GCMLD detector the optimum value

for the probability of false censoring will be the same as α.

4.5 Analysis of the ASIR-CFAR Detector

At the jth step, $j \neq 1, N$, the probability of false censoring , P_{FC}, is the probability that Q_j exceeds both $T_i Q_{j-1}$ and $T_i Q_{j+1}$ when Q_{j-1}, Q_j and Q_{j+1} are noise only samples (hypothesis H_{000}), that is,

$$P_{FC} = \Pr(Q_j > T_i Q_{j-1}, Q_j > T_i Q_{j+1} | H_{000}) \tag{4.20}$$

and can be written as

$$\begin{aligned} P_{FC} &= \left\{\frac{1}{\Gamma(L)}\right\}^3 \int_0^\infty dq_j^{L-1} \exp(-q_j) \int_0^{q_j/T_i} dq_{j-1}^{L-1} \exp(-q_{j-1}) \\ &\quad \cdot \int_0^{q_j/T_i} dq_{j+1}^{L-1} \exp(-q_{j+1}) \end{aligned} \tag{4.21}$$

where by evaluating the inner intagrals we obtain

$$\begin{aligned} P_{FC} &= \left\{\frac{1}{\Gamma(L)}\right\}^3 \int_0^\infty \left\{ q_j^{L-1} \exp(-q_j[1+2/T_i]) \sum_{r=0}^{L-1} \frac{(-1)(L-1)! q_j^{L-1-r} \frac{1}{T_i}^{L-1-r}}{(L-1-r)!} \right. \\ &\quad \cdot \sum_{k=0}^{L-1} \frac{(-1)(L-1)! q_j^{L-1-k} \frac{1}{T_i}^{L-1-k}}{(L-1-k)!} + q_j^{L-1} \exp(-q_j)(L-1)!^2 \\ &\quad \left. +2 q_j^{L-1} \exp(-q_j[1+1/T_i]) \sum_{r=0}^{L-1} \frac{(-1) q_j^{L-1-r} \frac{1}{T_i}^{L-1-r}}{(L-1-r)!} \right\} dq_j \end{aligned} \tag{4.22}$$

and P_{FC} is obtained to be

$$\begin{aligned} P_{FC} &= \sum_{r=0}^{L-1} \sum_{k=0}^{L-1} \frac{(1/T_i)^{2L-2-k-r}(3L-3-r-k)!((L-1)!)^{-1}}{(L-1-k)!(L-1-r)!(1+2/T_i)^{3L-2-r-k}} + 1 \\ &\quad -2 \sum_{r=0}^{L-1} \frac{((L-1)!)^{-1}(1/T_i)^{L-1-r}(2L-2-r)!}{(L-1-r)!(1+1/T_i)^{2L-1-r}} \end{aligned} \tag{4.23}$$

In the censoring procedure presented in section 4.4, the first and the last samples are tested separately, for possible interfering targets, from all the other samples in the reference window, since there is only one adjacent reference sample, that is q_2 for the

first sample and q_{N-1} for the last sample. Thus, the probability of false censoring the first sample can be written as

$$P_{FC} = \Pr(Q_1 > T_i Q_2 | H_{00}) \tag{4.24}$$

while the probability of false censoring the last sample is

$$P_{FC} = \Pr(Q_N > T_i Q_{N-1} | H_{00}) \tag{4.25}$$

In equations (4.24) and (4.25), hypothesis H_{00} denotes the case where the two samples involved in these tests, are noise only samples. Considering the expresion in (4.25) P_{FC}, can be written as a contour integral of the moment generating function, mgf, of the equivalent statistic $R_N = Q_N - T_i Q_{N-1}$ where q_N and q_{N-1} are the observations from the last and the $(N-1)$th reference cells respectively. The scaling constant T_i is selected so that the desired probability of false censoring, γ, is achieved. Thus,

$$\begin{aligned} P_{FC} &= \Pr(R_N > 0 | H_{00}) \\ &= -\frac{1}{2\pi i} \int_c \omega^{-1} \Phi_{R_N|H_{00}}(\omega) d\omega \end{aligned} \tag{4.26}$$

where the mgf of the equivalent statistic R_j is given by

$$\begin{aligned} \Phi_{R_j|H_{00}} &= E\left[\exp(-\omega(\sum_{i=1}^{L} q_{ij} - T_c \sum_{i=1}^{L} q_{i(j-1)}))\right] \\ &= \int_0^\infty \cdots \int_0^\infty \exp\left(-\sum_{i=1}^{L} q_{ij}\right) \exp\left(-\omega \sum_{i=1}^{L} q_{ij}\right) dq_{ij} \ldots dq_{Lj} \\ &\quad \cdot \int_0^\infty \cdots \int_0^\infty \exp\left(-\sum_{i=1}^{L} q_{i,j-1}\right) \exp\left(T_c \omega \sum_{i=1}^{L} q_{i,j-1}\right) dq_{i,j-1} \ldots dq_{L,j-1} \\ &= \left[\left(\frac{1}{1+\omega}\right)\left(\frac{1}{1-T_c\omega}\right)\right]^L \end{aligned} \tag{4.27}$$

In equation (4.26), the contour of integration c is crossing the real ω-axis at $\omega = c_1$ and is closed in an infinite semicircle in the left half ω-plane. c_1 is selected so that c encloses all the poles of $\Phi_{R_N|H_{00}}(\omega)$ that lie in the open left half ω-plane. For these two tests, P_{FC} is obtained by substituting equation (4.27) into (4.26), thus,

$$P_{FC} = \sum_{k=0}^{L-1} \binom{L+k-1}{k} \frac{T_i^k}{(1+T_i)^{L+k}} \tag{4.28}$$

That is the scaling constant is calculated from

$$P_{FC} = \begin{cases} \sum_{r=0}^{L-1} \sum_{k=0}^{L-1} \frac{(1/T_i)^{2L-2-k-r}(3L-3-r-k)!((L-1)!)^{-1}}{(L-1-k)!(L-1-r)!(1+2/T_i)^{3L-2-r-k}} + 1 & j \neq 1, N \\ -2\sum_{r=0}^{L-1} \frac{((L-1)!)^{-1}(1/T_i)^{L-1-r}(2L-2-r)!}{(L-1-r)!(1+1/T_i)^{2L-1-r}} & \\ \sum_{k=0}^{L-1} \begin{pmatrix} L+k-1 \\ k \end{pmatrix} \frac{T_i^k}{(1+T_i)^{L+k}} & j = 1, N \end{cases} \tag{4.29}$$

In Figure (4.3) we compare the censoring capabilities of the proposed detector in the case where time diversity transmission is employed, that is, $L = 4$. We assume that two interfering targets are present in the reference window. Clearly for both probabilities of false alarm considered, that is, 10^{-4} and 10^{-6}, when $L = 4$ the censoring probability of the ASIR-CFAR detector improves dramatically due to the enhanced performance offered by the time diversity transmission. For example when the signal to noise ratio is 20dB, for L =1 the probability of detection is approximately 0.45 while when L =4 the detection probability approaches unity.

The probability of false alarm, P_F, is equal to the probability that the output of the cell under test, q_0, exceeds the detection threshold, $T(J)q$, under hypothesis H_0. That is, from the test of expression (4.19), the probability of false alarm is given by

$$P_F = \Pr(Q_0 > T(J)Q|H_0) \tag{4.30}$$

where Q denotes the estimator of the noise level in the cell under test. Following the same procedure as in the derivation of the expression for the probability of false ecensoring, the probability of false alarm, P_F, is given by the contour integral

$$P_F = -\frac{1}{2\pi i}\int_C \omega^{-1}\Phi_{R|H_0}(\omega)d\omega \tag{4.31}$$

where the equivalent statistic R is given by

$$R = Q_0 - T(J)Q \tag{4.32}$$

The contour of integration is the same as that of equation (4.26) except c_1 is selected so that all the poles of $\Phi_{R|H_0}(\omega)$ that lie in the open left half ω-plane are enclosed.

The mgf of R under H_0 is given by

$$\begin{aligned}\Phi_{R|H_0}(\omega) &= E[\exp(-\omega(\sum_{i=1}^{L} q_{i0} - T\sum_{j=1}^{J}\sum_{i=1}^{L} q_{ij}))] \\ &= \int_0^\infty \cdots \int_0^\infty \exp\left(-\omega\sum_{i=1}^{L} q_{i0}\right)\exp\left(-\sum_{i=1}^{L} q_{i0}\right) dq_{i0}\ldots dq_{L0} \\ &\quad \cdot \int_0^\infty \cdots \int_0^\infty \exp\left(\omega T\sum_{j=1}^{J}\sum_{i=1}^{L} q_{ij}\right)\exp\left(-\sum_{j=1}^{J}\sum_{i=1}^{L} q_{ij}\right) dq_{ij}\ldots dq_{Lj} \\ &= (1+\omega)^{-L}(1-T\omega)^{-JL} \end{aligned} \tag{4.33}$$

Substitution of equation (4.33) into (4.31) and with the residue at $\omega = -1$ given by

$$\begin{aligned}\text{Res}_{\omega\to -1} &= \frac{1}{(L-1)!}\lim_{\omega\to -1}\frac{d^{L-1}}{d\omega^{L-1}}\left\{\frac{\omega^{-1}}{\omega(1-T\omega)^{JL}}\right\} \\ &= \frac{1}{(L-1)!}\lim_{\omega\to -1}\sum_{k=0}^{L-1}\binom{L-1}{k}(-1)^{L-1-k}\omega^{-(L-k)} \\ &\quad \cdot\frac{(JL+k-1)!}{(JL-1)!}\frac{T^k}{(1-T\omega)^{JL+k}} \end{aligned} \tag{4.34}$$

the probability of false alarm, P_F, is derived to be

$$P_F = \sum_{k=0}^{L-1}\binom{JL+k-1}{k} T(J)[1+T(J)]^{-(JL+k)} \tag{4.35}$$

The threshold multipliers $T(J), J = 1,\ldots,N-1$, are computed by solving $P_F = \alpha$. Observe that equation (4.35) is the expression for the probability of false alarm under the assumption that the censoring procedure correctly identifies the J reference samples that are identically distributed with the noise in the test cell.

4.6 Results

The performance of the ASIR-CFAR detector in multiple target situations is studied by means of computer simulation and compared to those of the CCA and GCMLD detectors. The GCMLD detector is analyzed in detail in [28]. The design expressions for the probability of false censoring and the probability of false alarm of the GCMLD-CFAR detector were presented in section 4.3.

An attractive feature of the proposed detector as in the case of the ACCA-CFAR detector, is the reduced amount of processing time required to implement the censoring procedure which makes an assessment of the background environment. As in chapter three, we assume that the heap sorting algorithm, which is the fastest sorting routine is used to rank order the data [33]. Also a DSP processor [34,35], employing special floating point hardware so that multiplications and additions take the same amount of time to be executed, is used. The maximum required number of machine cycles for the two detectors are derived to be

$$\tau_{GCMLD} = 2Nlog_2\frac{N}{2} + 4N + 1 \tag{4.36}$$

$$\tau_{ASIR} = 7N - 4 \tag{4.37}$$

In Figure 4.4, we show the the total execution time, expressed in machine cycles, versus the size of the reference window. Clearly the execution time of the proposed detector is much smaller than that of the GCMLD detector.

In Figures 4.5 to 4.7 we compare the censoring capabilities of the CCA, GCMLD and ASIR-CFAR detetcors. In Figure 4.5 we assume a window size of $N = 32$ and a probability of false alarm 10^{-6}. We show the probability of false censoring one, two and three interfering targets. As the number of interfering targets increases, the probability of censoring decreases in all three detectors considered and this may cause degradation in the probability of detection. In Figure 4.6 the window size is $N = 16$ and we study the censoring capabilities of all three detectors for two different values of false alarm probability, 10^{-4} and 10^{-6}, and for two interfering targets present in the reference window. The censoring capabilities of the CCA-CFAR detector are seriously degraded as shown, when the probability of false alarm becomes stricter, that is equal to 10^{-6}. On the other hand the censoring capabilities of the GCMLD and the ASIR-CFAR detectors are more robust especially when the signal to noise ratio is above 30dB. However, the GCMLD for values of signal to noise ratio less

than 30dB, shows also some degradation in the probability of censoring while the performance of the proposed detector is robust. For example, if the signal to noise ratio is 20dB the probability of censoring in the case of the GCMLD when $\alpha = 10^{-4}$, is approximately 0.52 while when $\alpha = 10^{-6}$ is approximately 0.22. In Figure 4.7, three interfering targets are present in the reference window and a probability of false alarm of 10^{-6} is assumed. The censoring capabilities of the three detectors are compared in terms of the size of the reference window. Both the GCMLD and the CCA-CFAR detectors suffer degradation in their censoring probability when the size of the window is reduced from $N = 32$ to $N = 16$ while the censoring capabilities of the ASIR-CFAR detector remain unchanged as shown. In summary, in all three detectors, as the number of interfering targets increases the probability of censoring degrades. As the false alarm probability becomes stricter and the size of the window smaller the performance of the GCMLD and the CCA-CFAR detectors is seriously degraded while the performance of the ASIR-CFAR detector is robust. It should be pointed out that in general it is desired to have α small, and keep N small to limit the number of false alarms and minimize the likelihood of encountering a large number of interfering targets in the reference window.

In Figure 4.8, we present the detection probability of the CA, CCA, and ASIR-CFAR detectors in homogeneous background environment. We have assumed that $N = 16, L = 1$ and $\alpha = 10^{-6}$. The detection performance of the CCA, GCMLD and ASIR-CFAR detectors is shown to be approximately the same. They are slightly superior than that of the CA-CFAR detector. This is due to the fact that sometimes the adaptive censoring procedures in the CCA, GCMLD and ASIR-CFAR detectors may censor some of the largest noise samples thereby slightly underestimating the noise level in the test cell. However, this effect is not significant.

In Figures 4.9 to 4.22, we compare the detection performance of the ASIR, GCMLD and CCA-CFAR detectors when two, three, four, six and ten interfering

targets are present in the N reference cells. In Figures 4.9 and 4.10, the detection performance of the ASIR, CCA and GCMLD detectors are shown for $\alpha = 10^{-4}$. Two interfering targets and a single pulse transmission have been assumed. In Figure 4.9 one interfering target is present in the leading and the other in the lagging reference window while in Figure 4.10 both interfering targets are in the lagging window. For $N = 16$, the CCA-CFAR detector suffers from the capture effect. When $N = 32$ the detection performance of the GCMLD detector is shown to be better for signal to noise ratio in the range of 15 to 25dB as shown in Figure 4.9. For example for probability of 0.9 the relative loss in signal to noise ratio of the ASIR-CFAR detector as compared to GCMLD is approximately 2dB. However, in the range of 0 to 15dB the detection performance of the ASIR-CFAR detector is shown to be better. In Figure 4.11, α is reduced to 10^{-6} and two interfering targets have been assumed. When $N = 32$, the detection performance of the GCMLD detector is superior to that of the ASIR and CCA-CFAR detectors. However, when the size of the window is reduced to $N = 16$ both the CCA-CFAR and GCMLD detectors suffer from the capture effect while the performance of the ASIR-CFAR detector is robust.

In Figures 4.12 to 4.16 we compare the detection performance of the CCA, GCMLD and ASIR-CFAR detectors for single pulse transmission and when three interfering targets are present in the reference window. In all cases where the reference window is small, $N = 16$, the detection performance of the CCA-CFAR detector is seriously degraded due to the capture effect. In Figures 4.12 and 4.13 we assume that $\alpha = 10^{-4}$. In Figure 4.12, the detection performance of the GCMLD detector is shown to be superior to that of the ASIR-CFAR detector. However, when all three interfering targets are present in the leading reference window as shown in Figure 4.13, the detection performance of the ASIR-CFAR detector is shown to be superior to both the CCA-CFAR and GCMLD detectors for both $N = 16$ and $N = 32$. In Figures 4.14 and 4.15 α is reduced to 10^{-6}. When $N = 32$ the detection performance

of the GCMLD detector is shown to be better than those of the CCA and ASIR-CFAR detectors. However, when the size of the window is reduced, $N = 16$, the GCMLD detector suffers from the capture effect while the detection performance of the proposed detector is robust. In Figure 4.16, we assume the presence of three weak interfering targets in the reference window and single pulse transmission. For $N = 32$ the detection performance of the GCMLD and the ASIR-CFAR detectors are almost identical and superior to that of the CCA-CFAR detector. However, when $N = 16$, clearly the detection performance of the ASIR-CFAR detector is superior to both the CCA-CFAR and GCMLD-CFAR detectors.

In Figures 4.17 and 4.18 we assume single pulse transmission and four interfering targets in the reference window. In Figure 4.17 where $\alpha = 10^{-4}$, for $N = 32$ the detection performance of the CCA-CFAR and GCMLD detectors are almost identical and superior to that of the ASIR-CFAR detector. When the size of the window is reduced to $N = 16$, both the CCA-CFAR and GCMLD detectors suffer from the capture effect while the detection performance of the ASIR-CFAR detector is robust. When the probability of false alarm becomes stricter, $\alpha = 10^{-6}$, as shown in Figure 4.18 the detection performance of the CCA-CFAR detector is degraded dramatically for both $N = 16$ and $N = 32$. When $N = 32$ the detection performance of the GCMLD detector is superior to that of the ASIR-CFAR detector in the range of 15 to 30dB. However, when the size of the window becomes smaller, $N = 16$, the detection performance of the ASIR-CFAR detector is superior.

In Figures 4.19 to 4.22 we consider the presense of a large number of interfering targets that appear in *every other cell* in the reference window. Although, the presence of ten interfering targets may not be realistic, we are comparing the three detectors to study their robustness in such acute environment. When the number of interfering targets is large, the detection performance of the CCA-CFAR detector is seriously degraded and in some cases as shown in Figure 4.19 and 4.22 the detection probability

is almost zero. In Figure 4.19, we assume the presense of ten strong (b=5) interfering targets in a reference window of size $N = 32$, and single pulse transmission. The detection performance of the GCMLD detector is shown to be superior to both the ASIR and CCA-CFAR detectors. The censoring procedure of the GCMLD detector, censors the large number of interfering targets more effectively since the reference noise samples are rank ordered and b=5. In Figure 4.20, we assume the presense of ten weak (b=0.4) interfering targets and ten interfering targets with the same radar cross section area (b=1.0) with the target in the test cell. Single pulse transmission and $\alpha = 10^{-6}$ is assumed. In the case where $b = 1.0$ the detection performance of the GCMLD detector is slightly superior to that of the ASIR-CFAR detector while when $b = 0.4$ the detection performance of the ASIR-CFAR detector is superior to that of the GCMLD detector. This is due to the fact, that the weak interfering target returns may be censored as noise samples by the censoring procedure of the GCMLD and therefore may not be censored. In Figures 4.21 and 4.22 the size of the window is reduced to $N = 16$. The detection performance of the proposed detector is shown to be superior to both the GCMLD and CCA-CFAR detectors. It should be pointed out that, in the presence of strong interfering targets and a large reference window, $N = 32$, as shown in Figure 4.19, the GCMLD detector was superior while in the case of a small reference window, $N = 16$, the ASIR-CFAR detector is shown to be superior even in the presense of strong interfering targets, $b = 10$, as shown in Figure 4.22.

In Figures 4.23 to 4.25, we assume $L = 4$ pulses are processed. As the number of interfering targets increases and the size of the reference window becomes smaller, the performance of the CCA-CFAR detector deteriorates while the detection performance of the proposed detector remains robust.

As we mentioned earlier it is generally desired to have α small and keep N small to limit the number of false alarms and minimize the likelihood of encountering

a large number of interfering targets in the reference window. The results presented demonstrated that in these situations the performance of the proposed detector is superior than that of the CCA-CFAR detector.

4.7 Summary and Conclusions

In this chapter, we have considered the problem of CFAR detection in multiple target situations. We have proposed and analyzed the ASIR-CFAR detector which determines and censors the samples that correspond to interfering targets, using an adaptive censoring procedure. The analysis of the CCA-CFAR detector was extended in time diversity combining. The performance of the ASIR-CFAR detector was shown to be superior as compared with the performance of the CCA and GCMLD-CFAR detectors when both the window size, and the design false alarm probability are small. Also the effect of the probability of false censoring on the design probability of false alarm in the case of the GCMLD and ASIR-CFAR detectors was studied. In addition, we have shown that the processing time required for the implementation of the proposed detector is less than the processing time required for the GCMLD-CFAR detector.

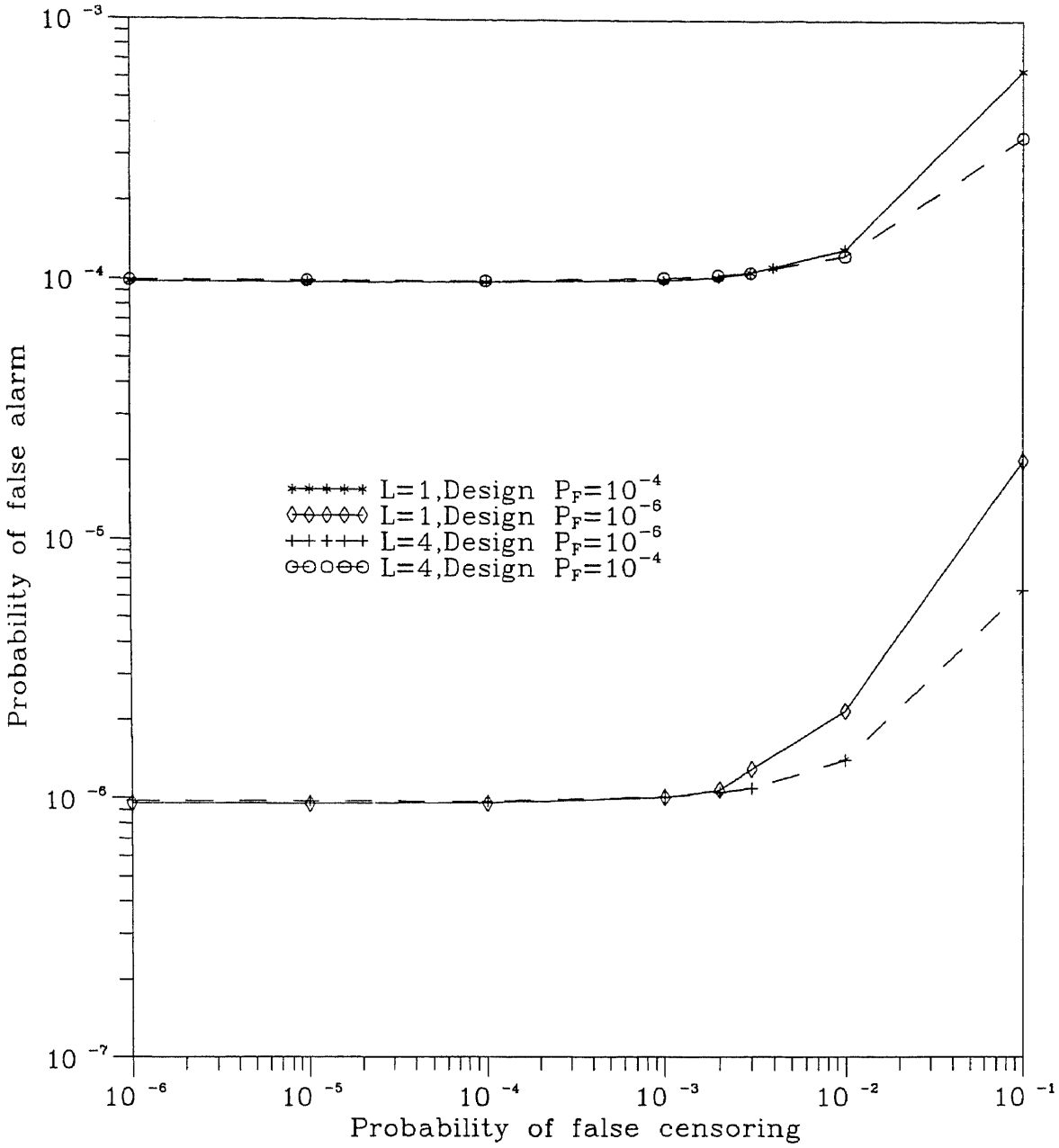

Figure 4.1. Probability of false alarm versus probability of false censoring of the ASIR-CFAR detector.

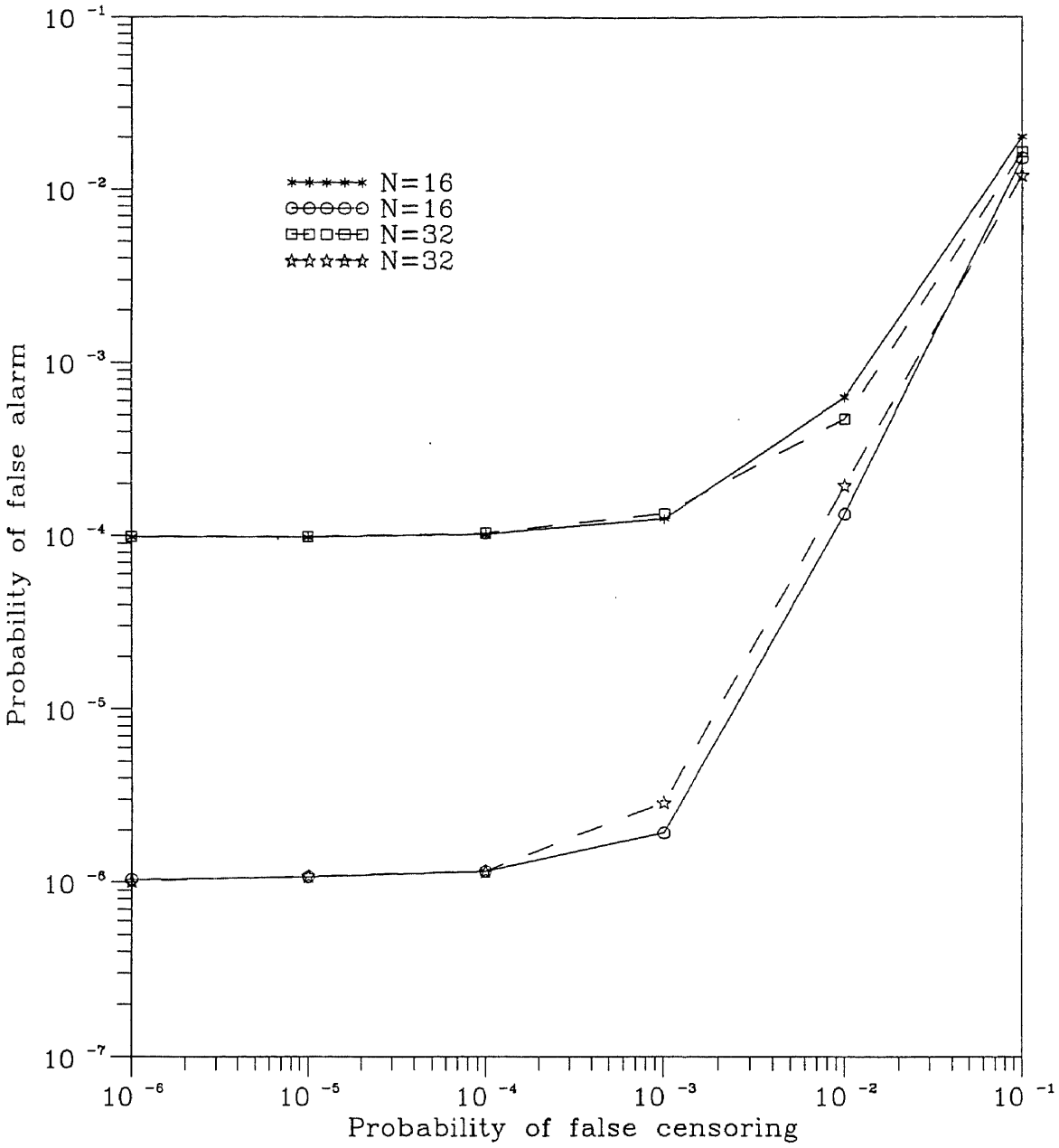

Figure 4.2. Probability of false alarm versus Probability of false censoring of the GCMLD-CFAR detector.

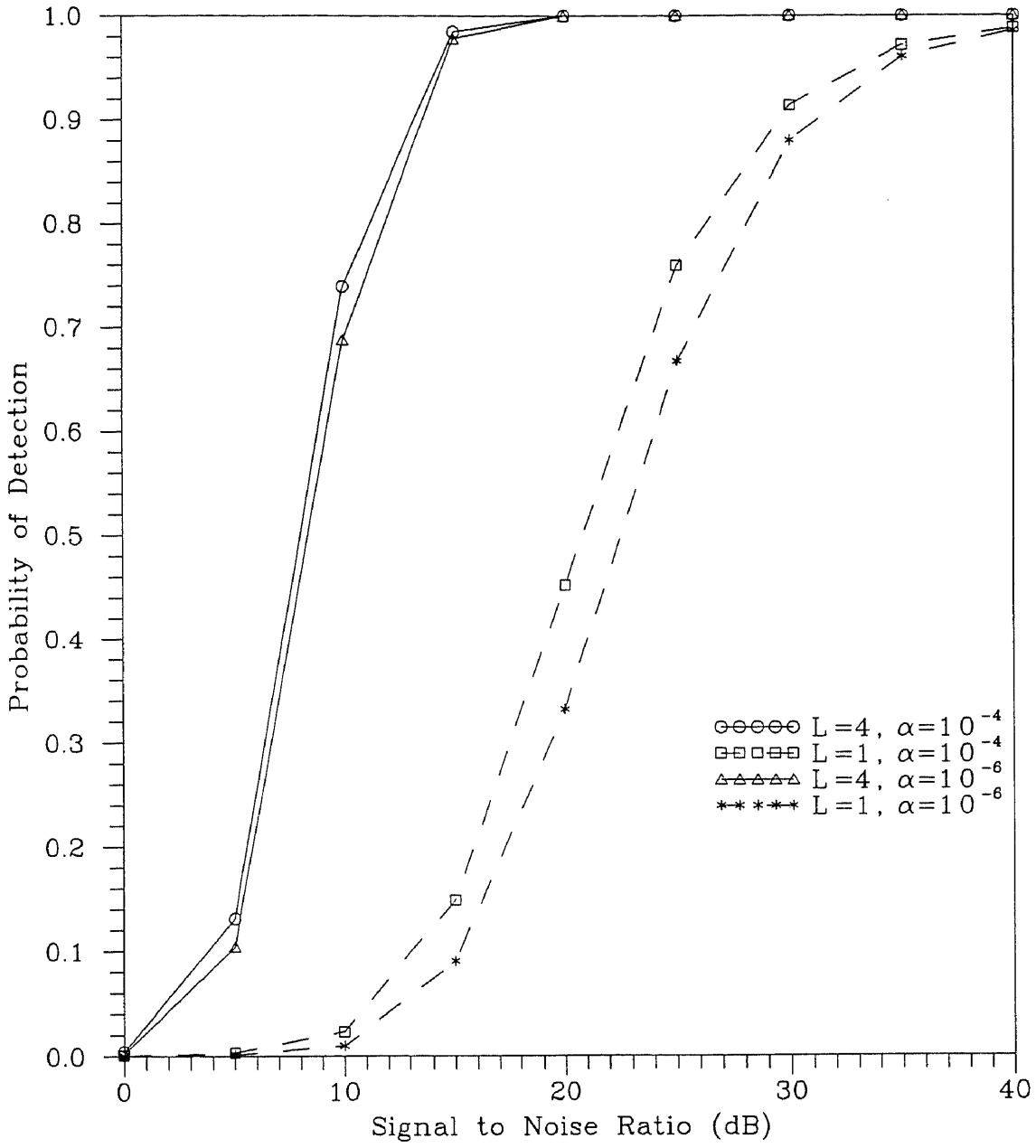

Figure 4.3. Probability of censoring two interfering targets for the ASIR-CFAR detector.
N=16, b=1.0 .

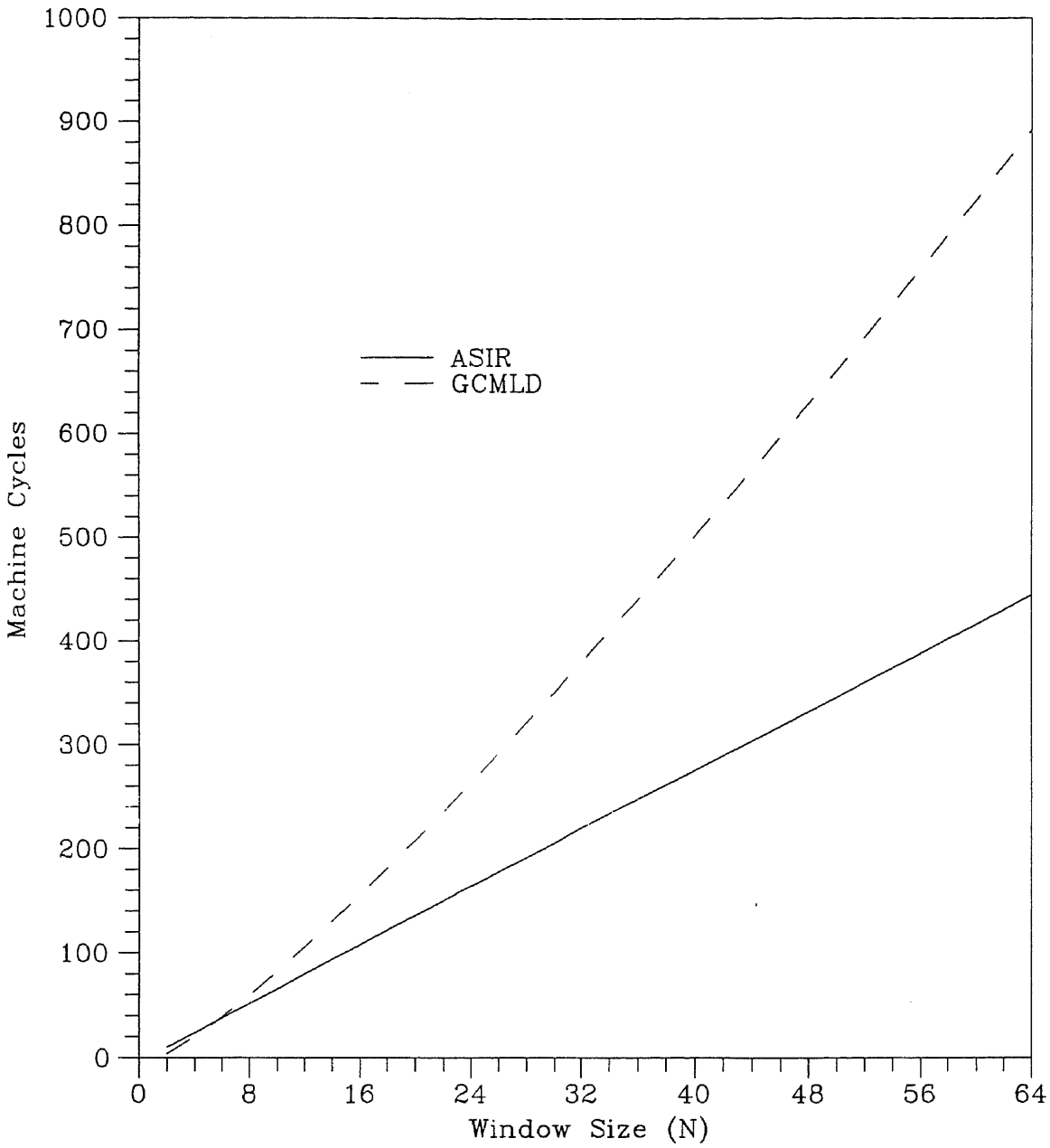

Figure 4.4. Total execution time in machine cycles versus the window size.

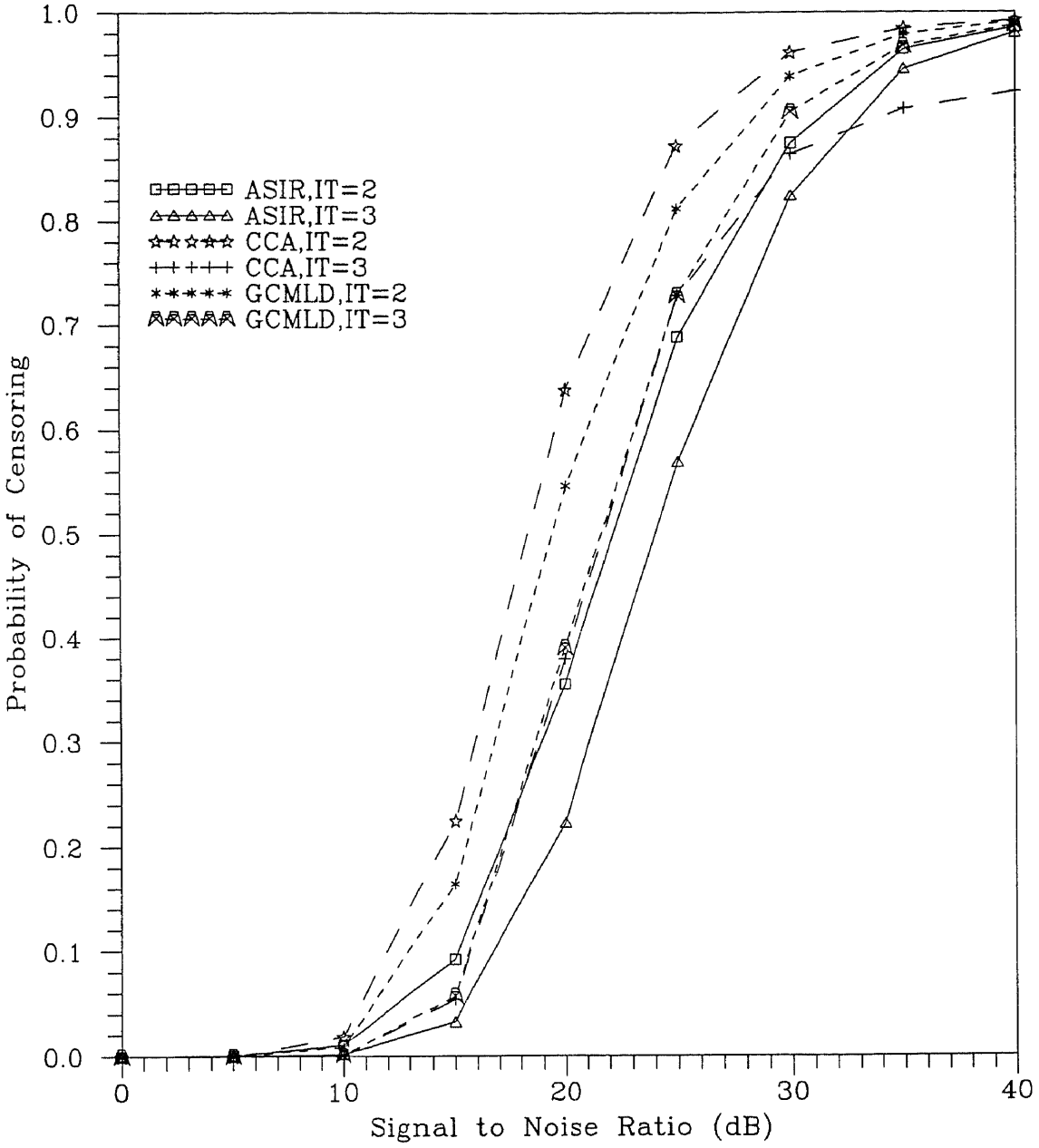

Figure 4.5. Probability of censoring number of interfering targets for the CCA,GCMLD and ASIR-CFAR detectors..
L=1, N=32, b=1.0, $\alpha=10^{-6}$, $\gamma=10^{-3}$

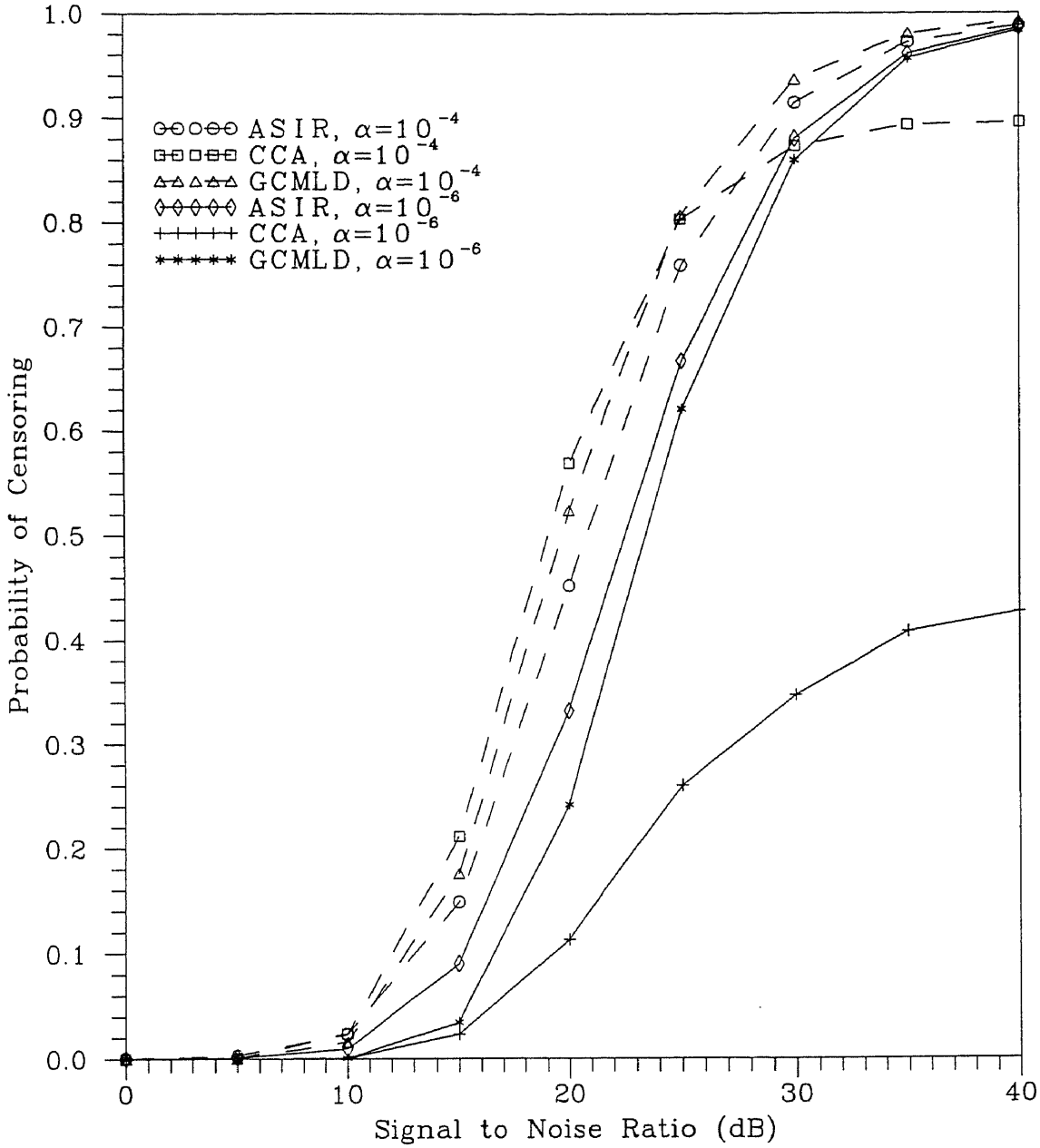

Figure 4.6. Probability of censoring two of interfering targets for the CCA,GCMLD and ASIR-CFAR detectors.
L=1, N=16, b=1.0,

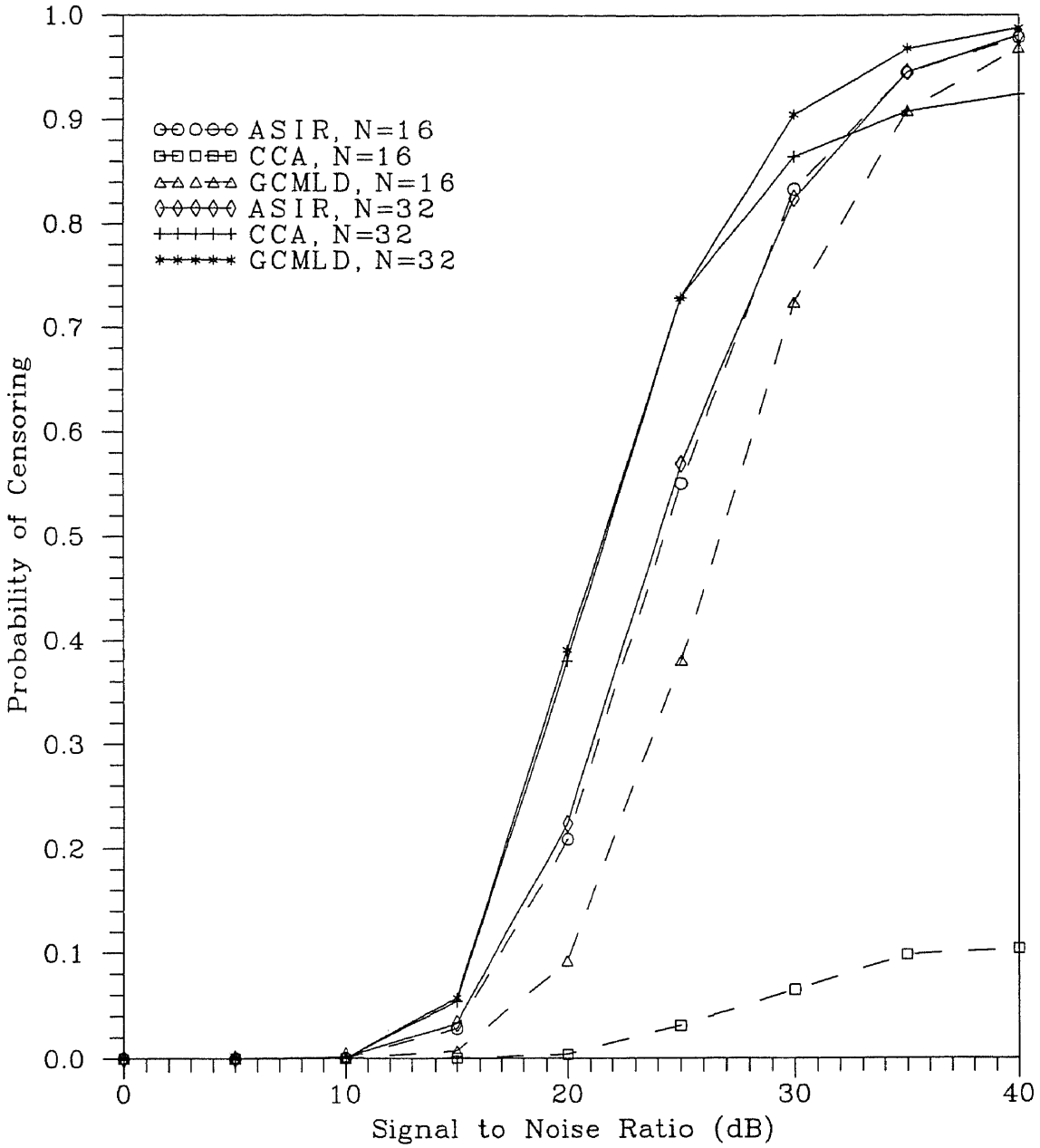

Figure 4.7. Probability of censoring three of interfering targets for the CCA,GCMLD and ASIR-CFAR detectors.
L=1, b=1.0, $\alpha=10^{-6}$, $\gamma=10^{-3}$

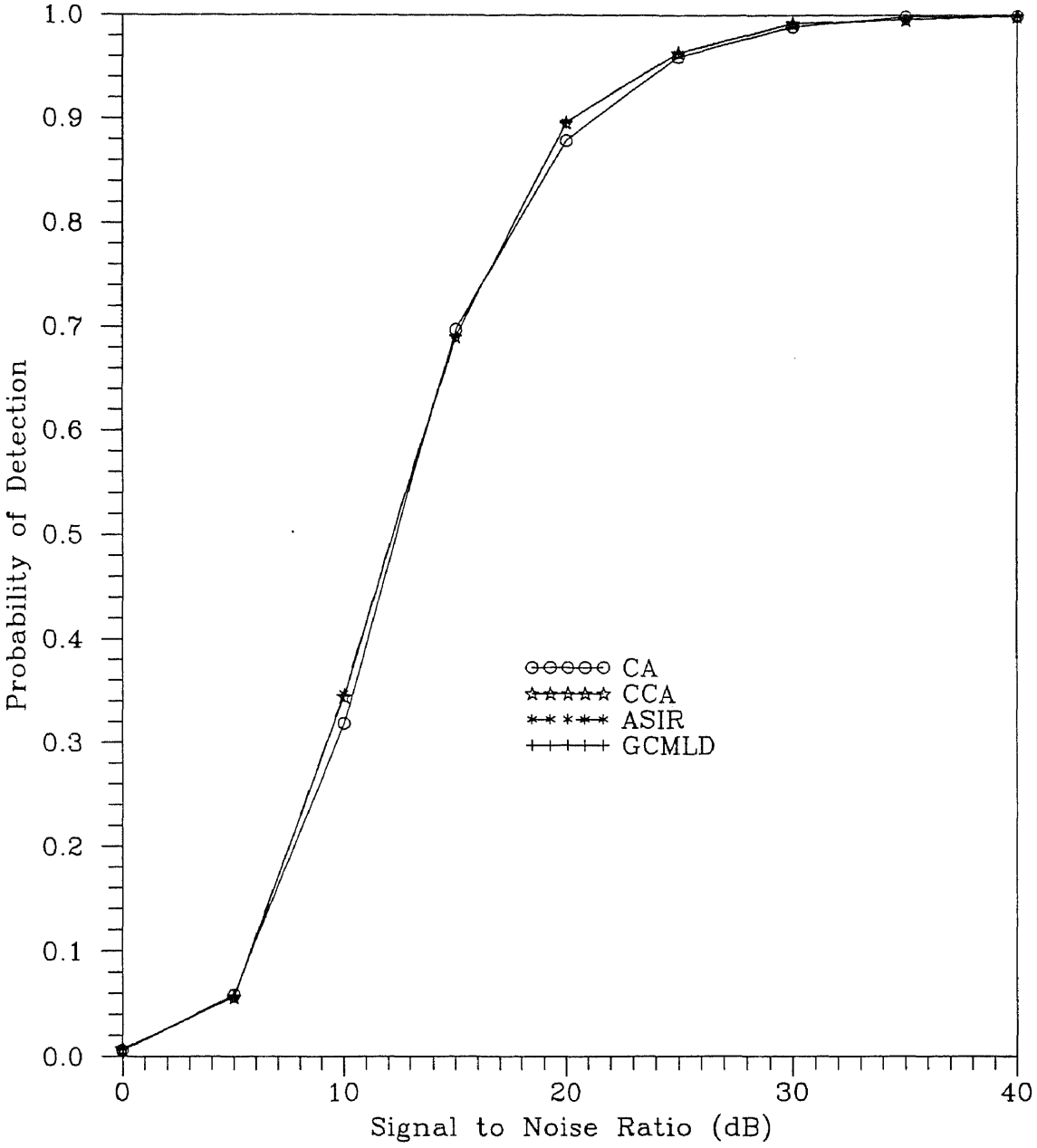

Figure 4.8. Probability of detection of the ASIR, CA, GCMLD and CCA–CFAR detectors in homogeneous background environment. N=16, L=1, $\alpha=10^{-6}$, $\gamma=10^{-3}$

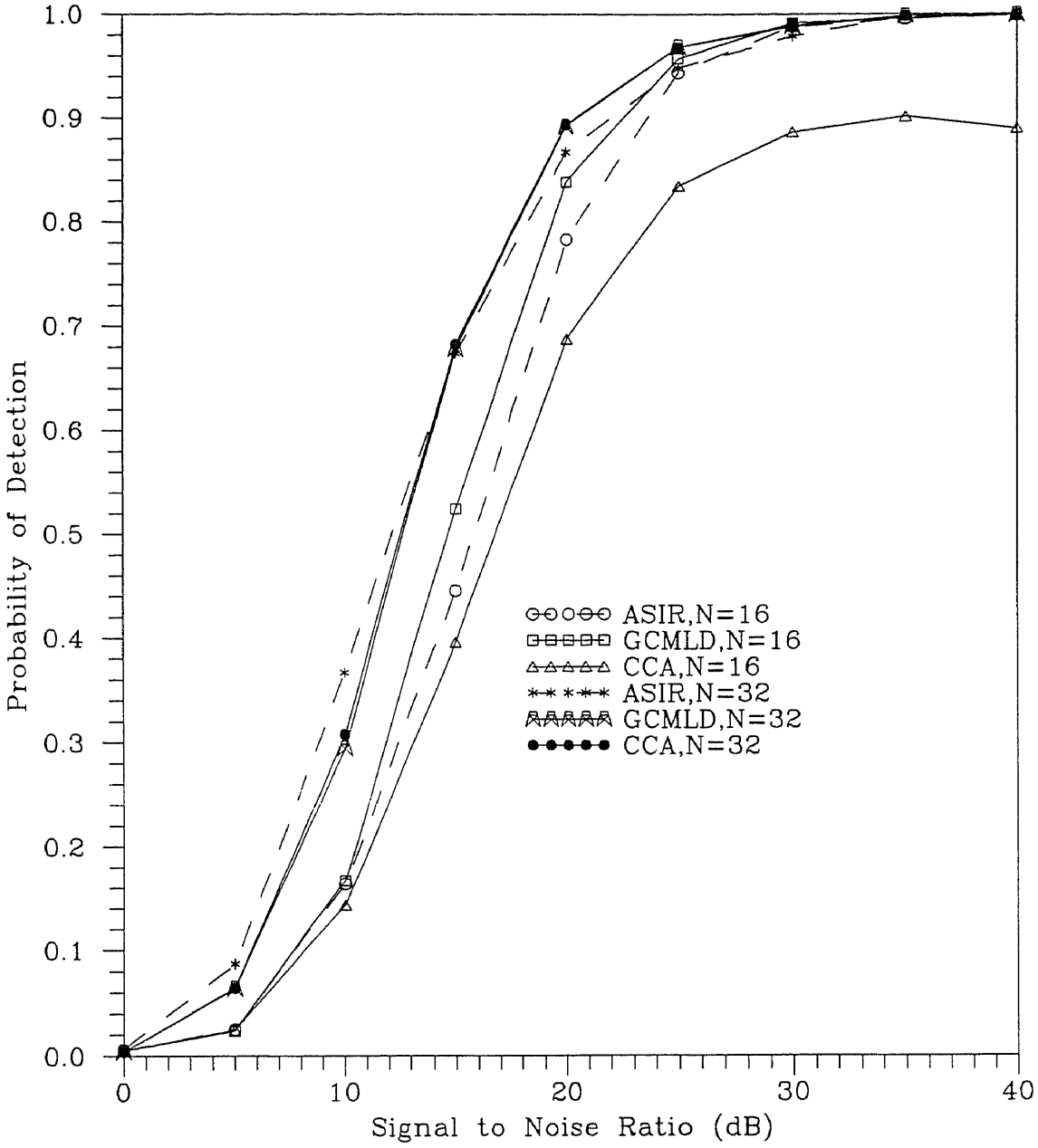

Figure 4.9. Probability of detection of the ASIR, GCMLD and CCA-CFAR detectors when two interfering targets are present. L=1, b=1.0, $\alpha=10^{-4}$, $\gamma=2\times10^{-3}$

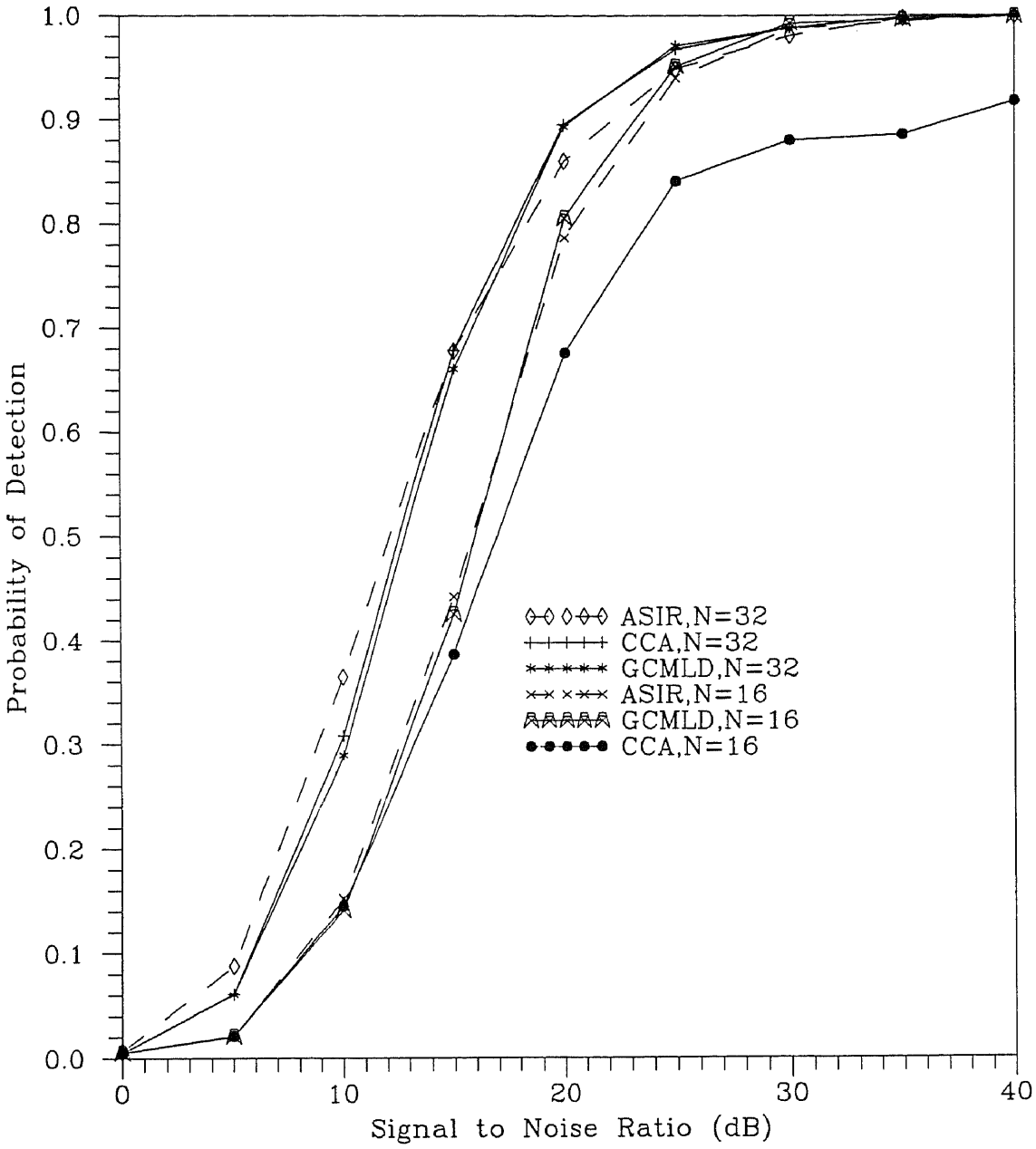

Figure 4.10. Probability of detection of the ASIR, GCMLD and CCA–CFAR detectors when two interfering targets are present in the lagging window.
L=1, b=1.0, $\alpha=10^{-4}$, $\gamma=2\times10^{-3}$

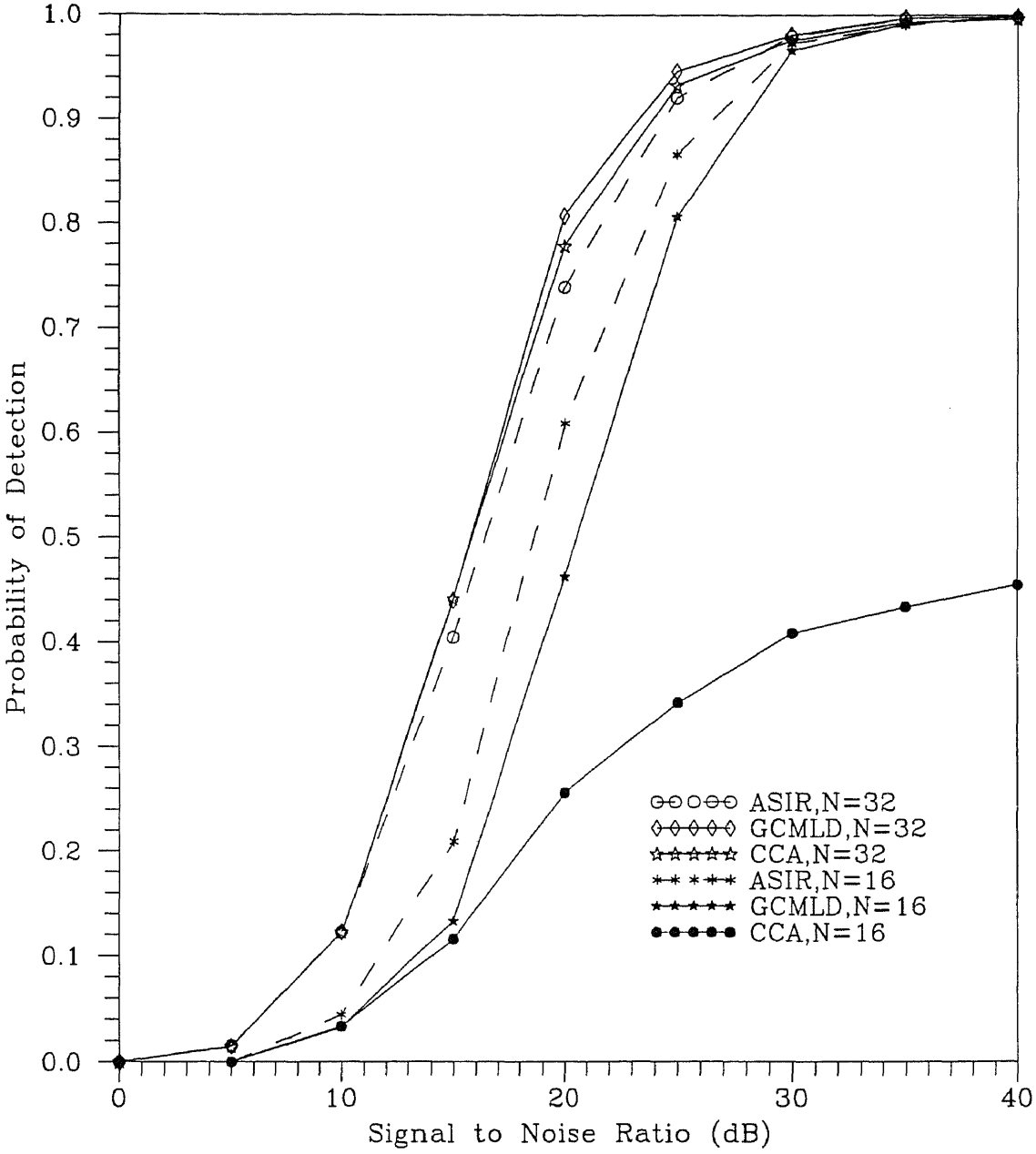

Figure 4.11. Probability of detection of the ASIR, GCMLD and CCA–CFAR detectors when two interfering targets are present in the leading window.
L=1, b=1.0, $\alpha=10^{-6}$, $\gamma=10^{-3}$

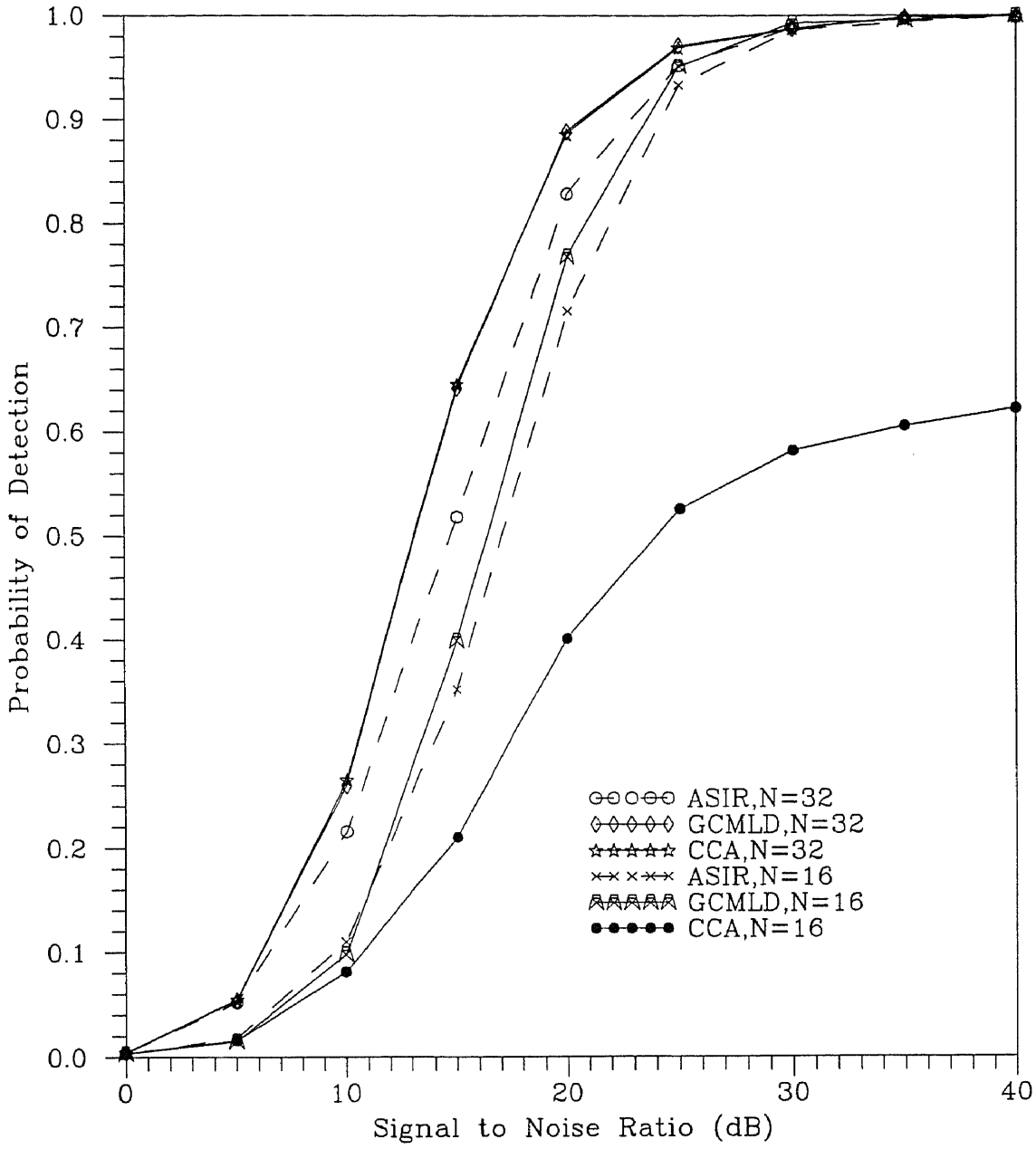

Figure 4.12. Probability of detection of the ASIR, GCMLD and CCA-CFAR detectors when three interfering targets are present.
L=1, b=1.0, $\alpha=10^{-4}$, $\gamma=2\times10^{-3}$

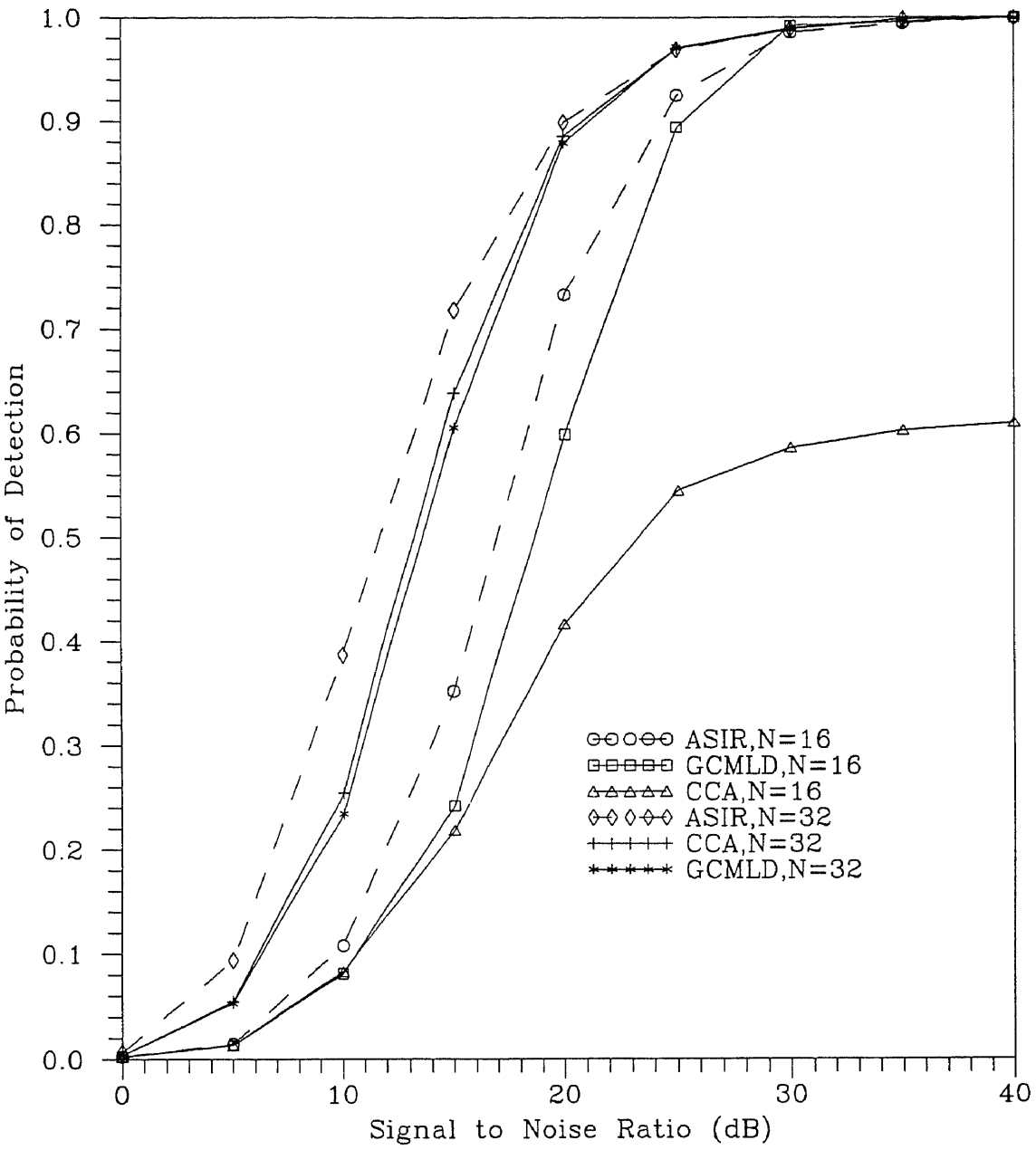

Figure 4.13. Probability of detection of the ASIR, GCMLD and CCA–CFAR detectors when three interfering targets are present in the leading window.
L=1, b=1.0, $\alpha=10^{-4}$, $\gamma=2\times10^{-3}$

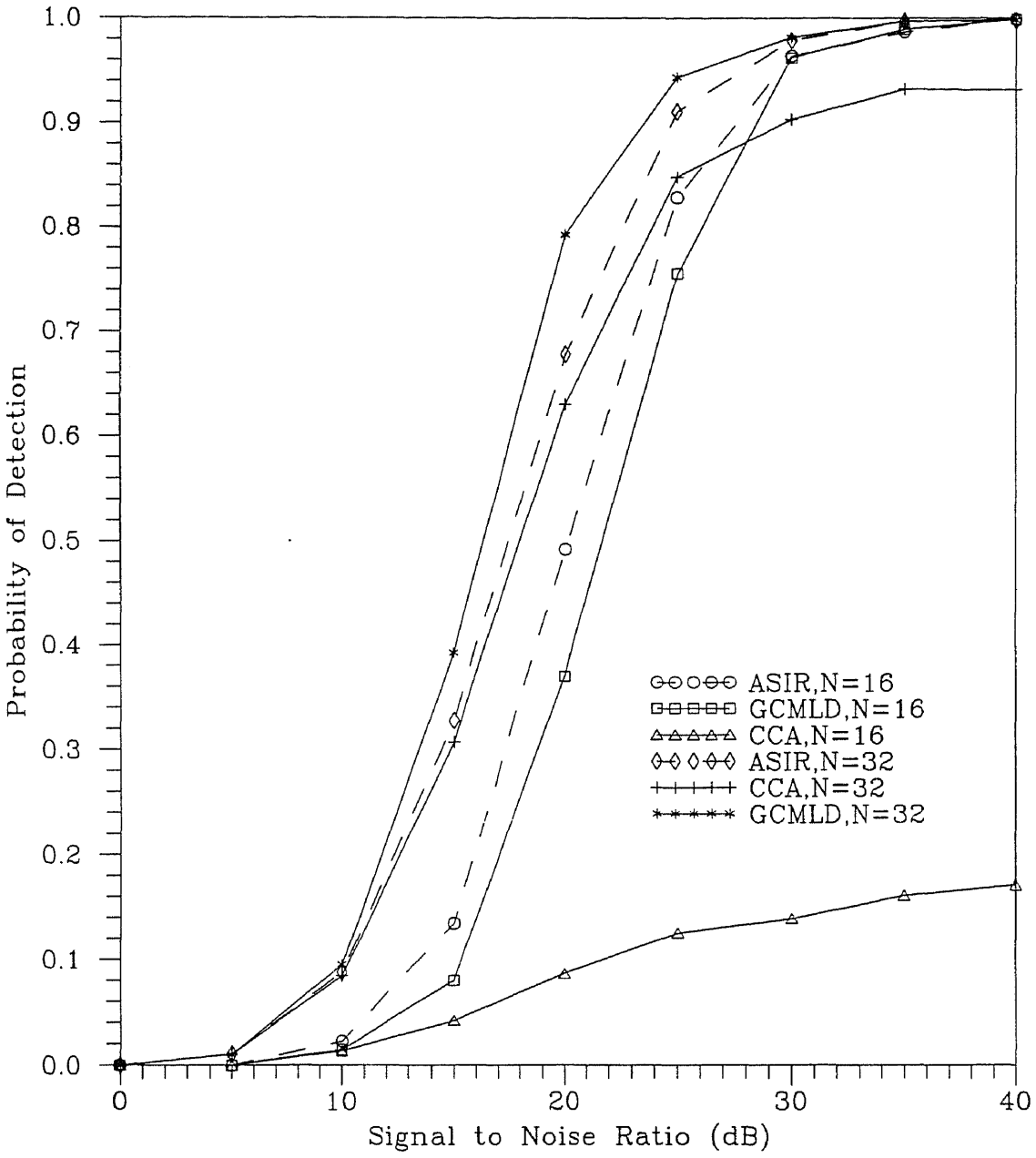

Figure 4.14. Probability of detection of the ASIR, GCMLD and CCA–CFAR detectors when three interfering targets are present.
L=1, b=1.0, $\alpha=10^{-6}$, $\gamma=10^{-3}$

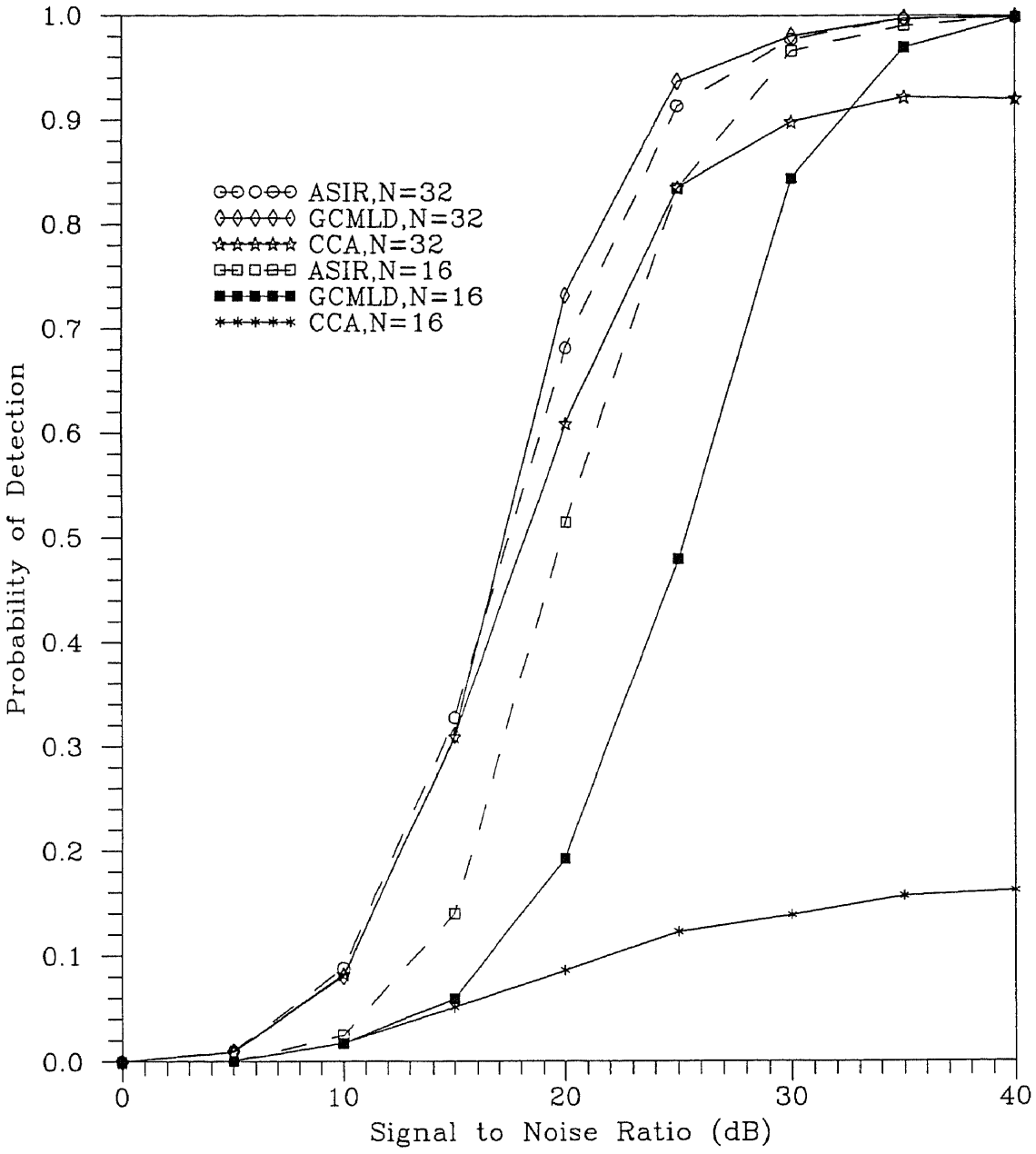

Figure 4.15. Probability of detection of the ASIR, GCMLD and CCA–CFAR detectors when three interfering targets are present in the leading window.
L=1, b=1.0, $\alpha=10^{-6}$, $\gamma=10^{-3}$

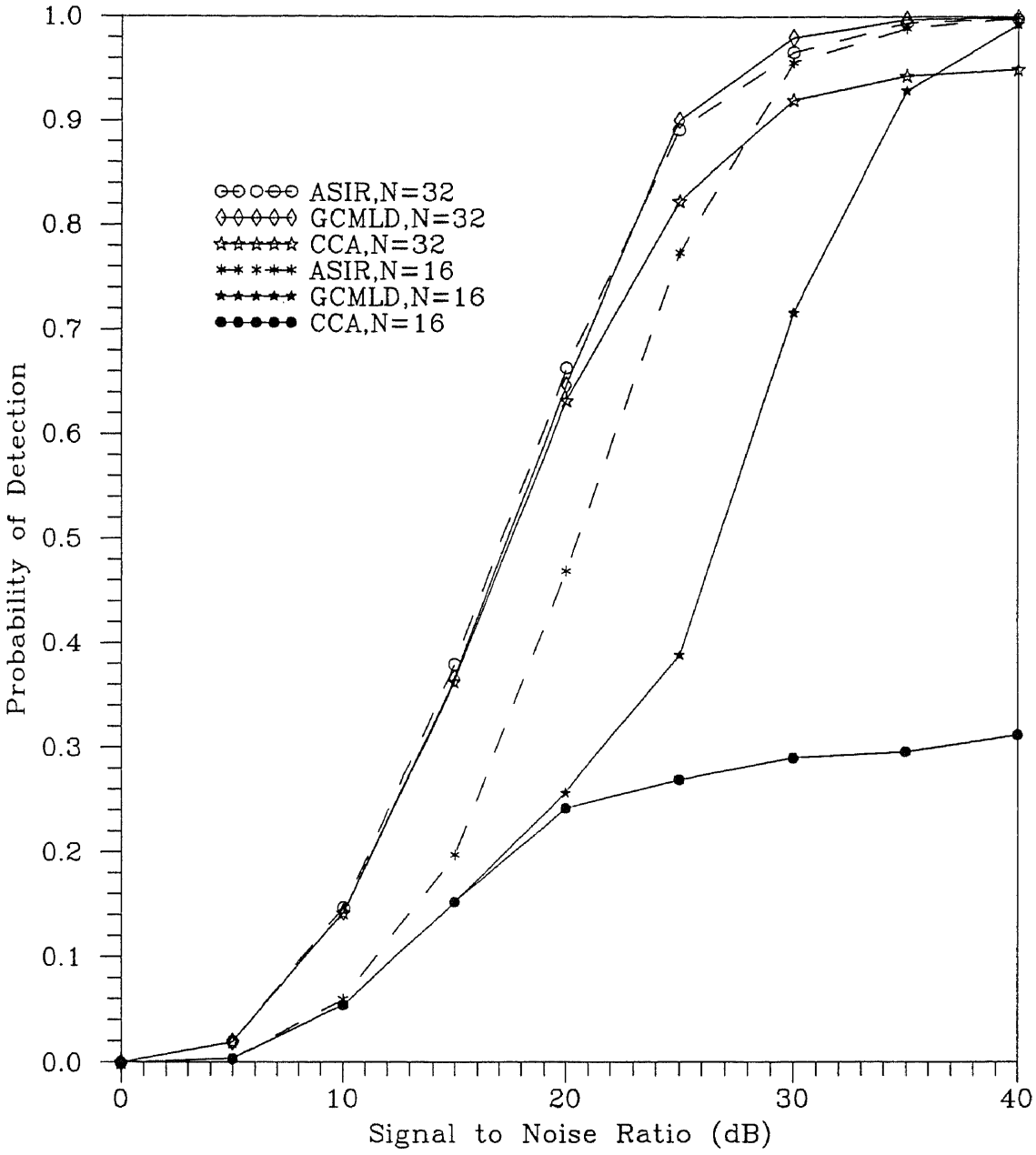

Figure 4.16. Probability of detection of the ASIR, GCMLD and CCA–CFAR detectors when three interfering targets are present.
L=1, b=0.4, $\alpha=10^{-6}$, $\gamma=10^{-3}$

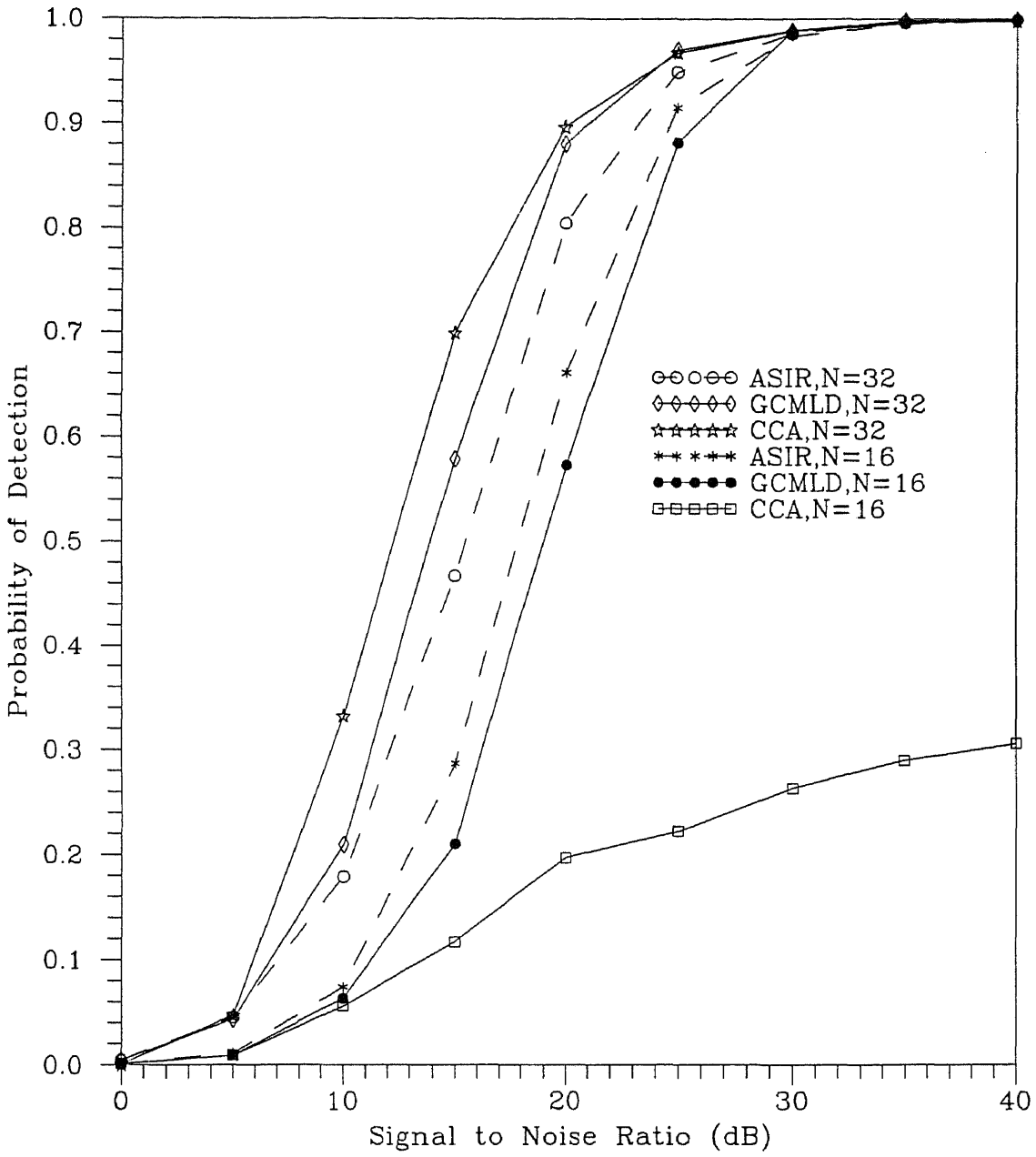

Figure 4.17. Probability of detection of the ASIR, GCMLD and CCA–CFAR detectors when four interfering targets are present.
L=1, b=1.0, $\alpha=10^{-4}$, $\gamma=2\times10^{-3}$

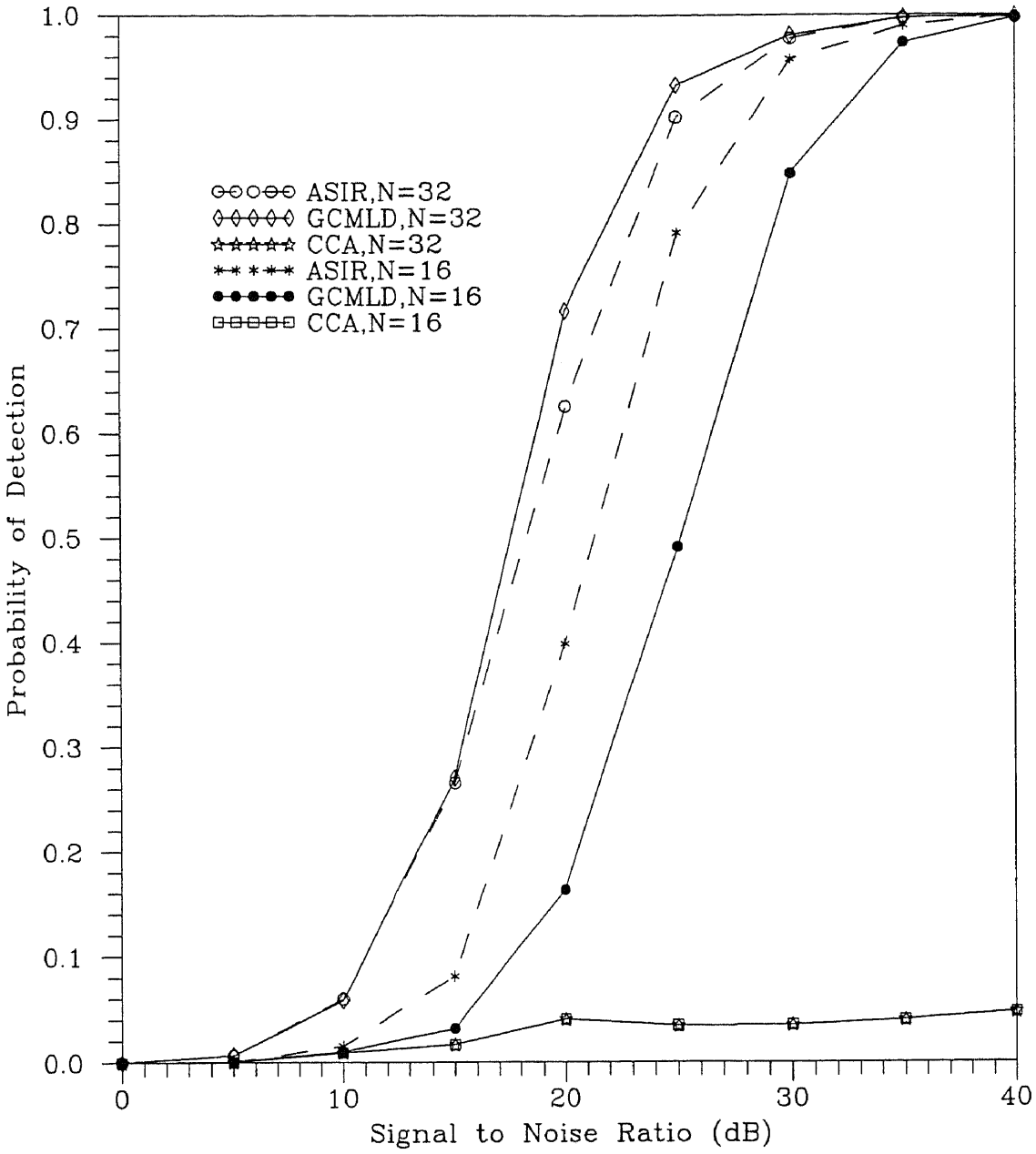

Figure 4.18. Probability of detection of the ASIR, GCMLD and CCA–CFAR detectors when four interfering targets are present.
L=1, b=1.0, $\alpha=10^{-6}$, $\gamma=10^{-3}$

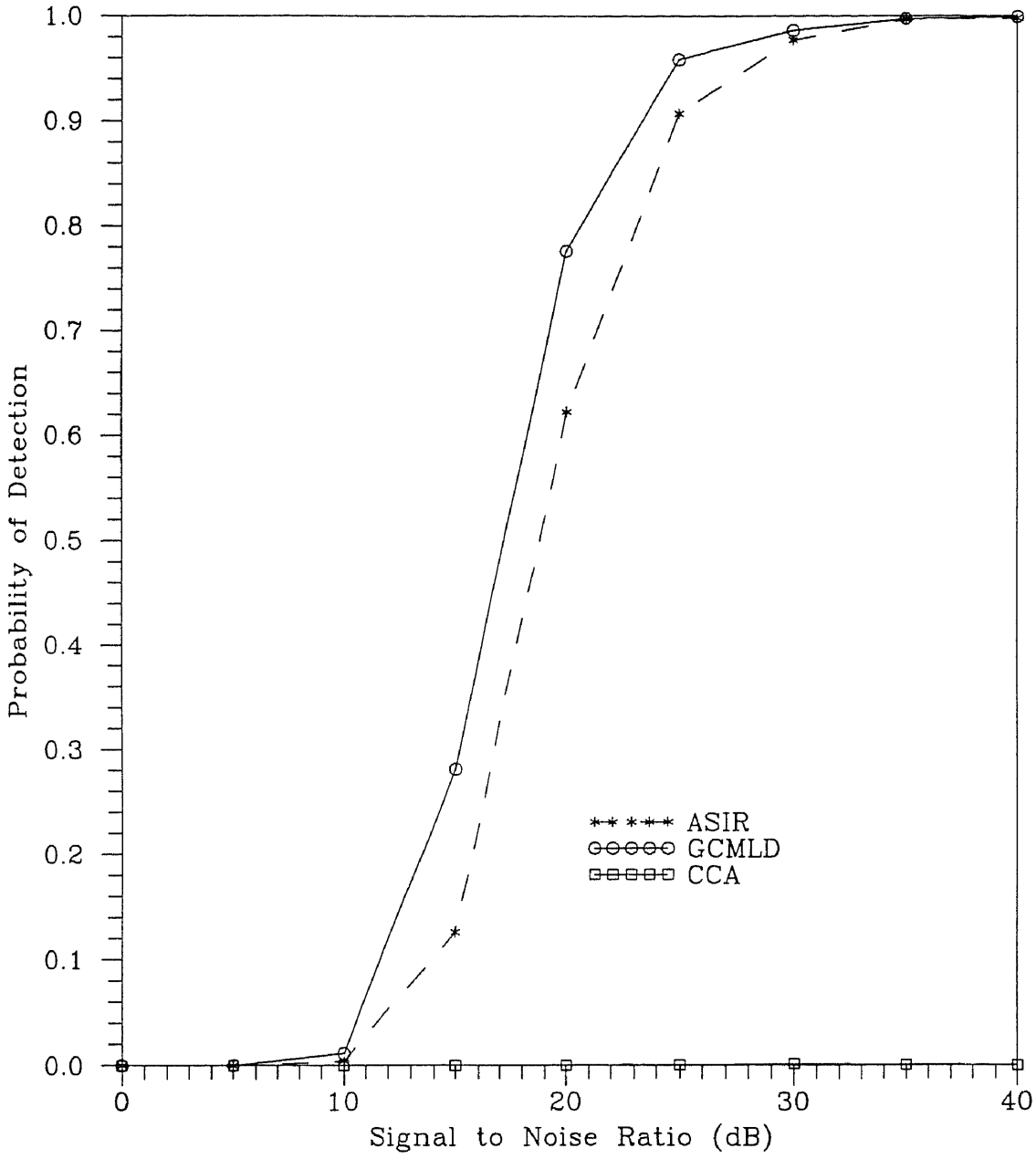

Figure 4.19. Probability of detection of the ASIR, GCMLD and CCA–CFAR detectors when ten interfering targets are present.
N=32, L=1, b=5.0, $\alpha=10^{-6}$, $\gamma=10^{-3}$

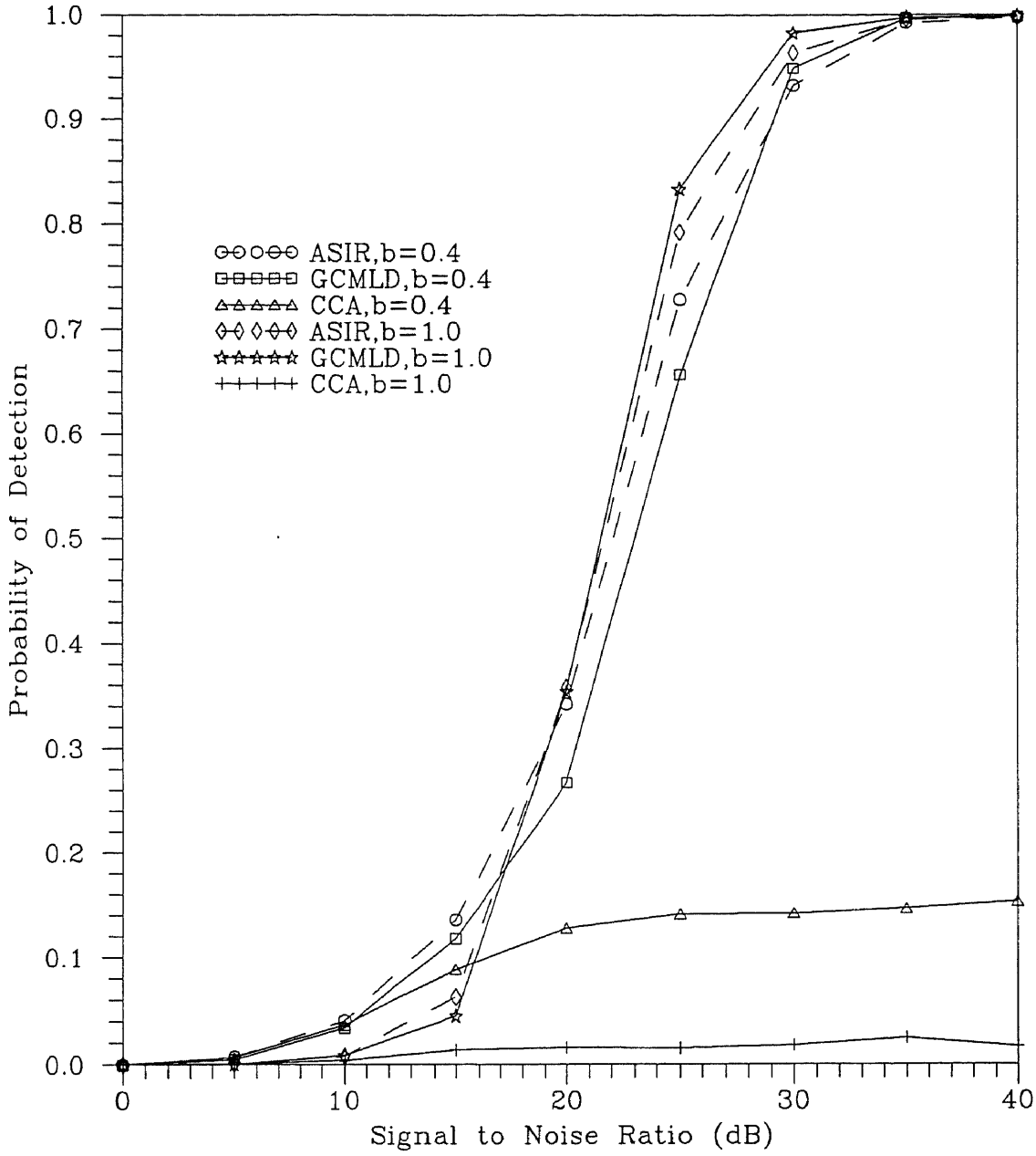

Figure 4.20. Probability of detection of the ASIR, GCMLD and CCA–CFAR detectors when ten interfering targets are present.
N=32, L=1, b=1.0, $\alpha=10^{-6}$, $\gamma=10^{-3}$

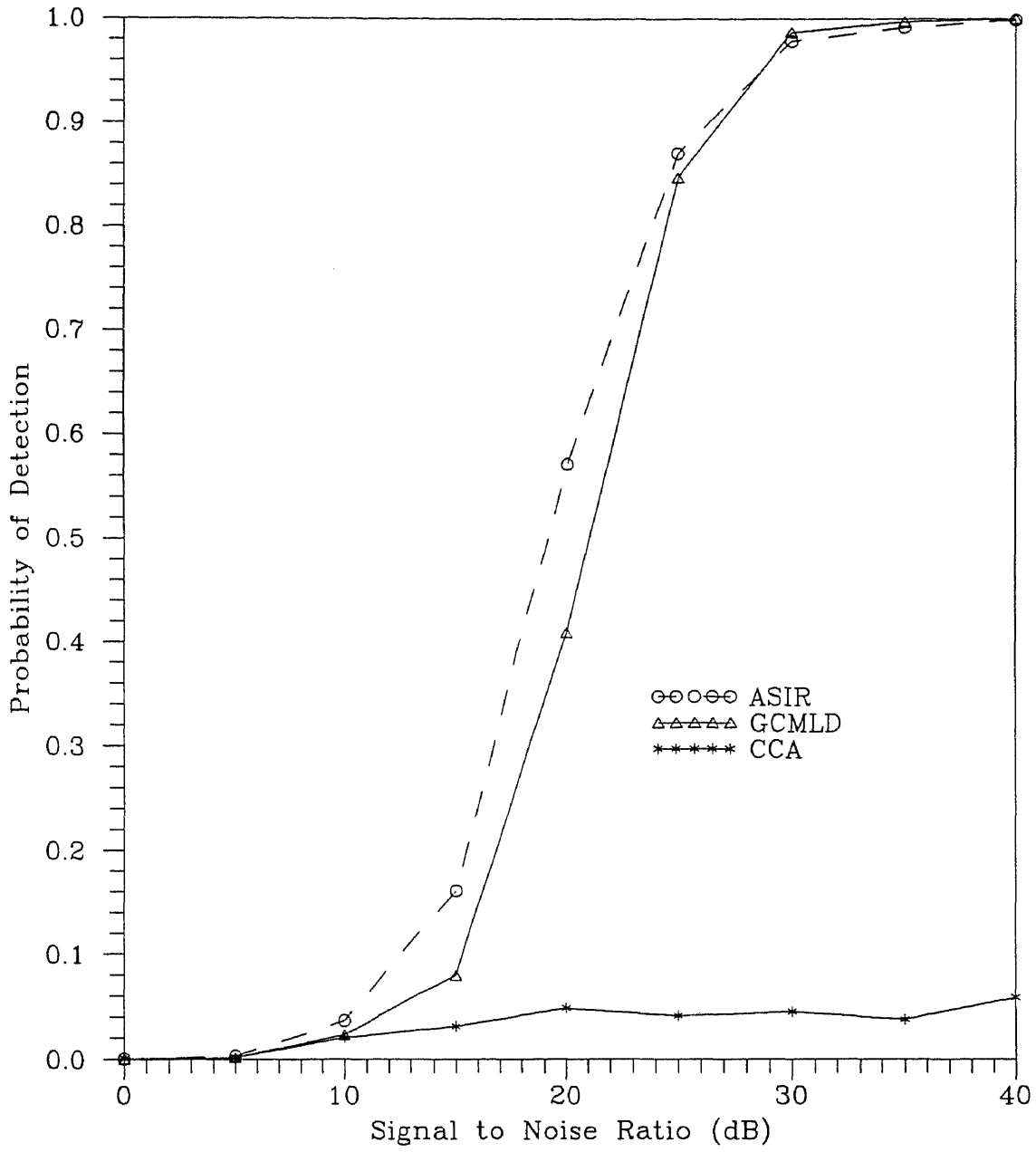

Figure 4.21. Probability of detection of the ASIR, GCMLD and CCA–CFAR detectors when six interfering targets are present.
L=1, N=16, b=1.0, $\alpha=10^{-4}$, $\gamma=2\times10^{-3}$

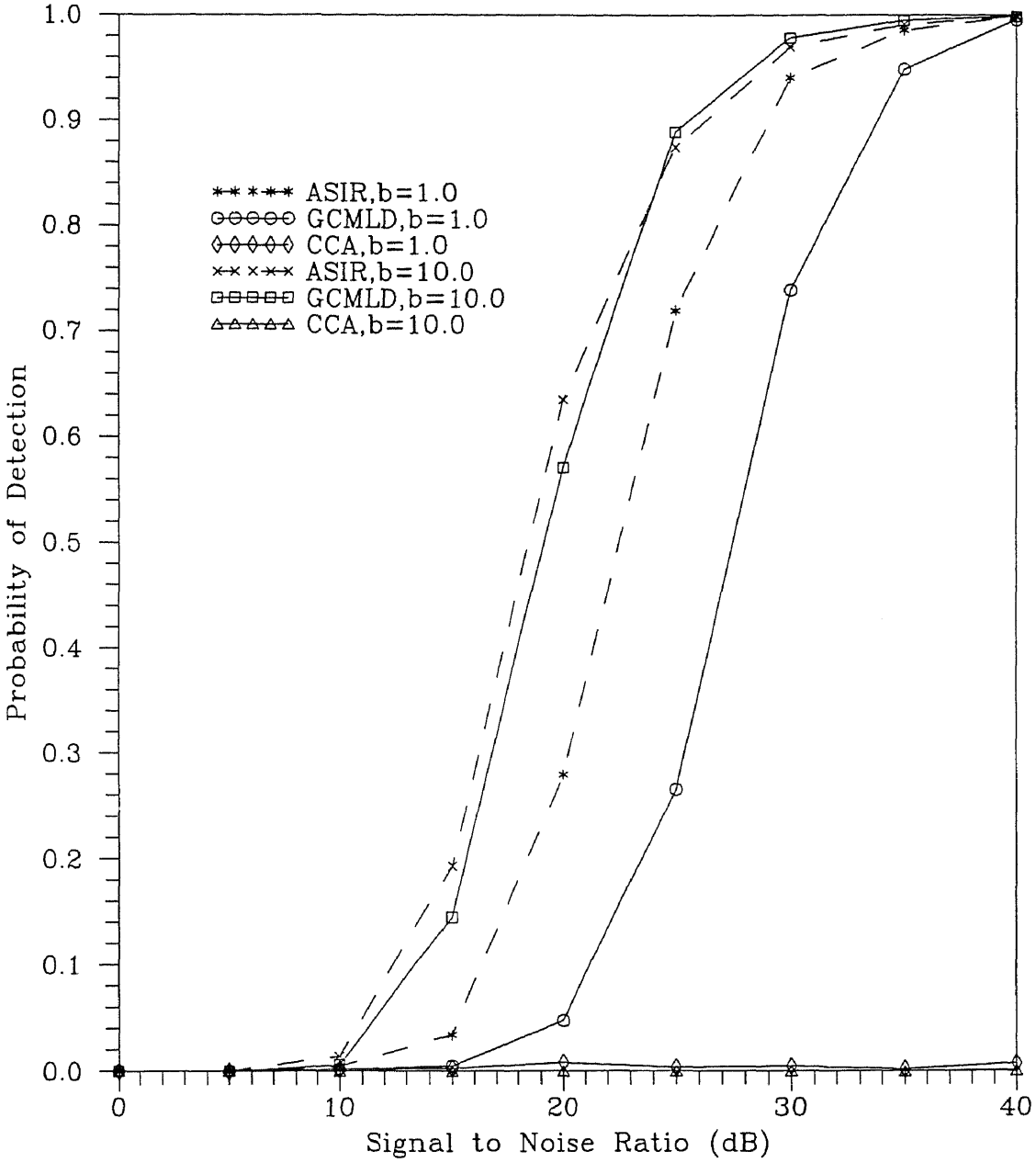

Figure 4.22. Probability of detection of the ASIR, GCMLD and CCA-CFAR detectors when six interfering targets are present.
L=1, N=16, b=1.0, $\alpha=10^{-6}$, $\gamma=10^{-3}$

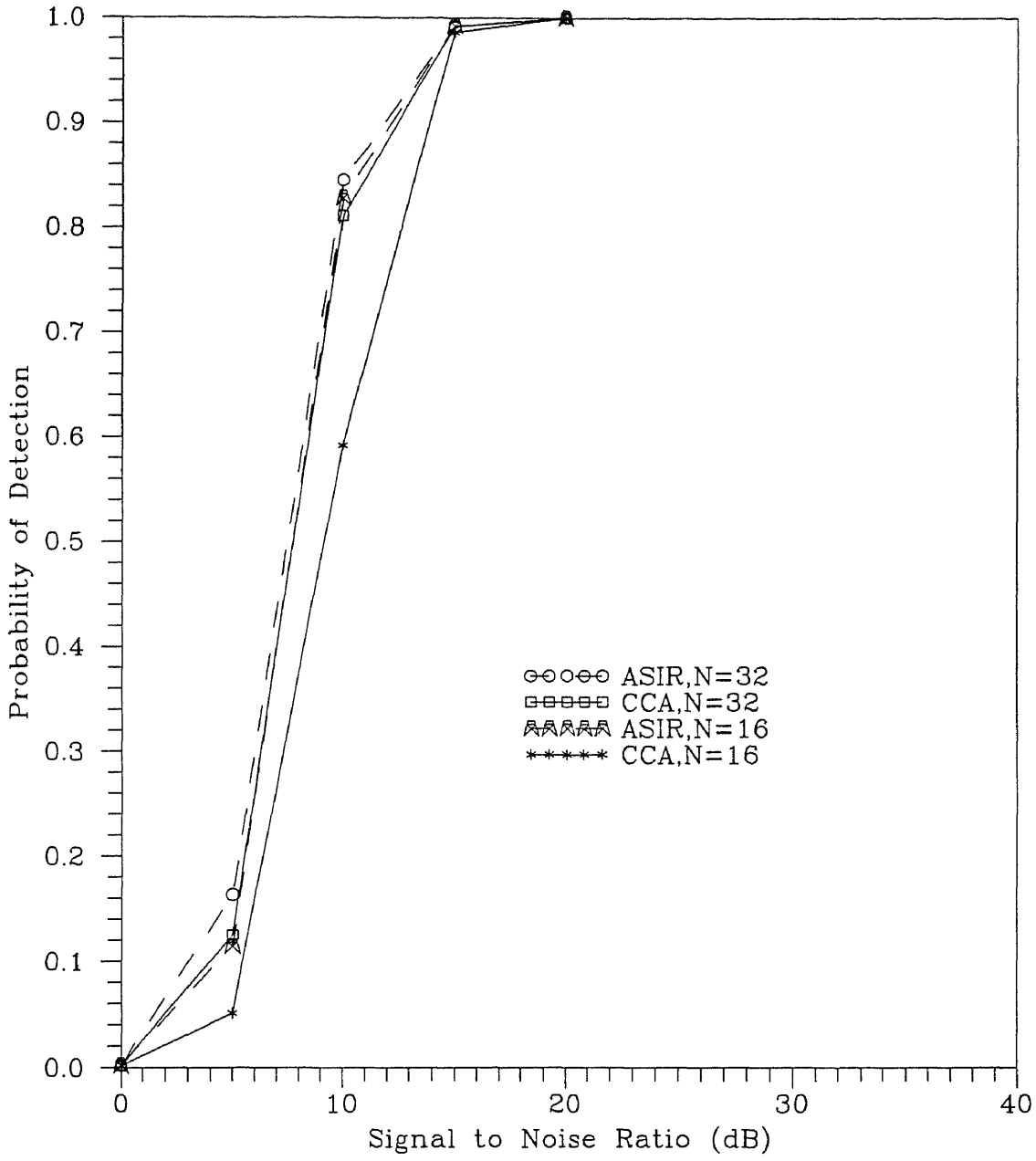

Figure 4.23. Probability of detection of the ASIR and the CCA-CFAR detectors when two interfering targets are present.
L=4, b=1.0, $\alpha=10^{-6}$, $\gamma=2\times10^{-3}$

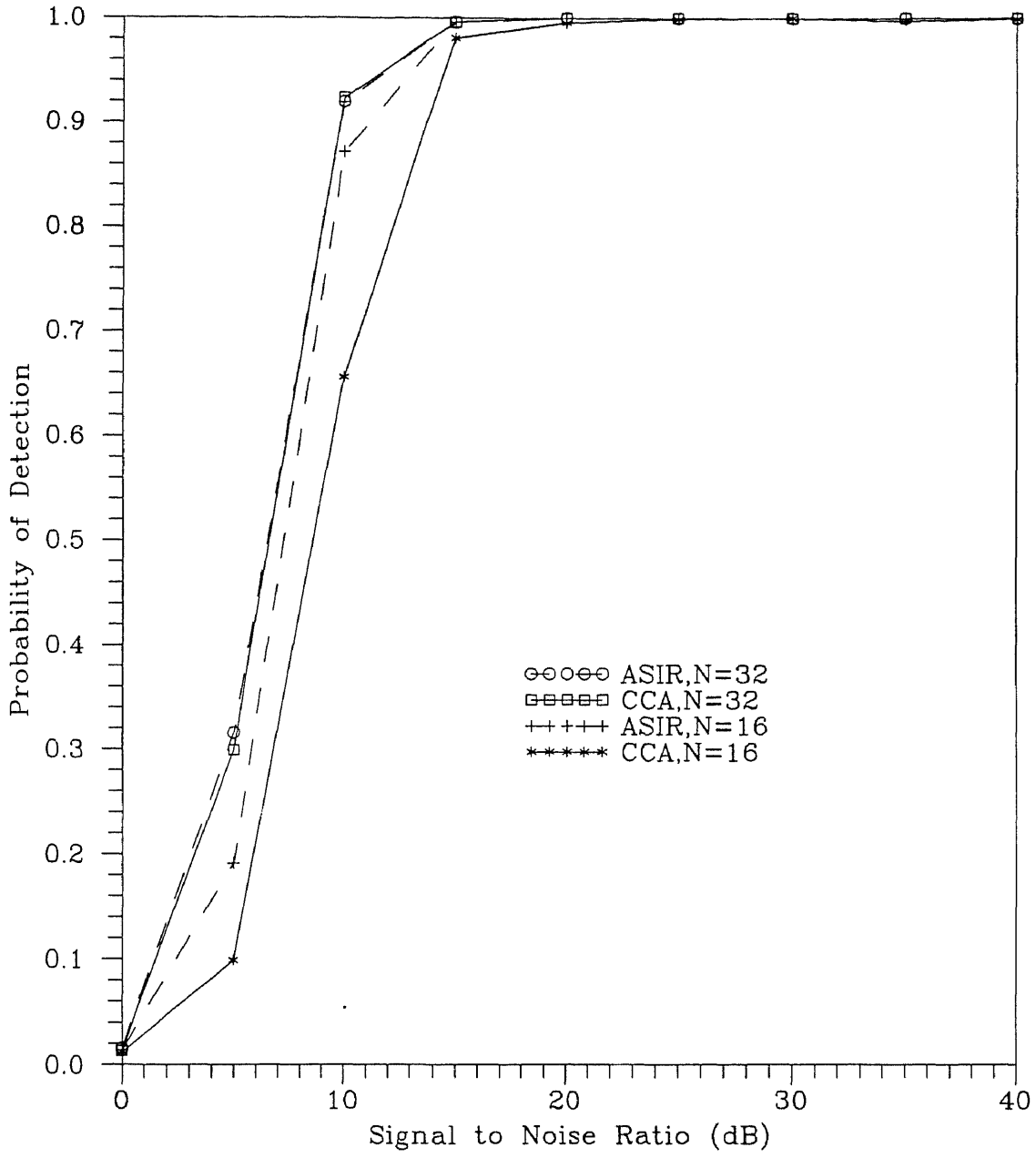

Figure 4.24. Probability of detection of the ASIR and the CCA-CFAR detectors when four interfering targets are present.
L=4, b=1.0, $\alpha=10^{-4}$, $\gamma=3\times10^{-3}$

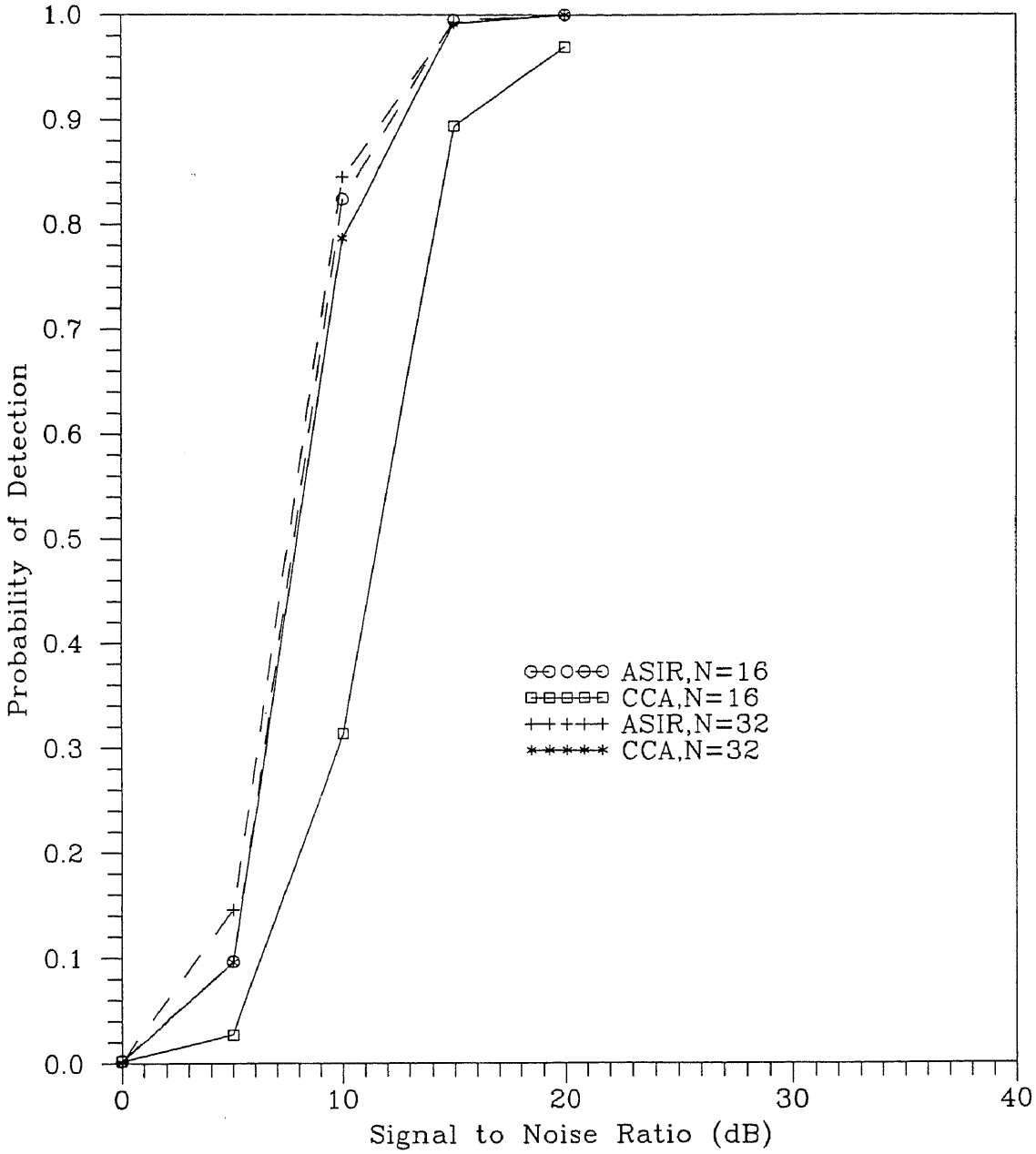

Figure 4.25. Probability of detection of the ASIR and the CCA-CFAR detectors when three interfering targets are present.
L=4, b=1.0, $\alpha=10^{-6}$, $\gamma=2\times10^{-3}$

Chapter 5

DATA DISCRIMINATOR AVERAGING CFAR DETECTOR IN MULTIPLE TARGETS AND NON-HOMOGENEOUS CLUTTER.

5.1 Introduction

In CFAR, all the samples that are generated from distributions which are different from the distribution that generates the noise in the test cell should be consored before the detection threshold is formed. In the previous chapter, we have assumed that the unwanted samples in the reference window are due to returns from interfering targets. A censoring procedure which censors these interfering target returns was proposed and analyzed. However, this is not the only source of interference, since some of the reference range cells may be also immersed in clutter as we saw in chapter three.

In this chapter, we consider the problem of CFAR detection when a number of range cells may contain interfering targets and/or a group of range cells may be immersed in clutter. We propose a data processing algorithm which performs two passes over the data. In the first pass, the objective of the algorithm is to censor possible interfering target returns that may be present in the reference cells of the test

cell. In the second pass the algorithm determines whether the test cell is in the clutter or the clear region, and selects only those samples which are identically distributed with the noise in the test cell to form the detection threshold. The proposed detector is referred to as the data discriminator (DD) CFAR processor. In addition, unlike the TM [27] and the ACGO-CFAR [30] detectors, the proposed detector does not rank order the reference noise samples which is a time consuming process before the application of the censoring procedure. We assume that all targets are flactuating according to the Swerling case II model and are embedded in uncorrelated Rayleigh envelope distributed clutter.

In section 5.2, we present a brief description and the design expression for the probability of false alarm of the TM-CFAR detector. In section 5.3, a description of the DD-CFAR detector is presented and the censoring procedure that the proposed detector uses to censor any unwanted samples is described. In section 5.4, we present the analysis of the DD-CFAR detector and we derive expressions for the probability of false censoring an interfering target, probability of false censoring a clutter power transition and the expression for the design probabilty of false alarm. In section 5.5, we present simulation results of the performance of the DD-CFAR detector as compared to other detectors that are tailord for each specific background environment. Finally in section 5.6, we present a summary along with our conclusions.

5.2 The TM-CFAR Detector

The trimmed mean CFAR detector [27], TM-CFAR, first orders the range cells according to their magnitude and then trims T_1 cells from the lower end and T_2 cells from the upper end before summing the rest. The noise level estimate, q, is set to be

$$q = \sum_{j=T_1+1}^{N-T_2} q_{(j)} \tag{5.1}$$

where $q_{(j)}$ denotes the jth ordered sample. The output of the test cell is then compared

to the adaptive threshold Tq, that is,

$$q_0 \underset{H_0}{\overset{H_1}{\gtrless}} T\,q \tag{5.2}$$

in order to determine the presence (H_1) or the absence (H_0) of a target in the test cell. The probability of false alarm, P_F, is equal to the probability that the output of the cell under test, q_0, exceeds the detection threshold, Tq, under hypothesis H_0. That is, from the test of expression (5.2), the probability of false alarm is given by

$$P_F = \Pr(Q_0 > Tq|H_0) \tag{5.3}$$

and is derived to be [27]

$$P_{FA} = \prod_{i=1}^{N-T_1-T_2} M_{V_i}(T) \tag{5.4}$$

where

$$M_{V_i}(T) = \frac{N!}{T_1!(N-T_1-1)!(N-T_1-T_2)} \tag{5.5}$$

$$\times \sum_{j=0}^{T_1} \frac{\binom{T_1}{j}(-1)^{T_1-j}}{\frac{N-j}{(N-T_1-T_2)}+T} \tag{5.6}$$

and

$$M_{V_i}(T) = \frac{a_i}{a_i+T} \qquad i = 2,\ldots,N-T_1-T_2 \tag{5.7}$$

where $a_i = (N-T_1-i+1)/(N-T_1-T_2-i+1)$. The value of the threshold multiplier T for a design probability of false alarm, α, is computed iteratively from equation (5.4) for a given value of T_1 and T_2. When there is no trimming, $(T_1 = 0, T_2 = 0)$ the TM-CFAR detector reduces to the CA-CFAR detector.

5.3 The DD-CFAR Detector

In this section, we propose the Data Discriminator CFAR, DD-CFAR, detector. The censoring procedure that the DD-CFAR detector employes to discard all the unwanted samples in the reference window, is deployed in two passes.

First Pass

During the first pass over the data, the censoring algorithm searches for interfering target returns. At the first step q_1 is compared with a scaled version of q_2, $T_i q_2$. The scaling constant T_i is selected to satisfy the design probability of false censoring $P_{FCI} = \gamma$. If $q_1 > T_i q_2$, it is declared to correspond to an interfering target return. Consequently, q_1 is censored. If $q_1 < T_i q_2$, one of two possible hypotheses might be true; either q_1 and q_2 are both noise only samples or q_2 is a sample from a distribution with a higher mean than the distribution of q_1. The second step of the censoring procedure depends on the outcome of the first one. If q_1 has been declared to be an interfering target return, the censoring algorithm proceeds by testing q_3. On the other hand, if the outcome of the first step is $q_1 < T_i q_2$, we proceed by testing q_2.

- In the former case, q_3 is compared to both $T_i q_2$ and $T_i q_4$. If $q_3 > T_i q_2$ and $q_3 > T_i q_4$, q_3 is decided to correspond to an interfering target return and is therefore censored. In a similar manner as before the algorithm proceeds by testing q_5. If both conditions are not satisfied, q_3 is decided to be a noise sample and q_4 is then tested.

- In the latter case, q_2 is compared to both $T_i q_1$ and $T_i q_3$. If $q_2 > T_i q_1$ and $q_3 > T_i q_3$, q_2 is censored as it is declared to correspond to an interfering target return and the algorithm proceeds by testing q_4. Otherwise, q_3 is tested in the nest step.

In general, q_j is compared to $T_i q_{j-1}$ and $T_i q_{j+1}$, If $q_j > T_i q_{j-1}$ and $q_j > T_i q_{j+1}$, q_j is censored and the algorithm proceeds by testing q_{j+2}. Otherwise, q_j is not censored and q_{j+1} is tested in the next step. The procedure continues in the same manner until a decision about q_{N-1} is made. If q_{N-1} is decided to be an interfering target return, the algorithm stops since its adjacent observation q_N cannot correspond to an interfering target return. If q_{N-1} has not been censored, a decision about q_N is made by comparing it with $T_i q_{N-1}$. If $q_N > T_i q_{N-1}$, q_N is censored. Otherwise q_N is

included in the threshold estimation process. Observe that in the first pass over the data, the algorithm does not search for interfering targets being in adjacent range cells as this case may be viewed as a cloud extended over a number of range cells which is handled by the algorithm implemented in the second pass over the data.

Second Pass

During the second pass over the data, the censoring algorithm processes the remaining samples to determine which ones are identically distributed with the noise in the test cell. Before any tests take place, a new array of data $q_1, \ldots, q_{\overline{M}}, q_{\overline{M}+1}, \ldots, q_{\overline{N}}$ is formed by reindexing the samples that survive the censoring process of the first pass. The test sample is located between $q_{\overline{M}}$ and $q_{\overline{M}+1}$. Since the number of samples censored from the leading range cells may be different than the number of samples censored from the lagging range cells, $\overline{M}$ may not be equal to $\overline{N}/2$. In this pass the algorithm begins by initializing two parameters, $k_1 = 0$ and $k_2 = \overline{N}$. q_1 is then compared with a scaled version of q_2, $T_c q_2$, where T_c is the scaling constant which is selected to satisfy the design probability of false censoring, $P_{FCC} = \beta$. If $q_1 > T_c q_2$ then the mean of $Q_1(\overline{Q_1})$ is decided to be greater than the mean of $Q_2(\overline{Q_2})$(where we use uppercase letters to denote random variables and lowercase letters to denote there corresponding observations). Thus, a high to low clutter power transition is assumed to occur in cell 1 (hypothesis H_{10}) and k_1 is updated to 1. In this event, the algorithm continues with the next step in which the samples q_2 and q_3 are considered. On the other hand, if $q_1 < T_c q_2$ two possible cases arise. Either q_1 and q_2 are identically distributed (hypothesis H_{00}) or a low to high clutter power transition occurs (hypothesis H_{01}). In order to determine which one of H_{00} or H_{01} is true, we then compare q_2 with $T_c q_1$. If $q_2 > T_c q_1$ hypothesis H_{01} is decided to be true and $k_1 = 1$. If $q_2 < T_c q_1$ hypothesis H_{00} is decided to be true and k_1 remains unchanged, i.e., $k_1 = 0$. The algorithm continues in the same manner until all the samples from the leading cells are tested. The value of k_1 is updated every time H_{10} or H_{01} is true. Observe that up to this point

the maximum possible value of k_1 is $\overline{M}-1$. Then, the last sample from the leading cells, $q_{\overline{M}}$, is compared with a scaled version of the first sample from the lagging cells, $T_c q_{\overline{M}+1}$. If $q_{\overline{M}} > T_c q_{\overline{M}+1}$ we decide that $\overline{Q_{\overline{M}}} > \overline{Q_{\overline{M}+1}}$, i.e., hypothesis H_{10} is true. Since the test cell is located between the cells indexed by $\overline{M}$ and $\overline{M}+1$, the low to high clutter power transition may occur in either the $\overline{M}$th cell or the test cell. It should be pointed out that in this test , it is not possible to determine the exact location of the clutter edge as the test cell is not considered by the censoring algorithm. In order to avoid a false alarm in the event that the transition occurs in the test cell, we assume that the noise in the test cell is identically distributed with $Q_{\overline{M}}$ and the second parameter k_2 is set equal to $\overline{M}$. At this point the algorithm stops and the estimate noise in the test cell is obtained by combining $q_{k_1+1},\ldots,q_{k_2}$ which have been determined to be identically distributed with the noise in the test cell. On the other hand, if $q_{\overline{M}} < T_c q_{\overline{M}+1}$ either H_{00} or H_{01} might be true. As before, we compare $q_{\overline{M}+1}$ with $T_c q_{\overline{M}}$. If $q_{\overline{M}+1} > T_c q_{\overline{M}}$ hypothesis H_{01} is decided to be true. Again the clutter power transition may occur in either the test cell or the $(\overline{M}+1)$th reference cell. As in the previous case, we decide that the edge is located in the test cell and therefore $k_1 = \overline{M}$, while k_2 remains unchanged, that is, all the leading samples are censored. If $q_{\overline{M}+1} < T_c q_{\overline{M}}$, hypothesis H_{00} is decided to be true and both k_1 and k_2 hold on to their previous values. The algorithm continues in the same manner until a clutter power transition is detected. When a clutter power transition is detected, the value of k_2 is updated accordingly while the value of k_1 does not change when the lagging samples are being tested. If no transition is detected $k_2 = \overline{N}$. Observe that when a transition is detected in the lagging cells, the algorithm stops without testing the remaining of the lagging cells. This is due to the fact that after the transition, it is not possible to determine whether any of the remaining cells are identically distributed with the noise in the test cell or not.

After the censoring procedure finishes, the noise level estimate, q, is set to be

$$q = \sum_{i=k_1+1}^{k_2} q_i \tag{5.8}$$

The output of the test cell is then compared to the adaptive threshold $T(J)q$, that is,

$$q_0 \underset{H_0}{\overset{H_1}{\gtrless}} T(J)q \tag{5.9}$$

in order to determine the presence (H_1) or absence (H_0) of a target in the test cell. The scaling constant $T(J)$ is chosen so that the design false alarm probability, α, is satisfied. The variable $J = k_2 - k_1$ is the number of samples that are included in the threshold estimation process.

5.4 Analysis of the DD-CFAR Detector

At the jth step, $j \neq 1, N$ of the first stage of the censoring procedure, the probability of false censoring an interfering target, P_{FCI}, is the probability that Q_j exceeds both $T_i Q_{j-1}$ and $T_i Q_{j+1}$ when Q_{j-1}, Q_j and Q_{j+1} are noise only samples (hypothesis H_{000}), that is,

$$P_{FCI} = \Pr(Q_j > TQ_{j-1}, Q_j > TQ_{j+1} | H_{000}) \tag{5.10}$$

and can be written as

$$\begin{aligned} P_{FCI} &= \left\{\frac{1}{\Gamma(L)}\right\}^3 \int_0^\infty dq_j^{L-1} \exp(-q_j) \int_0^{q_j/T_i} dq_{j-1}^{L-1} \exp(-q_{j-1}) \\ &\quad \cdot \int_0^{q_j/T_i} dq_{j+1}^{L-1} \exp(-q_{j+1}) \end{aligned} \tag{5.11}$$

where by evaluating the inner intagrals we obtain

$$\begin{aligned} P_{FCI} &= \left\{\frac{1}{\Gamma(L)}\right\}^3 \int_0^\infty \left\{ q_j^{L-1} \exp(-q_j[1+2/T_i]) \sum_{r=0}^{L-1} \frac{(-1)(L-1)! q_j^{L-1-r} \frac{1}{T_i}^{L-1-r}}{(L-1-r)!} \right. \\ &\quad \cdot \sum_{k=0}^{L-1} \frac{(-1)(L-1)! q_j^{L-1-k} \frac{1}{T_i}^{L-1-k}}{(L-1-k)!} + q_j^{L-1} \exp(-q_j)(L-1)!^2 \\ &\quad \left. +2 q_j^{L-1} \exp(-q_j[1+1/T_i]) \sum_{r=0}^{L-1} \frac{(-1) q_j^{L-1-r} \frac{1}{T_i}^{L-1-r}}{(L-1-r)!} \right\} dq_j \end{aligned} \tag{5.12}$$

and P_{FCI} is obtained to be

$$P_{FCI} = \sum_{r=0}^{L-1}\sum_{k=0}^{L-1}\frac{(1/T)^{2L-2-k-r}(3L-3-r-k)!((L-1)!)^{-1}}{(L-1-k)!(L-1-r)!(1+2/T)^{3L-2-r-k}} + 1 - 2\sum_{r=0}^{L-1}\frac{((L-1)!)^{-1}(1/T)^{L-1-r}(2L-2-r)!}{(L-1-r)!(1+1/T)^{2L-1-r}} \quad (5.13)$$

The probability of false censoring the first sample is

$$P_{FCI} = \Pr(Q_1 > T_i Q_2 | H_{00}) \quad (5.14)$$

while the probability of false censoring the last sample is

$$P_{FCI} = \Pr(Q_N > T_i Q_{N-1} | H_{00}) \quad (5.15)$$

In (5.14) and (5.15), hypothesis H_{00} denotes the case where the two samples involved in these tests, are noise only samples. For these two tests, P_{FCI} is obtained to be

$$P_{FCI} = \sum_{k=0}^{L-1}\binom{L+k-1}{k}\frac{T_i^k}{(1+T_i)^{L+k}} \quad (5.16)$$

That is the scaling constant is calculated from

$$P_{FCI} = \begin{cases} \sum_{r=0}^{L-1}\sum_{k=0}^{L-1}\frac{(1/T)^{2L-2-k-r}(3L-3-r-k)!((L-1)!)^{-1}}{(L-1-k)!(L-1-r)!(1+2/T)^{3L-2-r-k}} + 1 & j \neq 1, N \\ -2\sum_{r=0}^{L-1}\frac{((L-1)!)^{-1}(1/T)^{L-1-r}(2L-2-r)!}{(L-1-r)!(1+1/T)^{2L-1-r}} & \\ \sum_{k=0}^{L-1}\binom{L+k-1}{k}\frac{T_i^k}{(1+T_i)^{L+k}} & j = 1, N \end{cases} \quad (5.17)$$

In the second pass of the algorithm the probability of false censoring a clutter power transition, P_{FCC}, is defined as the probability to falsely decide the presence of a step discontinuity in the reference window when in fact no discontinuity is present. P_{FCC}, can be written as a contour integral of the moment generating function, mgf, of the equivalent statistic $R_j = Q_j - T_c Q_{j-1}$ where q_j and q_{j-1} are the observations from the jth and $(j-1)$th reference cells respectively. The scaling constant T_c is selected so that the desired probability of false censoring, γ, is achieved. Thus,

$$\begin{aligned} P_{FCC} &= \Pr(R_j > 0 | H_{00}) \\ &= -\frac{1}{2\pi i}\int_c \omega^{-1}\Phi_{R_j|H_{00}}(\omega)d\omega \end{aligned} \quad (5.18)$$

where the mgf of the equivalent statistic R_j is given by

$$\begin{aligned}\Phi_{R_j|H_{00}} &= E\left[\exp(-\omega(\sum_{i=1}^{L} q_{ij} - T_c \sum_{i=1}^{L} q_{i(j-1)}))\right] \\ &= \int_0^\infty \cdots \int_0^\infty \exp\left(-\sum_{i=1}^{L} q_{ij}\right) \exp\left(-\omega \sum_{i=1}^{L} q_{ij}\right) dq_{ij} \ldots dq_{Lj} \\ &\quad \cdot \int_0^\infty \cdots \int_0^\infty \exp\left(-\sum_{i=1}^{L} q_{i,j-1}\right) \exp\left(T_c\omega \sum_{i=1}^{L} q_{i,j-1}\right) dq_{i,j-1} \ldots dq_{L,j-1} \\ &= \left[\left(\frac{1}{1+\omega}\right)\left(\frac{1}{1-T_c\omega}\right)\right]^L \end{aligned} \tag{5.19}$$

In equation (5.18), the contour of integration c is crossing the real ω-axis at $\omega = c_1$ and is closed in an infinite semicircle in the left half ω-plane. c_1 is selected so that c encloses all the poles of $\Phi_{R_j|H_{00}}(\omega)$ that lie in the open left half ω-plane. Substituting equation (5.19) into equation (5.18), the residue at $\omega = -1$ is

$$\begin{aligned}\text{Res}_{\omega\to-1} &= \frac{1}{(L-1)!}\lim_{\omega\to-1}\frac{d^{L-1}}{d\omega^{L-1}}\left\{\frac{1}{\omega(1-T_c\omega)^L}\right\} \\ &= \frac{1}{(L-1)!}\lim_{\omega\to-1}\sum_{k=0}^{L-1}\binom{L-1}{k}\frac{d^k(1-T_c\omega)^{-L}}{d\omega^k}\frac{d^{L-1-k}(\omega^{-1})}{d\omega^{L-1-k}} \end{aligned} \tag{5.20}$$

and by using

$$\begin{aligned}\frac{d^n[uv]}{dx^n} &= \binom{n}{0} v\frac{d^n u}{dx^n} + \binom{n}{1}\frac{dv}{dx}\frac{d^{n-1}u}{dx^{n-1}} + \binom{n}{2}\frac{d^2v}{dx^2}\frac{d^{n-2}u}{dx^{n-2}} + \\ &\quad \ldots + \binom{n}{k}\frac{d^K u}{dx^k}\frac{d^{n-k}u}{dx^{n-k}} + \ldots \binom{n}{n} u\frac{d^n u}{dx^n} \end{aligned} \tag{5.21}$$

the probability of false censoring is derived to be

$$P_{FCC} = \sum_{k=0}^{L-1}\binom{L+k-1}{k}\frac{T_c^k}{(1+T_c)^{L+k}} \tag{5.22}$$

Equations (5.17) and (5.22) are used to calculate T_i and T_c so that $P_{FCI} = \gamma$ and $P_{FCC} = \beta$.

The probability of false alarm, P_F, is equal to the probability that the output of the cell under test, q_0, exceeds the detection threshold, $T(J)q$, under hypothesis H_0. That is, from the test of expression (5.9), the probability of false alarm is given by

$$P_F = \Pr(Q_0 > T(J)Q|H_0) \tag{5.23}$$

where Q denotes the estimator of the noise level in the test cell which is given by equation (5.8). Following the same procedure as in the derivation of the expression for the probability of false ecensoring, the P_F, is the contour integral

$$P_F = -\frac{1}{2\pi i}\int_C \omega^{-1}\Phi_{R|H_0}(\omega)d\omega \tag{5.24}$$

where the equivalent statistic R is given by

$$R = Q_0 - T(J)Q \tag{5.25}$$

The contour of integration is the same as that of equation (5.18) except c_1 is selected so that all the poles of $\Phi_{R|H_0}(\omega)$ that lie in the open left half ω-plane are enclosed. The mgf of R under H_0 is given by

$$\begin{aligned}
\Phi_{R|H_0}(\omega) &= E[\exp(-\omega(\sum_{i=1}^{L} q_{i0} - T\sum_{j=1}^{J}\sum_{i=1}^{L} q_{ij}))] \\
&= \int_0^\infty \cdots \int_0^\infty \exp\left(-\omega\sum_{i=1}^{L} q_{i0}\right)\exp\left(-\sum_{i=1}^{L} q_{i0}\right) dq_{i0}\ldots dq_{L0} \\
&\quad \cdot \int_0^\infty \cdots \int_0^\infty \exp\left(\omega T\sum_{j=1}^{J}\sum_{i=1}^{L} q_{ij}\right)\exp\left(-\sum_{j=1}^{J}\sum_{i=1}^{L} q_{ij}\right) dq_{ij}\ldots dq_{Lj} \\
&= (1+\omega)^{-L}(1-T\omega)^{-JL}
\end{aligned} \tag{5.26}$$

Substitution of equation (5.26) into (5.24) and with the residue at $\omega = -1$ given by

$$\begin{aligned}
\mathrm{Res}_{\omega\to -1} &= \frac{1}{(L-1)!}\lim_{\omega\to -1}\frac{d^{L-1}}{d\omega^{L-1}}\left\{\frac{\omega^{-1}}{\omega(1-T\omega)^{JL}}\right\} \\
&= \frac{1}{(L-1)!}\lim_{\omega\to -1}\sum_{k=0}^{L-1}\binom{L-1}{k}(-1)^{L-1-k}\omega^{-(L-k)} \\
&\quad \cdot\frac{(JL+k-1)!}{(JL-1)!}\frac{T^k}{(1-T\omega)^{JL+k}}
\end{aligned} \tag{5.27}$$

the design expression for the probability of false alarm, P_F, is

$$P_F = \sum_{k=0}^{L-1}\binom{JL+k-1}{k} T(J)^k(1+T(J))^{-(JL+k)} \tag{5.28}$$

Equation (5.28) is used to calculate the threshold multipliers $T(J), J = 1,\ldots,N$, so that $P_F = \alpha$.

In Figures 5.1 and 5.2, we plot the probability of false alarm versus the probability of false censoring a clutter edge (β) for $L = 1, 4$ and $\alpha = 10^{-4}$, for the DD-CFAR detector. The curves are parametric to different values of probability of false censoring an interfering target (γ). We observe that when γ is equal to 2×10^{-3} the probability of false alarm that is achieved by the DD-CFAR detector is equal to the design value. On the other hand when γ increases ($\gamma = 3 \times 10^{-3}, 4 \times 10^{-3}, 5 \times 10^{-3}$) the probability of false alarm increases irrespective of the value of β. When β is greater than 2×10^{-3}(γ kept at 2×10^{-3}) the probability of false alarm increases above the design value. This is due to the fact that when, β is large overcensoring is encouraged. Therefore, the probability of censoring some of the largest noise samples as clutter edge(s), which causes underestimating of the noise level in the test cell, is high. For values of β less than 2×10^{-3}, the DD-CFAR detector still achieves the design value of probability of false alarm, however, when β is smaller, this will discourage censoring of possible clutter edge(s). Thus, for $\alpha = 10^{-4}$ we choose the desired values of $P_{FCC} = 2 \times 10^{-3}$ and $P_{FCI} = 2 \times 10^{-3}$. Similarly in the case of multiple pulse ($L = 4$) the optimum choices are $P_{FCC} = 10^{-3}$ and $P_{FCI} = 10^{-3}$.

5.5 Results

The false alarm control and detection performances of the DD-CFAR detector for some nonhomogeneous background environments are evaluated and compared to those of the GO, SO, ACGO and TM-CFAR detectors. In the comparisons with the ACGO and the TM-CFAR detectors, we only considered single pulse transmission ($L = 1$) since the order statistics analysis for multiple pulse transmission is too cumbersome.

In Figures 5.3 and 5.4 the false alarm regulation properties of the DD-CFAR detector are shown for various values of the background noise level. The results show the CFAR properties of the DD-CFAR detector for $N = 16$ reference noise

samples and for single ($L = 1$) and multiple pulse ($L = 4$) transmission. Three desired probabilities of false alarm are considered $(10^{-2}, 10^{-3}, 10^{-4})$ and we assume $\beta = 2 \times 10^{-3}$ and $\gamma = 2 \times 10^{-3}$ in Figure 5.3 and $\beta = 10^{-3}$ and $\gamma = 10^{-3}$ in Figure 5.4. In both cases where $L = 1$ and $L = 4$ the false alarm probability of the proposed detector is shown to be robust for all the values of desired probability of false alarm considered.

In Figure 5.5, we study the false alarm regulation properties of the DD-CFAR detector in the presence of both one and two clutter power transitions for $L = 1$ and 4. We observe that the false alarm control performance is more robust when one transition is present since the probability of detecting one edge is higher than the probability of detecting both edges. Also, when the per pulse clutter to noise ratio C is small ($C < 12$dB) the number of false alarms when $L = 4$ is greater than the number of false alarms when $L = 1$. This is due to the fact that although the probability of detecting the edge(s) when $L = 4$ is higher than the probability of detecting the edge(s) when $L = 1$, the probability of false alarm when $L = 4$ is higher than the probability of false alarm when $L = 1$ due to the diversity in the system configuration. As C increases, the probability of correctly assessing the environment increases substantially especially when $L = 4$ thereby achieving more robust false alarm control performance than the case where $L = 1$.

In Figures 5.6 and 5.7, we compare the false alarm regulation properties of the DD-CFAR detector to those of the TM(k_1, k_2) and ACGO-CFAR detectors for $L = 1$. In the case of one clutter edge (Figure 5.6) the false alarm control performance of the DD and ACGO-CFAR detectors are comparable. The TM-CFAR detectors considered, are tailored to censor all 4 clear samples since $k_1 \geq 4$. We observe that as k_1 increases, the probability of false alarm of the TM-CFAR detector decreases, while as k_2 increases its probability of false alarm increases. In the presence of two clutter transitions as shown in Figure 5.7, the ACGO-CFAR detector censors all the high

power clutter samples from both the leading and the lagging range cells especially when C is large. Therefore, it severely underestimates the noise level in the test cell and its probability of false alarm approaches unity as C becomes large. The false alarm probability of the DD-CFAR detector is more robust than those of the TM-CFAR detectors, especially when C is large, because the TM-CFAR detectors use one or more clear cells in the threshold estimation process. In Figures 5.8 to 5.10 we study the false alarm regulation of the ACGO, TM and DD-CFAR detectors in the presence of two clutter power transitions, extending at various locations in the leading and lagging reference window. In Figures 5.9 and 5.10 where the clutter to noise ratio is 20dB and 30dB respectively, the false alarm probability of the ACGO-CFAR detector is the highest. This is due to the fact that the censoring procedure of the ACGO-CFAR detectors, underestimates the noise level in the test cell since all the high power samples are censored. In Figures 5.8 and 5.9 the DD-CFAR detector has the highest probability of false alarm since the censoring procedure may miss the clutter edges for low clutter to noise ratio (10dB,20dB). However, when the clutter to noise ratio is high (30dB) as shown in Figure 5.10 the performance of the proposed detector is superior as compared to the others.

In Figure 5.11, we present the detection probability of the GO, CA, ACGO, DD-CFAR and the ideal detector. We have assumed that $N = 16, L = 1$ and $\alpha = 10^{-4}$. The performance of all detectors is approximately the same with the ideal detector superior as expected. In Figure 5.12, we study the detection performance of the DD-CFAR and the TM-CFAR detectors when interfering targets in homogeneous noise are present in the reference window. The GO and SO-CFAR detectors are not shown since as we saw in chapter 2 they both yield extremely poor detection performance in this environment. We have assumed that four interfering targets whose radar cross section is the same (b=1.0) with the target in the test cell are present in the reference window. The dashed curves represent the performance of the DD-CFAR detector.

The notation for example DD(1, 3) in the figure means that one interfering target is present in the leading window and three interfering targets are present in the lagging window. The detection probability of the TM-CFAR detector does not depend on the location of the interfering targets since the outputs of all the reference range cells are rank ordered before any censoring takes place. However, the detection probability for the TM-CFAR detector depends on the preassigned censoring points. The case where TM(0, 4) is superior to all others. In this case the largest four samples in the reference window are censored. This is equivalent to assuming exact a priori knowledge about the number of interfering targets since four interfering targets have been assumed in the reference cells. When however the assessment of the interfering environment is not correct and the number of higher ordered samples that are censored is less than the actual number of interfering targets in the reference window, the performance of the TM-CFAR detector is seriously degraded as shown for example in the case of TM(0, 1). Unlike the TM-CFAR detector the performance of the proposed detector is robust. Also a similar comparison of the proposed detector with the ACGO-CFAR detector is presented in Figure 5.13. The detection performance of both detectors is shown to be approximately the same.

In Figures 5.14 to 5.19 we compare the GO, ACGO, TM and DD-CFAR detectors in the presence of clutter power transition in the leading window and a number of interfering targets in the lagging window. All the interfering targets are assumed to have the same radar cross section area with the target in the test cell (b= 1.0). All camparisons are shown for $N = 16$, $L = 1$ and for $C = 10, 20, 30$dB. The detection performance of the GO-CFAR detector is seriously degraded in the presence of interfering targets in the reference window due to the capture effect. In the case where exact a priori information is available about the interfering environment, the performance of the TM-CFAR detector is superior to all others. For instance in Figure 5.14 the case of TM(4, 2) is superior to all others, since 4 samples from the leading and

two samples from the lagging window are trimmed, which is equivalent to an exact knowledge of the environment. However, in the case where there is no trimming in the lagging window, TM(4, 0), the detection performance of the TM-CFAR detector is seriously degraded. On the other hand, the detection performane of the ACGO and DD-CFAR detector remain robust. However, in the case where the number of interfering targets increases as shown in Figures 5.17 to 5.19, the DD-CFAR detector is slightly superior as compared with the ACGO-CFAR detector. This is due to the fact that as the number of interfering targets present in the leading or lagging reference window increases the detection performance of the ACGO-CFAR detector degrades as shown in Figure 3.1 of chapter 3.

In Figures 5.20 to 5.25 the SO, ACGO and the DD-CFAR detectors are compared in the presence of one and two interfering targets in the leading or the lagging reference window and when a clutter power transition ($C = 10, 20, 30$dB) is present in the lagging reference window. The test cell is assumed to be in the clear and the interfering targets have the same radar cross section (b=1.0) with the target in the test cell. Single pulse transmission and a reference window of $N = 16$ is assumed. The detection performance of the SO-CFAR detector is superior to all others as shown in Figures 5.20 to 5.22, since this constitutes the best environment for the SO-CFAR. However, in the case where an interfering target is present in both the leading and the lagging reference window the detection performance of the SO-CFAR detector is seriously degraded due to the capture effect as shown in Figures 5.23 to 5.25. The detection performance of the DD-CFAR detector is shown to be better as compared to that of the ACGO-CFAR detector especially when the clutter to noise ratio is high (30dB). As the clutter to noise ratio becomes higher the censoring procedure of the DD-CFAR detector is more effective.

In Figure 5.26, we study the detection probability of the DD-CFAR detector for $L = 1$ and 4 in the presence of three interfering targets and different background

environments. Since C is high, the probability of detecting the possible clutter edges is high, therby obtaining a robust estimate of the noise level in the test cell. We observe that the detection performance in all three bachground environments is robust and fairly close to the performance of the ideal detector. The detection probability of the DD-CFAR detector is greatly improved when $L = 4$ due to the enhanced performance offered by the diversity transmission. For example, considering the environment of case (a) for $L = 1$ and a signal to noise ratio of 15dB the probability of detection is approximately 0.49. For the same signal to noise ratio, where $L = 4$ the detection probability achieved by the DD-CFAR detector almost doubles and is equal to one.

In Figure 5.27, we compare the required processing time of the TM, ACGO and the DD-CFAR detectors for $L = 1$. We have assumed that in the order statistics processors (TM and ACGO-CFAR) the heap sorting algorithm which is the fastest sorting routine [33] is used to rank order the data. When the heap sort is used, $N \log_2 N$ comparisons are required to sort the data. We have also assumed that a single DSP processor [34,35], employing special floating point hardware so that multiplications and additions take the same amount of time to be executed, is used. The maximum required number of machine cycles for the three detectors are derived to be

$$\tau_{TM} = 2Nlog_2N + N + 2 \tag{5.29}$$

$$\tau_{ACGO} = 2Nlog_2\frac{N}{2} + 4N + 1 \tag{5.30}$$

$$\tau_{DD} = 11N - 2 \tag{5.31}$$

We observe that when

$$N \geq 2^{4.5} \tag{5.32}$$

the execution time of the DD-CFAR detector is smaller than the execution time of the ACGO-CFAR detector. The execution time of the TM-CFAR detector is approximately the same to that of the ACGO-CFAR detector.

5.6 Summary and Conclusions

In this chapter, we have considered the problem of CFAR detection when some of the range cells may contain interfering targets and/or a group of range cells may be immersed in the clutter. We proposed the Data Discriminator CFAR detector, DD-CFAR, which performs two passes over the data. In the first pass, the objective of the algorithm is to censor all possible interfering target returns that may be present in the reference cells of the test cell. In the second pass the algorithm determines whether the test cell is in the clutter or the clear region and selects only those samples which are identically distributed with the noise in the test cell to form the detection threshold. The most attractive feature of the DD-CFAR detector, is that unlike the TM and ACGO-CFAR detectors, it does not rank order the reference noise samples which is a time consuming process, and yet achieves robust performace as compared with the order-based statistics counterparts.

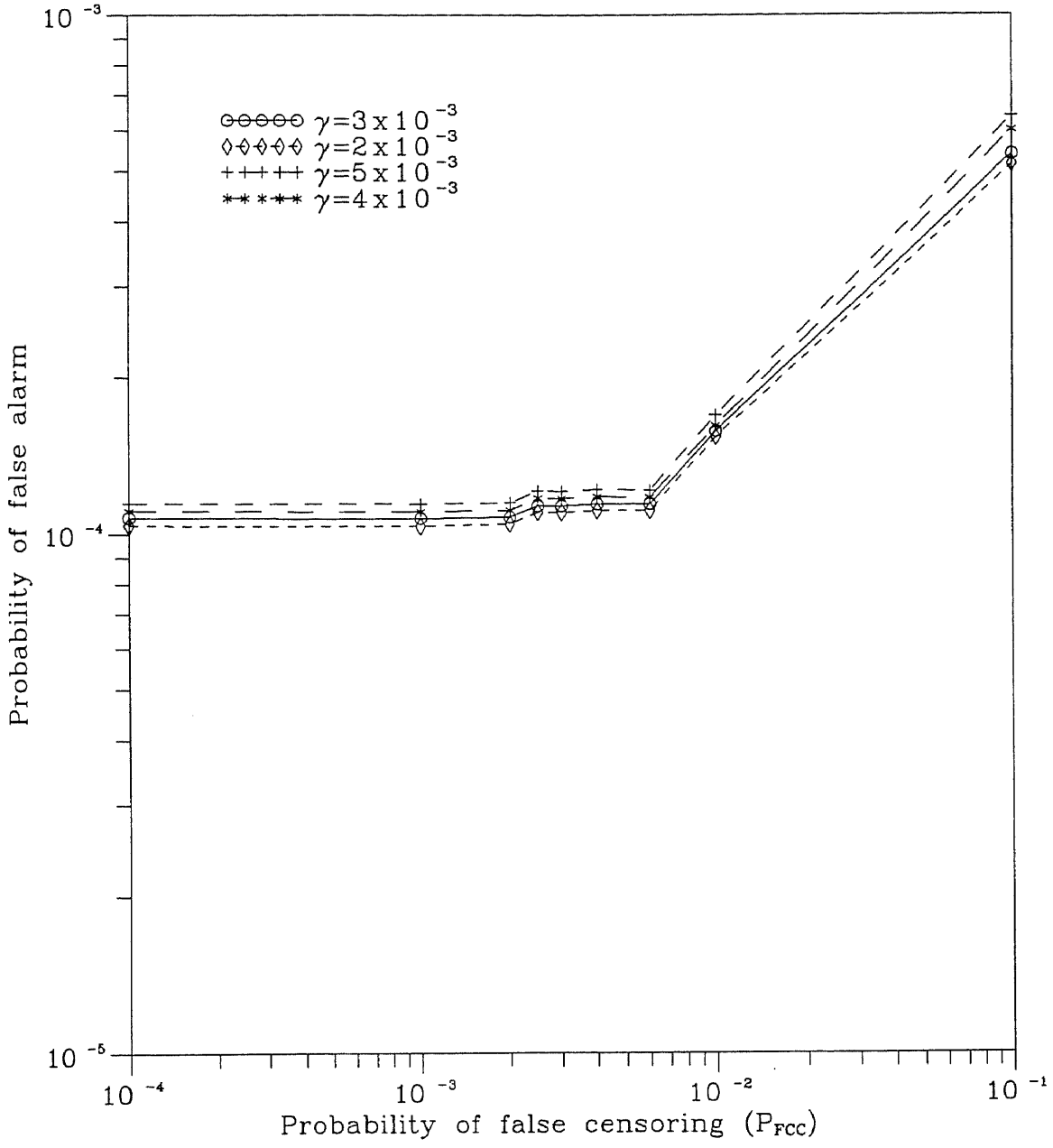

Figure 5.1. Probability of false alarm versus probability of false censoring of the DD-CFAR detector. L=1, $a=10^{-4}$.

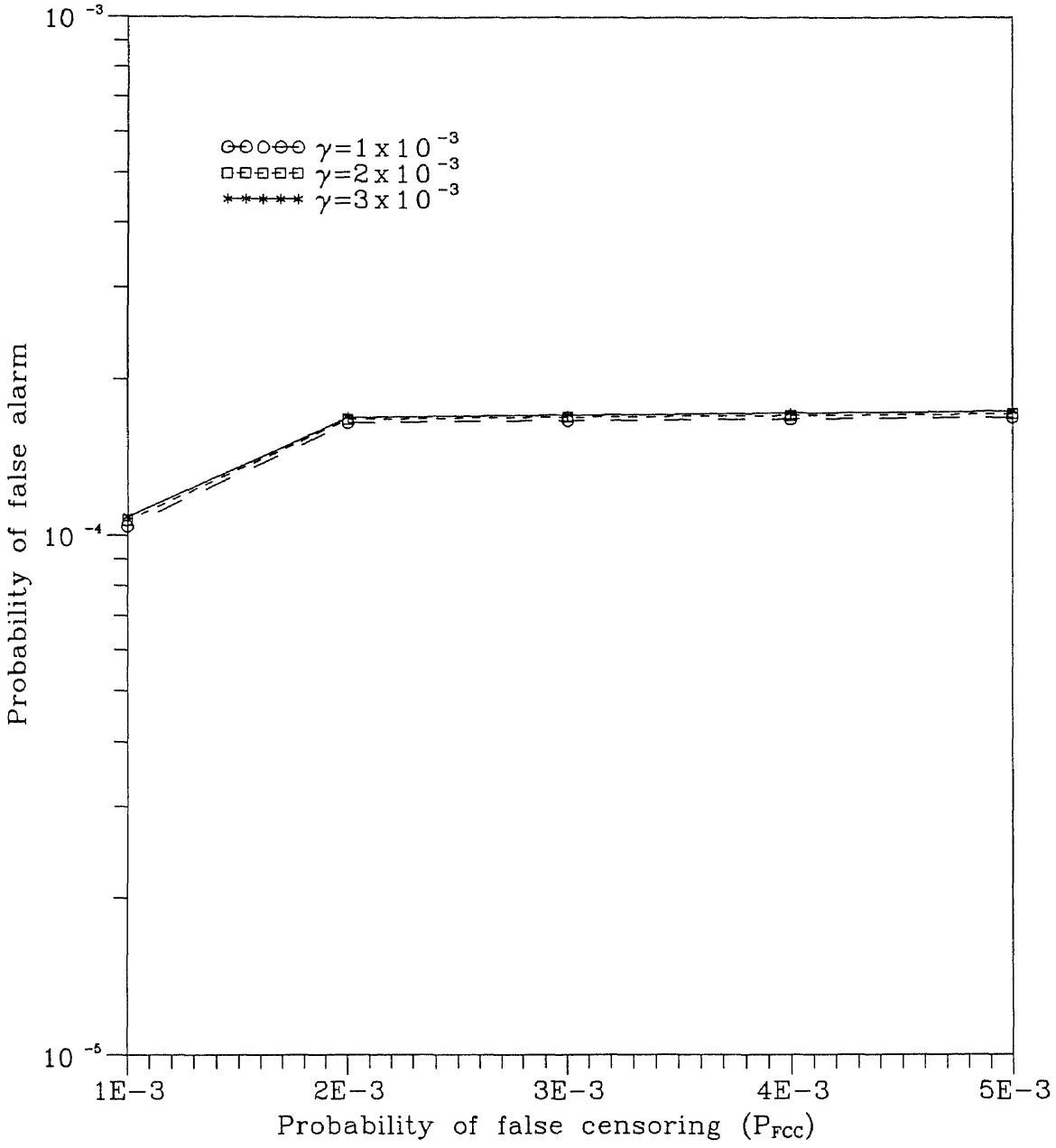

Figure 5.2. Probability of false alarm versus probability of false censoring of the DD-CFAR detector. L=4, $a=10^{-4}$.

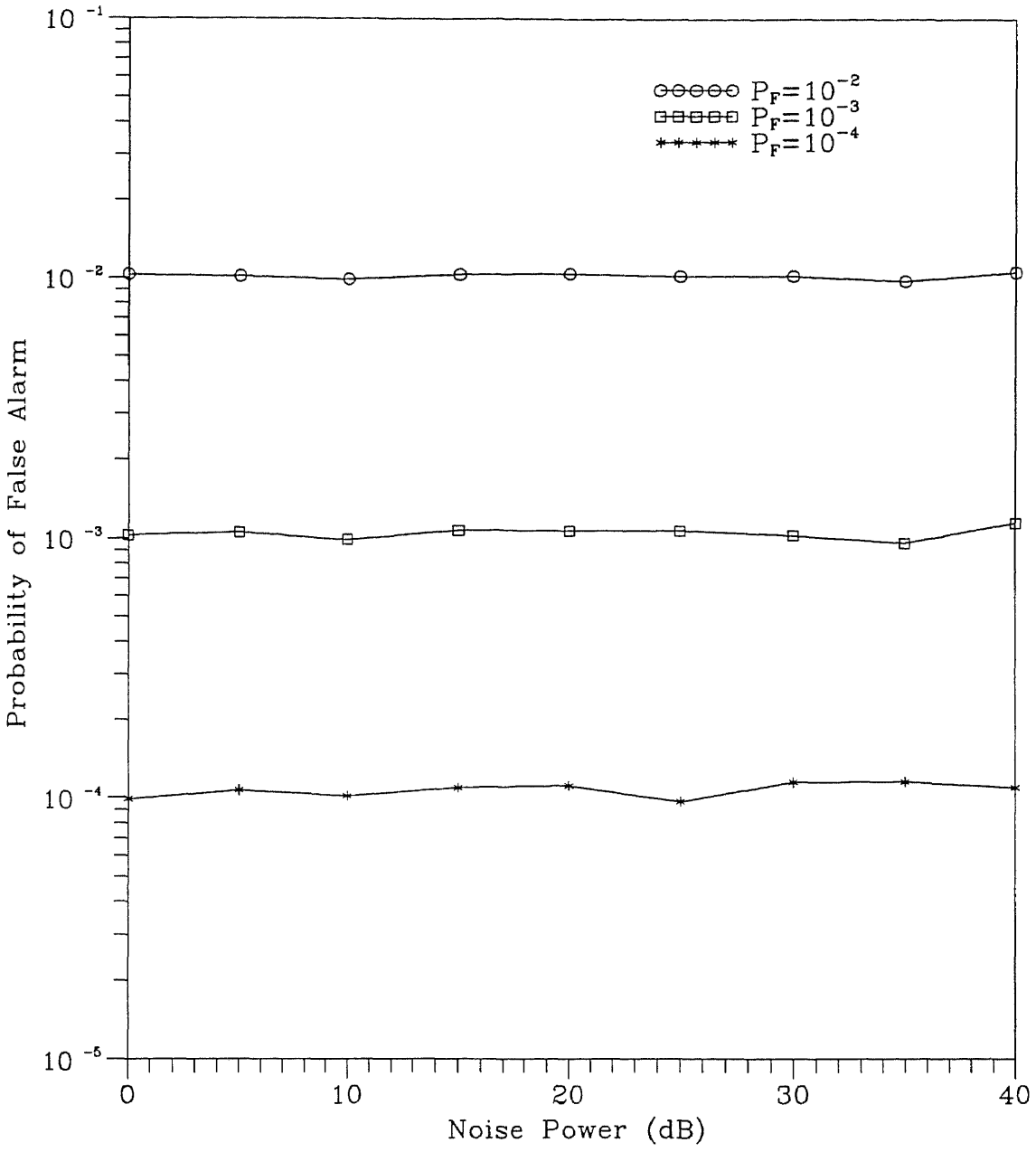

Figure 5.3. Probability of false alarm versus noise power (dB) L=1, $\beta=2\times10^{-3}$, $\gamma=2\times10^{-3}$

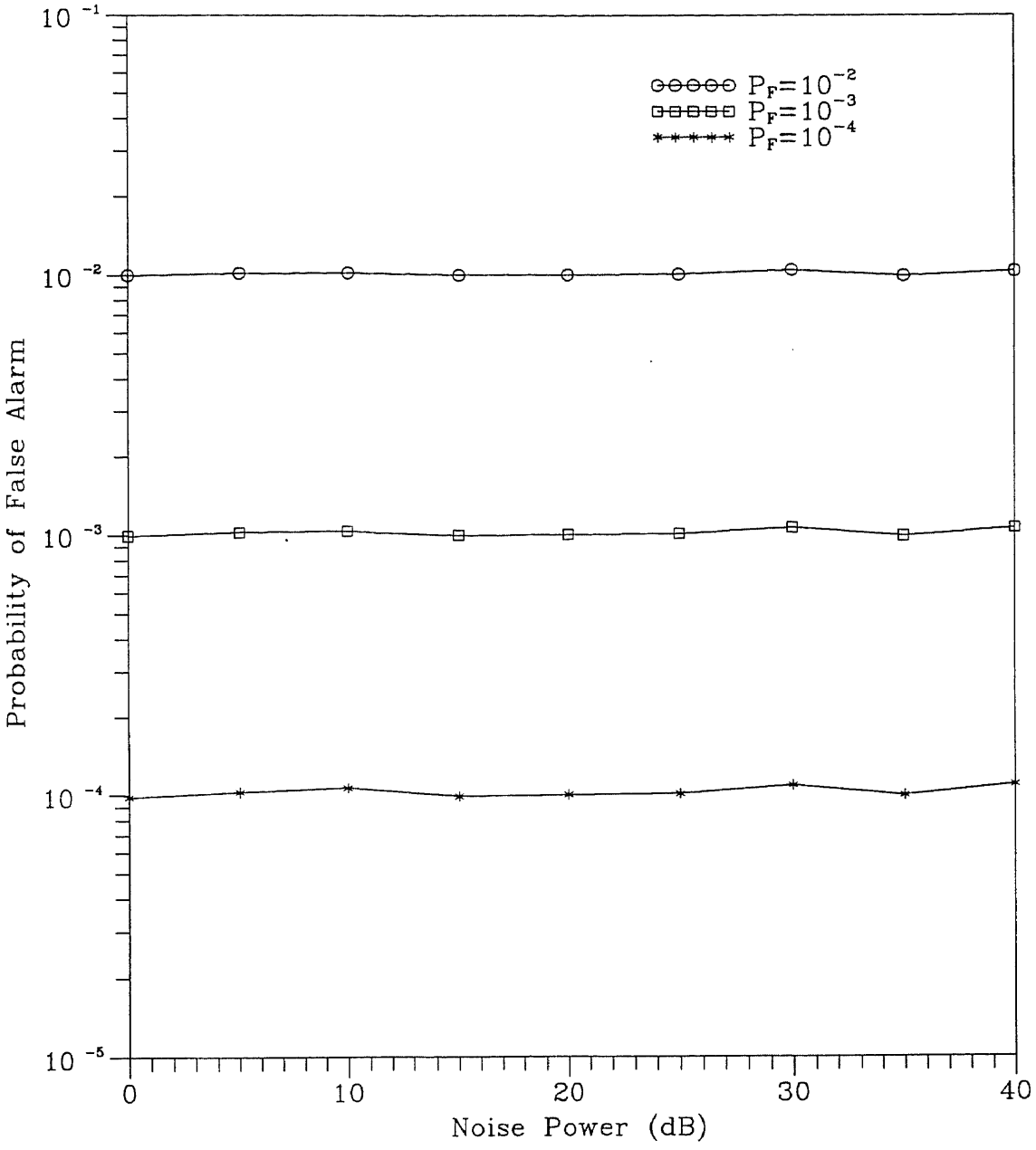

Figure 5.4. Probability of false alarm versus noise power (dB) L=4, $\beta=10^{-3}$, $\gamma=10^{-3}$

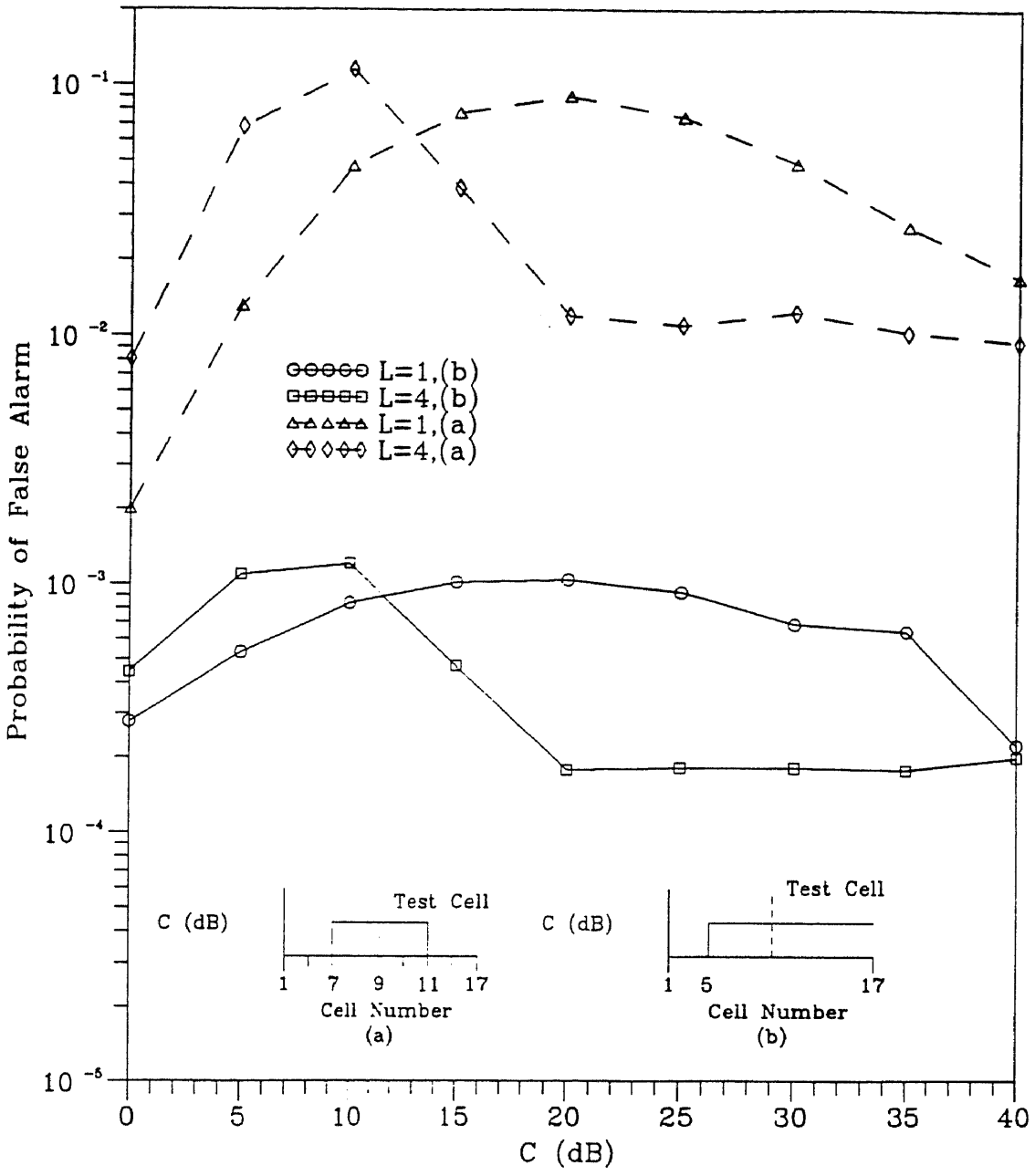

Figure 5.5. Probability of false alarm of the DD−CFAR detector in the in the presence of one and two clutter power transitions.
N=16, $\alpha=10^{-4}$

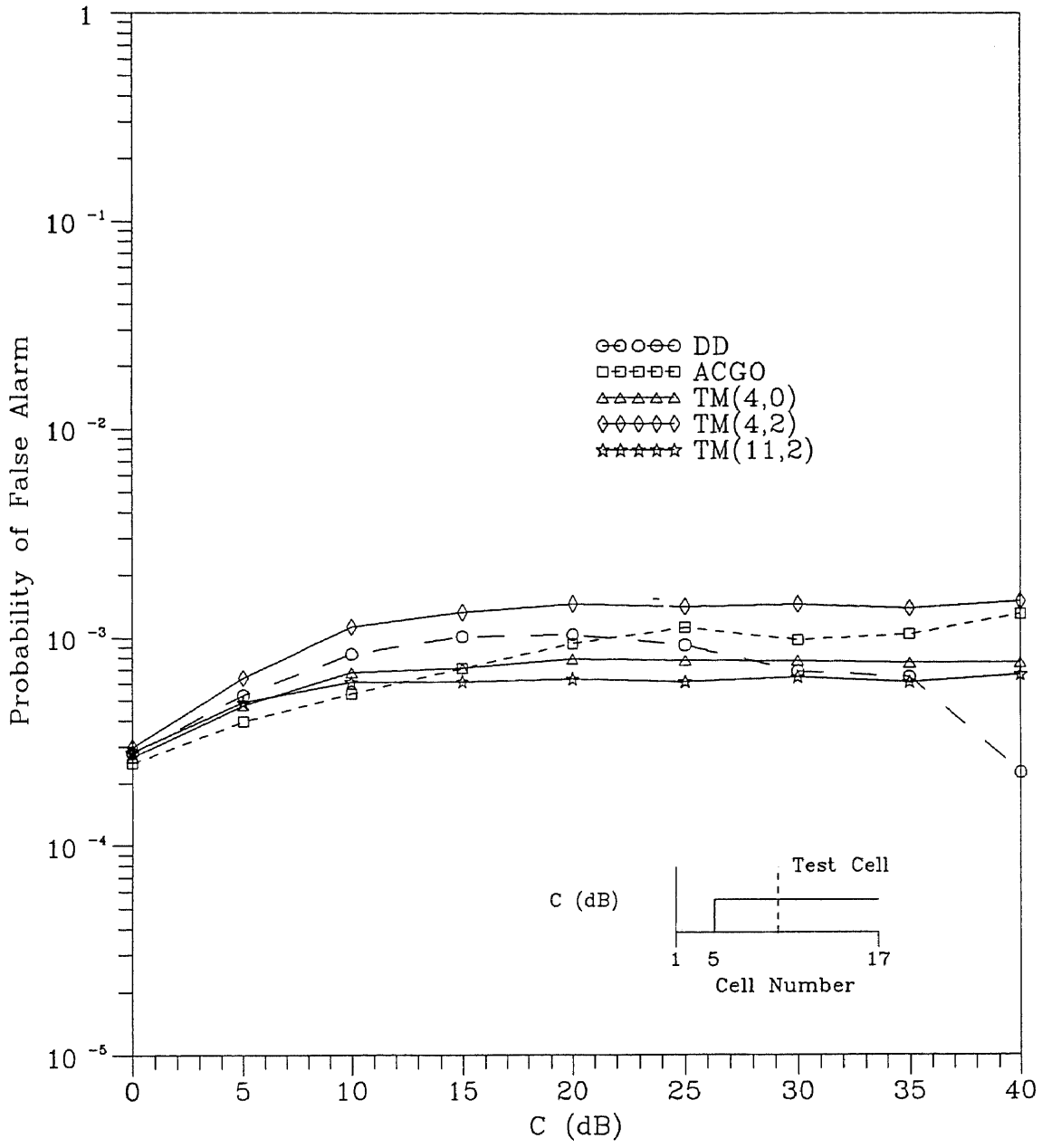

Figure 5.6. Probability of false alarm of the DD,TM and the ACGO-CFAR detectors in the presence of one power transition.
N=16, L=1, $\alpha=10^{-4}$, $\beta=2\times10^{-3}$, $\gamma=2\times10^{-3}$.

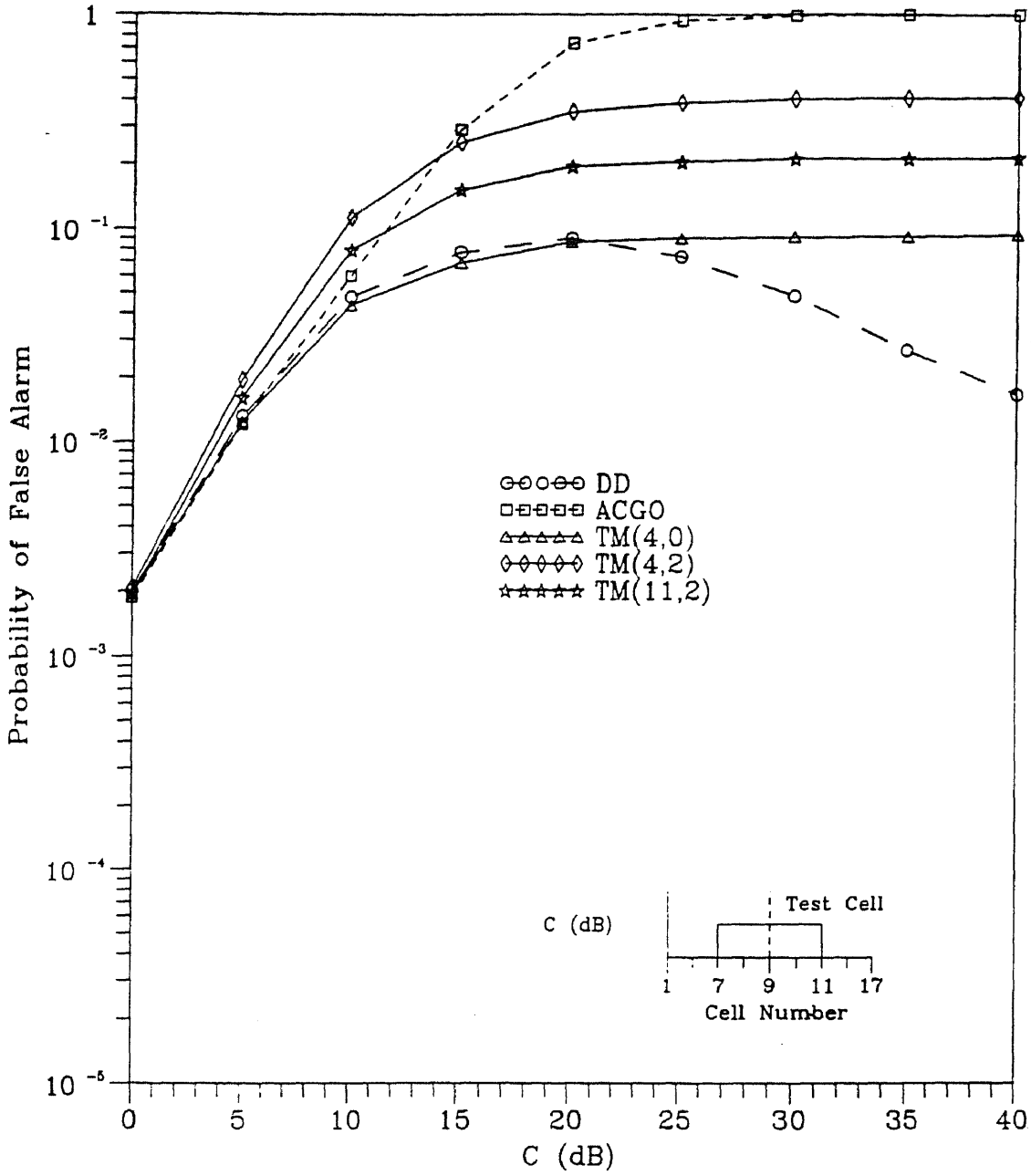

Figure 5.7. Probability of false alarm of the DD,TM and the ACGO-CFAR detectors in the presence of two clutter power transitions.
N=16, L=1, $\alpha=10^{-4}$, $\beta=2\times10^{-3}$, $\gamma=2\times10^{-3}$.

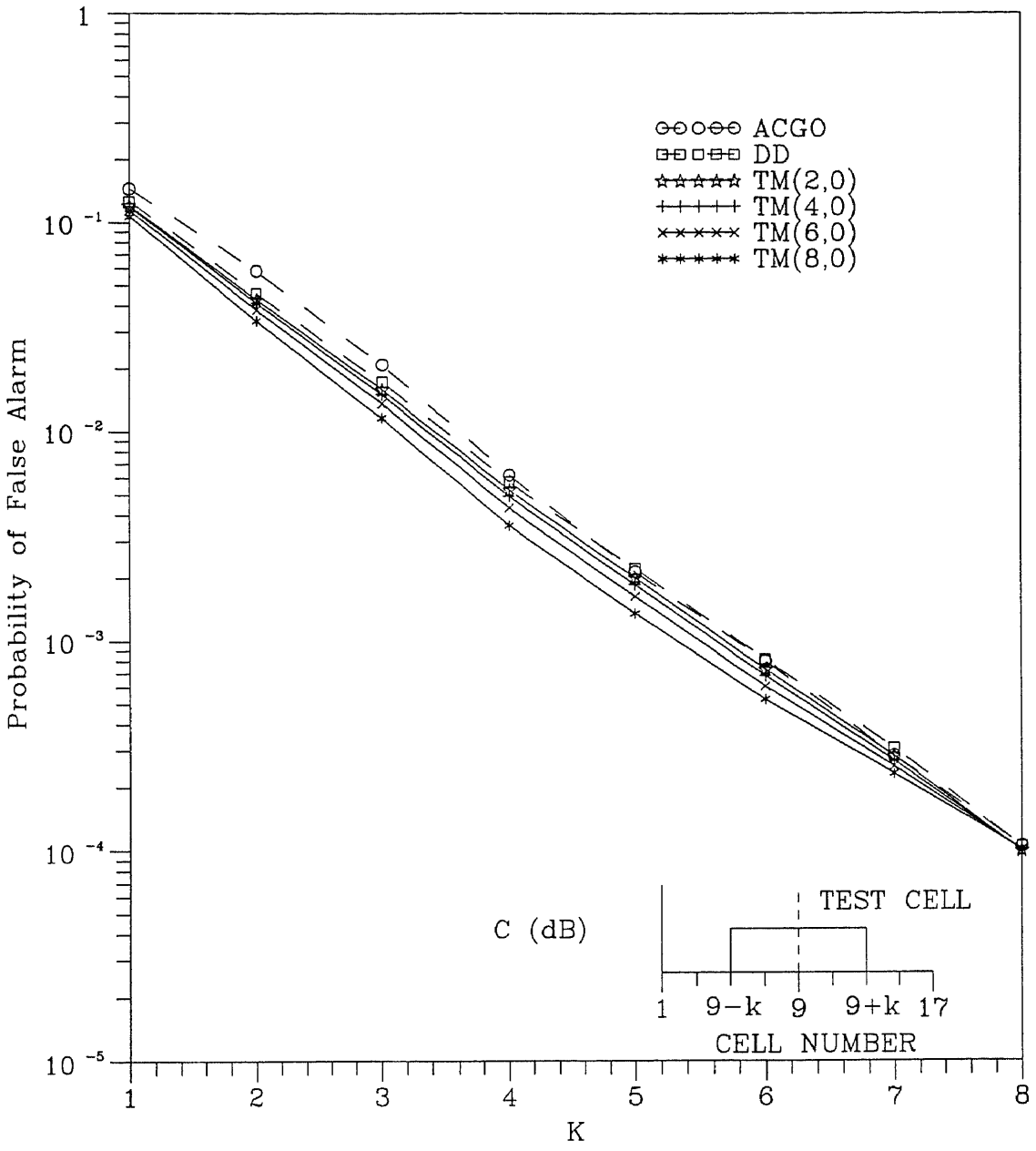

Figure 5.8. Probability of false alarm of the DD,TM and the ACGO-CFAR detectors when the test cell and 2K reference cells are in the clutter.
C=10dB, N=16, L=1, $\alpha=10^{-4}$, $\beta=2\times10^{-3}$, $\gamma=2\times10^{-3}$.

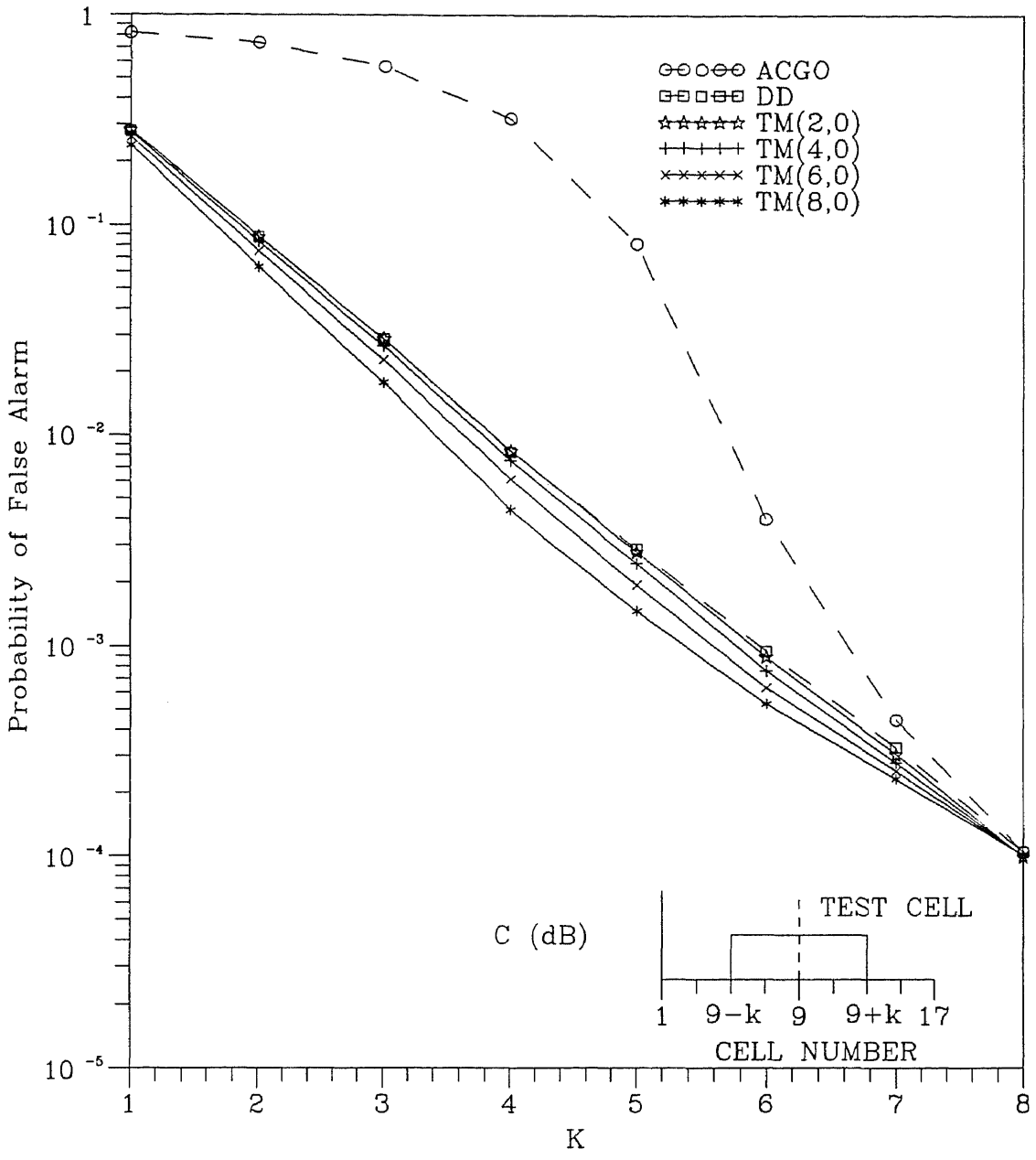

Figure 5.9. Probability of false alarm of the DD,TM and the ACGO–CFAR detectors when the test cell and 2K reference cells are in the clutter.
C=20dB, N=16, L=1, $\alpha=10^{-4}$, $\beta=2\times10^{-3}$, $\gamma=2\times10^{-3}$.

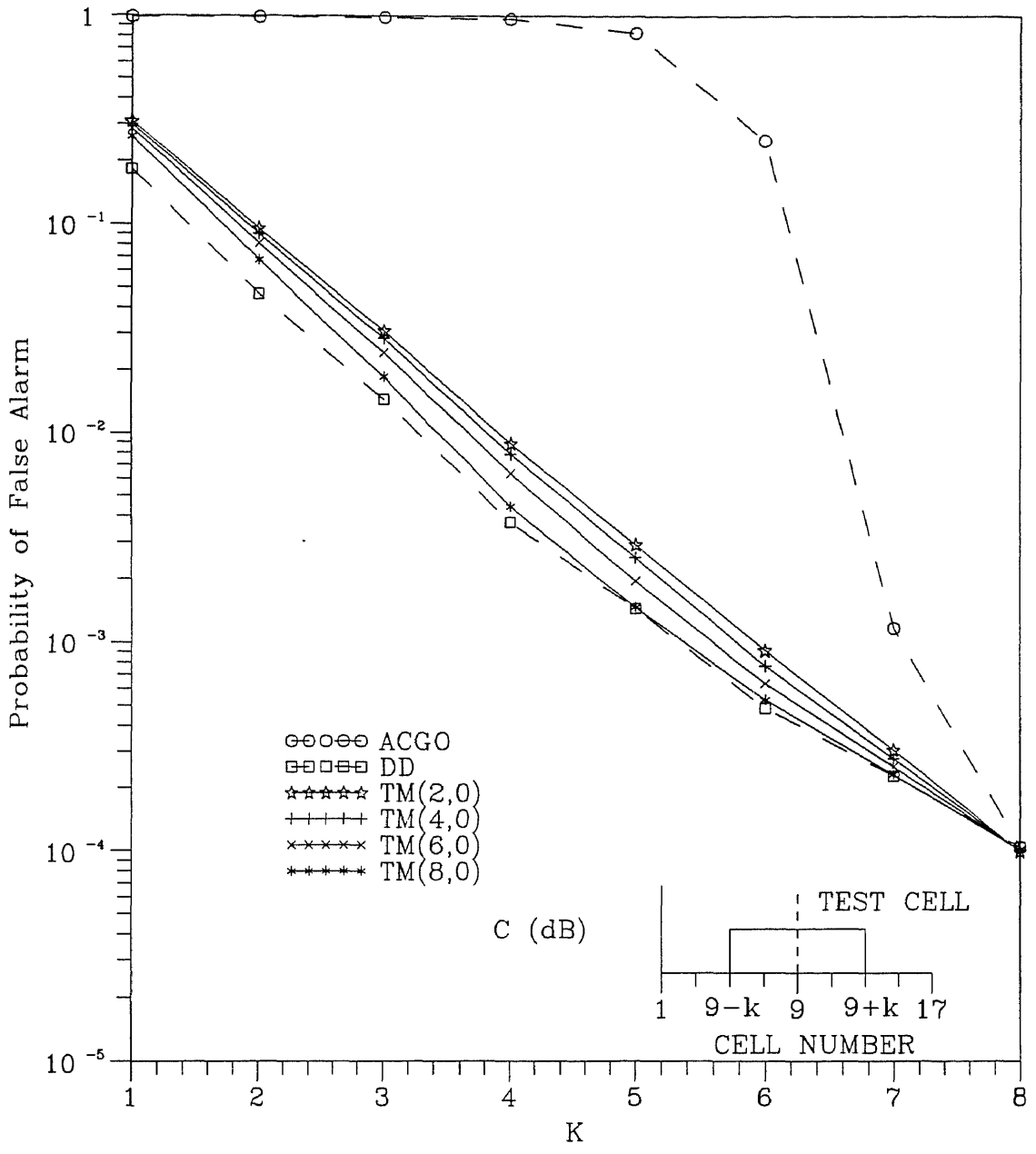

Figure 5.10. Probability of false alarm of the DD,TM and the ACGO–CFAR detectors when the test cell and 2K reference cells are in the clutter.
C=30dB, N=16, L=1, $\alpha=10^{-4}$, $\beta=2\times10^{-3}$, $\gamma=2\times10^{-3}$.

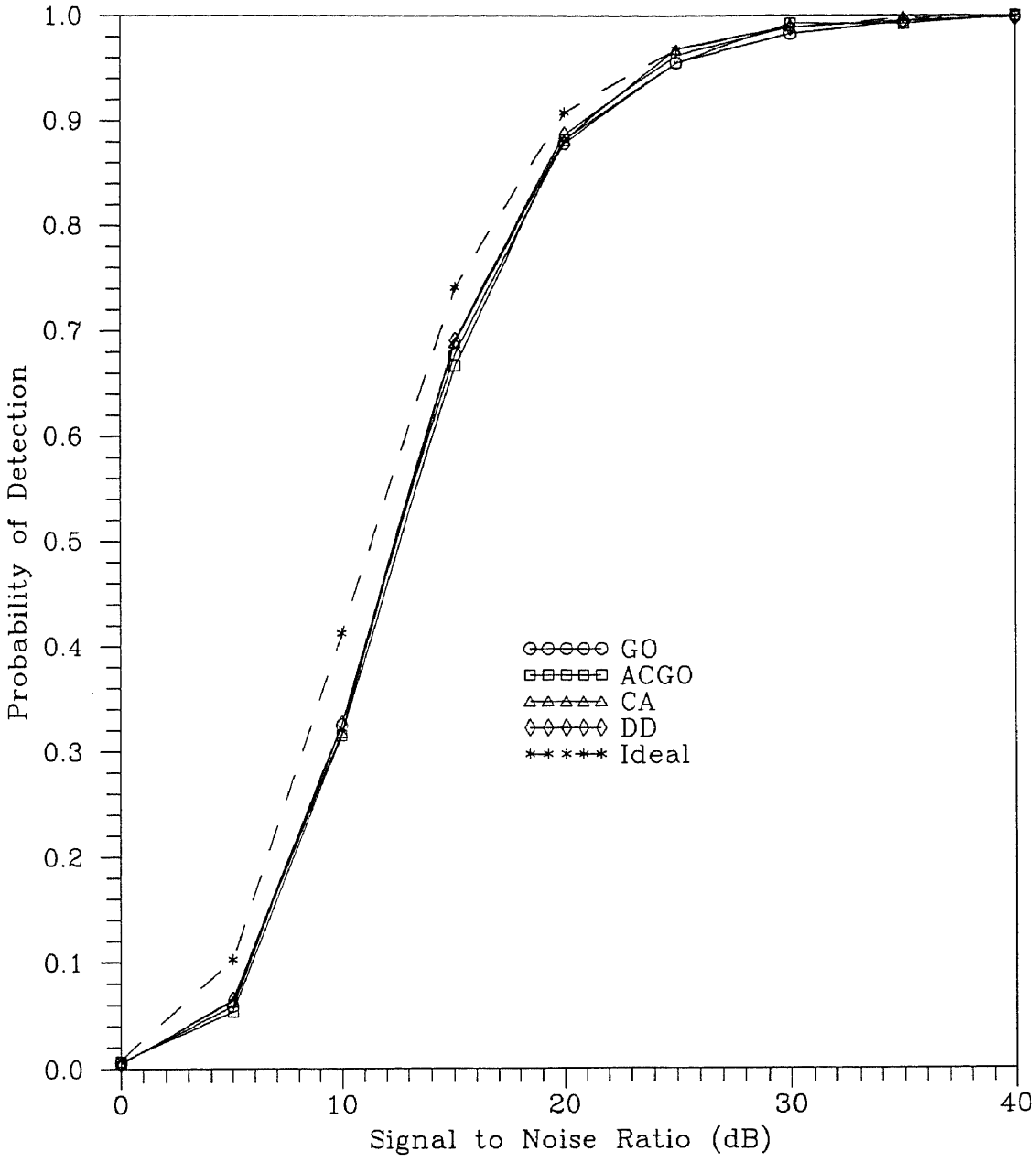

Figure 5.11. Probability of detection of the DD,ACGO,GO,CA-CFAR, and the Ideal detectors in homogeneous background environment.
N=16, L=1, $\alpha=10^{-4}$, $\beta=2\times10^{-3}$, $\gamma=2\times10^{-3}$.

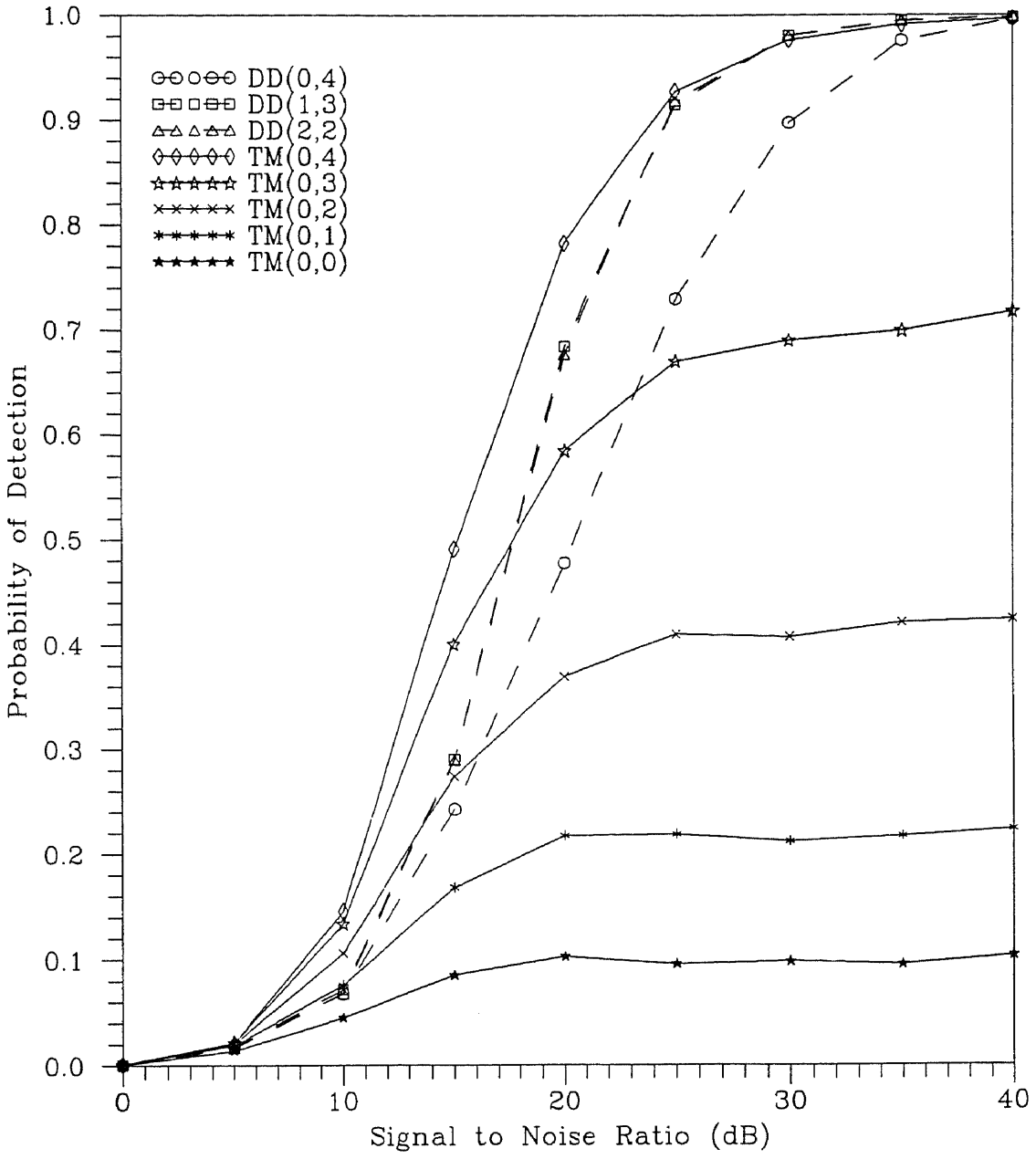

Figure 5.12. Probability of detection of the DD and TM-CFAR detectors when a number of interfering targets are present in the reference window.
N=16, b=1.0, L=1, $\alpha=10^{-4}$, $\beta=2\times10^{-3}$, $\gamma=2\times10^{-3}$.

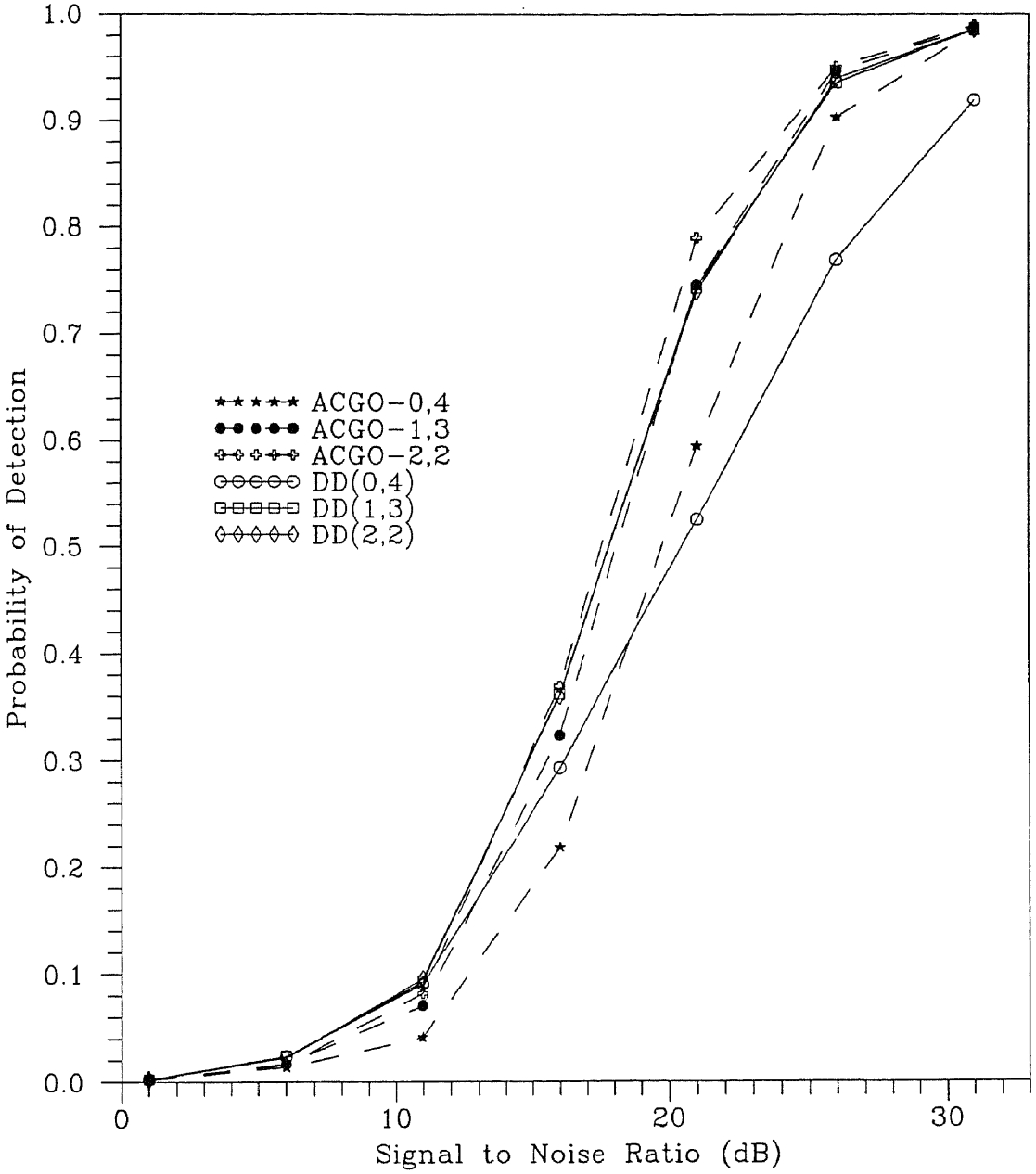

Figure 5.13. Probability of detection versus SNR(dB) of the ACGO-CFAR and the DD-CFAR detectors in the presence of four interfering targets.
N=16, b=1.0, $\alpha=10^{-4}$.

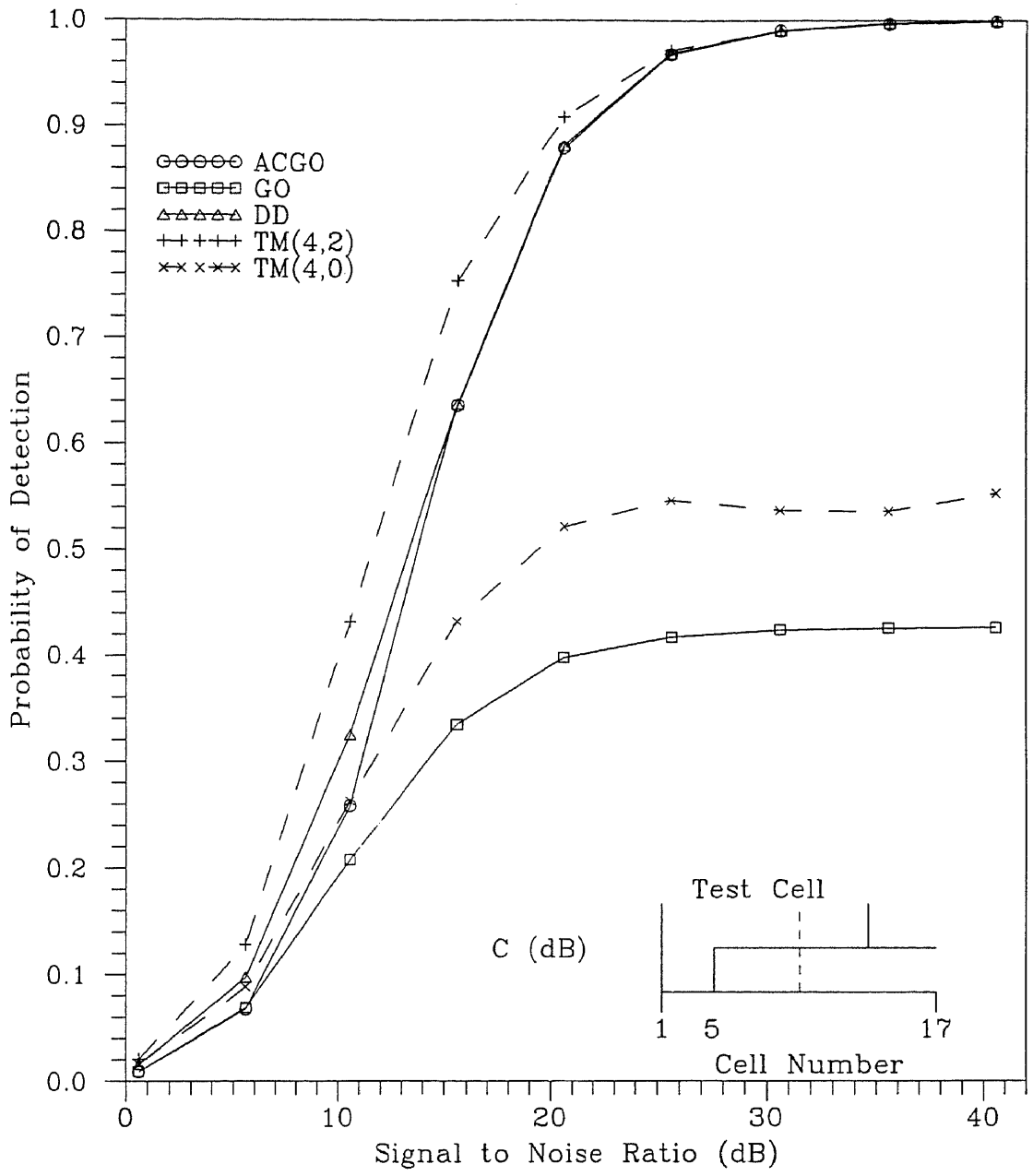

Figure 5.14. Probability of detection of the DD,ACGO,GO and TM-CFAR detectors when one interfering target and a clutter power transition are present in the reference window.
C=10dB, N=16, b=1.0, L=1, $\alpha=10^{-4}$, $\beta=2\times10^{-3}$, $\gamma=2\times10^{-3}$.

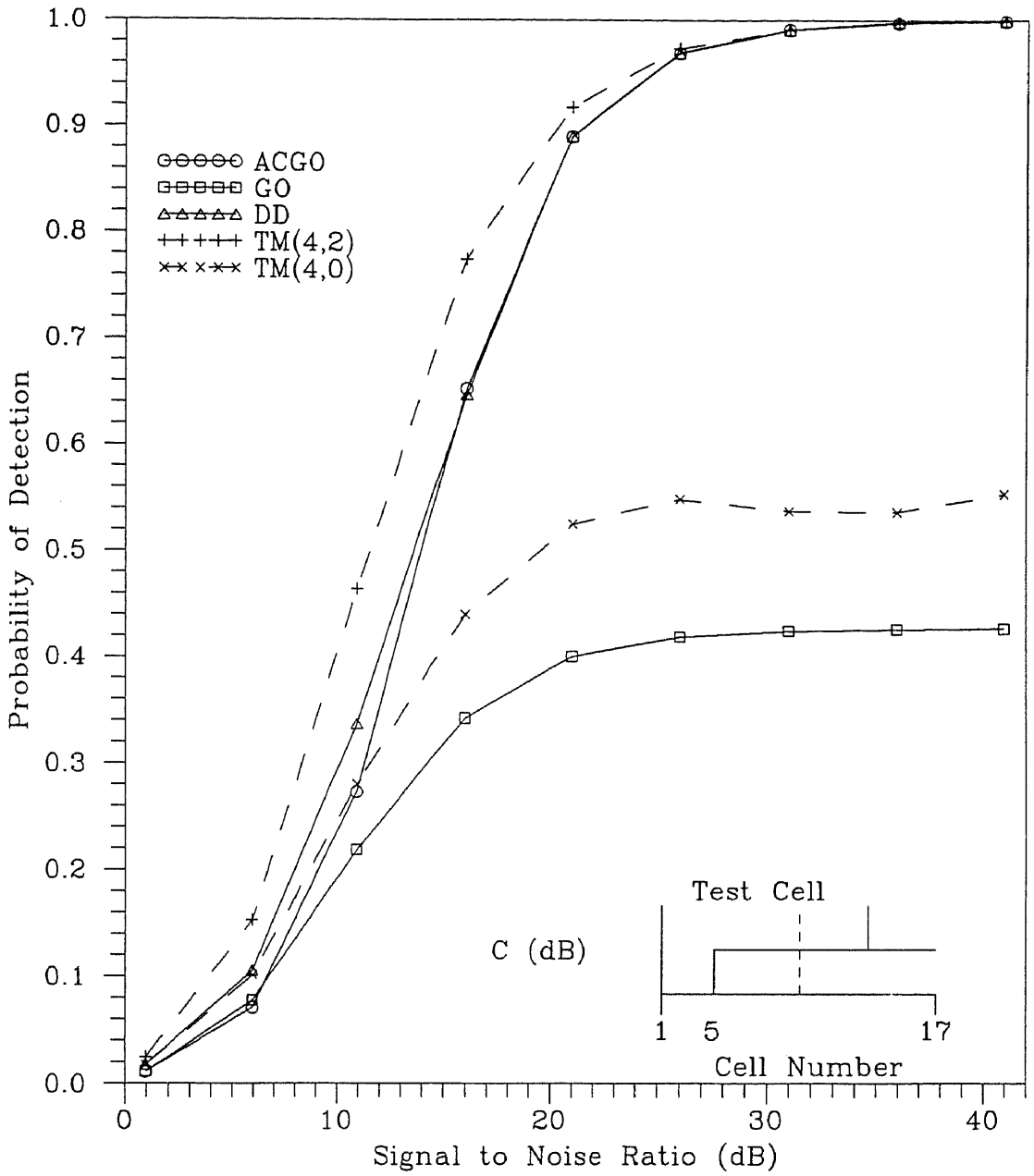

Figure 5.15. Probability of detection of the DD,ACGO,GO and TM-CFAR detectors when one interfering target and a clutter power transition are present in the reference window.
C=20dB, N=16, b=1.0, L=1, $\alpha=10^{-4}$, $\beta=2\times10^{-3}$, $\gamma=2\times10^{-3}$.

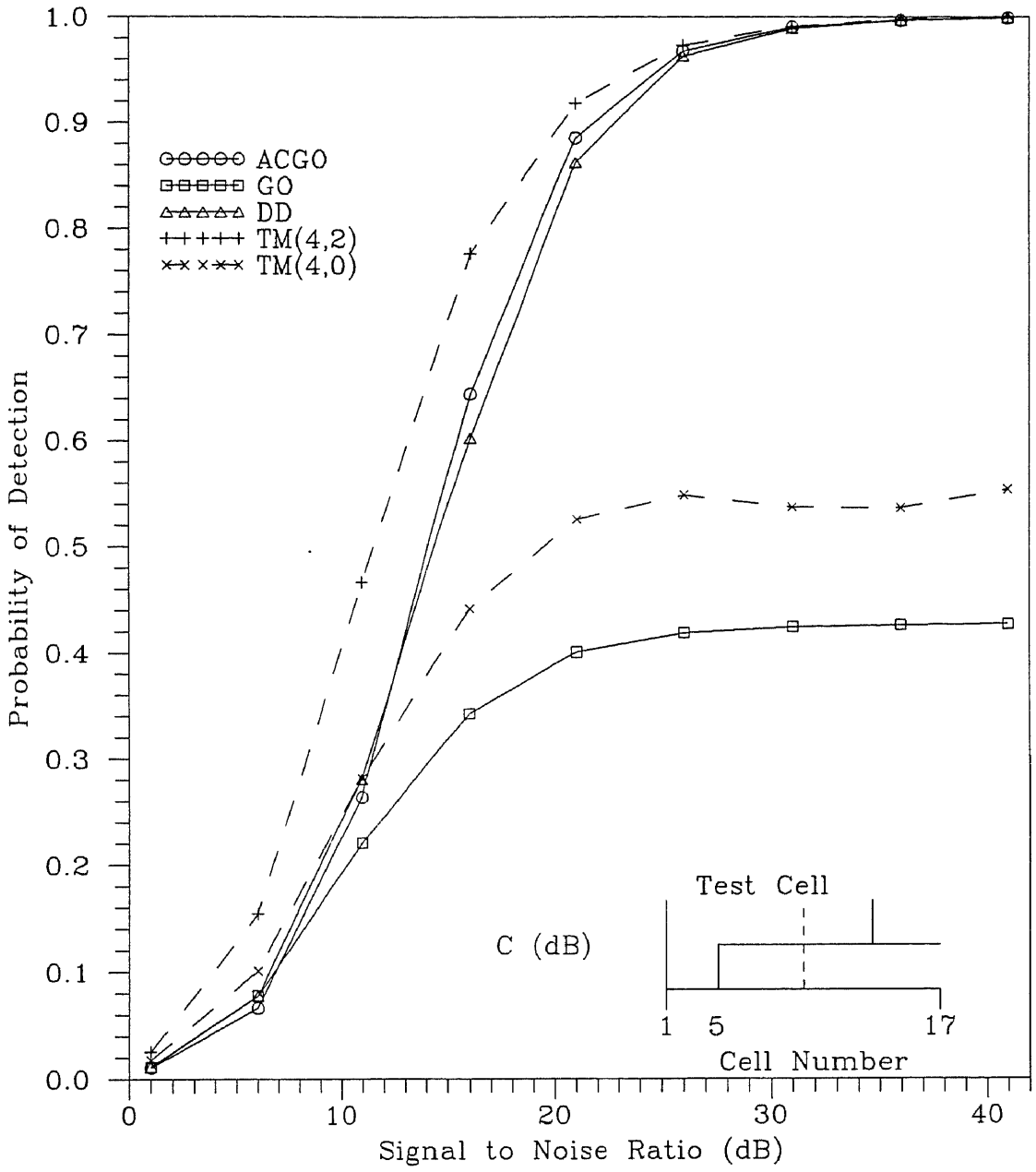

Figure 5.16. Probability of detection of the DD,ACGO,GO and TM−CFAR detectors when one interfering target and a clutter power transition are present in the reference window.
C=30dB, N=16, b=1.0, L=1, $\alpha=10^{-4}$, $\beta=2\times10^{-3}$, $\gamma=2\times10^{-3}$.

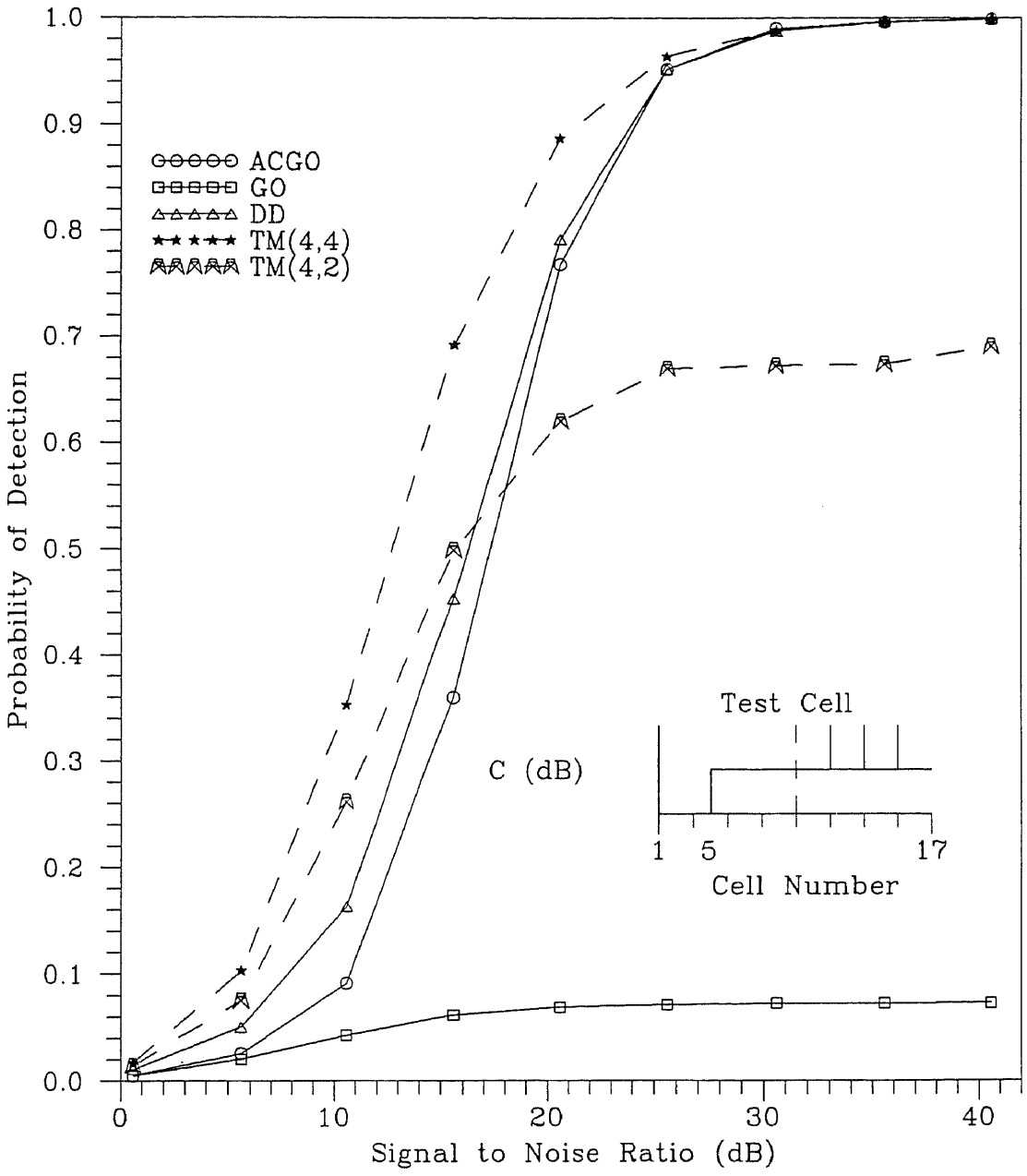

Figure 5.17. Probability of detection of the DD,ACGO,GO and TM-CFAR detectors when three interfering targets and a clutter power transition are present in the reference window.
C=10dB, N=16, b=1.0, L=1, $\alpha=10^{-4}$, $\beta=2\times10^{-3}$, $\gamma=2\times10^{-3}$.

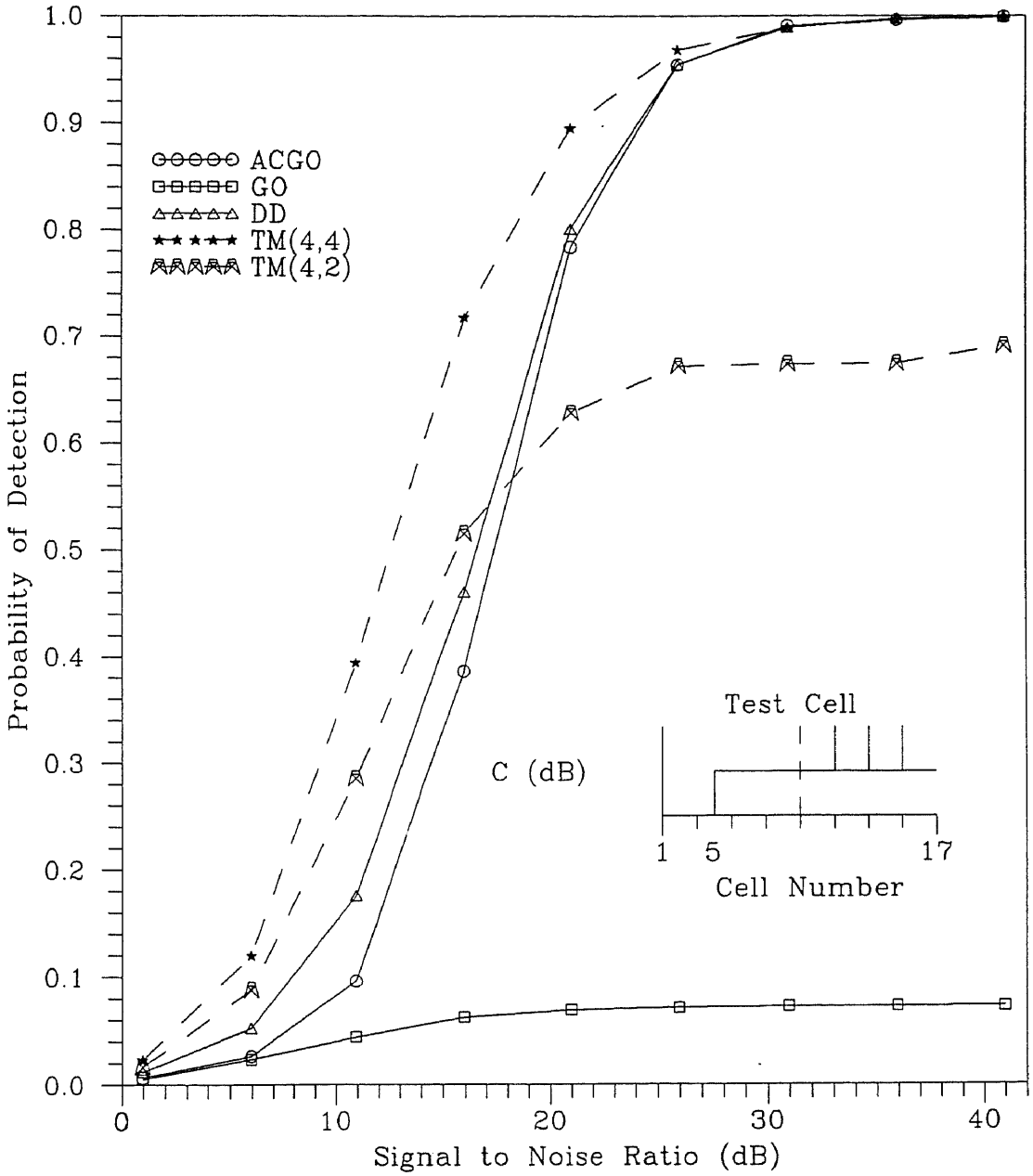

Figure 5.18. Probability of detection of the DD,ACGO,GO and TM-CFAR detectors when three interfering targets and a clutter power transition are present in the reference window.
C=20dB, N=16, b=1.0, L=1, $\alpha=10^{-4}$, $\beta=2\times10^{-3}$, $\gamma=2\times10^{-3}$.

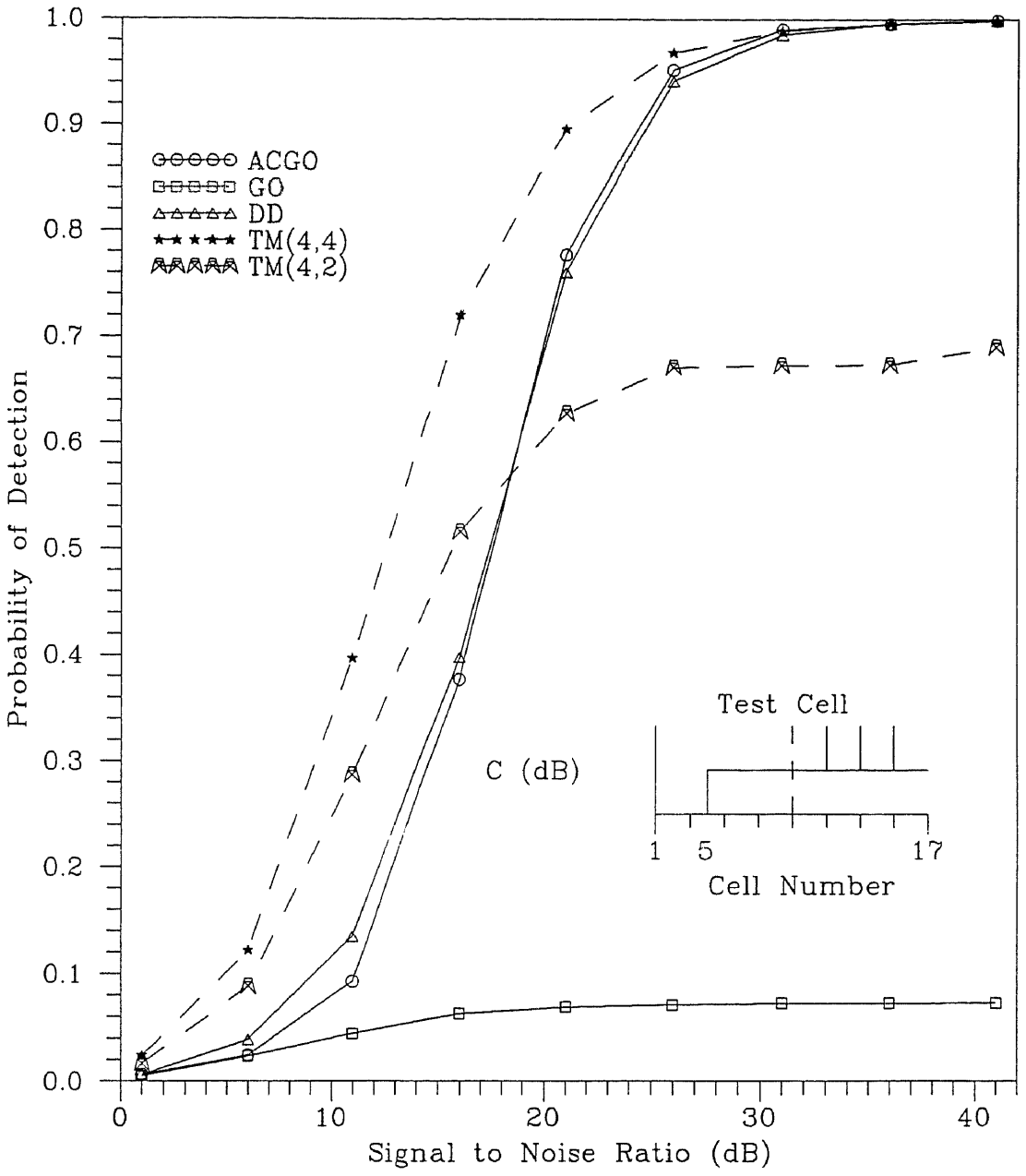

Figure 5.19. Probability of detection of the DD,ACGO,GO and TM-CFAR detectors when three interfering targets and a clutter power transition are present in the reference window. C=30dB, N=16, b=1.0, L=1, $\alpha=10^{-4}$, $\beta=2\times10^{-3}$, $\gamma=2\times10^{-3}$.

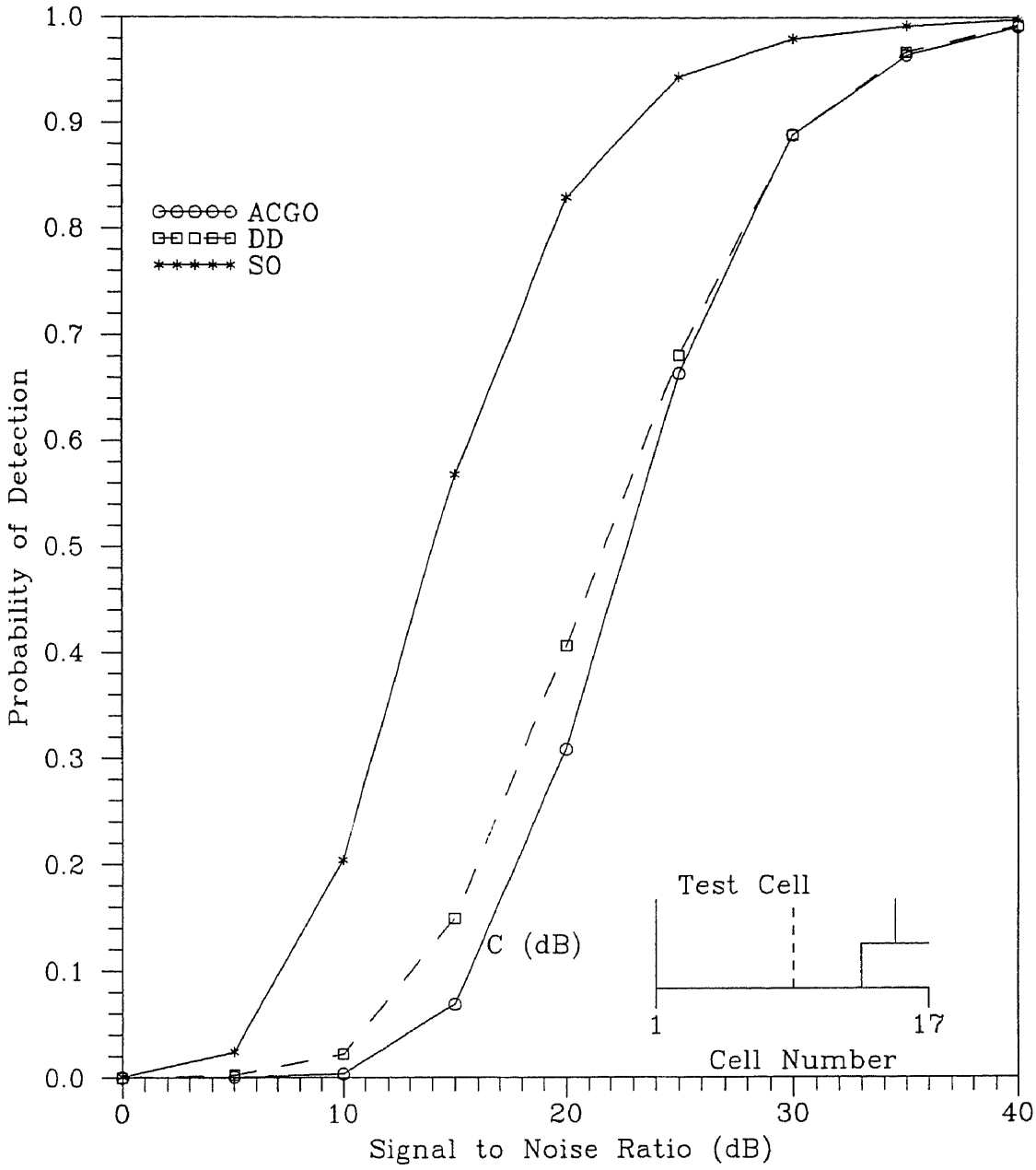

Figure 5.20. Pobability of detection of the DD,SO and ACGO-CFAR detectors when a clutter power transition and one interfering target are present while the test cell is in the clear.
C=10dB, N=16, b=1.0, L=1, $\alpha=10^{-4}$, $\beta=2\times10^{-3}$, $\gamma=2\times10^{-3}$.

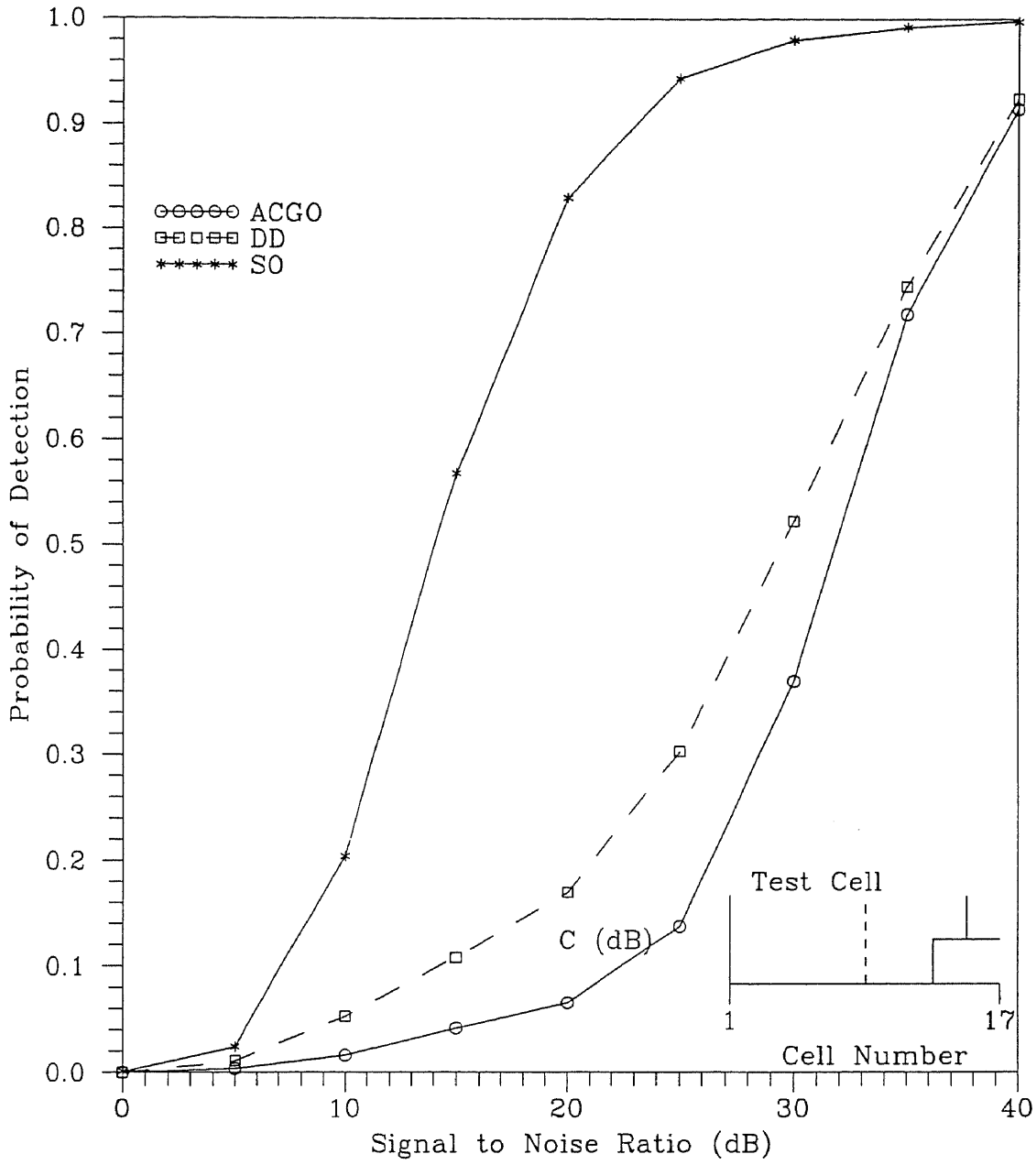

Figure 5.21. Pobability of detection of the DD,SO and ACGO-CFAR detectors when a clutter power transition and one interfering target are present while the test cell is in the clear.
C=20dB, N=16, b=1.0, L=1, $\alpha=10^{-4}$, $\beta=2\times10^{-3}$, $\gamma=2\times10^{-3}$.

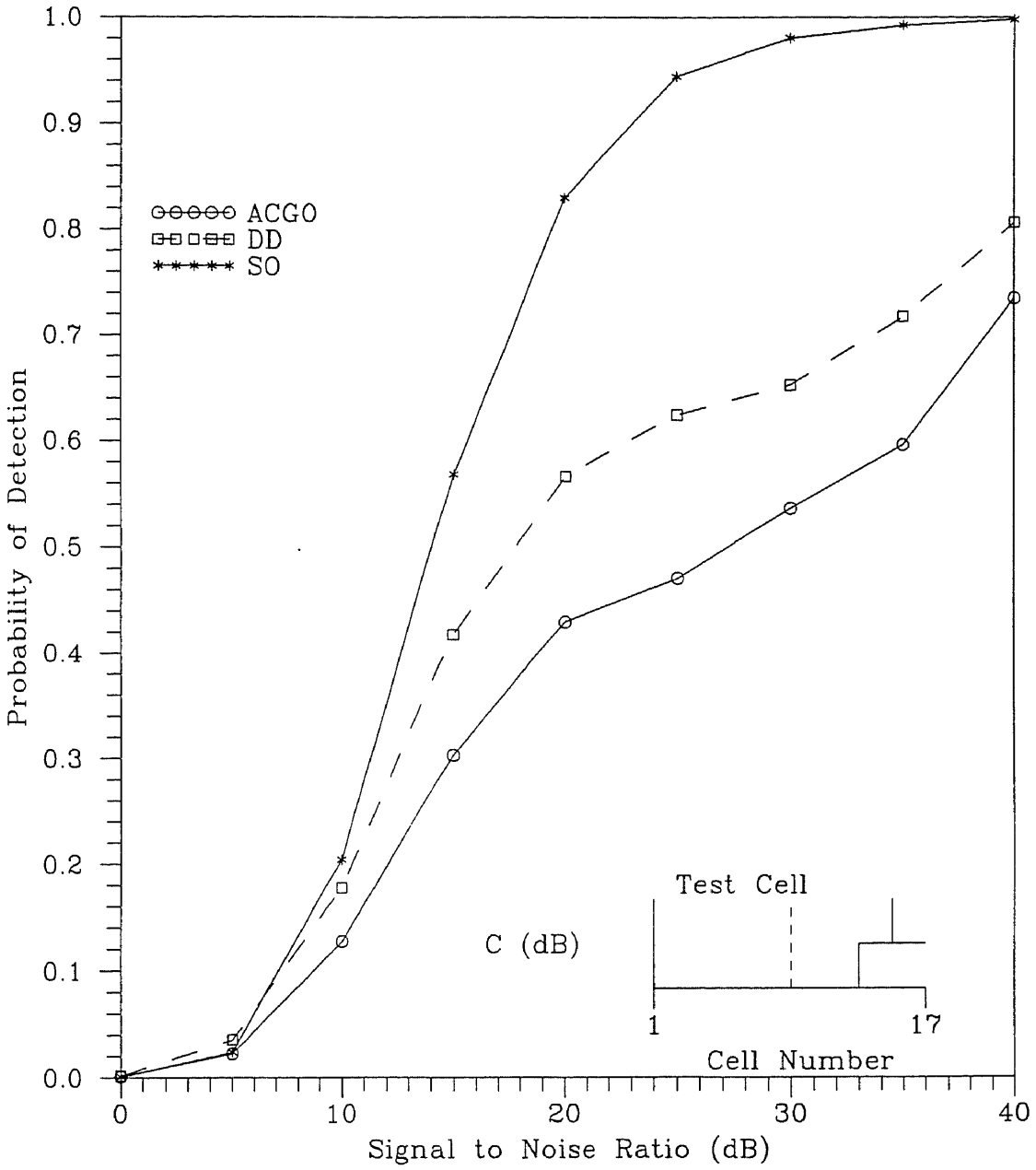

Figure 5.22. Pobability of detection of the DD,SO and ACGO-CFAR detectors when a clutter power transition and one interfering target are present while the test cell is in the clear.
C=30dB, N=16, b=1.0, L=1, $\alpha=10^{-4}$, $\beta=2\times10^{-3}$, $\gamma=2\times10^{-3}$.

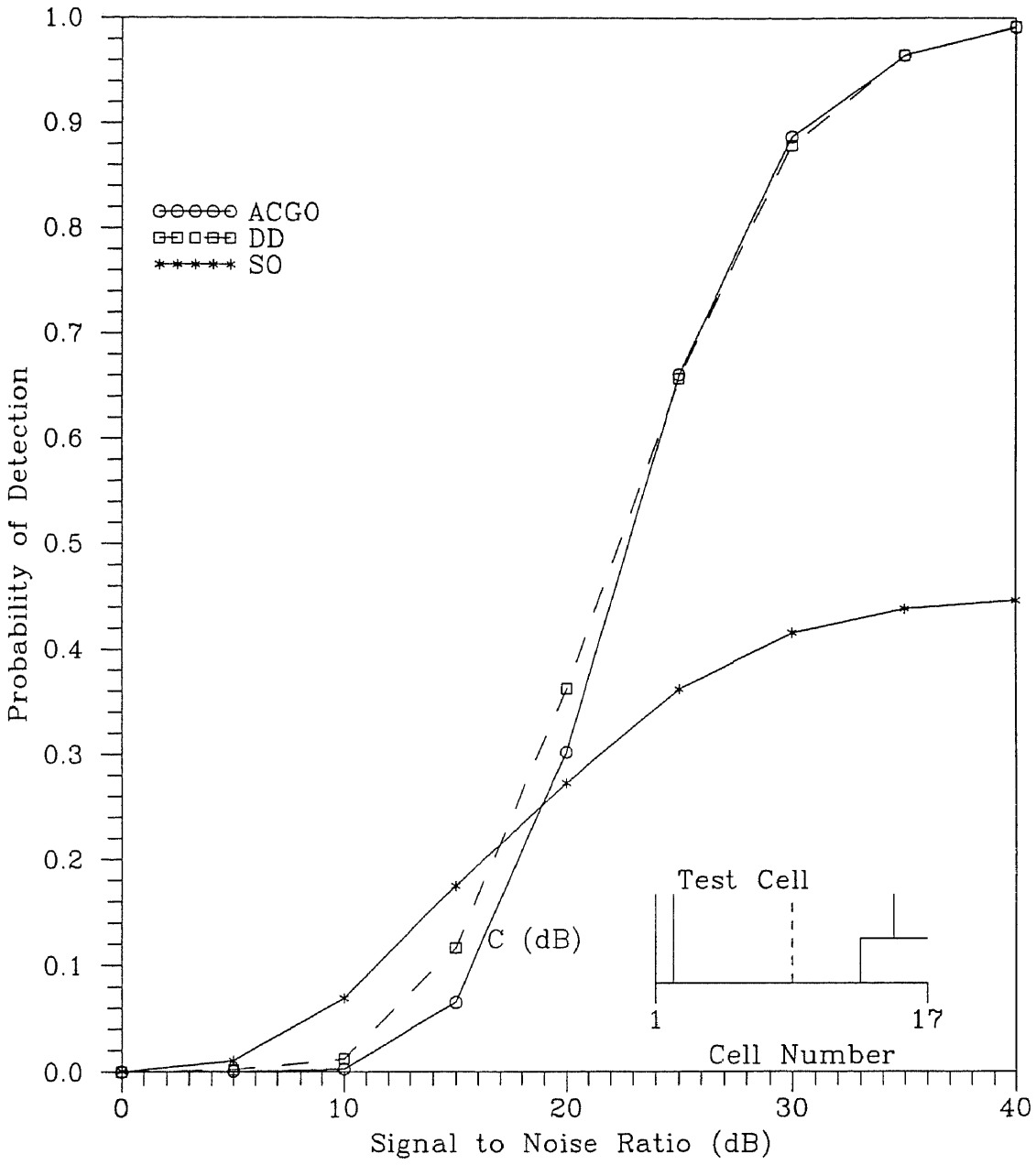

Figure 5.23. Pobability of detection of the DD,SO and ACGO-CFAR detectors when a clutter power transition and two interfering targets are present while the test cell is in the clear.
C=10dB, N=16, b=1.0, L=1, $\alpha=10^{-4}$, $\beta=2\times10^{-3}$, $\gamma=2\times10^{-3}$.

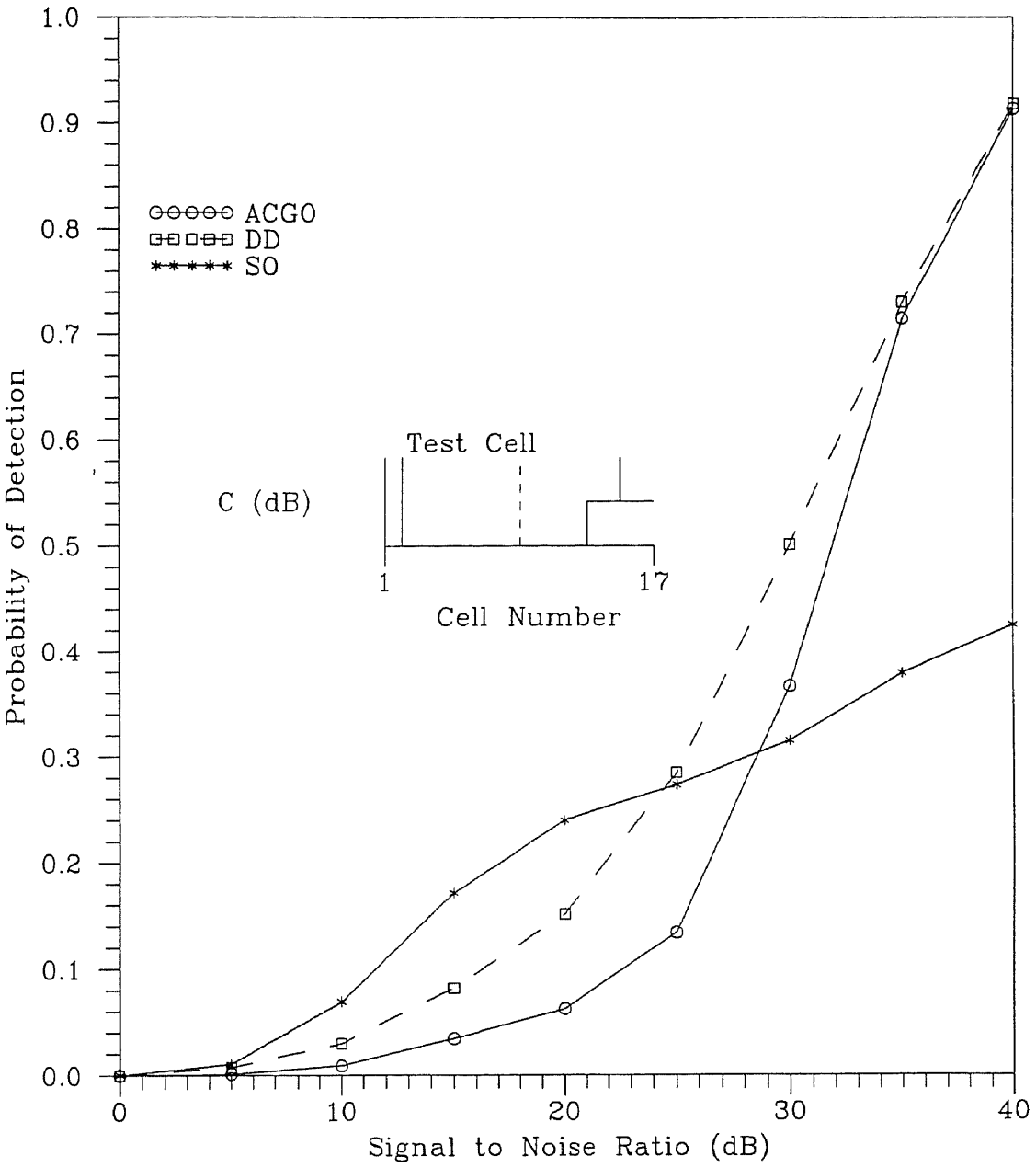

Figure 5.24. Probability of detection of the DD, ACGO and the SO-CFAR detectors when a clutter power transition and two interfering targets are present while the test cell is in the clear.
N=16, b=1.0, L=1, C=20dB, $\alpha=10^{-4}$, $\beta=2\times10^{-3}$, $\gamma=2\times10^{-3}$

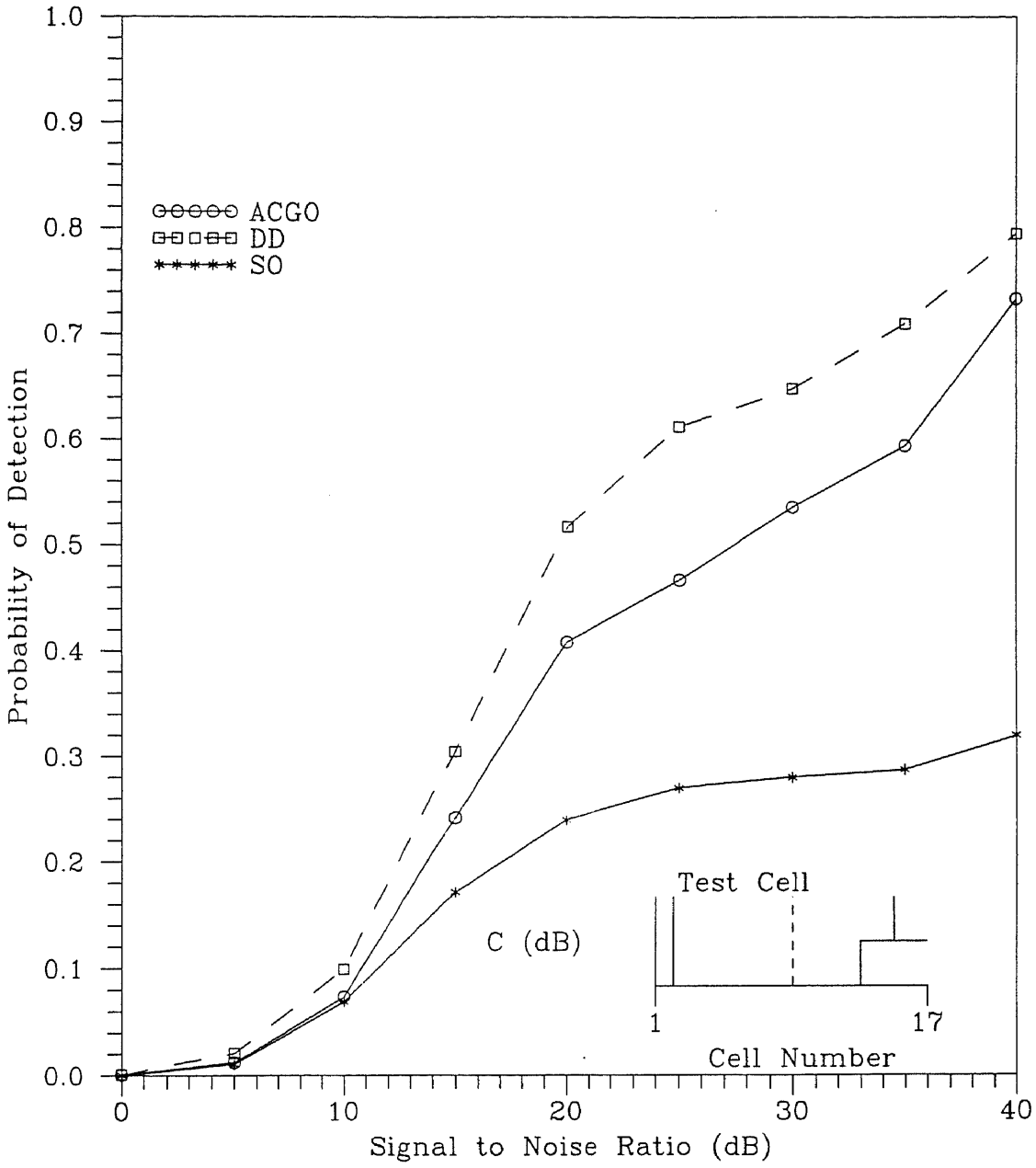

Figure 5.25. Pobability of detection of the DD,SO and ACGO-CFAR detectors when a clutter power transition and two interfering targets are present while the test cell is in the clear.
C=30dB, N=16, b=1.0, L=1, $\alpha=10^{-4}$, $\beta=2\times10^{-3}$, $\gamma=2\times10^{-3}$.

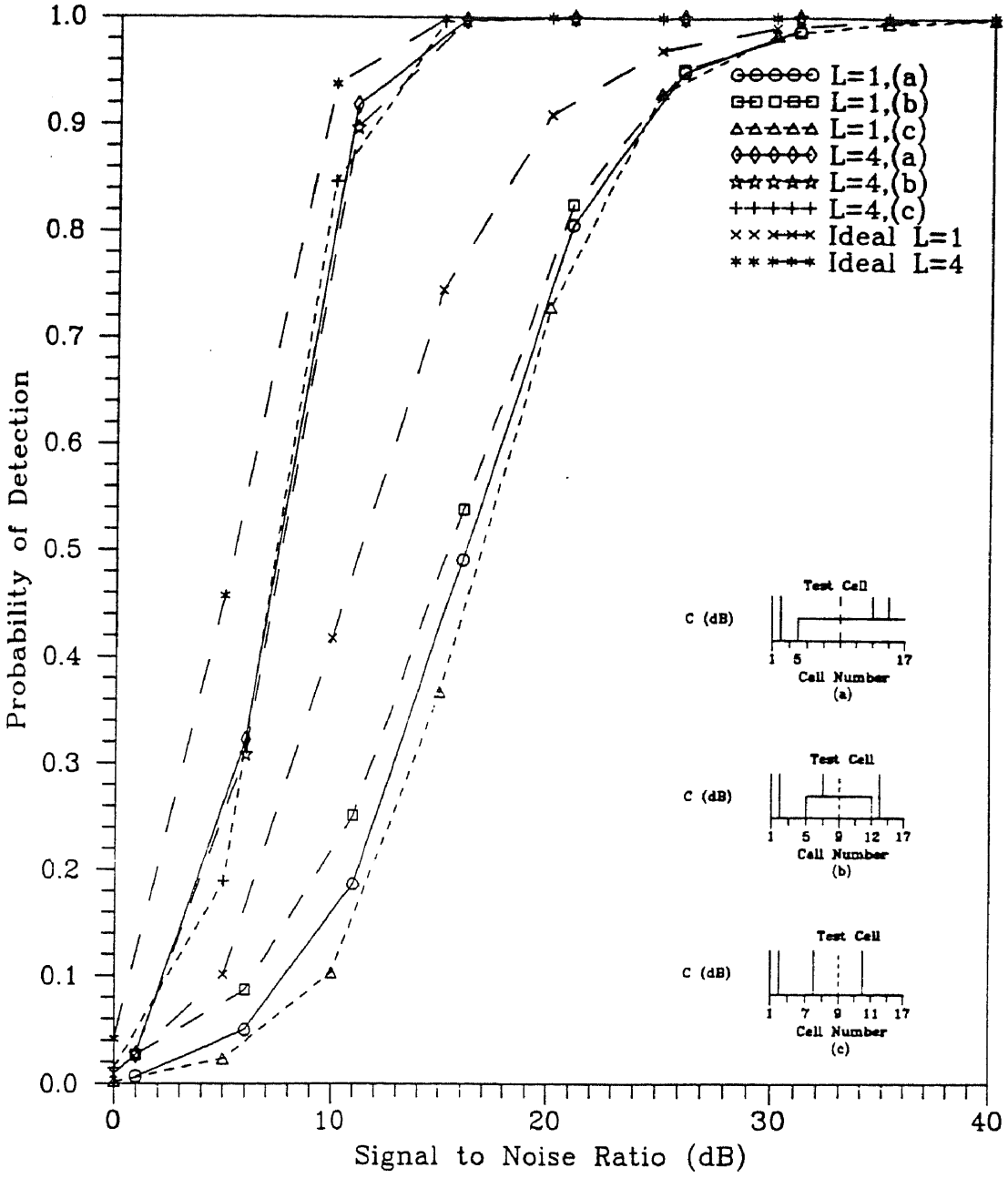

Figure 5.26. Probability of detection versus SNR (dB) of the DD-CFAR detector.
C=30dB, $\alpha=10^{-4}$

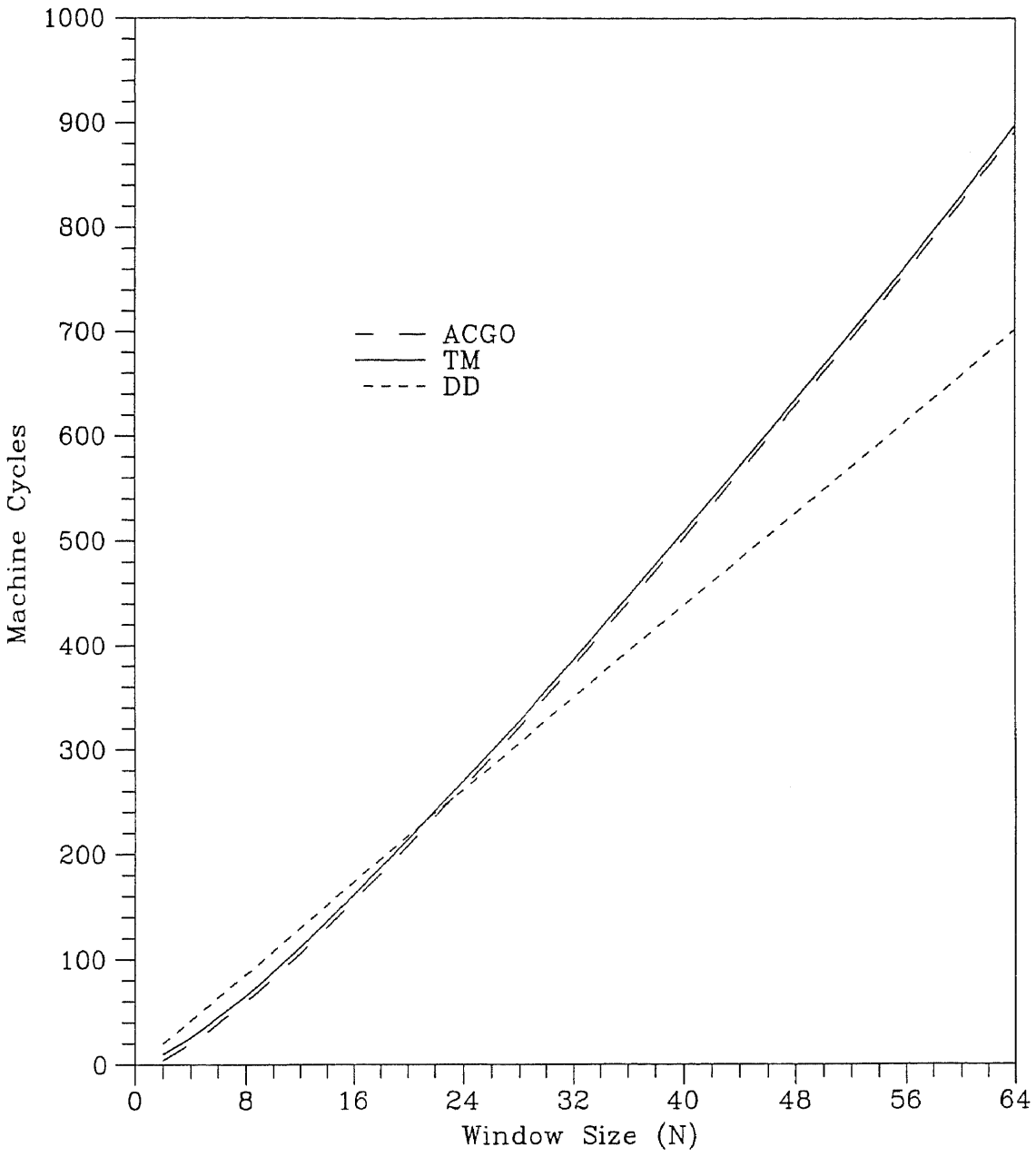

Figure 5.27. Total execution time in machine cycles versus the window size.

Chapter 6

OPTIMUM DETECTION OF RAYLEIGH SIGNALS IN NONSTATIONARY NOISE-THE (RCA) CFAR DETECTOR

6.1 Introduction

In adaptive thresholding techniques, the detection threshold is set so that the detector adapts to changes in the background environment. As we saw in chapter one, one such processor is the Cell Avaraging CFAR detector, CA-CFAR, [10] in which the estimate of the noise power in the cell under test is equal to the arithmetic mean of the outputs of the nearby range cells. The CA-CFAR detector achieves constant false alarm rate when the noise samples are independent and identically distributed. As we saw in previous chapters, in real environment the noise samples may not be homogeneous. Non-homogeneities in the background environment may be continously distributed in the form of a cloud and/or may manifest themselves as spikes in individual cells. Consequently as we saw in chapter 1, the CA-CFAR detector may neither achieve the design false alarm probability nor a high detection probability.

In this chapter, we propose a new adaptive thresholding procedure for Rayleigh envelope distributed signals and noise, where noise power residues instead of noise power estimates are processed. Hence, the proposed detector is referred to as the *residual cell averaging* (RCA) CFAR detector. We show that it is the optimum

constant false alarm rate (CFAR) detector when the noise samples are statistically independent and identically distributed in the sense that its detection performance approaches that of the ideal (fixed threshold) detector as the number of noise samples becomes very large. We also discuss the merits of the proposed technique in rejecting interferences in the noise samples.

In Section 6.2, we describe the RCA-CFAR detector, and in section 6.3 the analysis of the proposed detector is presented. Our results are presented in Section 6.4. Our conclusions are briefly stated in Section 6.5.

6.2 The RCA-CFAR Detector

The sequence of observations $q_1, q_2, \ldots, q_{2M+1}$ is stored in the tapped delay line, as shown in Figure 6.1. The tap in the middle of the delay line is designated as before to be the one under test. The samples in the taps lagging the test tap have been reindexed. They are denoted by $q_{M+1}, \ldots, q_{2M}$. Furthermore, in order to study the optimality of the proposed detector, we assume that the reference samples, $q_1, q_2, \ldots, q_{2M}$, are due to noise alone. The reference noise samples are governed by the exponential distribution with probability density function (pdf)

$$p_{Q_i}(q_i) = \frac{1}{\mu} \exp(-q_i/\mu), \qquad q_i \geq 0$$
$$i = 1, \ldots, 2M \tag{6.1}$$

where μ denotes the average noise power at the receiver input. The test tap, may contain either noise alone or target plus noise. In the event that the test tap contains a target, in addition to noise, the test sample is exponentially distributed as well, since the envelope of the desired signal is Rayleigh distributed. However, the parameter of the distribution governing the observation in the tap under test is different from μ.

Thus, the conditional pdf of the output of the test tap is

$$p_{Q_0|H_i}(q_0|H_i) = \begin{cases} \frac{1}{\mu}e^{-q_0/\mu} \\ \qquad q_0 \geq 0 \text{ for } H_0 \\ \frac{1}{\mu(1+S)}e^{-q_0/\mu(1+S)} \\ \qquad q_0 \geq 0 \text{ for } H_1 \end{cases} \tag{6.2}$$

where hypothesis H_0 denotes the noise only case, while hypothesis H_1 means that a target is also present in the test cell. The noise samples are assumed to be statistically independent from each other. Also the target is independent from the noise. The outputs of the reference cells, $q_1, q_2, \ldots, q_{2M}$, are first subtracted and the new samples are then combined to yield an estimate, q, of the noise variance (power) in the cell under test. q is then scaled by a constant, T , in order to achieve the design probability of false alarm, α. The output of the cell under test, q_0, is compared to the adaptive threshold, Tq, in order to make a decision about the presence or the absence of a target in the test cell. In the next section we show the analysis of the RCA-CFAR detector.

6.3 Analysis of the RCA-CFAR detector

In order to obtain an estimate of the noise variance in the test cell, we first subtract the outputs of all the adjacent reference cells from each other, that is,

$$z_i = q_i - q_{i+1}, \qquad i = 1, \ldots, 2M-1$$

$$z_{2M} = q_{2M} \tag{6.3}$$

Lemma: Given two exponential random variables X and Y with the same parameter, μ, the probability density function of the random variable $W = X - Y$ is given by

$$p_W(w) = \frac{1}{2\mu}\exp(-|w|/\mu) \quad -\infty < w < \infty \tag{6.4}$$

The proof of the above lemma is straightforward since [31]

$$p_W(w) \;=\; p_X(w) * p_Y(-w) \tag{6.5}$$

where "$*$" denotes the convolution operation. Thus, the pdf of the noise residue Z_i is given by

$$p_{Z_i}(z_i) = \frac{1}{2\mu}\exp(-|z_i|/\mu) \quad -\infty < z_i < \infty \tag{6.6}$$

for $i = 1, \ldots, 2M-1$, and

$$p_{Z_{2M}}(z_{2M}) = \frac{1}{\mu}\exp(-z_{2M}/\mu) \qquad z_{2M} \geq 0 \tag{6.7}$$

The system of $2M$ equations depicted by expression (6.3) have a unique solution which can be written as

$$q_i = \sum_{j=i}^{2M} z_j \qquad i = 1, \ldots, 2M \tag{6.8}$$

Also, the jacobian of the transformation is equal to one. Therefore, the likelihood function, [32] $L[z_1, \ldots, z_{2M}]$, of the noise residues is given by

$$L[z_1, \ldots, z_{2M}] = p_{Q_1 \ldots Q_{2M}}(\sum_{j=1}^{2M} z_j, \sum_{j=2}^{2M} z_j, \ldots, z_{2M}) \tag{6.9}$$

where $p_{Q_1 \ldots Q_{2M}}(.,.,\ldots,.)$ denotes the joint pdf of the random variables $Q_1, \ldots, Q_{2M}$. Since the noise samples are statistically independent, the likelihood function, $L[z_1, \ldots, z_{2M}]$ can be written as

$$L[z_1, \ldots, z_{2M}] \;=\; \frac{1}{\mu^{2M}}\;\exp[-\frac{1}{\mu}\sum_{i=1}^{2M}\sum_{j=i}^{2M} z_j] \tag{6.10}$$

Combining the terms in the double summation in equation (6.10), the likelihood function, $L[z_1, \ldots, z_{2M}]$, of the random variables $Z_1, \ldots, Z_{2M}$, may be written as

$$L[z_1, \ldots z_{2M}] \;=\; \frac{1}{\mu^{2M}}\;\exp(-\frac{1}{\mu}\sum_{i=1}^{2M} i z_i) \tag{6.11}$$

Theorem 1 [37]

A statistic $T(\mathbf{Z})$ of a random vector $\mathbf{Z}$ with range I is sufficient for a parameter $\boldsymbol{\theta}$ in Θ (parameter space), if and only if there exists a function $g(t, \boldsymbol{\theta})$ defined for t in I and $\boldsymbol{\theta}$ in Θ, and a function h defined on R^L such that the likelihood function

$$L = g(T(\mathbf{z}), \boldsymbol{\theta})h(\mathbf{z}), \tag{6.12}$$

for all $\mathbf{z} \in R^L, \boldsymbol{\theta} \in \Theta$. Applying theorem 1 to the likelihood function of equation (6.11) we obtain the sufficient statistic

$$T(z_i, \ldots, z_{2M}) = \sum_{i=1}^{2M} i z_i \tag{6.13}$$

Theorem 2 [37]

Let,

$$L = \exp\left[\sum_{i=1}^{n} c_i(\boldsymbol{\theta}) T_i(\mathbf{z}) + d(\boldsymbol{\theta}) + S(\mathbf{z})\right] \tag{6.14}$$

and let C denote the interior of the range of $(c_1(\boldsymbol{\theta}), \ldots c_n(\boldsymbol{\theta}))$. If the equations

$$E[T_i(\mathbf{z})] = T_i(\mathbf{z}), \quad \text{for} \quad i = 1, \ldots, n \tag{6.15}$$

have a solution

$$\hat{\boldsymbol{\theta}}(\mathbf{z}) = [\hat{\theta}_1(\mathbf{z}), \ldots, \hat{\theta}_n(\mathbf{z})] \tag{6.16}$$

for which $\{c_1[\hat{\theta}(z)], \ldots, c_n[\hat{\theta}(z)] \in C$, then $\hat{\boldsymbol{\theta}}$ is the unique maximum likelihood estimate of $\boldsymbol{\theta}$.

Hence, by theorem 2, we obtain that the maximum likelihood estimate, $\hat{\mu}$, of the parameter μ is given by

$$\hat{\mu} = \frac{1}{2M} \sum_{i=1}^{2M} i \, z_i \tag{6.17}$$

In order to make a decision about the presence or the absence of a target in the test cell, we perform the test

$$q_0 \underset{H_0}{\overset{H_1}{\gtrless}} T\, q \tag{6.18}$$

where q is equal to the sufficient statistic $2M\hat{\mu}$ where $\hat{\mu}$ is given by equation (6.17). The probability of false alarm, P_F, may be written as a contour integral that is,

$$P_F = -\frac{1}{2\pi i} \int_c \omega^{-1} \Phi_{Q_0|H_0}(\omega) \Phi_Q(-T\omega) d\omega \tag{6.19}$$

$\Phi_{Q_0|H_0}(\omega)$ denotes the moment generating function, mgf , of the random variable Q_0 under hypothesis H_0, while $\Phi_Q(\omega)$ denotes the mgf of the estimator, Q, of the noise

variance in the test tap. Similarly, the probability of detection, P_D , is given by

$$P_D = -\frac{1}{2\pi i}\int_c \omega^{-1}\Phi_{Q_0|H_1}(\omega)\Phi_Q(-T\omega)d\omega \tag{6.20}$$

In expressions (6.19) and (6.20) the contour of integration c consists of a vertical path in the complex ω-plane that is crossing the real ω-axis at $\omega = c_1$. It is closed in an infinite semicircle in the left half ω-plane. The choice of c_1 will be presented later in the analysis. The mgf of Q_0 under hypothesis H_j, $j = 0, 1$, is defined to be

$$\Phi_{Q_0|H_j}(\omega) = E[\exp(-\omega Q_0) \mid H_j] \tag{6.21}$$

where E [·] denotes the expectation operator. Thus, using equations (6.2) and (6.21), the mgf of Q_0 under H_j, j = 0,1 is obtained to be

$$\Phi_{Q_0|H_j}(\omega) = \begin{cases} 1/(1+\mu\omega) & H_0 \\ 1/[1+\mu(1+S)\omega] & H_1 \end{cases} \tag{6.22}$$

Similarly, using equation (6.1),the mgf of Q may be shown in a straightforward manner to be

$$\Phi_Q(\omega) = \frac{1}{(1+\mu\omega)^{2M}} \tag{6.23}$$

The contour integral of expression (6.19) is evaluated in terms of the simple pole at $\omega = -1/\mu$, while the contour integral of expression (6.20) is evaluated in terms of the simple pole at $\omega = -1/\mu(1+S)$. Observe that the poles of $\Phi_Q(\omega)$ lie in the right-half ω-plane since Q is a positive random variable. In evaluating (6.19) c_1 lies in the open interval $(-1/\mu, 0)$, while in evaluating (6.20) c_1 lies in the open interval $(-1/\mu(1+S), 0)$. Hence, the probability of false alarm is obtained to be

$$P_F = \frac{1}{(1+T)^{2M}} \tag{6.24}$$

and the probability of detection is

$$P_D = \frac{1}{(1+\frac{T}{1+S})^{2M}} \tag{6.25}$$

As the number of reference range cells becomes very large ($M \rightarrow \infty$), the probability of false alarm approaches

$$P_F = \exp(-T) \tag{6.26}$$

while the probability of detection approaches

$$P_D = \exp\left(-\frac{T}{1+S}\right) \tag{6.27}$$

Equations (6.26) and (6.27) are the expressions which describe the performance of the ideal (fixed threshold) detector. Thus, the RCA-CFAR detector is the optimum CFAR processor when the noise samples are statistically independent and identically distributed in the sense that its detection performance approaches that of the ideal detector as the number of reference noise samples becomes very large.

6.4 Results

An attractive feature of the RCA-CFAR detector is the fact that the noise residues become partially correlated to the same degree if the adjacent samples are identically distributed. To see this, consider the correlation coefficient, ρ_i, between Z_i and Z_{i+1}. ρ_i is defined to be

$$\rho_i = \frac{E[Z_i Z_{i+1}] - E[Z_i]E[Z_{i+1}]}{\sigma_{Z_i}\sigma_{Z_{i+1}}} \tag{6.28}$$

for $i = 1, \ldots, 2M-1$. $\sigma^2_{Z_i}$ denotes the variance of Z_i. Since Q_i, Q_{i+1} and Q_{i+2} are identically distributed, then Z_i and Z_{i+1} are also identically distributed with zero mean and variance $2\mu^2$. It can be shown in a very straightforward manner that $E(Z_i Z_{i+1}) = -\mu^2$. Hence, $\rho_i = -1/2$. Also the correlation coefficient between Z_i and Z_j is equal to zero when $|i-j| \neq 0$ or 1. That is, the correlation matrix, $\mathbf{\Lambda}$, of the noise residues is a tridiagonal matrix. The elements of the main diagonal are all equal

to 1, and the elements of the two off diagonal entries are all equal to -1/2. That is,

$$\Lambda = \begin{bmatrix} 1 & -1/2 & 0 & \dots & 0 \\ -1/2 & 1 & -1/2 & \dots & 0 \\ 0 & -1/2 & \ddots & \dots & 0 \\ \vdots & & & & \vdots \\ 0 & \dots & & -1/2 & 1 \end{bmatrix} \tag{6.29}$$

Assuming that a clutter edge with SNR= C appears in the ith cell, then using equation (6.28), it may be readily shown that

$$\rho_j = -1/2 \quad j \neq i-2, i-1 \tag{6.30}$$

$$\rho_{i-2} = -\{2[1+(1+C)^2]\}^{-1/2} \tag{6.31}$$

$$\rho_{i-1} = -\{(1+C)[2(1+(1+C)^2)]^{-1/2}\} \tag{6.32}$$

We observe from equation (6.31) that when the edge is large, ρ_{i-2} approaches zero, while ρ_{i-1} approaches $-1/\sqrt{2}$. Now, let us assume that an interfering signal with SNR= I appears in the ith cell. Using equation (6.28) as before, it may be shown that

$$\rho_j = -1/2 \quad j \neq i-2, i-1, i \tag{6.33}$$

$$\rho_{i-2} = \rho_i = -\{2[1+(1+I)^2]\}^{-1/2} \tag{6.34}$$

$$\rho_{i-1} = -[1+1/(1+I)^2]^{-1} \tag{6.35}$$

We observe from equation (6.34) that when the interference is large, ρ_{i-2} and ρ_i approach zero, while ρ_{i-1} approaches unity. The above change in the correlation coefficient allows us to identify the non-homogeneities in the clutter power distribution which may then be censored by simply observing the consistency in the degree of correlation between adjacently received samples.

The detection performance of the RCA-CFAR detector, is presented in Figures 6.2 and 6.5 for various values of M and a homogeneous noise background environment. In Figure 6.2, the design probability of false alarm is $\alpha = 10^{-4}$, while in Figure 6.3, the

design probability of false alarm is $\alpha = 10^{-6}$. As expected, the detection probability of the RCA-CFAR detector approaches that of the ideal detector as the number of reference noise samples increases. In Figure 6.4, we present the CFAR loss of the RCA-CFAR detector. The CFAR loss is defined to be the increase in signal to noise ratio (dB) that is required so that the CFAR processor achieves the same detection probability with the ideal detector with that SNR. In obtaining these results, we have assumed a detection probability of 0.9. The false alarm regulation properties of the RCA-CFAR detector have been evaluated by means of computer simulation for various values of the background noise level. We have assumed a design probability of false alarm $\alpha = 10^{-4}$. The results are presented in Figure 6.5. We observe that the actual false alarm probability is close to the design value irrespective of the average power of the background noise.

6.5 Summary and Conclusions

In this chapter, we have proposed the RCA-CFAR processor in which noise power residues are combined to obtain the adaptive threshold. The detection performance of the RCA-CFAR detector is identical to the detection performance of the CA-CFAR detector. In a homogeneous background environment the CA-CFAR detector is preferred because it requires less processing of the received observations. However, the fact that the noise residues that are processed by the proposed detector become partially correlated enables us to identify non-homogenieties that may be present in the real environments, by observing the consistency of the degree of correlation where no such feature is available in the CA-CFAR detector.

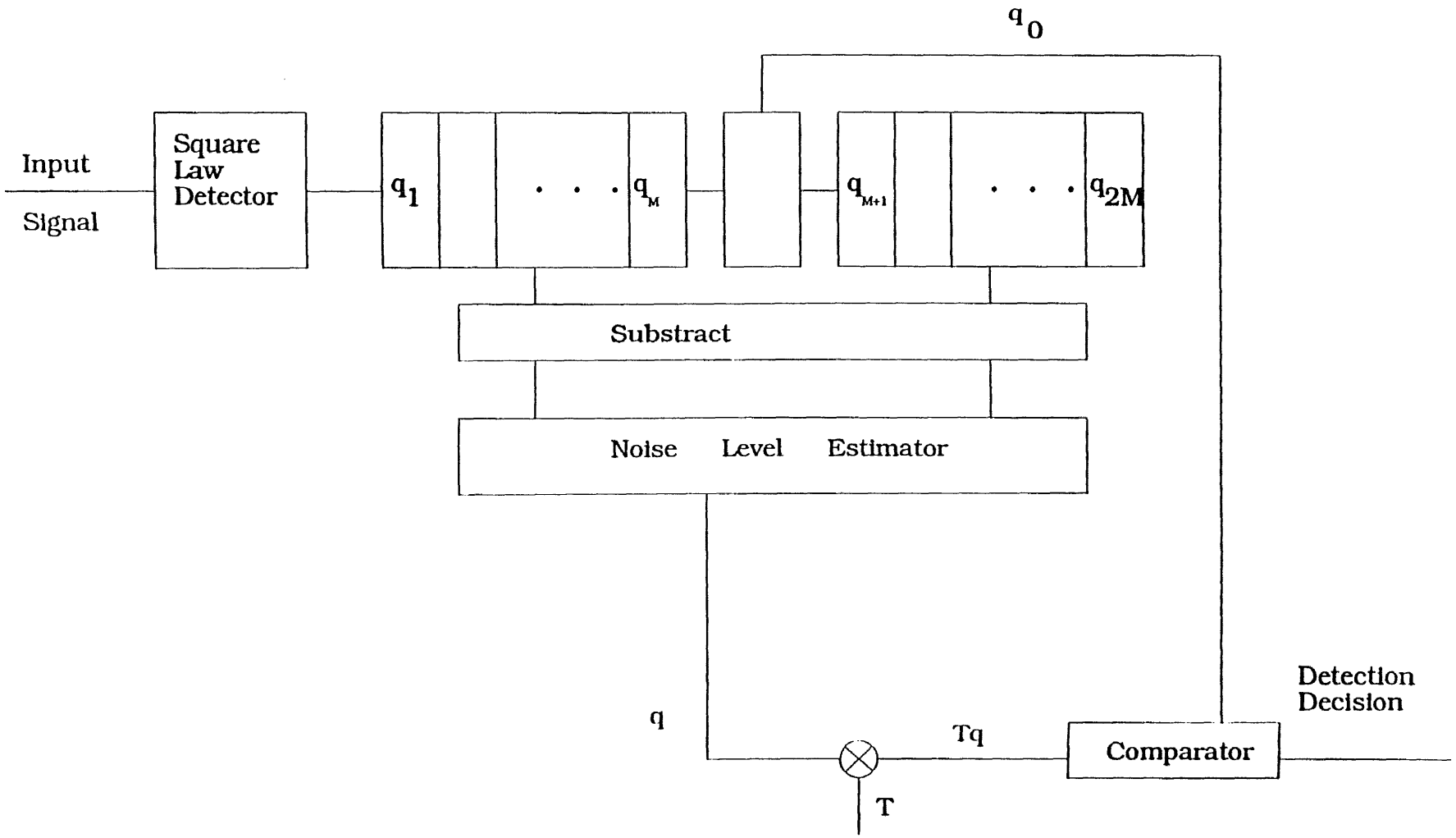

Figure 6.1 Residual Cell Averaging CFAR Detector

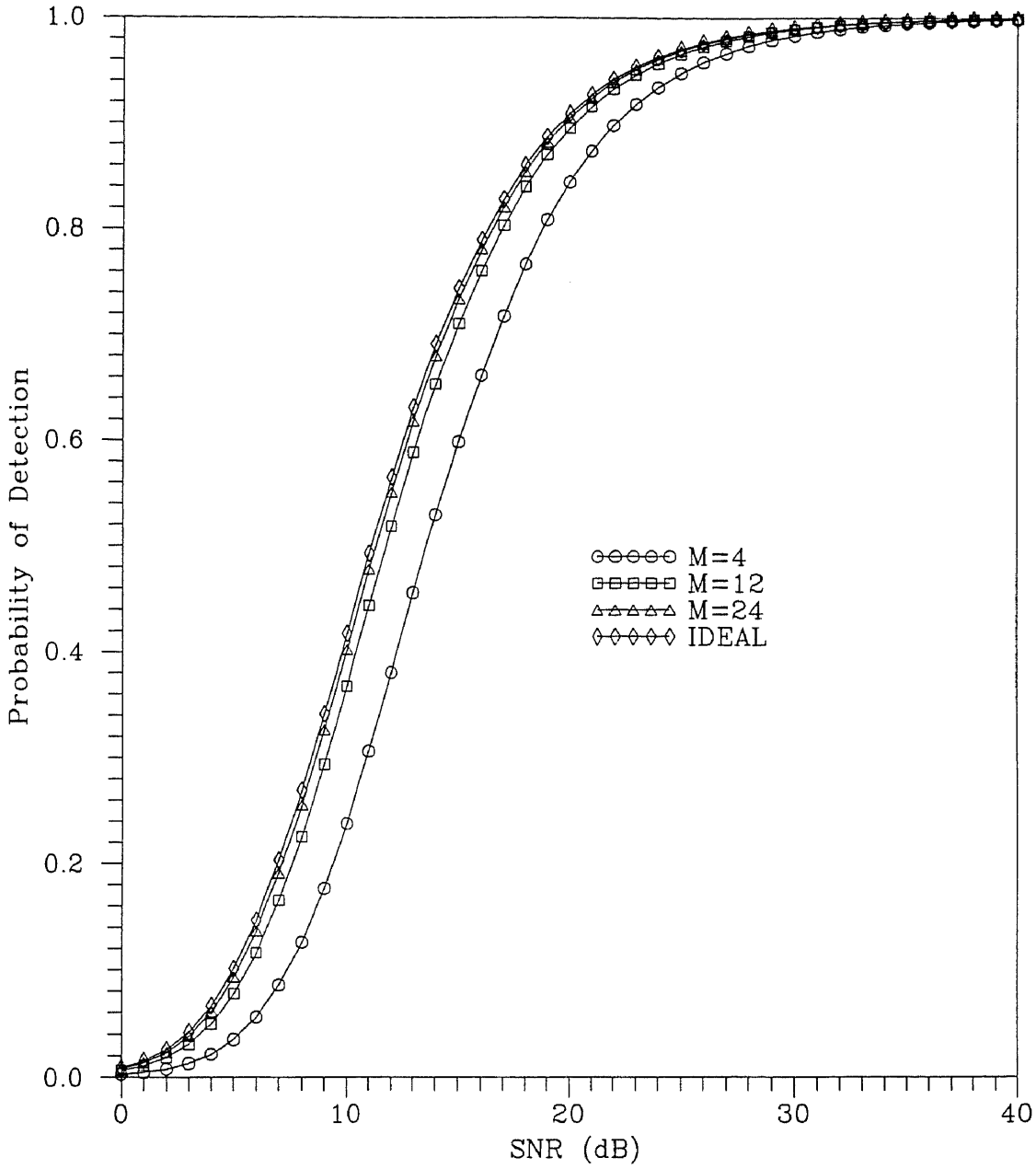

Figure 6.2. Probability of detection versus SNR (dB) with the number of reference cells as a parameter.
$\alpha = 10^{-4}$

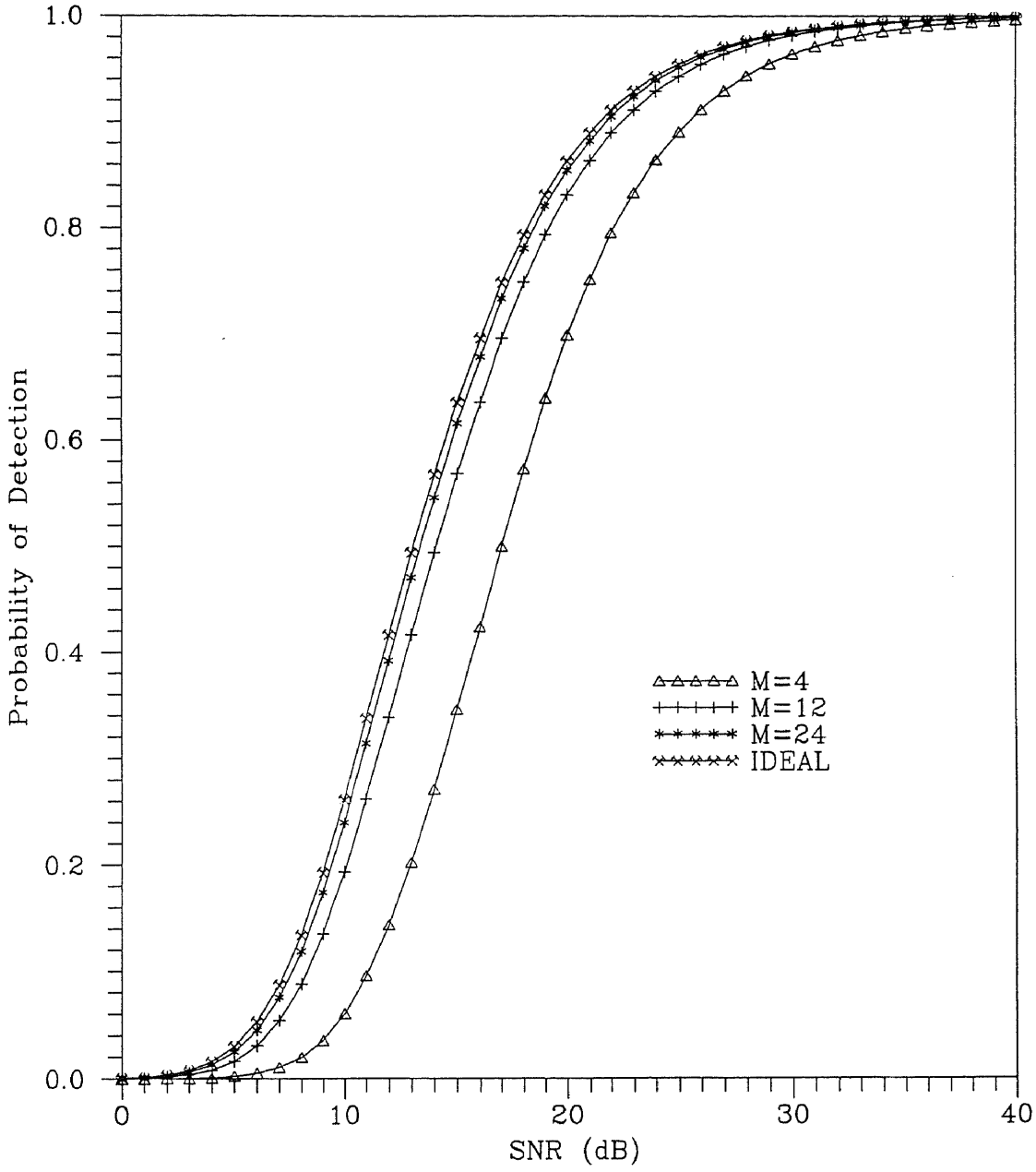

Figure 6.3. Probability of detection versus SNR (dB) with the number of reference cells as a parameter.
$\alpha = 10^{-6}$

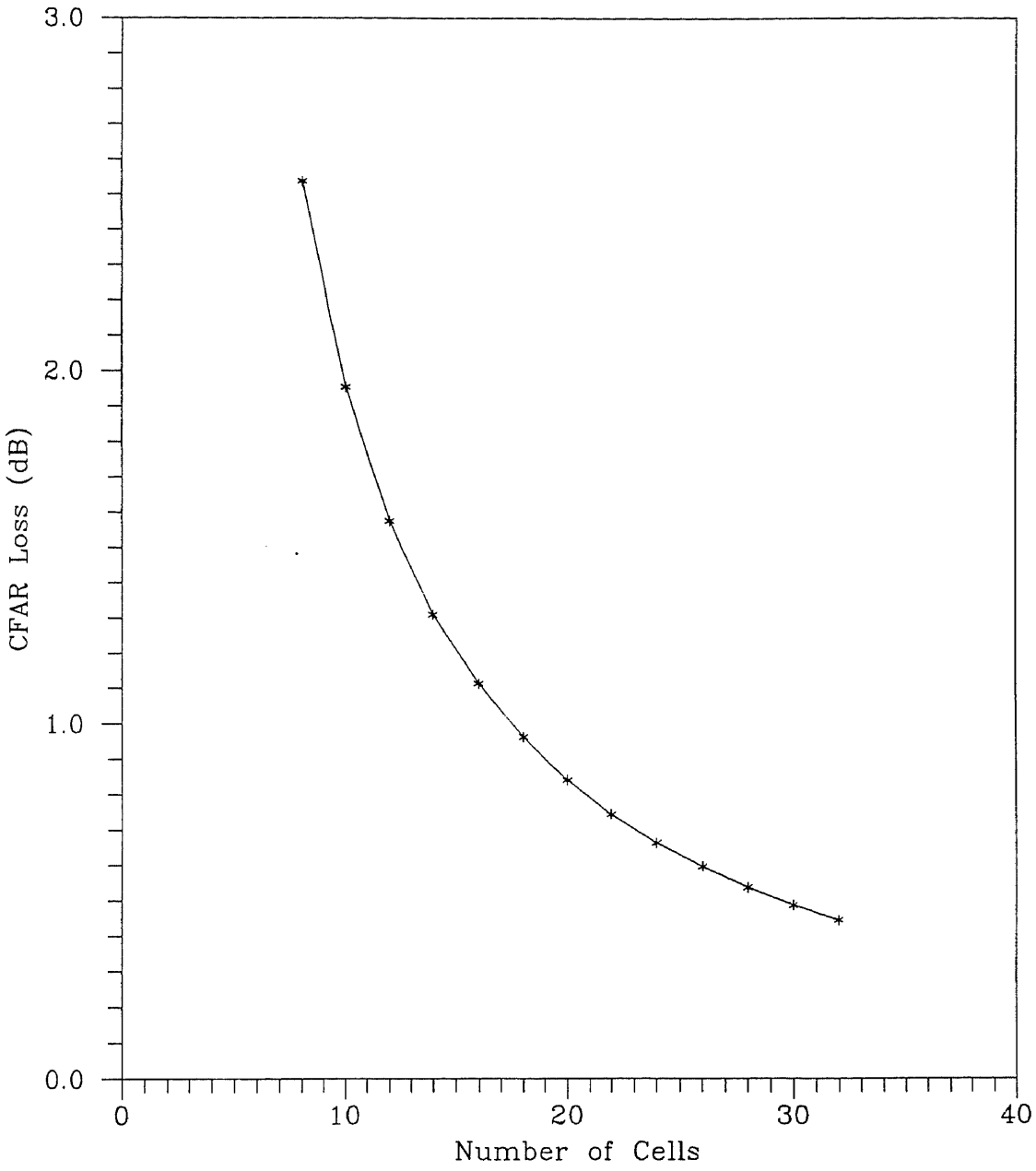

Figure 6.4. CFAR Loss versus number of cells.
$\alpha=10^{-6}$, $P_D=0.9$

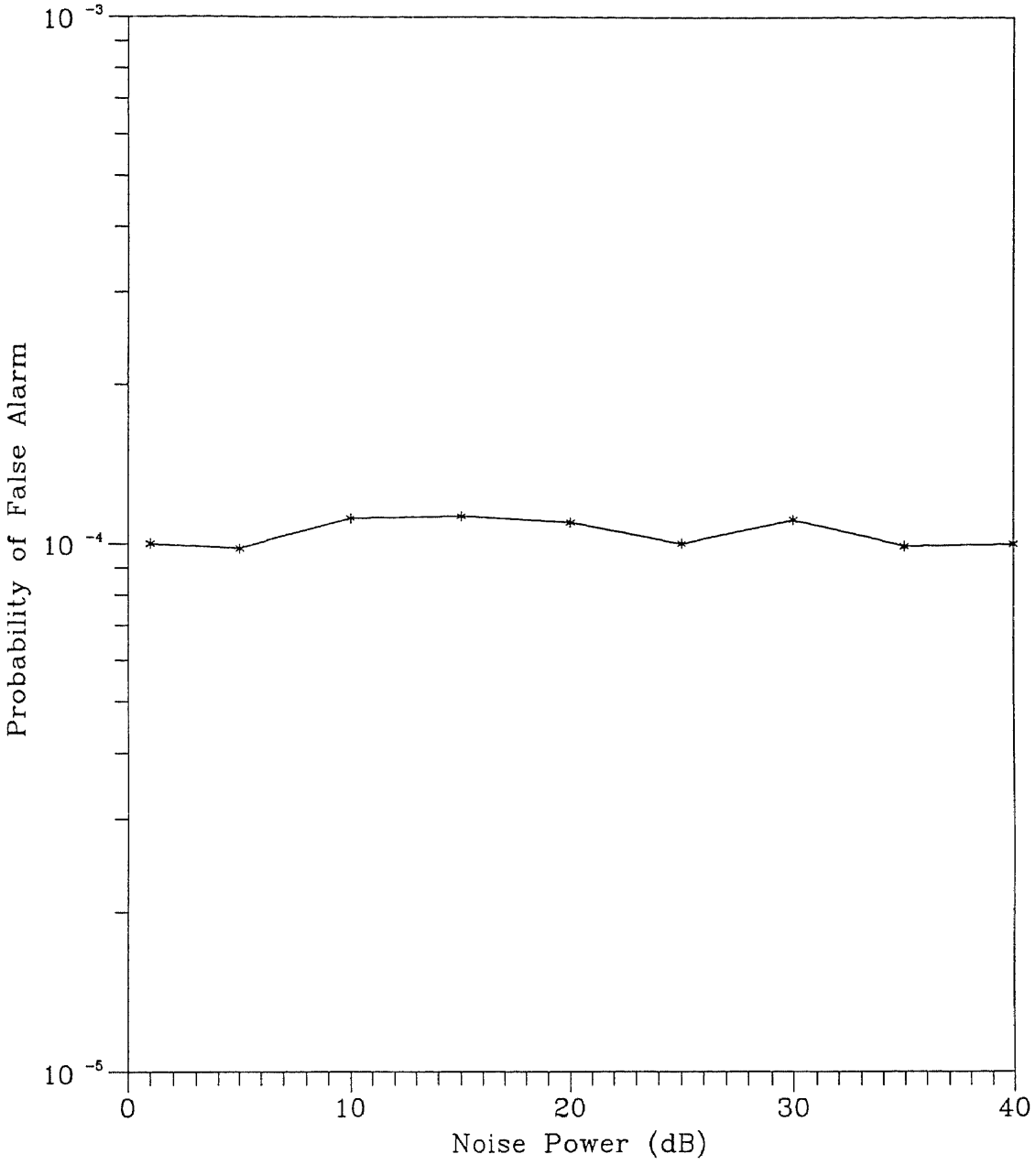

Figure 6.5. Simulation probability of false alarm versus noise power (dB);
$\alpha = 10^{-4}$

Chapter 7

SUMMARY AND CONCLUSIONS

In this dissertation, new adaptive thresholding technigues for CFAR processing in non-homogeneous background environments were proposed and analyzed in time diversity transmission. We developed various signal processing algorithms in which the samples in the reference window of the cell under test, that may yield a poor estimate of the noise level, were effectively censored. First we presented the analysis for single pulse transmission of the GO and SO-CFAR detectors. Then the results were extended for time diversity transmission. A comparison of the performance for both detectors in single pulse and multiple pulse transmission was presented, demonstrating the enhanced performance of both detectors when time diversity was employed.

The presence of clutter power transitions in the range resolution cells of a constant false alarm rate detector may cause an excessive number of false alarms or impaired target detectability as we saw in chapter one. We proposed a CFAR detector algorithm, the Automatic Censored Cell Averaging CFAR detector, ACCA-CFAR, which determines whether the test cell is in the clutter or the clear region and selects only those samples which are identically distributed with the noise in the test cell to form the detection threshold. Its most attractive feature was the fact that the unwanted samples were efficiently censored without having to rank order. The required processing time for a decision to be reached was shown to be less than that

of the order-based statistics processor (ACGO). In addition, when two clutter power transitions were present, one in the leading and the other in the lagging reference window, the false alarm regulation properties of the proposed detector was shown to be robust, while none of the CFAR detectors in the literature perform well.

In real operating environment, reflections from other targets may appear as spikes in the reference window of the cell under test, causing the detection threshold to be raised too high. Thus, the primary target in the test cell may be missed. The Adaptive Spiky Interference Rejection, ASIR-CFAR, detector which determines and censores the interfering targets by performing cell-by-cell tests was proposed and analyzed, in multiple target situations. The detection performance of the proposed detector was compared to those of the CCA and GCMLD detectors in both homogeneous and interfering environments. Also the analysis of the CCA-CFAR detector was extended for multiple pulse transmission. In addition, we studied the effect of the probability of false censoring on the false alarm regulation of both the GCMLD and the proposed detector. Comparison of the GCMLD and the proposed detector in terms of the required processing time was also presented.

Then, the Data Discriminator CFAR detector, DD-CFAR, was proposed and analyzed in the presence of clutter power transitions and/or interfering target returns in the range resolution cells. The DD-CFAR processor performs two passes over the data. In the first pass, the algorithm censors any possible interfering target returns that may be present in the reference cells of the test cell. In the second pass the algotithm determines whether the test cell is in the clutter or the clear region and selects only those samples that are identically distributed with the noise in the test cell to form the detection threshold. The false alarm control and detection performance of the DD-CFAR detector for non-homogeneous background environment was compared to those of the ACGO, TM, GO and SO-CFAR detectors. Unlike the TM and ACGO-CFAR processors, the proposed detector does not require rank ordering of the received

data. As the number of reference cells increases, the processing time required by the DD-CFAR processor, was shown to be less than the processing time required by other CFAR detectors.

Finally, we proposed a new adaptive thresholding procedure for Rayleigh envelope distributed signals and noise, where noise power residues instead of noise power estimates are processed and is referred to as the Residual Cell Averaging detector, RCA-CFAR. We showed that it is the optimum constant false alarm rate (CFAR) detector, when the noise samples are statistically independent and identically distributed, in the sense that its detection performance approaches that of the ideal (fixed threshold) detector as the number of noise samples becomes large. However, the fact that the noise residues become partially correlated to the same degree, if the adjacent samples are identically distributed, enables us to identify non-homogeneities in the clutter power distribution, which may be censored, by simply observing the consistency in the degree of correlation between adjacently received samples.

As mentioned throughout this dissertation, clutter power transitions may be present in the reference window of the cell under test. We have assumed that the parameter of the cell that contains the clutter edge is $\mu = 1 + C$, where the adjacent cell which is in the clear has parameter μ that is normalized to unity. A more realistic approach can be considered in which the clutter power transition is extended gradually among range cells.

Recently a number of CFAR processors that exhibit robust performance have been proposed in the literature. However, a crucial point that is usually underestimated is the amount of processing time required to implement the different processing algorithms. A study should be made where possible use of parallel processing algorithms is possible. An evaluation of the performance of different processing algorithms with respect to different parameters, such as processing time, utilization, complexity and cost should also be investigated.

In chapter four, we proposed the ASIR-CFAR detector for multiple target situations. The processing algorithm of the ASIR-CFAR detector can be applied in case where random interfering pulses, such as those generated from nearby radars or pulse jammers, are present at the reference window of the primary target. Random interfering pulses, with an average repetitive frequency comparable to that of the radar, will coincide in time with only a small fraction of the pulses in any received pulse train [7].

Finally the decision algorithm of the DD-CFAR detector can be studied in conjuction with distributed systems where decision from various sensors are being processed to make the final decision according to some decision rule (AND,OR).

Appendix A

Scaling Constants of the CA,GO and SO-CFAR Detectors

P_{FA}	N=16		N=24		N=32	
	L=1	L=4	L=1	L=4	L=1	L=4
10^{-4}	0.778	0.275	0.468	0.1773	0.334	0.1305
10^{-6}	1.371	0.3855	0.778	0.2445	0.54	0.179
10^{-8}	2.162	0.501	1.154	0.313	0.778	0.227

CA-CFAR Detector

P_{FA}	N=16		N=24		N=32	
	L=1	L=4	L=1	L=4	L=1	L=4
10^{-4}	1.358	0.511	0.833	0.333	0.602	0.265
10^{-6}	2.420	0.720	1.400	0.460	0.983	0.38
10^{-8}	3.840	0.940	2.090	0.592	1.425	0.497

GO-CFAR Detector

P_{FA}	N=16		N=24		N=32	
	L=1	L=4	L=1	L=4	L=1	L=4
10^{-4}	2.444	0.6479	1.277	0.4001	0.851	0.28
10^{-6}	5.131	0.94	2.347	0.564	1.475	0.39
10^{-8}	9.905	1.269	3.916	0.736	2.302	0.502

SO-CFAR Detector

Appendix B

Scaling Constants for the DD-CFAR Detector

T(1)	9990
T(2)	98.97
T(3)	20.54
T(4)	8.999
T(5)	5.309
T(6)	3.641
T(7)	2.7275
T(8)	2.162
T(9)	1.7825
T(10)	1.5117
T(11)	1.31
T(12)	1.15428
T(13)	1.0308
T(14)	0.93068
T(15)	0.8478
T(16)	0.7782

$$L = 1, P_F = 10^{-4}$$

T(1)	22.7
T(2)	4.612
T(3)	2.3065
T(4)	1.5021
T(5)	1.1051
T(6)	0.8712
T(7)	0.7178
T(8)	0.6098
T(9)	0.5298
T(10)	0.4682
T(11)	0.41933
T(12)	0.37965
T(13)	0.34677
T(14)	0.31912
T(15)	0.29555
T(16)	0.2752

$$L = 4, P_F = 10^{-4}$$

Bibliography

[1] Eaves, J.L., and E.K. Reedy. "Principles of Modern Radar." Van Nostrant, New York, 1987

[2] Barton, D.K. "Modern Radar System Analysis.", Artech House, Massachussets, 1988

[3] Swerling, P. "Probability of Detection for Fluctuating Targets." RM-1217, March 17, 1954

[4] Van Trees, H.L. "Detection, Estimation, and Modulation Theory." Part I, Wiley, 1968

[5] Helstrom, C.W. "Statistical Theory of Signal Detection." Pergamon Press, 1960

[6] Whalen, A.D. "Detection of Signals in Noise." Academic Press, New York, 1971

[7] DiFranco, J.V., and W.L. Rubin. "Radar Detection." Artech House, Dedham MA, 1980.

[8] Levanon, N. "Radar Principles." Wiley, 1988

[9] Skolnik, I.M."Introduction to Radar Systems." McGraw-Hill, 1980

[10] Finn, H.M., and R.S. Johnson. "Adaptive Detection Mode with Threshold Control as a Function of Specially Sampled Clutter Estimates." *RCA Review*, VOL. 29, No. 3, pp 414-464, 1968.

[11] Hansen, V.G. "Constant False Alarm Rate Processing in Search Radars." *Proceedings of the IEE International Radar Conference*, pp.325-332, 1973.

[12] Hansen, V.G., and J.H. Sawyers. "Detectability Loss due to Greatest-of Selection in a Cell Averaging CFAR." *IEEE Transactions on Aerospace and Electronic Systems*, Vol. AES-16, pp. 115-118, 1980.

[13] Moore, J.D., and N.B. Lawrence. "Comparison of Two CFAR Methods Used With Square-Law Detection of Swerling I Targets." *Proceedings of the 1980 IEEE International Radar Conference* pp.403-409, 1980.

[14] Weiss, M. "Analysis of some Modified Cell-Averaging CFAR Processors in Multiple Target situations." *IEEE Transactions on Aerospace and Electronic Systems*, Vol. AES-18,No. 1, pp. 102-114, 1982.

[15] Trunk, G.V. "Radar Resolution of Targets using Automatic Detection." *IEEE Transactions on Aerospace and Electronic Systems*, Vol. AES-14,No. 5, pp. 750-755, 1978.

[16] Barkat, M., and P.K. Varshney. "Adaptive Cell Averaging CFAR Detection with Multiple Estimators." *Proceedings of the IV European Signal Processing Conference*, pp. 355-358, 1988

[17] Barkat, M. "On Adaptive Cell Averaging CFAR Radar Signal Detection." Ph.D. Dissertation, Syracuse University, 1987.

[18] McLane, P.J., P.H. Wittke, and C. Ips. "Threshold Control for Automatic Detection in Radar Systems." *IEEE Transactions on Aerospace and Electronic Systems*,Vol. AES-18,No. 2, pp. 242-248, 1982.

[19] Al-Hussaini, E.K., and B.M. Ibrahim. "Comparison of Adaptive Cell-Averaging Detectors for multiple target situations.", *IEE Proceedings*, Pt. F, Vol. 133, No. 3, pp. 217-223, 1986.

[20] Barkat, M., and P.K. Varshney. "A Weighted Cell-Avaraging CFAR Detector for Multiple Target Situations." *Proceedings of the 21st Annual Conference on Information Sciences and Systems*, Baltimore, Maryland, Mar. 25-27, pp. 118-123, 1987.

[21] Barboy, B., E. Lomes, and E. Perkalski. "Cell-Averaging CFAR for multiple target situations."*IEE Proceedings*, Pt. F, Vol. 133, No. 2, pp. 176-186, 1986.

[22] Rohling, H. "Radar CFAR thresholding in clutter and multiple target situations." *IEEE Transactions on Aerospace and Electronic Systems*,Vol. AES-19, No. 4, pp. 608-621, 1983.

[23] Elias-Fuste, A.R., M.G. Mercado, and E.R. Davo. "Analysis of Some Modified Ordered Statistic CFAR: OSGO and OSSO CFAR." *IEEE Transactions on Aerospace and Electronic Systems*, Vol. AES-26, No. 1, pp. 197-202, 1990.

[24] Rickard, J.T., and G.M. Dillard. "Adaptive Detection Algorithms for Multiple Target Situations." *IEEE Transactions on Aerospace and Electronic Systems*,Vol. AES-13,No. 4, pp. 338-343, 1977.

[25] Ritcey, J.A. "Performance Analysis of the Censored Mean Level Detector." *IEEE Transactions on Aerospace and Electronic Systems*,Vol. AES-22,No. 4, pp. 443-454, 1986.

[26] Al-Hussaini, E.K. "Performance of the Greater-of and Censored Greater-of Detectors in Multiple Target Environments." *IEE Proceedings*, Pt. F, Vol. 133, No. 3, pp. 193-198, 1988.

[27] Gandhi, P.P. and S.A. Kassam. "Analysis of CFAR Processors in Nonhomogeneous Background." *IEEE Transactions on Aerospace and Electronic Systems*, Vol. AES-24, No. 4, pp. 443-454, 1988.

[28] Barkat, M., S.D. Himonas, and P.K. Varshney. "CFAR Detection for Multiple Target Situations." *IEE Proceedings*, Pt. F, Vol. 136, No. 5, pp. 193-209, 1989.

[29] Himonas, S.D., and M. Barkat. "Automatic Censored CFAR Detection for Nonhomogeneous Environments.", *IEEE Transactions on Aerospace and Electronic systems*, Vol. AES-28, No. 1, pp. 286-304, 1992.

[30] Himonas, S.D. "Adaptive Censored Greatest-of CFAR detection." *IEE Proceedings*, Pt. F, Vol.139, No.3, pp.247-255, 1992

[31] Papoulis, A. "Probability, Random Variables and Stochastic Processes." McGraw-Hill, New York, 1984.

[32] Rohatgi, V.K. "An Introduction to Probability Theory and Mathematical Statistics." Wiley, 1976

[33] Aho, A.V., J.E. Hopcrofd, and J.D. Ullman. "The Design and Analysis of Computer Algorithms." Addisson Wesley, Massachussets, 1974.

[34] Hennessy, J.L., and D.A. Patterson. "Computer Architecture and Quantitative Approach." Morgan Kaufman, California, 1990.

[35] "TMS32C40 User's Guide", Texas Instruments, 1991

[36] Wozencraft, J.M., and I.M. Jacobs. "Principles of Communication Engineering." John Wiley, New York, 1965.

[37] Bickel, P.J., and K.A. Doksum. "Mathematical Statistics." Holden-Day,Inc., Oakland, California, 1977